Mechanistic studies of a cell-permeant peptide designed to enhance myosin light chain phosphorylation

Almansour, Khaled

Award date:
2017

Awarding institution:
University of Bath

Mechanistic Studies of a Cell-permeant Peptide Designed to Enhance Myosin Light Chain Phosphorylation

Khaled Fahad Almansour

A thesis submitted for the degree of Doctor of Philosophy
University of Bath
Department of Pharmacy and Pharmacology

September 2017

Declaration of authorship

I declare that I am the author of this thesis, and all the work described therein was carried out by myself personally, except where I have indicated via references or acknowledgments.

Name: **Khaled Fahad A Almansour**

Date: **02-May-2018**

Signature: 

Contents

Acknowledgments

First and foremost, I offer my sincerest gratitude to my lead supervisor, Prof. Randy Mrsny, who has supported me throughout my PhD with his patience and knowledge. I was extremely lucky to work in his lab and under his supervision. I am also grateful to my second supervisor. Dr. Ian Eggleston for his valuable advice and support during my studies. I attribute the completion of this thesis to the support and encouragement that I have received from both my supervisors.

I would like to express my gratitude to all the Mrsny research group, for their friendly advice and support. In particular, I would like to thank Alistair Taverner who helped me with the *in vivo* work. Also, I thank Dr. Eggleston's group for sharing their views on issues related to the project. In addition, I am grateful to all my friends and colleagues in lab 5W 3.22 for their companionship and for providing such a pleasurable and friendly working atmosphere.

Similarly, I am taking this opportunity to express my gratitude to my sponsors, at the University of Hail and the Ministry of Education in Saudi Arabia, for their funding and support.

My deepest gratitude goes to my parents, Fahad and Nawair, for their love and support my entire life and throughout my PhD. Also, I would like to thank my brothers and sisters for their continued encouragement.

Lastly, I am indebted to my wife, Shahad, who has been extremely supportive throughout my PhD and has made countless sacrifices to help me in getting to this stage.

September, 2017
Bath, UK

List of abbreviations

AJC	Apical junctional complex
AMP	Antimicrobial peptide
APS	Ammonium Persulfate
AUC	Area under the curve
Boc	*tert*-butyloxycarbonyl
BSA	Bovine serum albumin
BVES	Blood vessel epicardial substance
Caco-2	Human colorectal adenocarcinoma cells
CaM	Calmodulin
CAR	Coxsackie and adenovirus receptor
CK2	Casein kinase 2
CM	Carboxymethyl
CPI-17	C-kinase potentiated protein phosphatase-1 inhibitor-17 kDa
CPP	Cell-penetrating peptide
CRB3	Crumbs homologue 3
DAPI	Diamidinophenylindole
DEAE	Diethylaminoethyl
DIC	Diisopropylcarbodiimide
DIEA	Diisopropylethylamine
DMEM	Dulbecco's modified Eagle's medium
DMF	Dimethylformamide
DMSO	Dimethyl sulfoxide

ECL	Extracellular loop
EDTA	Ethylenediaminetetraacetic acid
EtOH	Ethanol
FBS	Foetal bovine serum
FITC	Fluoresceinisothiocyanate
FLIP	Fluorescence loss in photobleaching
Fmoc	9-fluorenylmethyloxycarbonyl
FRAP	Fluorescence recovery after photobleaching
GI	Gastrointestinal
GLP	Glucagon-like peptide
HBSS	Hanks' balanced salt buffer solution
HEK	Human embryonic kidney cells
HOBt	Hydroxybenzotriazole
IBD	Inflammatory bowel disease
IESC	Intestinal epithelial stem cell
ILI	Intraluminal intestinal injection
INF-γ	Interferon-γ
JAM	Junctional adhesion molecule
LAL	*Limulus* amebocyte lysate
LPS	Lipopolysaccharide
LY	Lucifer yellow
MAGI	membrane-associated guanylated kinase inverted protein
MBHA	Methyl benzhydrylamine

MDCK	Madin Darby canine kidney cells
MeOH	Methanol
MLC	Myosin light chain
MLCK	Myosin light chain kinase
MLCP	Myosin light chain phosphatase
MLC-pS^{19}	Myosin light chain phosphorylation at serine 19
MoA	Mechanism of action
MTS	3-(4,5-Dimethylthiazol-2-yl)-5-(3-carboxymethoxyphenyl) -2-(4-sulfophenyl)-2H tetrazolium
MUPP1	Multi-PDZ domain proteins
MYPT1	Myosin targeting subunit-1
OA	Okadaic acid
OtBu	*tert*-Butyl ester
P/S	Penicillin and Streptomycin
PALS1	Protein associated with Lin-7
PATJ	Protein associated to TJ
Pbf	Pentamethyl-2,3-dihydrobenzofuran- 5-sulfonyl
PBS	Phosphate buffer saline
PD	Pharmacodynamic
PE	Permeability enhancer
PEG	Polyethylene glycol
PFA	Paraformaldehyde
pI	Isoelectric point

PIK	Membrane-permeant peptide inhibitor of MLCK
PIP	Membrane-permeant peptide inhibitor of MLCP
PK	Pharmacokinetic
PKC	Protein kinase-C
PP1-δ	Protein phosphatase 1-δ
PP2A	Protein phosphatase 2 A
PVDF	Polyvinylidene floride
PyBOP	(benzotriazol-1-yloxy)-tripyrrolidinophosphonium hexafluorophosphate
RIPA	Radioimmunoprecipitation assay buffer
SAR	Structure activity relationship
SBTI	Soybean trypsin inhibitor
SC	Subcutaneous
SDS-PAGE	Sodium dodecyl sulfate polyacrylamide gel electrophoresis
SGLT1	Na-dependent glucose transporter
sIgA	Secretory immunoglobulin A
SPPS	Solid phase peptide synthesis
TAMP	TJ-associated MARVEL protein
tBu	*tert*-Butyl
TEER	Trans-epithelial electrical resistance
TEMED	Tetramethylethylenediamine
TFA	Trifluoroacetic acid
TIPS	Triisopropylsilane

TJ	Tight junction
TNF-α	Tumour necrosis factor-α
TRITC	Tetramethylrhodamine isothiocyanate
ZO	Zonula occluden

Abstract

Oral delivery of therapeutic peptides has been a continuous target for the pharmaceutical industry, as most of these drugs are currently administered by parenteral routes. However, a major challenge limiting the success of oral delivery of these drugs is their poor permeability across the intestinal epithelial barrier. Extensive research efforts have investigated different strategies to overcome the epithelial barrier and enhance the oral bioavailability of therapeutic peptides. One of the most widely used strategies is the application of permeability enhancer (PE) agents that are co-administered with peptide drugs to facilitate their permeability across the intestinal epithelial barrier. The safety of most of the available PE agents, however, has always been questioned, because most PE agents act non-specifically in altering intestinal epithelial permeability which in many cases has been associated with epithelial damage.

The work presented here investigates a novel strategy to overcome the intestinal epithelial barrier challenge and enhance the oral bioavailability of therapeutic peptides. This is by manipulating an endogenous mechanism that is used by the intestinal epithelial cells to dynamically regulate the permeability across the tight junction (TJ) structures by increasing myosin light chain phosphorylation at serine 19 (MLC-pS^{19}), which is regulated by MLC kinase (MLCK) and MLC phosphatase (MLCP). A small membrane-permeant peptide inhibitor for MLCP, called PIP 640 peptide, was rationally designed to selectively alter MLCP activity in a manner that increases MLC-pS^{19} to transiently enhance TJ permeability for therapeutic peptides. The PIP 640 peptide was designed to be relatively stable in the intestinal lumen, as it is intended to be co-administered orally with therapeutic peptides. It was initially examined for enhanced TJ permeability of fluorescent dextran and for toxicity induction *in vitro*. Accordingly, efforts were devoted to explore potential modifications of the peptide sequence that might optimize the PIP 640 peptide function. Moreover, studies were performed to examine the biochemical changes of TJ protein structures associated with the permeability

enhancement function of the PIP 640 peptide. Finally, we investigated different aspects of the PIP 640 peptide permeability enhancement function *in vivo*. An overall outcome of these studies was that the PIP 640 peptide can enhance TJ permeability *in vitro* and *in vivo* without causing apparent damage to the epithelial barrier. This outcome suggest that the PIP 640 peptide has the potential to be used as a PE for therapeutic peptides.

List of figures

List of tables

Chapter 1 : Introduction to oral protein delivery

Chapter 1

1.1. Gastrointestinal (GI) tract of the digestive system anatomy and physiology

The human digestive system is a multi-organ system that extends from the mouth to the anus [1]. This system mainly consists of an alimentary tube, called the GI tract, and accessory organs. The alimentary tube includes the oral cavity, pharynx, esophagus, stomach, small intestine, large intestine, and rectum [1]. The alimentary tube is functionally linked to several accessory organs, such as the salivary glands, the gallbladder, the liver, and the pancreas (Figure 1.1) [1]. Food digestion, nutrient absorption, and waste elimination are the main functions of the GI tract [1]. Food digestion occurs in different places within the GI tract in a functionally coordinated manner. Beginning in the mouth, food is mechanically broken down by chewing and exposure to salivary fluid containing digestive enzymes such as salivary amylase that function to break down sugars [1]. Macerated food then reaches the stomach where digestion continues by the actions of digestive enzymes, such as pepsin, that is particularly well-suited to function in harsh acidic conditions (~ pH 1-2) that facilitates protein unfolding [1]. Food processed by the stomach, now known as chyme, then passes through the pyloric sphincter to enter the duodenum where it is mixed with a bicarbonate-based, alkaline (~ pH 8), buffer containing enzymatic cocktail produced in the pancreas [1, 3]. Via this mixing, the pH of the luminal contents of the duodenum is typically brought to ~ pH 5-6 [3]. As chyme moves along the subsequent segments of the small intestine, the jejunum followed by the ileum where the pH of the luminal contents is brought to ~ 7.4, although the pH at the epithelial cell surface can be slightly acidic [3-5]. Enzymes present at the beginning of the small intestine are focused on degrading large materials (such as proteins) while later in the GI tract appear to facilitate digestive events of smaller materials (such as peptidases) [1, 4]. The ultimate goal of this digestive juggernaut is to breakdown complex food stuff, through a serious coordinated enzymatic actions, to release individual nutrient components (amino acids, nucleotides, lipids, *etc*.), that can be readily absorbed via selective uptake mechanisms for located at the luminal surface of the intestinal [1]. The remaining unabsorbed materials

are transported to the large intestine before being execrated from the body through the anus [1].

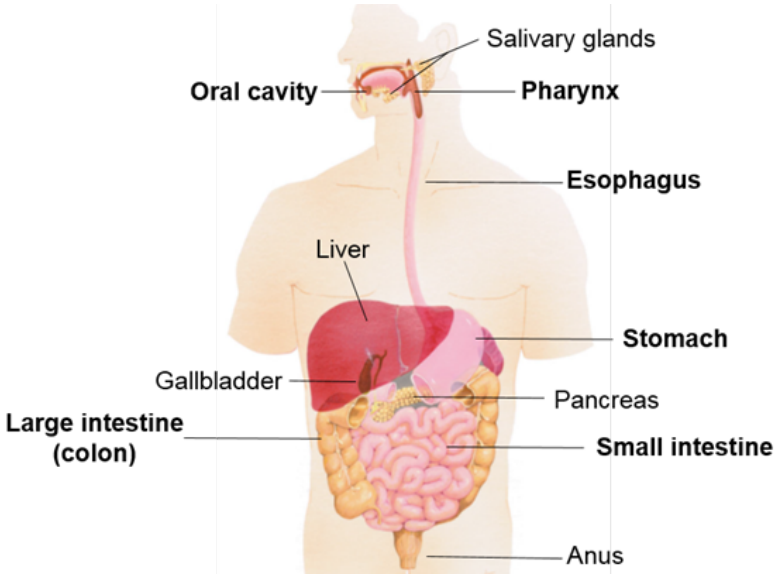

Figure 1.1: Diagram showing the recognized regions of the GI tract. Components that comprise the alimentary tube are in bold. This image was adopted from Scanlon *et al*.,2014 [1] with permission of F. A. Davis publications.

The small intestine is ~ 7 m in length with a mucosal surface that is increased dramatically by *plica circulares* folds (Figure 1.2 A) [1, 6]. These folds in the mucosal layer establish projections in the luminal surface of the small intestine called villi; the base of these villi called crypts that the surface area for molecule diffusion [1]. The small intestine consist of four major layers; mucosa, submucosa, external muscular layers that provide intestinal movement, and an outer layer of connective tissues called serosa (Figure 1.2 B) [1].

The mucosa is composed of a single layer of columnar epithelial cells. Enterocytes are the most prominent of these cell types in terms of number [2]. In addition to the villi arrangements of the small intestine, the absorptive

surface area generated by enterocytes is further increased by specialized apical membrane projections known as microvilli [1, 2]. The specialized apical surface environment established by microvilli, called the epithelial brush border, contains a variety of digestive enzymes that function to complete the digestion of food into nutrients that can be readily absorbed by transporters that specifically recognize distinct nutrients by their physicochemical properties [7].

Immediately beneath the monolayer of cells that comprise the intestinal epithelium is a non-cellular matrix of proteins and glycoproteins known as the basement membrane. And immediately beneath the basement membrane is a network of blood capillaries and lymphatic vessels that are themselves followed by thin layer of muscle (Figure 1.2 B) [1, 6]. The submucosal layer contains more blood and lymphatic vessels in addition to nerve fibres (Figure 1.2 B). Due to large luminal surface area of the small intestine and its high content of blood vessels in both mucosal and submucosal layers [1, 6], the small intestine is not only the main site of nutrient uptake, but has also been considered as a promising site for drug absorption, as most marketed drugs are formulated and administrated for absorption at this tissue [8].

1.2. Small intestinal epithelium composition and maintenance

There are a variety of cell types in the small intestine, many of which are regionally restricted to crypt and villus structures that characterize this region of the alimentary tract (Figure 1.3) [1, 2]. These cells contribute in various ways to the many functions of the intestinal epithelia. Enterocytes are the most common cells, performing both digestive and absorptive functions [2]. The remaining cells, representing only a fraction of the small intestinal epithelium are involved in functions that include secretion and protection [2, 9, 10]. Enteroendocrine cells produce a varierty of different hormones that have not only important locally, but also have sysemic physiological actions [11]. For

example, enteroendocrine cells secrete glucagon-like peptides (GLP) that are essential for maintaining glucose homeostasis [11]. Goblet cells produce and secrete mucus at the luminal intestinal surface to establish an important barrier to pathogen entry; Paneth cells have a protective role by the secretion of antimicrobial peptides (AMPs) [9, 10]. The small intestinal epithelium also contains microfold cells (M cells) that mediate luminal antigens transport to subepithelial concentrations of immune cells (Peyer's patch) for presentation to the immune system (Figure 1.3) [1, 2].

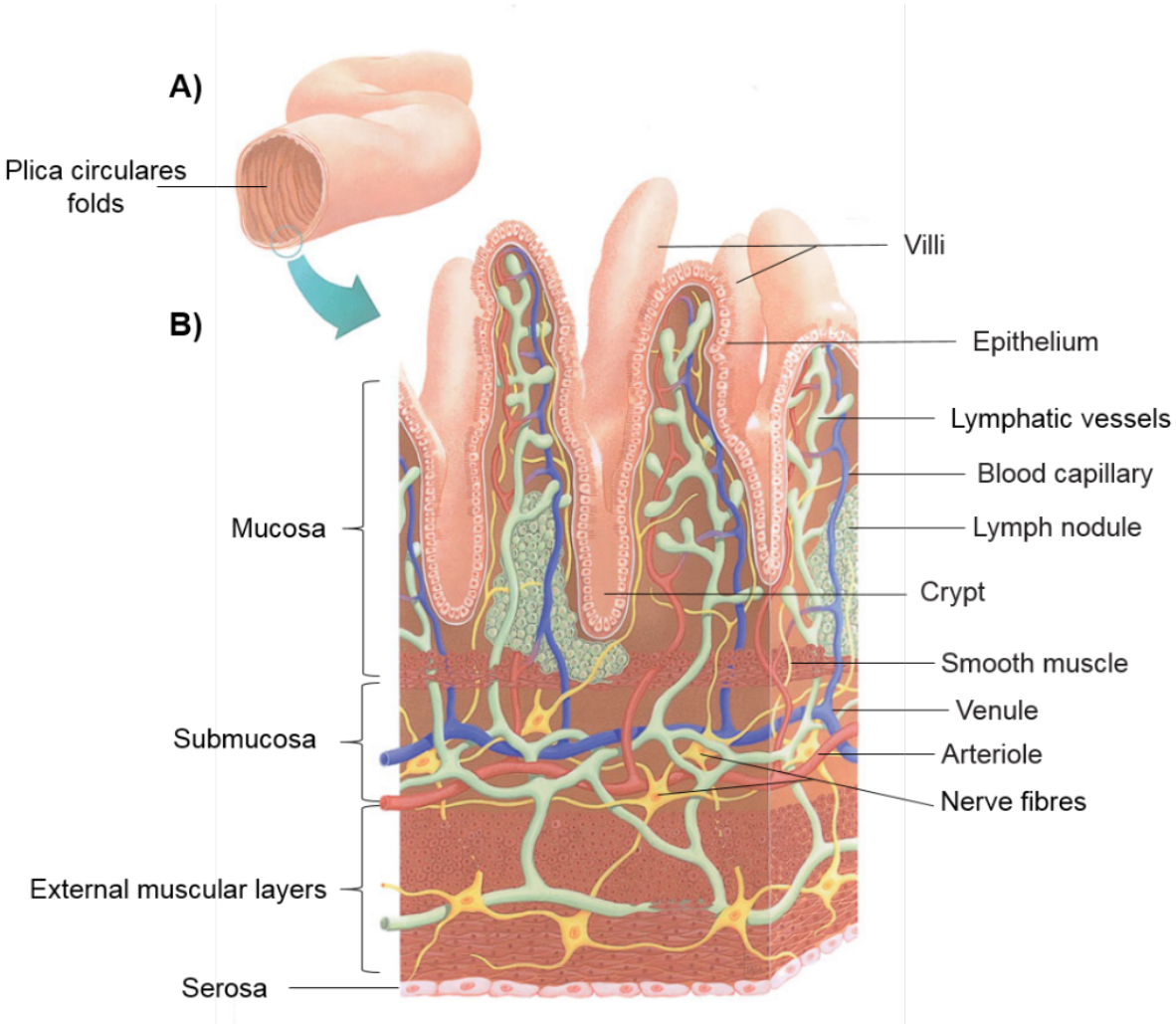

Figure 1.2: Diagram illustrating the cellular organization of the small intestine. **A)** Cross-section of the intestine showing the gross appearance of the luminal surface. **B)** A magnified segment of the small intestine showing the four layers of the small intestine described in the text. This image was modified from Scanlon *et al.*,2014 [1] with permission of F. A. Davis publications.

.

Chapter 1

The intestinal epithelial layer establishes a biological barrier against luminal toxins and microorganisms, which is important for health [2, 12]. The integrity of the intestinal epithelial barrier is maintained by various mechanisms. Initially, the epithelial cells undergo a continuous renewal process that can compensate for damage resulting from the exposure to different substances from the external environment, such as alcohol and drugs [2, 13]. This renewal process is regulated by both intestinal epithelial stem cells (IESCs) and stromal stem cells (Figure 1.3) [2]. Another protective mechanism is provided by goblet cells that secrete mucin proteins. In addition, other molecules such as trefoil factor 3 (TFF3) that can cross-link with mucins to further enhance its protective function (Figure 1.3) [2, 10]. Paneth epithelial cells produce additional AMPs, such as defensin proteins, that can be secreted into the intestinal lumen in response to exposure to viable bacteria or their endotoxins [9]. This function of Paneth cells beside the luminal secretory immunoglobulin A (sIgA), which secreted from the immune cells located beneath the epithelial cells, provide a further protective function against luminal pathogens (Figure 1.3) [2].

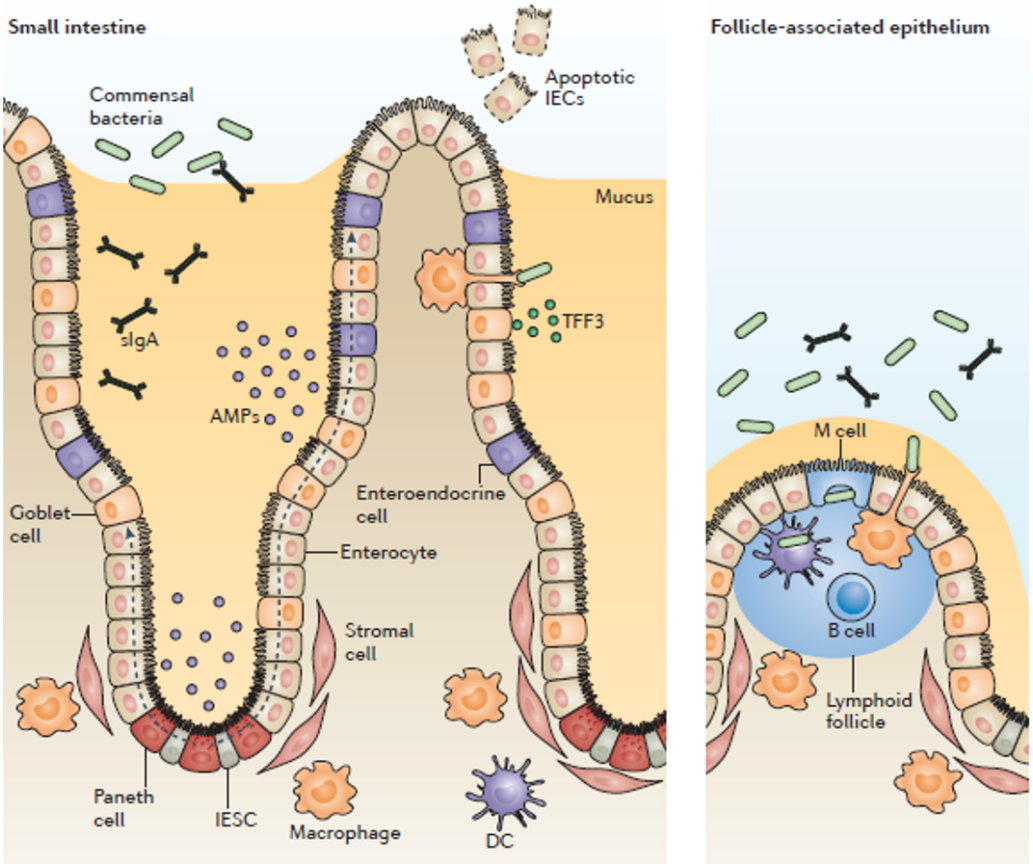

Figure 1.3: Components of the intestinal epithelium. It contains different epithelial cells; enterocytes, enteroendocrine cells, goblet cells and Paneth cells. Microfold cells (M cells) localized in the follicle-associated epithelium that cover the lymphatic follicles that contain immune cells. The intestinal epithelial stem cell (IESC) and stromal stem cells regulate the continuous renewal of the epithelial cell layer. Migration of differentiated epithelial cells occurs from crypt to villus, as indicated by the dashed arrows. Goblet cells and Paneth cells secrete mucus and antimicrobial peptides (AMPs), respectively, which provide protection to the intestinal epithelium. Subepithelial immune cell, such as dendritic cells (DCs) macrophages are responsible for sampling luminal antigens and presenting them to the immune system. This figure was obtained from Peterson *et al*.,2014 [(2)] with permission of Nature publishing group.

1.3. Small intestinal epithelial barrier function

Intestinal epithelial cells are polarized, meaning that they are organized in a way where there are distinct apical and basolateral compartments [14]. This polarized organization is stabilized by different cell-cell contacts on the lateral membranes between adjacent epithelial cells, called junctions [12, 14]. These junctions include gap junctions, desmosomes and the apical junctional complex (AJC) [14, 15]. Gap junctions function as cell-cell channels that allow communication between adjacent cells via the exchange of ions and signalling molecules [15]. Desmosomes are transmembrane adhesive proteins that are linked to intermediate cytoskeletal filaments, which stabilize cell-cell contacts [14]. The AJC is the most apical of these cell-cell contacts, consisting of tight junction (TJ) and adhesion junction structures, which work together to establish a close approximation of adjacent cell membranes at the apical neck of neighbouring epithelial cells [14].

This organisation of intestinal epithelial cells establishes two possible pathways for molecules to pass across polarized small intestinal epithelial cells; transcellularly, through the cell membrane, or paracellularly, between adjacent cells [12] . The TJ is a protein complex that functions to seal and control transport of solutes and ions through the paracellular route [14]. This controlled permeability across the intestinal epithelium that is mediated by the function of the TJ is referred to as barrier function (Figure 1.4) [12].

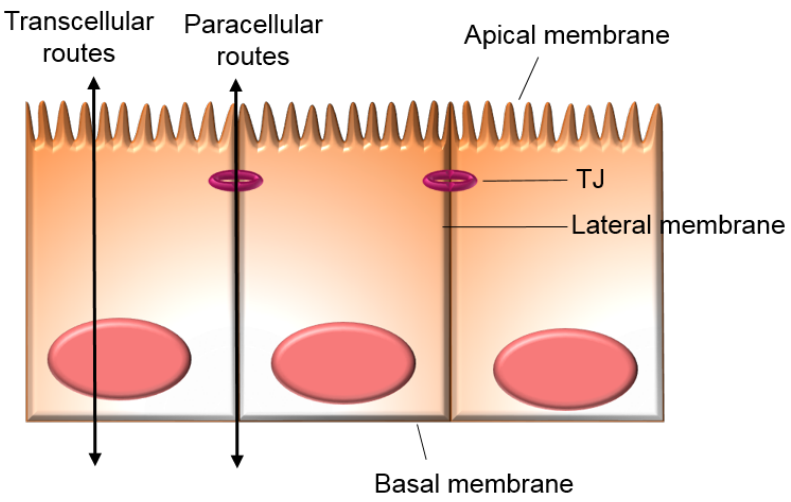

Figure 1.4: Permeability pathways across the intestinal epithelial barrier. Transcellular permeability is mediated by specific transporters. Paracellular permeability is controlled by TJ protein complex.

1.4. Transcellular permeability across the small intestinal epithelial barrier

The transcellular route is primarily restricted by the hydrophobic properties of the lipids that make up the epithelial cell membrane, which allows the passive transport of small, lipophilic molecules [16], but not large hydrophilic molecules, such as therapeutic peptides [5]. Various mechanisms can faciliate the transcellular transport of hydrophilic molecules across the intestinal epithelial barrier [16, 17]. This can occur via transporters that are molecule-specific, such as the Na^+-dependent glucose transporter (SGLT1) that mediates glucose absorption across the small intestinal epithelium [16]. The movement of hydrophilic molecules that are too large to engage transporters that function to absorb nutrients can traverse small intestinal enterocytes via mechanisms involving endocytosis and vesicular trafficking, termed transcytosis. The efficiency of transcytosis for the oral delivery of large hydrophilic molecules, such as therapeutic peptides, is typically very poor. While uptake from the luminal surface via receptor-mediated endocytosis involving clathrin or caveolin or non-selective entry via pinocytosis usually

results in destruction of vesicle contents after intracellular trafficking to lysosomes [16-18].

1.5. TJ components and their role in intestinal epithelial barrier

The way in which the molecular architecture of TJ elements is involved in the regulation of TJ function is still poorly understood. However, remarkable progress has been made towards understanding the ultrastructural arrangement of TJ components. In the early 1960's, TJs were described as a fusion of cell membranes of neighbouring cells that reduces the distance between cells and regulates the diffusion of molecules [19]. A few years later, electron microscopy studies revealed that TJ contains a network of transmembrane strands that were observed to be organized differently within various epithelial tissues [20]. Subsequently, many integral and peripheral membrane proteins were discovered and found to be important in regulating TJ function.

1.5.1. Transmembrane proteins (integral membrane proteins)

1.5.1.1. Claudins

Claudins are ~20 kDa transmembrane proteins that exist in approximately 27 isoforms in the human body [21]. Most claudins have a similar transmembrane tetra-spanning structure with a short N-terminal region, two extracellular loops (ECLs) and a C-terminal tail (Figure 1.5) [22]. The cytoplasmic tail of claudins has a PDZ binding domain to facilitate interactions with TJ scaffolding proteins, primarily to the *zonula occludens* (ZO) protein family, to provide a connection to the actomyosin cytoskeleton [22, 23]. Claudin proteins are able to associate with each other in the same cell membrane (*cis*-interaction) or between adjacent cell membranes (*trans*-interaction) [22, 24]. These interactions could occur between the same claudin isoforms, which is

called homophilic interaction, or between different claudin isoforms, which is called heterophilic interaction (Figure 1.5) [22, 24].

Claudin proteins have different functional properties. Several claudins, so called sealing claudins, have been found to tighten the paracellular barrier, *e.g*. claudin-1, claudin-3 [25, 26]. Pore-forming claudins, *e.g.* claudin-2 and claudin-15, create paracellular channels that allow charge- and size-selective permeability to ions and small molecules [27, 28]. This is supported by the observation that overexpression of pore-forming claudins, *e.g.* claudin-2, a cationic-selective claudin, enhanced the TJ permeability of cations but not macromolecules, such as 4 kDa dextran [27]. Claudin pore charge selectivity is determined by an electrostatic force generated by the presence of charged amino acids on the first extracellular loop (ECL) [29, 30]. The first ECL contains two conserved cysteine residues believed to stabilize the ECL folding by a disulfide bond to position specific amino acids that function in this perm-selective function (Figure 1.5) [30, 31].

Disrupting this disulfide bond has been associated with losing claudin function. This was observed when mutating either of the cysteines in claudin-5, a sealing claudin, reduced the trans-epithelial electrical resistance (TEER) and induced mannitol flux *in vitro* [31]. Moreover, Na^+ flux was significantly reduced by mutating the two conserved cysteine residues in claudin-2, a cation-selective claudin [32]. These studies demonstrate that the first ECL regulates the pore- and charge-selectivity properties of claudins. However, the second ECL was found to play a part in connecting claudins of adjacent cells, or *trans*-interaction. For example, the second ECL has been shown to contribute to the barrier function of claudin-5 [33, 34]. Thus, it has been concluded that both ECLs are necessary for optimum claudin functions.

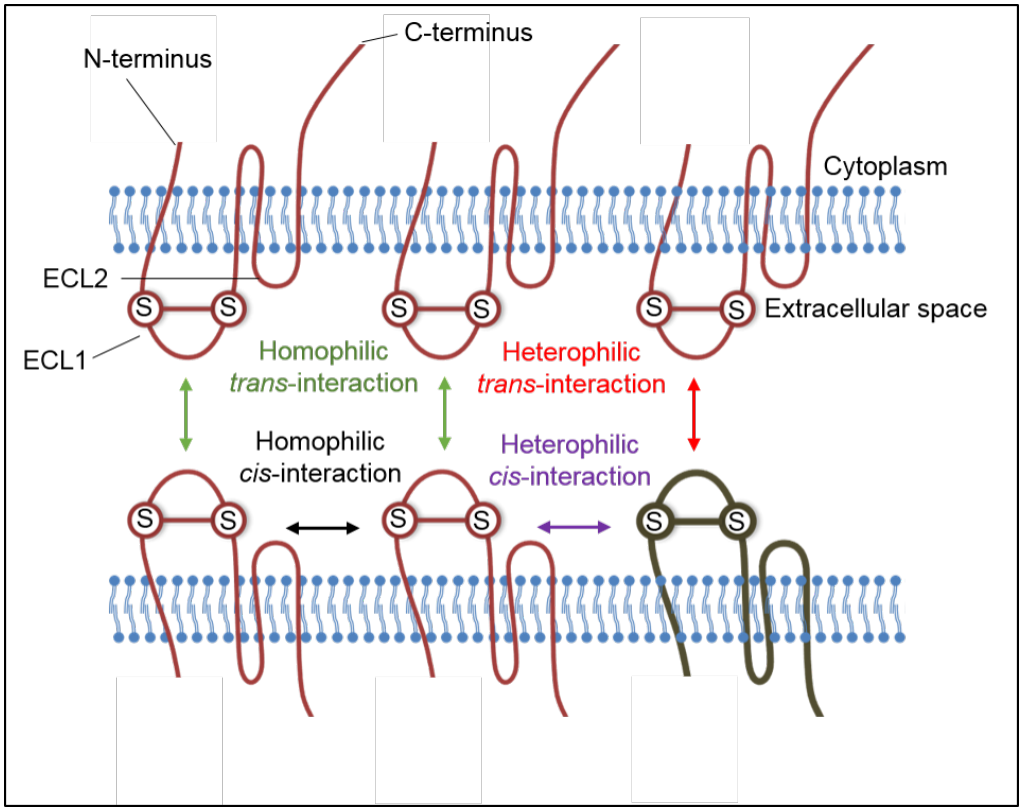

Figure 1.5: Diagram illustrating the structural components of claudin proteins and possible forms of interaction between claudin proteins. As shown, the tetra-span transmembrane structure has a short N-terminus, two extracellular loops (ECL-1, ECL-2) and a C-terminal tail. Homophilic *trans*-interaction and homophilic *cis*-interaction, which are indicated with green and black arrows, respectively, occur between the same claudin isoform. Heterophilic *trans*-interaction and heterophilic *cis*-interaction, which are indicated with red and violet arrows, respectively, occur between different claudin isoforms. S-S is disulfide bridge that stabilizes ECL-1.

Accumulated data has suggested that claudins are critical elements for TJ protein assembly. Initially, expressing either claudin-1 or claudin-2 in mouse fibroblasts that lack of TJs was sufficient to produce TJ-like cell contacts [35]. Furthermore, TJ-associated MARVEL proteins (TAMPs, which include occludin, tricellulin and MARVELD3) were only recruited into TJ in fibroblasts when co-expressed with claudin-1 [35, 36]. This observation might be explained by the *cis*-interactions found between claudin-1 and TAMPs [37]. These studies emphasise the fundamental role of claudin family members in TJ protein assembly but do not suggest an absolute role. Co-expression of TAMPs with claudin-1 in TJ-free human embryonic kidney cells, (HEK)-293, has been shown to modify the morphology of claudin-1 strands to a more physiological shape [37]. Hence, collaboration between claudins and other TJ proteins seems to be essential for their proper, coordinated, function in TJ structure development.

Though the direct role of claudins in TJ macromolecule permeability is still being evaluated [38], many studies have provided strong evidence for the involvement of claudins in macromolecule permeability. An observation derived from intestinal biopsies from patients with early diagnosed Crohn's disease, an intestinal disease characterized by an impairment in epithelial barrier function, has supported the idea that claudins might play an early regulatory role in inducing leaky gut [39], as changes in the expression and distribution of different claudin proteins was detected in patients' samples at an early disease state and before the development of severe epithelial damage [39]. In addition, claudin-1 knock-out mice present with severe defects in the epidermal barrier of the skin, which enhanced the flux of membrane impermeable tracers [26]. Recent studies have shown that a peptide mimicking the ECL-1 of claudin-1 induced a TJ opening to large molecules preferentially by reorganisation of claudin-1 and claudin-5 [40]. Together, this suggests that claudins can regulate TJ macromolecule permeability.

1.5.1.2. TJ-associated MARVEL proteins (TAMPs)

TAMPs contain a MARVEL domain (MAL and related proteins for vesicle trafficking and membrane link), a four-transmembrane helix structure that is essential for their cell membrane localization (Figure 1.6) [41]. TAMPs comprise three proteins: occludin (MARVELD1), tricellulin (MARVELD2) and MARVELD3 [36, 41]. The association of the tetra-spanning structure of the MARVEL domain of all TAMPs generates two ECLs and one cytoplasmic loop [36]. This leaves both the N- and the C-terminal tails of TAMPs in the cytoplasm, where they play roles in both interacting with and recruiting other TJ proteins for TJ barrier function. The growing knowledge about TAMPs suggests that TAMP family members work as partners with overlapped contributions in regulating TJ function [36].

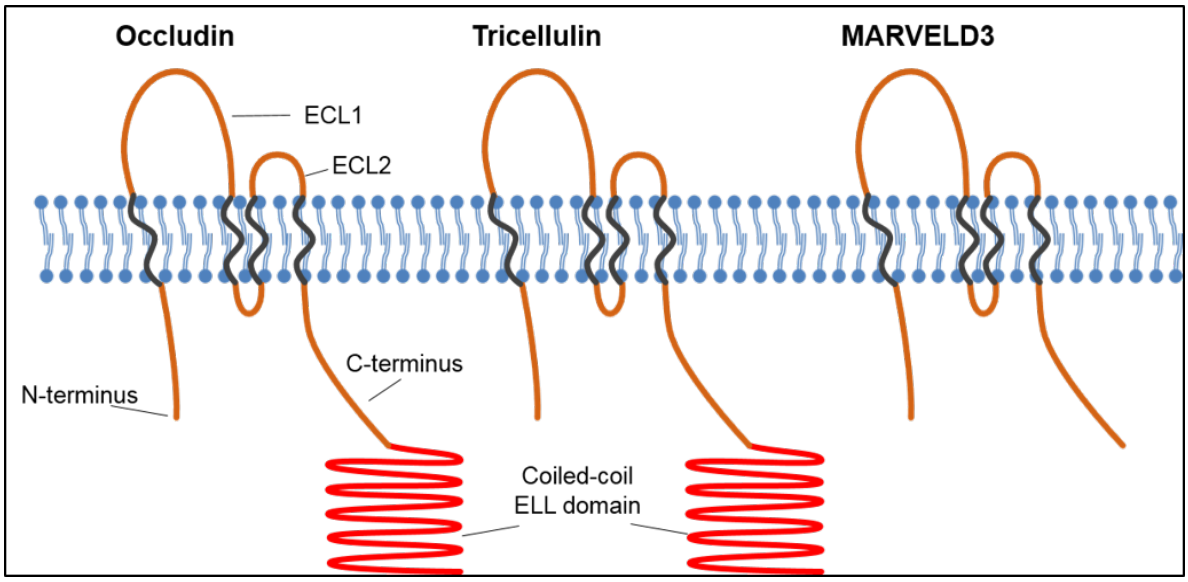

Figure 1.6: Structural similarities between TJ-associated MARVEL proteins (TAMPs); occludin, tricellulin and MARVELD3. All TAMPs contain the MARVEL domain, a four-transmembrane helix structure, highlighted in black. The C-terminal tails of both occludin and tricellulin contain a coiled-coil ELL domain.

Occludin was the first integral protein discovered at the bi-cellular interfaces of epithelial cells [42], and since then many studies have been conducted to define its structural basis that contributes to TJ function. The C-terminal tail of occludin has a coiled-coil structure that shows a similar sequence to the ELL domain of RNA polymerase II elongation factor-ELL (Figure 1.6) [43, 44]. This domain connects occludin to the GUK domain of the ZO-1 scaffolding protein to mediate occludin binding to actin microfilaments [23, 44]. The occludin C-terminus is susceptible to many phosphorylation events, many of which are linked with regulating occludin function [45]. In Caco-2 monolayers, the inhibition of casein kinase 2 (CK2), which mediates phosphorylation of serine 408 (S^{408}) within the C-terminal tail of occludin, stabilized interactions of ZO-1 and claudin-2 with occludin at TJs [46]. This resulted in an increase in the TEER of the monolayers and a reduction in the TJ permeability of ions, reflecting the essential role of occludin, particularly the C-terminal end, in regulating TJ protein function [46]. It has been suggested that both ECLs of occludin are essential for its TJ localization, as the application of synthetic peptides mimicking the ECLs of occludin interferes with TJ localization of occludin [47, 48]. However, the expression of truncated versions of occludin, with either or both ECL1 and ECL2 removed, in MDCK cells has shown that ECL2 alone was able to recruit occludin to TJs [49].

Early studies based on reduced occludin expression argued against the importance of occludin for TJ barrier function, as occludin knock-out mice showed normal TJ morphology and did not demonstrate enhanced intestinal permeability [50, 51]. However, occludin knock-out mice do developed significant and a complex series of multi-organ pathologies [51]. It has been suggested that the non-significant effect on barrier function of occludin knock-out was because other TAMP members compensated for the lack of occludin in the mouse [52]. Supporting this idea is the observation that knockdown of occludin in MDCK cells showed redistribution of tricellulin protein to bi-cellular junctions, a member of the TAMPs family that is normally restricted to tricellular junctions [52]. However, many studies have also suggested a direct role of occludin in regulating barrier function. For example, occludin downregulation has been

suggested as a central cause in inflammatory bowel diseases (IBD)-associated TJ barrier dysfunction [45, 53]. Moreover, occludin knockdown induced leaky TJs with perm-selective profiles showing solutes with a diameter of up to 62 Å being transported [54]. This enhanced transport was associated with increased claudin-4 and claudin-15 expression at the TJs and redistributed tricellulin to bi-cellular interfaces [54]. Thus, claudins might have also contributed to compensating for occludin loss. All together, these findings indicate that the role of occludin is still unclear but it appears to play a critical role in normal events of TJ assembly and barrier function.

Tricellulin was the first TJ-related protein normally restricted to tri-cellular junctions [55]. Similar to occludin, tricellulin possesses the tetra-spanning MARVEL domain required for membrane association [41]. A sequence comparison between occludin and tricellulin has shown strong similarities [36]. The C-terminus of tricellulin has a ELL-domain similar to that of occludin, by which the latter uses to bind ZO-1 (Figure 1.6) [23, 56]. Moreover, it was found that *in vitro* binding of tricellulin to ZO-1 was attenuated by an ELL-domain mutation of tricellulin [56]. Therefore, it has been suggested that tricellulin binds to ZO-1 via the same C-terminal domain as occludin [56]. However, binding to ZO-1 seems to be unnecessary for tricellulin cell membrane association, as tricellulin located at cell contacts in the absence of ZO-1 when co-expressed with claudin-3 in fibroblasts [52]. This does not reflect the ability of tricellulin to self-associate at cell-cell contacts, as claudins can recruit TAMPs to cell contacts [36]. In addition, claudin-3 has a *cis*-connection to tricellulin [37].

Many studies have demonstrated that both tricellulin and occludin functions are closely related. Occludin knockdown in mouse EpH4 epithelial cells alter the distribution of tricellulin to bi-cellular junctions. Moreover, suppressing tricellulin expression in the same cell line increased occludin levels at tricellular contacts [55]. Although the reduction of tricellulin levels was replaced by occludin at tri-cellular locations, this redistribution of occludin to tri-cellular locations failed to provide sealing outcomes at these locations. This was supported by the observation that tricellulin knockdown of EpH4 cells showed

lower TEER compared to a wild-type cells. Moreover, the cells were permeable to large molecules, such as 4 kDa dextran [55]. Consistent with the data obtained in EpH4, overexpression of tricellulin in the low-TEER cell line, MDCK II cells with low endogenous tricellulin expression, reduces the permeability to 4 and 10 kDa dextrans [57]. These findings support the conclusion that tricellulin limits macromolecule permeability at tri-cellular junctions [57]. Like occludin, tricellulin is known to be multiply phosphorylated. However, less is known about the role of phosphorylation in tricellulin function [58]. In studies using a human pancreatic cancer cell line, HPAC, a phosphorylation event was detected in tricellulin in response to depletion of the cellular level of Ca^{2+} that was associated with the redistribution of tricellulin to the cytoplasm. This effect was reversed when the cellular Ca^{2+} was restored [58]. This study suggests that phosphorylation events might play a role in tricellulin membrane integration.

MARVELD3 was subsequently defined as a member of the TAMP family that contains the four transmembrane helixes of the MARVEL domain [36, 59]. Unlike occludin and tricellulin, MARVELD3 has a shorter C-terminus that lacks the coiled-coil component of the C-terminus tail (Figure 1.6). This observation has suggested that MARVELD3 does not bind to ZO-1 [36, 59]. Co-immunoprecipitation studies using Caco-2 cell lysates revealed that MARVELD3 can associate with both occludin and tricellulin [36]. Moreover, fluorescent imaging showed co-localization of MARVELD3 with other TAMP members and ZO-1 at the TJ both *in vitro* and *in vivo* [36]. MARVELD3 knockdown in Caco-2 cells increased the time required for the cells to develop normal TEER [36]. However, no changes were detected in the overall distribution or expression of other TJ proteins [59]. Taken together, MARVELD3 seems to be less essential for TJ assembly, but still contributes to regulating TJ barrier function.

1.5.1.3. Other membrane integral proteins

Blood vessel epicardial substance (BVES) is a tri-spanning transmembrane domain protein defined in various epithelial cells TJs [60, 61]. Pull-down

experiments showed that the C-terminus of BVES interacts with ZO-1 [60]. BVES knockdown in human corneal epithelial HCE cells has been associated with a decrease in the monolayer TEER values and disrupted barrier integrity [60]. Accordingly, an essential role of BVES in TJ assembly has been suggested; however, less is known about the role of BVES in TJ permeability.

Another type of TJ integral membrane protein are those with a single-span transmembrane domain, which include junctional adhesion molecules (JAMs), crumbs homologue 3 (CRB3), and the angulin protein family. A few years after the discovery of occludin as the first integral membrane protein, the JAM family was identified and shown to be concentrated at TJs of both endothelial and epithelial cells [62]. JAMs are part of immunoglobulin superfamily (IgSF), as they contain two extracellular immunoglobulin (Ig)-like domains [62]. The JAM family encompasses three homologous proteins: JAM-A, JAM-B and JAM-C, which are widely distributed in the human body [63]. Additionally, proteins that are structurally related to the JAM family have been identified, such as the Coxsackie and adenovirus receptor (CAR), which has a lesser role in regulating barrier [63]. Depletion of CAR in the mouse intestine does not interfere with epithelial integrity [63]. While the length of the cytoplasmic C-terminus of all JAMs and their related proteins varies, all bind to the PDZ domain of the ZO-1 scaffolding protein [64]. It is been suggested that the JAM family has a role in regulating barrier function, since JAM-A -deficient mice have shown a deficiency in the intestinal barrier function that was permeable to 4 kDa dextran [65]. JAM proteins are also expressed in the circulating leukocytes [66, 67]. Therefore, they have been linked with the trans-epithelial and endothelial migration of leukocytes and the induction of various mucosal inflammations [63, 65]. These data support the role of JAM in regulating paracellular permeability. However, JAM proteins do not seem to have an essential role in the assembly of TJ proteins, since overexpression of JAMs in fibroblasts failed to reconstitute TJ strand-like structures [68]. This data suggests that JAM proteins are recruited to cell-cell contacts by other TJ proteins.

The CRB3 protein is the mammalian homologue of the *Drosophila* transmembrane protein Crumbs, a protein that is expressed in the marginal zone of invertebrate epithelial cells and is essential for cell polarity [69]. CRB3 was found to be associated with the TJs *in vitro* in both Caco-2 and MDCK cells and in many organs *in vivo* [70, 71]. It is been reported that the CRB3 intracellular C-terminus forms complexes with different scaffolding proteins, *e.g.* protein associated to TJ (PATJ) and protein associated with Lin-7 (PALS1), that play roles in TJ development [70, 71]. Modulating the expression of these proteins has shown some disorganization of TJ proteins without disrupting overall TJ integrity [70, 71]. Although less is known about the role of CRB3 in regulating TJ permeability, these findings suggest that CRB3 does not seem to be a critical player in determining TJ permeability compared to other TJ transmembrane proteins.

The angulin protein family consists of three proteins: lipolysis-stimulated lipoprotein receptor (LSR/ angulin 1), immunoglobulin-like domain-containing receptor 1 (ILDR 1/ angulin 2) and ILDR 2 (angulin 3) [72, 73]. All angulin proteins have closely related structures, and all possess an extracellular immunoglobulin-like domain [72, 73]. The angulin family along with tricellulin have been known to be the protein components of the tricellular junctions [55, 72, 73]. Studies in mice showed that angulin protein expression varies within tissues; however, at least one protein of the angulin family was found in each epithelial tissue [73]. Angulin-1 knockdown in EpH4 cells was associated with tricellulin redistribution [72]. This observation led to the demonstration that the C-termini of angulin proteins bind to tricellulin [72, 73]. Downregulation of angulin-1 in EpH4 reduced the monolayer TEER and increased permeability of 40 kDa dextran [73]. Despite the small surface of the tricellular junctions compared to that of the bi-cellular junctions, the function revealed for angulin proteins and tricellulin shows how essential tricellular proteins are to maintaining the epithelial barrier integrity.

1.5.2. Cytosolic scaffolding proteins

A network of cytoplasmic proteins is located peripherally to TJ proteins. These scaffolding proteins generally bind to each other and connect transcellular proteins to the cell's cytoskeleton [74]. ZO-1, was the first TJ protein to be discovered in both epithelial and endothelial cells [75]. ZO-2 and ZO-3 are two proteins that are structurally related to ZO-1 that were found to bind to ZO-1 [76, 77]. Among all TJ scaffolding proteins, the ZO protein family is believed to be a central component within the TJ scaffolding network, mediating TJ transmembrane proteins binding to the cytoskeleton [23]. The N-terminus of all members of the ZO protein family members contains three protein binding domains: three PDZ domains (postsynaptic density 95/discs large/zona occludens-1), Src homology 3 domain (SH3) and an apparently inactive guanylate kinase homology domain (GUK) where the TJ proteins associate with ZO proteins (Figure 1.7) [78]. The C-terminal ends of ZO proteins vary in length; however, they are all associated with the F-actin cytoskeleton either directly through an actin-binding region (ABR), such as ZO-1 and ZO-2, or indirectly via other scaffolding proteins such as cortactin and cingulin, such as ZO-3 [79]. Many other TJ scaffolding proteins have been identified, such as membrane-associated guanylated kinase inverted proteins (MAGI), the multi-PDZ domain proteins (MUPP1), and cingulin proteins; all have similarities in their protein binding domains to the ZO protein family [23]. These proteins were found to play a supportive role to the ZO protein family in TJ assembly; but specific functions of these proteins have not been fully defined [23].

Single knock-out or knockdown studies of scaffolding proteins have produced various outcomes. ZO-3 deficiency in mice and in the F9 teratocarcinoma cell line have shown normal overall TJ structure and epithelial appearance [80]. Similarly, mice lacking of cingulin show no significant effect on TJ assembly or barrier function [81]. These findings might suggest that either some scaffolding proteins are not essential for TJ formation or that the presence of many other scaffolding proteins can compensate for any protein

loss. For example, ZO-3-deficient mice have increased ZO-2 localization in their TJs [80]. On the other hand, ZO-1 and ZO-2 are known to have a vital role in TJ assembly and barrier function. *In vivo*, lethality was observed in mice embryos lacking either ZO-1 or ZO-2.[82, 83] Consistently, ZO-1 knockdown was shown to weaken the barrier function for macromolecule permeability in both MDCK and EpH4 epithelial cells [84, 85].

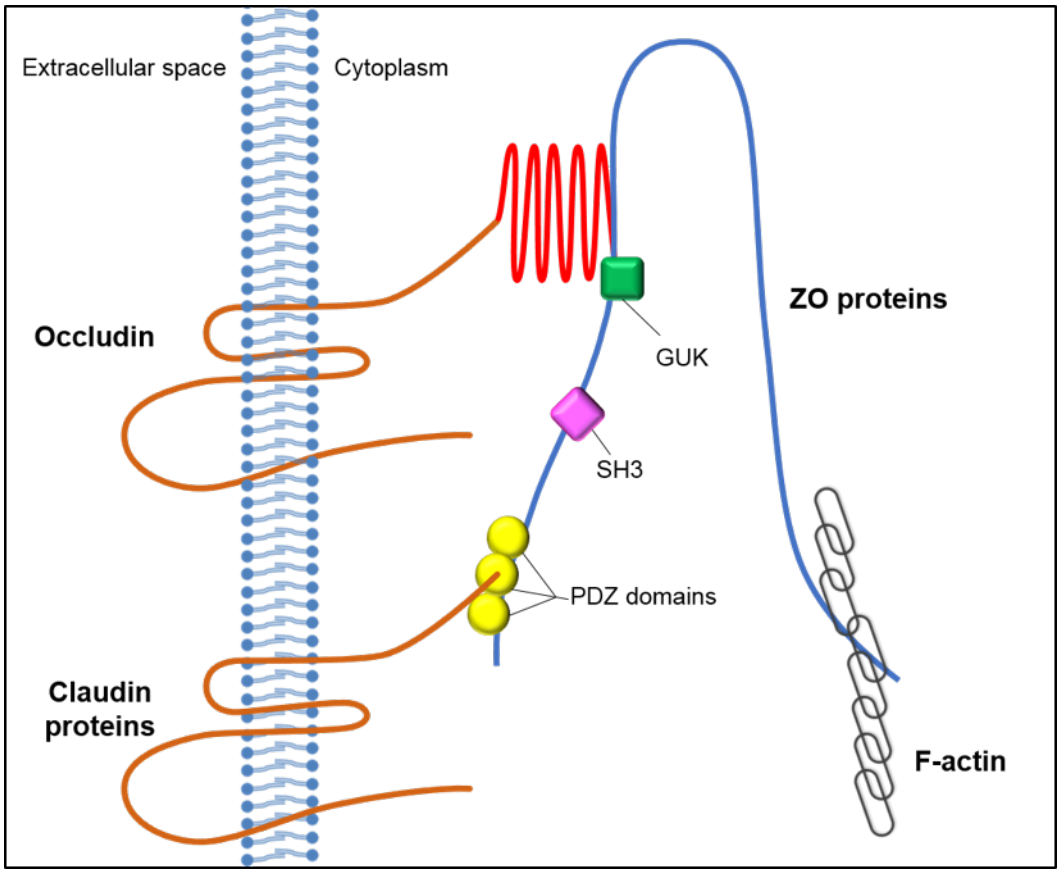

Figure 1.7: Schematic representation of cytoplasmic *zonula occludens* (ZO) scaffolding proteins showing their binding domains to TJ membrane integral proteins, such as occludin and claudins. The N-terminus of ZO proteins contains three protein binding domains: three PDZ domains (postsynaptic density 95/discs large/zona occludens-1), Src homology 3 domain (SH3) and a guanylate kinase homology domain (GUK). The C-terminus of ZO proteins is connected to F-actin.

1.5.3. Cytoskeletal elements

A direct association between perijunctional actomyosin filaments and the junctional protein complexes has been revealed with the aid of electron microscopy [86]. Since then, more efforts have been devoted to understanding the influence of the cytoskeleton on TJ structure and function. Disruption of actin filaments is associated with occludin internalization and loss of barrier function [87], an observation that has suggested the potential role of the perijunctional actin filaments in providing stability to TJ structures. In addition, a mechanism mediating actomyosin filaments contraction, triggered by increasing myosin light chain phosphorylation at serine 19 (MLC-pS^{19}) via MLC kinase (MLCK) (Figure 1.8), was found to play a key role in inducing TJ permeability in response to various physiological and pathological stimuli [53, 88]. The MLCK-dependent alteration of TJ permeability was linked to changes in the distribution of selected TJ proteins that occurred secondarily to the induction of MLC-pS^{19} [53, 89]. This function of MLCK is reversed by the action of MLC phosphatase (MLCP) [90, 91] (Figure 1.8). In addition, endogenous inhibition of MLCP by a specific protein inhibitor called C-kinase potentiated protein phosphatase-1 inhibitor-17 kDa (CPI-17) was found to increase MLC-pS^{19} levels and enhance TJ permeability [92]. Overall, these studies suggest that the perijunctional cytoskeleton is essential for regulation of TJ barrier function.

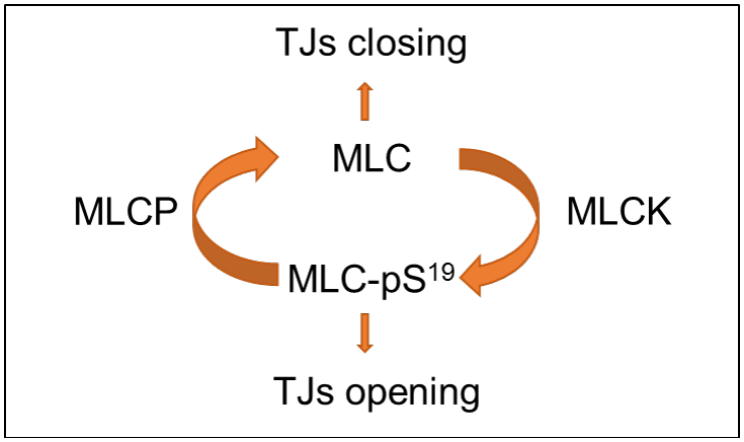

Figure 1.8: Schematic representation of the endogenous mechanism that regulates TJ permeability through alteration of myosin light chain (MLC) phosphorylation status. MLC kinase (MLCK) increases MLC phosphorylation at serine 19 (MLC-pS^{19}) that enhances TJ permeability. This process is reversed by MLC phosphatase (MLCP).

1.6. Protein remodelling associated with intestinal TJ permeability

As described above, many proteins have been discovered as components of endothelial and epithelial TJs. The expression of these proteins varies between different tissue barriers, helping to define their distinct profiles of paracellular permeability. In the intestinal epithelia, several intracellular mechanisms could trigger the dynamic modulation of TJ proteins that either promotes regulated permeability or induces barrier dysfunction, outcomes associated with physiological and pathological TJ permeability, respectively. This section will review the current knowledge of TJ protein modulation associated with paracellular permeability in the intestine.

1.6.1. Nutrients regulating TJ permeability

Over the years, studies have improved our understanding of how nutrients alter TJ permeability. Initially, it was reported that high luminal sugar content transiently enhanced the TJ permeability of small hydrophilic molecules [93]. This phenomenon appears to function as a physiological strategy to alter TJ permeability, which could transiently increase nutrient uptake by providing a secondary uptake route through the paracellular space. Examination of this hypothesis led to the discovery that MLCK was activated as a consequence of increased Na^+-glucose co-transport; events that led to increased glucose-mediated TJ permeability [88]. Freeze-fracture electron microscopy of TJ during glucose-mediated TJ permeability showed dilations in TJ structures lacking the ZO-1 protein without affecting the total ZO-1 cellular levels [94]. As ZO-1 is a central scaffolding element holding transmembrane proteins at TJs, this finding suggested that the reduction of ZO-1 linked to the TJs might be responsible for inducing TJ permeability during the activation of Na^+-glucose. An analysis of fluorescence recovery after photobleaching (FRAP) in Caco-2 cells that stably express fluorescent TJ proteins has defined the kinetic behaviour of TJ proteins associated with active Na^+-glucose cotransport [95]. ZO-1 assembly at TJs reduced during Na^+-glucose co-transport activity, an effect reversed by MLCK inhibition that stabilized ZO-1 at TJs [95]. No

significant changes were observed on other TJ proteins, such as claudin-1, occludin and actin [95]. This reorganization required the ZO-1 ABR domain that is involved in binding to actin cytoskeleton [95]. Moreover, expression of the ABR domain in Caco-2 cells disrupted the function of ZO-1 and prevented MLCK-mediated barrier regulation [45, 95].

Other diet-derived substances that are found in low concentrations in the diet, such as the medium chain fatty acid, capric acid, are well known to induce TJ permeability via intracellular pathways [96]. Hence, sodium caprate, in millimolar concentrations, has been used as a permeability enhancer of poorly absorbed drugs. This will be discussed in great detail in another section. Dietary minerals such as Zn^{2+}, a trace element, have been reported to be essential for maintaining TJ barrier integrity. Thereby, Zn^{2+} depletion was found to play a causative role in the development of IBD *in vivo* [97]. This was investigated in detail *in vitro* using Caco-2 cell monolayers grown in medium lacking Zn^{2+}; TEER was reduced and paracellular permeability was enhanced [98]. This effect was shown to be due to downregulation of occludin and ZO-1 levels at TJs that induced a leaky epithelium permeable to neutrophils, which induced inflammation and subsequently damaged the epithelium [98]. In contrast to Zn^{2+} reduction in the outer environment, minimizing intracellular Zn^{2+} in both Caco-2 cells and mouse colon by using cell-permeable Zn^{2+} chelator resulted in TJ barrier deficiency but with different changes to TJ protein composition [99]. Reducing the intracellular Zn^{2+} was associated with depletion in the cellular levels of occludin and claudin-3, a sealing claudin, with no effect on ZO-1. Although both extracellular and intracellular Zn^{2+} depletion was associated with a leaky epithelium, Zn^{2+} supplementation induced barrier function in *in vitro* models and reduced colitis-associated colon damage in mice [97, 98].

1.6.2. Intestinal disorder-induced TJ barrier dysfunction

The intestinal lumen contains a variety of microbial colonies that play an essential role in gut physiology, *e.g.,* in improving digestion [100]. Nevertheless, this microbial community also produces toxins that could cause serious problems when translocated into the blood circulation. Thus, gut epithelia with sealed TJs perform a critical task in preventing the passage of luminal pathogens into mucosal tissues while permitting selective permeability of other substances, such as nutrients [45]. Under certain conditions, toxins and pathogens from the lumen could leak through the epithelial TJs leading to the induction of local tissue inflammation that subsequently could lead to systemic complications [101]. This phenomenon is associated with intestinal inflammatory diseases such as Crohn's disease and ulcerative colitis, which together are called IBD and characterized by leaky intestinal epithelia [45].

1.6.2.1. TJ permeability associated with inflammatory mediators

Accumulated evidence from both *in vivo* and *in vitro* studies have refined the role of the molecular remodelling of TJ proteins in determining TJ permeability behaviour in response to different cytokines during IBD. Similar to the physiological TJ opening mentioned above, MLCK activation was reported to be an essential process for the induction of IBD-associated TJ permeability [53, 102]. This barrier defect was shown to be reversed by inhibiting MLCK [53, 103]. Intracellular signalling induced by TNF-α and INF-γ, defined as the main inflammatory mediators of TJ barrier defects in Crohn's disease, can activate MLCK, which in turn induces occludin endocytosis leading to changes in the TJ protein complex sufficient to enhance macromolecule permeability [45, 53, 54]. This so called leaky pathway has been detailed through a series of *in vitro* studies that have suggested that the time of exposure to pro-inflammatory cytokines is a critical factor defining the changes to TJ protein complexes. Short (~ 4 h) exposure to TNF-α and INF-γ was enough to induce only occludin endocytosis that resulted in enhanced TJ permeability to molecules with a diameter of up to ~60 Å, in a non-charge selective manner [53, 54, 103].

Treating Caco-2 monolayers with TNF-α and INF-γ for ~ 48 h up-regulated claudin-2 and down-regulated claudin-4 at TJs, claudins demonstrated to enhance TJ permeability and sealing, respectively [104]. Accordingly, it has been concluded that these changes to claudin proteins might play a role in disrupting the epithelial barrier function in IBD [104]. However, less is known about whether these changes to claudin proteins in response to long exposure to TNF-α and INF-γ have an influence on TJ permeability profiles in terms of size and charge compared to a shorter exposure.

Unlike the type of barrier defect mediated by TNF-α and INF-γ, interleukin-13 (IL-13), a cytokine associated with ulcerative colitis, reduces TEER with no effect on macromolecule permeability [102, 105]. This was accompanied by increasing claudin-2 expression at TJs, resulting in increased charge-selective permeability to cations [102]. Although the intracellular signalling pathway(s) responsible for reorganizing TJ protein complexes is presumed to be different in each of these cases, these studies have demonstrated that TJ protein remodelling is critical for determining TJ permeability behaviour.

1.6.2.2. Life style factors mediate TJ reorganization

Several studies in the literature have established a role of life style-related factors, such as alcohol consumption and stress, in inducing TJ protein reorganization and the enhancement of luminal endotoxin permeability. Chronic alcohol consumption was found to enhance the translocation of endotoxins into blood circulation, which was linked to alcoholic liver disease [106]. Studies investigating the mechanism of action of ethanol and its metabolite, acetaldehyde, have shown that they induce TJ permeability through the reorganization of occludin and ZO1 [107]. Treating Caco-2 cell monolayers with acetaldehyde reduced TEER and enhanced the TJ permeability to macromolecules, FITC-inulin (~11 Å) [107]; both changes in TJ structures and altered interactions between occludin and ZO-1 were observed [107, 108]. A recent *in vivo* study provided evidence for TNF-α involvement and

MLCK activation in generating TJ leakage associated with chronic alcohol consumption [109], a similar scenario to leaky TJs associated with IBD. However, changes in TJ protein complexes produced by alcohol are distinct from those occurring with IBD. These studies suggested that similar cellular signalling pathways could induce macromolecule permeability by developing TJ complexes with distinctive features.

Psychological stress was reported to increase the level of endotoxin permeability to the blood stream that could result in disease initiation or progression [110]. Both physiological and pathological stimuli were found to play a role in stress induced TJ permeability. Under acute stressful conditions, the body requires a higher level of energy. Therefore, a wide array of stress-related signalling hormones, *e.g.* glucocorticoids, are released in different organs to provide and maintain energy supplies, nutrients and minerals, by reducing wastage and increasing absorption [110]. In this case, the intestine responds by activating the epithelial Na^+-glucose pathway, a physiological pathway, which enhances TJ permeability, a transient event that ends by removing the cause of stress [88, 110]. Mechanistic studies using HT-29 cell monolayers and mice showed that chronic stress-induced TJ permeability is associated with up reglation of claudin-2, which was mediated by overexpression of the endotoxin-sensitive protein toll-like receptor-4 (TLR-4) [111]. Furthermore, it was found that the TLR-4 activation resulted in the activation of the NF-κB pathway, which is involved in production of various cytokines, and is also correlated with stress-induced barrier dysfunction involving increased claudin-2 expression [111]. Therefore, it is been suggested that cytokine production is involved in chronic stress-induced TJ protein reorganization [110].

1.6.3. Studies clarifying the dynamic organization of TJ proteins

The knowledge that is currently available about TJ dynamic remodelling was not fully realized by only studying TJ regulation induced by naturally existing mechanisms, *e.g.,* physiological and pathological pathways. Monitoring the influence of artificial techniques on the regulation of TJ function has also contributed to a better understanding of TJ organization. These techniques can be categorized into two main groups: synthetic tools that can be used to target specific TJ proteins, such as synthetic peptidomimetics and RNA interference techniques, and the application of permeability enhancers primarily used to improve the permeability of drugs across the TJ barrier, which occurs through the reorganization of TJ proteins. This part will focus on summarizing studies involving peptidomimetics and permeability enhancers that induce transient modulation of TJ proteins.

1.6.3.1. Peptides targeting TJ proteins.

In polarized epithelial cells, TJ integral membrane proteins establish extracellular associations with neighbouring cells that regulate paracellular permeability. Amongst the known TJ integral membrane proteins, claudins and occludin have a fundamental role in generating these interacting complexes that regulate TJ barrier properties. Structural studies of claudins and occludin have revealed that both ECLs are important determinants of the function of these proteins at TJs. Peptides designed to emulate the ECLs of claudins and occludin have been used to define the role of these protein domains in modulating TJ protein assembly. Such a strategy has not only contributed valuable knowledge on the organization of TJ structure and function, but has also provided promising tools to enhance drug permeability.

Several studies have concluded that the ECL2 of occludin is essential for its TJ recruitment [47, 49, 112]. Application of 18-mer peptide mimicking residues 210-228 of the ECL2 of occludin on human intestinal epithelial T84 cell

monolayers, prevented TJ barrier re-establishment on T84 cells after Ca^{2+} repletion [112]. This was suggested to occur by disrupting the organization of claudin-1, occludin and JAM-A in forming TJ structures [112]. Consistent with this, a study investigating the role of claudin-1 ECLs in determining TJ function has shown that a 27-mer peptide related to residues 53-80 of claudin-1 ECL1 reduced barrier function and increased macromolecule permeability in both T84 cell monolayers and in rats *in vivo* [113]. This was accompanied by the rearrangement of claudin-1, occludin, JAM-A, and ZO-1 proteins. Although several studies performed on different epithelial barriers, have reported that disruption of claudin-1 or occludin can induce distinct changes to TJ protein complexes associated with TJ barrier dysfunction, both peptides, which target ECL-1 and ECL-2 of claudin-1 and occludin, respectively, have been shown to induce similar modulations to TJ proteins in intestinal epithelia [112, 113]. This might suggest that in intestinal epithelia, claudin-1, a sealing claudin, and occludin have a communication by which they regulate TJ permeability when exposed to an external stimulus targeting their extracellular domains. Therefore, claudin-1 and occludin might be considered markers to monitor intestinal epithelial TJ permeability function.

Another example of peptides modulating TJ barrier function is a peptide-related to claudin-1 ECL-1 residues 53-81, similar to the previously mentioned peptide mimicking ECL-1 of claudin-1, but Cys54 and Cys64 mutated to serine residues, called C1C2 peptide [114]. This peptide was designed to enhance the permeability of hydrophilic drugs across tissue barriers by modulating claudin-1 sealing properties at the TJs [114]. The C1C2 peptide was first tested for its capacity to enhance the permeability of nerve fibres towards analgesics within the peripheral nervous system that are surrounded by the perineurium barrier. Within 2 days of pre-treatment of C1C2, claudin-1 levels were reduced in the inner perineurium layer of rats sciatic nerve, and accordingly, an enhancement in the effect of membrane-impermeable analgesics was achieved, indicating an increase in the analgesics permeability [114].

A further study to confirm the mode of action of the C1C2 peptide was performed in different epithelial and endothelial cell monolayers, including the following: Caco-2, MDCK-II and primary mouse microvascular endothelial cells (pMBMECs). These cell lines have distinct barrier properties due to their different claudin expression patterns. This study has revealed consistent changes in TJ protein complexes that mediate a reversible reduction of TEER and the enhancement of macromolecule permeability 4- 6 h after treating these monolayers with the C1C2 peptide [40]. Immunofluorescent staining has shown that the permeability enhancement induced by C1C2 peptide was associated with the redistribution of claudin-1, claudin-2, claudin-3, claudin-4, claudin-5 and occludin in both MDCK-II and Caco-2 monolayers and claudin-3, claudin-5 and occludin in pMBMECs monolayers [40]. An observation suggested a direct disruption of TJ proteins by the C1C2 peptide [40, 114]. However, investigating the direct interference of C1C2 peptide upon the distribution of different claudins using HEK-293 cells transfected with one claudin at a time revealed that the C1C2 peptide only disrupted claudin-1- and claudin-5-based TJs [40]. This finding suggested that the C1C2-induced modulation of TJ proteins, apart from claudin-1 and claudin-5, might be mediated by a heterophilic *trans*- or *cis*-interaction with claudin-1 and claudin-5 [40].

Exposure to a peptide related to claudin-2 ECL1 called C2C2 for 24 h neither altered TJ protein distribution nor affected TJ barrier function in all cell culture models studies [40, 114]. This was particularly surprising for the intestinal epithelial cell model, Caco-2, since many studies have shown that interference with claudin-2 changes the TJ barrier function in the intestine [28, 115]. Moreover, TJ barrier dysfunction associated with some intestinal diseases has been linked with modifying claudin-2 expression [104]. This might suggest that unlike claudin-1 and claudin-5, which have sealing functions, claudin-2-mediated TJ permeability is more strongly regulated by intracellular signalling.

1.6.3.2. Permeability enhancers inducing TJ permeability

Oral delivery of protein and peptide therapeutics is limited by the intestinal epithelial barrier [5]. Therefore, many delivery strategies, *e.g.,* mucoadhesives and nanoparticles, have been examined for their ability to enable oral delivery of these biopharmaceuticals [116]. Over ~ 250 permeability enhancers (PEs) have been used to improve drug permeability across intestinal epithelia either transcellularly via enhancing the drugs diffusion through the plasma membrane or paracellularly by modulating TJ proteins [5]. In general, a number of these PEs for delivering biopharmaceutics have been shown to be safe, although their capacity to enhance their uptake has been less than efficacious or inconsistent [5, 96].

Sodium caprate is an example of a well-studied PE that exists in dietary products, *e.g.,* milk, and is one of the most promising PEs for enhancing oral drug delivery [5, 117]. The mechanism of action by which sodium caprate modulates intestinal epithelial TJ proteins and enhances permeability has been investigated in different tissue barrier models. In each model, sodium caprate was shown to induce different modifications to TJ proteins that enhanced permeability [118]. These changes in TJ modulation have been suggested to be due to differences in TJ protein composition between tissue barriers [119].

Many reports have agreed on the role of cytoskeleton contraction mediated by MLCK as a primary cause of paracellular permeability induced by sodium caprate in Caco-2 cells [96, 120-122]. Treating Caco-2 cells with 10 mM of sodium caprate induced a rapid, time-dependent reduction of TEER and induction of large molecule permeability, up to 10 kDa dextran [121, 122]. A study reported that changes to TJ protein organization was only observed after extended exposure times to sodium caprate of > 60 min [121]. Exposure to 10 mM of sodium caprate for 60 min reduced ZO-1 and occludin abundance at TJs in Caco-2 cell monolayers [121]. Studies have shown that MLCK activation is

correlated with rapid changes to ZO-1 cell distribution [94, 95]. Moreover, extended activation times for MLCK result in a constant effect on ZO-1 that could induce multiple changes to TJ proteins and TJ barrier function [54, 95]. This might be the case with a long exposure to sodium caprate, as long-lasting activation of MLCK reorganized ZO-1 and occludin to form larger pores that were responsible for dramatic changes of permeability profile at the beginning and after a long exposure to sodium caprate.

A brief sodium caprate exposure (~ 30 min) to enhance TJ permeability was associated with the activation of cytoskeleton contraction and claudin-1 displacement from TJs [122]. Monolayers of the human colon cell line, HT-29/B6, have a higher TEER value than Caco-2 cells; exposure of HT-29/B6 monolayers to ≥ 10 mM sodium caprate induced a similar time-dependent reduction profile of TEER reduction and TJ permeability [118]. Immunofluorescent microscopy studies demonstrated tricellulin and claudin-5 redistribution from tri-cellular and bi-cellular TJs after ~ 30 min, with no effect on other TJ proteins [118]. None of these responses involved the activation of MLCK as observed in Caco-2 cell monolayers, suggesting a direct interference with tricellulin and claudin-5 [118]. Comparison of findings obtained with HT-29/B6 cells Caco-2 cells, regardless of variations between their barrier properties, suggest that the fast onset of TJ permeability induced by sodium caprate in intestinal epithelia involves regulation of claudins and tricellulin. This observation may reflect structure/function features of the TJ that enable their rapid dissociation from the plasma membrane. For example, claudins are palmitoylated proteins, a post-translational modification found to facilitate certain aspects of membrane trafficking [123].

1.7. Therapeutic peptides and issues that hinder their oral delivery

Since the discovery of human insulin as the first therapeutic peptide for the treatment of diabetes, production of therapeutic proteins and peptides has increased over the years to represent currently ~ 10 % of all the

pharmaceutical products in the global market, a figure which is also expected to increase in the future [117, 124]. This is because proteins, in general, can control specific functions in the human body mediated via discrete membrane receptors that generate selective cell signalling process [125]. Among all the marketed peptides, which are mostly delivered by parenteral routes, only a few can be delivered by the oral route (Table.1) [5, 117]. Developing oral peptide formulations has been an ongoing target for the pharmaceutical industry for many reasons [5, 117]. Oral peptide formulations might enhance patient compliance to treatment, as patients prefer oral administration of drugs over injection [5, 117]. Moreover, oral administration of peptides would reduce the cost associated with the production and application of injectable dosage forms, which include sterilization, needle disposal and staff/patient training in some instances [5]. In addition, oral delivery for some therapeutic peptides can mimic their physiological release in the body. For example, insulin uptake from the intestine results in direct hepatic delivery via the portal vein, which mimics its natural release from the pancreas which also goes directly to the liver [5].

Table 1.1: Commercially available oral therapeutic peptides [5, 117].

Peptide drug	MW (Da)	Applications
Cyclosporine	1202	Immunosuppressant
Desmopressin	1069	Diabetes Insipidus
Taltirelin	477	Spinocerebellar degeneration
Glutathione	307	Acquired immune deficiency syndrome (AIDS)-related cachexia/ cystic fibrosis
Linaclotide	1526	Irritable bowel syndrome
Vancomycin	1449	Pseudomembranous colitis
Colistin	1155	Multi drug resistant bacterial infections
Tyrothricin	1228	Pharyngitis.

MW: molecular weight

There are many challenges to oral delivery of peptide therapeutics. First of all, these drugs are water soluble and too large to readily transport across the intestinal epithelial cells [5]. Moreover, peptide therapeutics are typically susceptible to degradation by GI tract digestive enzymes including the gastric enzyme pepsin and intestinal enzymes secreted by the pancreas or enterocytes, such as trypsin and chymotrypsin [5, 126]. In addition, drug absorption in the intestine, generally, requires its complete dissolution and solubility that can be pH-dependent [5]. This could be an issue for some peptide drugs, such insulin, which has better solubility in mild acidic medium than the neutral medium of the intestine [5]. However, most of these problems can be solved with the aid of existing pharmaceutical technologies. For example, the stability of peptide drugs in the GI tract can be improved by enteric coating or an oral dosage form and/or application of drug excipients, such as protease inhibitors, while solubility of insulin can be enhanced by acidifying agents [5, 117]. This leaves poor permeability across the intestinal epithelial barrier as the main challenge for the oral delivery of peptide therapeutics [5, 117].

Chapter 1

1.8. Aims of this project

This project represents an extension to previous work aimed at developing a novel strategy to enhance the oral permeability of therapeutic peptides across the TJ of intestinal epithelial cells by manipulating an endogenous pathway. This strategy involved examining the ability of rationally designed membrane permeant peptide inhibitors of MLCP, PIP peptides, to alter the activity of MLCP resulting in a transient induction of MLC-pS^{19} that could enhance the permeability of therapeutic peptides through TJ structures. Previous work on PIP peptides has suggested that these peptides can enhance TJ permeability by enhancing MLC-pS^{19}, as anticipated [*127*]. However, much less was known about how these peptides alter the activity of MLCP or how their effect was associated with TJ structure. The current project focused on improving our understanding of the mechanism of action (MoA) of one of the lead PIP peptides: PIP 640 peptide.

Specific aims of the current project:

- Validate and optimize the permeability enhancement function of PIP 640 peptide and evaluate its safety *in vitro.*

- Characterize the biochemical changes associated with TJ proteins induced by the actions of the PIP 640 peptide *in vitro*.

- Investigate different aspects of the PIP 640 peptide-induced permeability enhancement *in vivo.*

Chapter 2 : Materials and methods

Chapter 2

2.1. Reagents and materials

Solvents and reagents for peptide synthesis and characterisation were purchased from Novabiochem, Sigma-Aldrich, and Rathburn Chemicals. Reagents and materials for cell biology studies were purchased from Sigma-Aldrich, Fisher Scientific, Invitrogen, Phoenix Pharmaceuticals, Novabiochem, Tocris Bioscience, 2B Scientific, Sartorius, Promega, BIO-RAD, and Santa Cruz Biotech unless otherwise stated. All primary and secondary antibodies were obtained from Santa Cruz Biotech, Abcam, Invitrogen, Cell Signalling Technologies and LI-COR. All reagents, materials, and antibodies that were used to perform all experiments are listed in Table 2.4, Table 2.5, Table 2.6 and Table 2.7.

2.2. Solution preparation

Solutions and media that were used for cell biology studies were commercially prepared and sterilised unless otherwise stated. Solutions which were prepared in the lab, were made by dissolving the required materials in Milli-Q water (18.2 MΩ.cm at 25 °C) followed by adjusting the pH as appropriate with HCl before making up to the final volume. The pH values of solutions were adjusted using a ceramic junction reference electrode that is connected to a Thermo Orion model 420 pH meter (Thermo Scientific, UK). The pH meter was calibrated by measuring different commercially obtained reference standard solutions (pH buffers) that have known pH values at room temperature (Thermo Scientific, UK). The calibration process was performed by placing the electrode in two pH buffers that bracket the desired sample pH; the first buffer usually has pH 7 and the second buffer should be near the expected sample pH, pH 10. All solutions that were prepared in the lab were sterilised by autoclaving at 121 °C for 15 minutes or by filtration using a 0.2 µm filter.

2.3. Peptide synthesis and characterization

2.3.1. Peptide synthesis and biotinylation protocols

All peptides were synthesized by 9-fluorenylmethyloxycarbonyl (Fmoc) solid phase peptide synthesis (SPPS) strategy using D-amino acids. Peptides were generally synthesised on 0.25 g of Rink amide methyl benzhydrylamine (MBHA) resin (0.6 mmol/g loading) to obtain peptides with an amidated C-terminus [128, 129]. For the synthesis of a C-terminally biotinylated peptide, 0.25 g of biotin-PEG Nova Tag™ resin (0.34 mmol/g loading) was used to produce a C-terminally biotinylated peptide with PEG spacer between the peptide and the biotin [130, 131]. Removal of the Fmoc group was performed with 20 % (v/v) piperidine in dimethylformamide (DMF) [128, 132]. The first coupling process was performed manually in a disposable plastic vessel with diisopropylcarbodiimide (DIC) and hydroxybenzotriazole (HOBt) as coupling agents in the presence of diisopropylethylamine (DIEA). Successful manual removal of Fmoc from the resin and coupling of the first amino acid were confirmed by Kaiser colour test (Kaiser reagents composed of 100 mM ninhydrin in ethanol (EtOH), 2.1 M phenol in EtOH, and 0.02 mM potassium cyanide in pyridine) [133]. A few drops of each Kaiser reagents were added to a sample of the Fmoc de-protected resin prior to heating to ~100 °C for 1 minute. Appearance of a dark blue colour in the resin sample indicated the presence of free amino functions capable of reacting with ninhydrin. Upon completion of the first amino acid coupling, the remaining coupling processes were performed on an automated Symphony Quartet peptide synthesizer (Gyros Protein Technologies, USA) with (benzotriazol-1-yloxy)-tripyrrolidinophosphonium hexafluorophosphate (PyBOP) as coupling reagent with DIEA. N-terminal biotinylation of peptides was performed during the automated process using a biotin-*p*-nitrophenyl ester (biotin-ONp) reagent [134]. Quantities of all D-amino acids, biotin-ONp, and coupling reagents used were equal to 3 equivalents of the resin. The amount of DIEA used during all coupling steps was equal to 6 equivalents of the resin. All peptides were cleaved from the resin and side chain protection groups removed by treatment with 1mL of a mixture of 95% of trifluoroacetic

acid (TFA), 2.5% water, and 2.5% triisopropylsilane (TIPS) per 1g resin and incubating at room temperature for 3 h[132].

2.3.2. Peptides purification and characterization by HPLC and mass spectrometry

All cleaved peptides were purified by reversed-phase semi-preparative high performance liquid chromatography (RP-HPLC), and purified materials were characterized by analytical RP-HPLC with electrospray mass spectrometry being used to verify peptide identity. Semi-preparative RP-HPLC was performed on a Dionex HPLC system, using a Phenomenex Gemini 5µm C-18 (250 x 10 mm) column, and a flow rate of 2.5 mL/min. Analytical RP-HPLC was performed using a Dionex UltiMate 3000 HPLC system (Dionex, UK), using a Phenomenex Gemini 5µm C-18 (150 x 4.6 mm, Phenomenex, UK) column, and a flow rate of 1 mL/min. Mobile phase for both analytical and semi-preparative HPLCs was: A) 0.1% (v/v) of TFA in water and B) 0.1% (v/v) TFA in acetonitrile. The semi-preparative RP-HPLC gradient used was T = 0 min, B = 5%; T = 25 min, B = 95%; T = 35 min, B = 95%; T = 35.1 min, B = 5%; T = 40 min, B = 5%. The analytical RP-HPLC gradient used was T = 0 min, B = 5%; T = 10 min, B = 95%; T = 15 min, B = 95%; T = 15.1 min, B = 5%; T = 18 min, B = 5%. Mass spectrometry analysis of all peptides was performed using a microTOF instrument from Bruker Daltonics run in positive ion mode (Bremen, Germany).

2.4. Cell culture handling and maintenance

2.4.1. General methodology

The human colorectal adenocarcinoma (Caco-2) cell line (American Type Culture Collection, ATCC, USA) was used to perform all *in vitro* cell-based studies. All plastic-ware, which was used to culture and maintain cells, was purchased pre-sterilised. For general cell maintenance, cells were cultured in 75 cm^2 flasks using Dulbecco's modified Eagle's medium (DMEM)

supplemented with 10% (v/v) of foetal bovine serum (FBS) and 1% (v/v) of an antibiotic mixture (P/S) containing penicillin (100 unit/mL) and streptomycin (100 µg/mL); known as complete DMEM. Cells were maintained in 5% CO_2 at 37 °C in a humidified incubator. All cell culture work was performed in a biosafety tissue culture hood applying the required aseptic techniques to keep cell cultures free from contamination by microorganisms. This included use of sterile cell culture tools and cleaning the working area using 70 % (v/v) EtOH in water and/or a UV lamp. For further sub-culturing or seeding onto semi-permeable membrane supports, cells were split at a point of ~80 % confluence in T75 flasks. To split cells, spent media was removed and cells were washed once with pre-warmed phosphate buffered saline (PBS). Washed cells were then treated with 10 mL/flask of trypsin/ethylenediaminetetraacetic acid (EDTA) solution for ~ 5 min or until cell detachment was completed. An equal volume of pre-warmed complete DMEM was then added to the flask to inactivate the trypsin. Cells were then transferred to centrifuge tubes and pelleted at 125 x g for 10 min using AccuSpin™ 400 (Fisher scientific, UK). After removal of the media, pelleted cells were suspended with 1 mL of complete DMEM prior to further dilution with the same medium to achieve a split ratio of ~ 1:10. Cells were then either placed in fresh culture flasks or seeded on semi-permeable membrane supports to perform *in vitro* studies.

Trypsin/EDTA solution was prepared as follows: 2% (w/v) of EDTA stock solution was prepared by dissolving 0.5 g in 25 mL PBS prior to passing through a 0.2 µm filter. Then, 100 mL of 10x trypsin (2.5%, v/v) was mixed with 10 ml of 2% EDTA stock in 890 ml of sterile PBS to give a working concentration of 0.25% Trypsin/0.02% EDTA solution. The trypsinization solution was stored in aliquots at - 20°C.

2.4.2. Cells storing and reconstituting protocols

Reconstitution of frozen cells was performed by placing a vial retrieved from the liquid nitrogen dewar in a pre-warmed water bath at 37 °C. Thawed cells were transferred to a 15 mL tube containing pre-warmed cell medium and centrifuged for 10 min at 125 x g. After discarding the supernatant, pelleted cells were suspended with fresh medium of sufficient volume to produce the desired cell concentration for growth as mentioned in Section 2.4.1.

To store cells frozen in liquid nitrogen, cells that had reached ~80 % confluency on 75 cm^2 flask were trypsinized and centrifuged as stated in Section 2.4.1. After discarding the supernatant, pelleted cells were suspended with cryopreserving medium composed of 10 % (v/v) of dimethyl sulfoxide (DMSO) and 20 % (v/v) of FBS in DMEM. These cell suspensions were divided into cryotubes (1 mL/tube) and stored at -20 °C for 1 h prior to being placed in a -80 °C freezer overnight. On the next day, cell vials were transferred to liquid nitrogen for long-term storage.

2.5. Analysis of barrier function

2.5.1. Cell seeding

Caco-2 cells were seeded into the apical chamber of a 1.2 cm^2 (0.4 µm pore size) polyester membrane of 12-well Transwell® plates at a cell density of 7 x 10^4/well. Cells were left to grow for ~ three weeks to produce polarized monolayers. During this time cells were maintained in DMEM medium supplemented with 10 % (v/v) FBS and 1 % P/S with 400 µL in the apical chamber and 800 µL in the basolateral chamber. One well in each plate was left without cells for blank reading. Cell medium in each well was replaced with fresh medium every two days.

2.5.2. Transepithelial electrical resistance (TEER) measurement

TEER measurements were used to monitor cell growth, formation, and changes in epithelial cell barrier function [88, 135]. Caco-2 cell monolayer confluency is usually demonstrated by a TEER value of > ~ 300 $\Omega \cdot cm^2$ [135]. TEER measurement was performed using EVOM2™ epithelial voltmeter (World Precession Instruments, UK) using chopstick-like silver/silver-chloride electrodes that were 4 mm wide and 1 mm thick. Prior to each use, the electrodes were sterilized using 70 % (v/v) of ethanol in water then washed with and calibrated in Hanks' balanced salt buffer solution (HBSS). TEER values were obtained by placing one electrode in the apical chamber and the other in the basolateral chamber as per supplier's instructions. Cell monolayer TEER values of each well were calculated by subtracting the blank well TEER value from the TEER value measured for each cell monolayer with that value then multiplied by the filter surface area.

2.5.3. Fluorescent solutes used to study TJ permeability

Evaluation of paracellular permeability of Caco-2 *in vitro* is commonly performed by measuring apical to basolateral transport of different poorly-permeable solutes of different molecular weights, such as fluorescent dextrans [118, 135, 136]. In our work, we assessed the extent of TJ opening by studying apical to basolateral transport of 4 kDa fluorescein isothiocyanate (FITC)-dextran, 10 kDa FITC-dextran, and 70 kDa tetramethylrhodamine isothiocyanate (TRITC)-dextran across Caco-2 cell monolayers. In addition, the permeability of fluorescent dextran having different net charge across Caco-2 cell monolayers was also examined: positively-charged FITC-diethylaminoethyl-dextran (FITC-DEAE-dextran) and negatively-charged FITC-carboxymethyl-dextran (FITC-CM-dextran), both having a molecular weight of 4 kDa. The listed molecular weights of all of these dextrans represent an approximate average of a pooled material collected by size-fractionation.

2.5.4. Time-course assessments of TEER change of monolayers and fluorescent dextran transport induced by PIP peptides

Studies were performed on polarized Caco-2 cell monolayers as defined by the measured TEER value as defined in Section 2.5.2. Transport experiments were initiated by discarding cell medium and washing apical and basal monolayer surfaces once with 400 µL and 800 µL of HBSS, respectively. Subsequently, this buffer was removed and replaced with fresh HBSS in both apical and basolateral chambers and monolayers were left at 37 °C for 30 min to equilibrate. Upon completion of the equilibration period, a study baseline TEER measurement was performed and a background sample that served as the initial time point for the transport study was collected.

To start a study, apical buffer was removed and replaced with 400 µL of fresh HBSS buffer containing the required fluorescent dextran for each test (each prepared at a stock working concentration of 1 mg/mL) with or without a PIP peptide; fresh HBSS (800 µL) was exchanged in the basal compartment. For each time point of a study, a TEER measurement was performed followed by collection of the basal media, which was then replaced with fresh HBSS medium to the basal chamber. The extent of transported dextran was determined by measuring the fluorescence present in the HBSS samples collected from the basal compartment over time (FITC; Ex 490 nm/ Em 520. TRITC; Ex 540 nm/ Em 610 nm) using FLUOstar® Omega Microplate Readers (BMG Labtech, Germany).

2.5.5. Induction of TJ barrier loss by proinflammatory cytokines

This was performed as described in the literature [*54, 137, 138*] to compare TJ barrier loss induced by proinflammatory cytokines with changes in TJ barrier properties induced by PIP peptides. A mixture of the human proinflammatory cytokines tumour necrosis factor alpha and interferon gamma (TNFα/INFγ) were added to the basal chamber medium of Caco-2 cell monolayers

containing DMEM medium without P/S antibiotic to induce TJ barrier loss. Specifically, Caco-2 cell monolayers were treated with 10 ng/mL INFγ overnight prior to addition of 5 ng/mL TNFα for 4 h. After induction of TJ barrier dysfunction, media containing proinflammatory cytokines was discarded and cell monolayers were washed once with HBSS, 400 µL in the apical chamber and 800 µL in the basal chamber. Subsequently, transport of different-sized fluorescent dextran molecules across Caco-2 cell monolayers was as described in Section 2.5.4.

2.6. Protein characterization

2.6.1. Protein extraction for immunoblotting (western blotting)

Upon completion of an experiment, cell media in the apical and basal compartments was discarded prior to washing monolayers thrice with ice cold PBS. Cells were then lysed by adding 100 µL radioimmunoprecipitation assay buffer (RIPA) that contained a cocktail of protease and phosphatase inhibitors (25 µL/mL each), added to the apical surface of each Transwell® filter. Lysed cells were scraped into Eppendorf tubes and placed on ice for 10 min prior to centrifugation at 10,000 x g for 10 min at 4 °C using Heraeus™ Fresco™ 17 Microcentrifuge (Fisher scientific, UK). Supernatants obtained from this centrifugation step were then diluted with electrophoresis sample buffer (composed of 500 µL/mL 4x NuPAGER® lithium dodecyl sulfate (LDS), 200 µL/mL NuPAGER® reducing agent, and 300 µL/mL Milli-Q water) in a 1:1 ratio prior to separation by sodium dodecyl sulfate polyacrylamide gel electrophoresis (SDS-PAGE) as described in Section 2.11.

2.6.2. Protein extraction for immunoprecipitation, native-immunoblotting and pull-down assay with biotinylated PIP peptides

Proteins were extracted using the same method as in Section 2.6.1. However, cells were harvested from 75 cm^2 flasks and lysed using a 1 mL of lysis buffer composed of 50 mM Tris at pH 7.4, 200 mM NaCl, 10 mM EDTA, 20% (v/v) of glycerol, and 1% (v/v) Nonidet P40.

2.7. Determination of extracted protein

2.7.1. Detergent-compatible Bradford assay

The Bradford colorimetric assay is commonly used to determine the protein concentration of a solution [139]. This assay uses the protein-binding capacity of Coomassie blue dye that results in an absorption maximum shift from 465 nm (un bound dye, green colour) to 595 nm (dye bound to protein, blue colour) [139]. Unfortunately, the traditional Bradford reagent is incompatible with cell lysis buffers containing detergents [139]. Thus, the Pierce™ detergent compatible Bradford reagent was used that is compatible with commonly used detergents. For these protein determinations, bovine serum albumin (BSA) was used as a standard protein.

2.7.2. General methodology

Protein determinations were performed in a 96-well plate using 10 µL of cell lysates and 300 µL of Pierce™ detergent-compatible Bradford reagent. Plates were incubated for 10 min at room temperature on a plate shaker. The intensity of Bradford dye converted to 595 nm emission was determined using a FLUOstar® Omega Microplate Reader. Protein concentrations were determined using a plotted BSA standard curve with the following concentrations: 25 µg/mL, 20 µg/mL, 15 µg/mL, 10 µg/mL, 5 µg/mL, 2.5 µg/mL.

2.8. Immunoprecipitation protocol

Immunoprecipitation of proteins was performed on confluent Caco-2 cells grown in 75 cm^2 flasks. Separate flasks of cells were treated with the PIP 640 peptide for set times. Untreated cells were used as controls. Treated cells were then washed with HBSS once and lysed as described in Section 2.6.2. Cell lysates containing ~ 500 µg of total protein were quantified as described in Section 2.7.2 and mixed with a primary antibody recognizing the protein of interest (Section 2.16, Table 2.6); this solution was incubated with rotation for 1 h at 4 °C. Subsequently, 20 µL of agarose beads was added to each sample and the suspension was mixed by gentle rotation overnight at 4 °C. Agarose beads were then collected by centrifugation at 1,000 x g for 5 mins at 4 °C and washed thrice by centrifugation with 500 µL of the same lysis buffer for each wash. After the final wash, agarose beads were re-suspended with 50 µL of electrophoresis sample buffer (described in Section 2.6.1) and the agarose bead-associated proteins separated by SDS-PAGE prior to Western immunoblotting analysis (Section 2.11).

2.9. Pull-down assay with biotinylated peptides

Confluent Caco-2 cells grown in 75 cm^2 flask were lysed as described in Section 2.6.2. Lysates were divided equally, with each being prepared from cells treated with a different concentration of biotinylated PIP 640 peptide and rotated slowly for 3 h at 4 °C, each then being combined with 50 µL of streptavidin magnetic beads that had been pre-equilibrated with 500 µL of lysis buffer. Samples were incubated with gentle rotation for 1 h at 4 °C. Biotinylated PIP 640 peptide-bound beads were pulled-down using a magnet and washed thrice with 500 µL lysis buffer, being captured each time using the magnet pull-down step as above. After the final wash, the streptavidin magnetic beads were suspended in 50 µL of electrophoresis sample buffer and proteins associated with these beads being separated by SDS-PAGE prior to Western immunoblotting analysis as described in Sections 2.6.1 and 2.11.

2.10. Detection of myosin light chain phosphatase protein components interacting with PIP 640 peptide

A 75 cm^2 flask of Caco-2 cells was lysed as described in Section 2.6.2. An aliquot of the lysate was combined with each PIP peptide to be tested and then incubated by gentle rotation for 3 h at 4 °C. Subsequently, 10 µL of each lysate-PIP peptide sample was mixed with 40 µL of a non-denaturing sample buffer (Native sample gel buffer, Table 4). Proteins present in these preparations were separated by native gel electrophoresis (Section 2.11.1) prior to western immunoblotting analysis as described in Section 2.11.4.

2.11. SDS-PAGE and native-PAGE immunoblotting

2.11.1. Gel preparation for SDS-PAGE and native-PAGE immunoblotting

The resolving element of the gels used in these studies was prepared by mixing the ingredients described in Table 2.1; the solution being poured into 8 cassettes of 1 mm thickness each and allowed to polymerize at room temperature for 60 min. Ingredients of the stacking gel described in Table 2.2 were mixed and immediately poured into the cassettes over the resolving gel prior to inserting a comb to form the desired number of wells where protein samples are loaded.

2.11.2. Buffers for electrophoresis and immunoblotting

Electrophoresis running buffer for both SDS-PAGE and native PAGE was prepared by combining 3 g of Tris and 14 g of glycine in 1 L of Milli-Q water; the SDS-PAGE running buffer also contained 1 g of SDS. Protein transfer onto polyvinylidene fluoride (PVDF) membranes was performed using a buffer that was composed of 1.5 g of Tris, 7 g glycine, and 200 mL methanol (MeOH) in 800 mL Milli-Q water. Tris buffer saline (TBS) was composed of 5 mL of 2 M

Tris-HCl (pH 7.5) and 37 mL of 4 M NaCl in 957.5 mL Milli-Q water. TBS containing 0.1 % (v/v) of Tween®20 (TBS-T) was used for washing, BSA blocking, and antibody incubation of PVDF membranes.

Table 2.1: Reagents used to prepare the resolving gel used for both SDS-PAGE and native-PAGE

Reagent (resolving gel)	SDS-PAGE	Native-PAGE
Milli-Q water	24 mL	24 mL
40 % acrylamide/bis-acrylamide (29:1)	16.8 mL	16.8 mL
Tris-HCl buffer (1.5 M, pH=8.8)	14 mL	14 mL
10 % (w/v) of SDS in Milli-Q water	560 µL	----
10 % (w/v) of Ammonium Persulfate (APS) in Milli-Q water	560 µL	560 µL
Tetramethylethylenediamine (TEMED)	56 µL	56 µL

Table 2.2: Reagents used to prepare the stacking gels used for both SDS-PAGE and native-PAGE

Reagent (stacking gel)	SDS-PAGE	Native-PAGE
Milli-Q water	11.6 mL	11.6 mL
40 % acrylamide/bis-acrylamide (29:1)	3 mL	3 mL
Tris-HCl buffer (0.5 M, pH=6.8)	5 mL	5 mL
10 % (w/v) of SDS in Milli-Q water	200 µL	-----
10 % (w/v) of APS in Milli-Q water	200 µL	200 µL
Tetramethylethylenediamine (TEMED)	20 µL	20 µL

2.11.3. SDS-PAGE and electrophoretic transfer

SDS-polyacrylamide gels were placed in an XCell™ Sure Lock Mini-cell electrophoresis box (Invitrogen, UK) with SDS-PAGE running buffer (Section 2.11.2). Cell lysates were mixed with sample buffer, heated for 5 min at 95°C, and then loaded into wells generated by the removal of the comb (20 µL/well). Samples were electrophoresed at 160 V for ~ 2 h to separate proteins. Upon completion of proteins separated by gel electrophoresis were electro-transferred onto PDVF membranes using an XCell™ Blot module (Invitrogen, UK) at 30 V for 90 min. Membranes were then blocked by 2% BSA (w/v) in TBS-T for 1h at room temperature prior to an overnight incubation at 4 °C with an appropriate primary antibody diluted in TBS-T (Section 2.16 Table 2.6). On the next day, membranes were washed with TBS-T thrice, for 5 min each, then incubated with infrared (IR) dye-labelled secondary antibody diluted in TBS-T (Section 2.16 Table 2.7). Afterwards, membranes were washed thrice with TBS-T and imaged using the Odyssey CLX imaging system (LI-COR, UK). Images were analyzed using the Image Studio Lite software, version 5.2.

2.11.4. Native-PAGE immunoblotting protocol

Native-PAGE immunoblotting was performed using a running buffer that does not include SDS, as mentioned in Section 2.11.2, following a similar method to that described in Section 2.11.3, except that protein electro-transfer onto PDVF membranes was carried out overnight with 30 V at 4 °C.

2.12. Confocal microscopy and immunofluorescent staining

2.12.1. Confocal microscopy and image analysis

All images were collected at 63x magnification using a Zeiss LSM 510 META confocal microscope equipped with 3 laser lines: diode (Ex 405 nm), argon (Ex 488 nm) and helium-neon (Ex 543 nm). Filters with different ranges were used to collect the emitted fluorescence including: (Em 550-625 nm, red), (Em 420-480 nm, blue) and (Em 505-530 nm, green). Z-stacks were collected at 1 µm intervals to generate xz plan images. Collected images were analyzed using Zeiss LSM Image Browser software, version 4.2.0.121. Maximum excitation/emission wavelengths of fluorophores used in confocal images are described in Table 2.3.

Table 2.3: Maximum excitation/emission wavelengths of fluorophores used in confocal microscopy.

Fluorophores	Ex (nm)	Em (nm)
Alexa 488 (Green)	495	519
Alexa 546 (Red)	556	573
Diamidinophenylindole (DAPI) (Blue)	358	461

2.12.2. Immunofluorescent staining

2.12.2.1. Intracellular localization of biotinylated PIP peptides

Caco-2 cell monolayers, incubated at 37 °C, 5% CO_2, were treated apically with different analogues of biotinylated PIP peptides dissolved in HBSS buffer; HBSS was used as a control. Upon completion of the incubation period, cell monolayers were washed thrice with HBSS to remove extracellular peptides prior to fixing with 4 % (w/v) paraformaldehyde (PFA) in PBS for 20 min. Fixed cell monolayers were washed thrice with 500 µL of PBS, each for 2 min on a plate rocker and then incubated with 50 mM NH_4Cl in PBS for 20 min

as a quenching reagent to reduce background fluorescence resulting from residual aldehyde groups generated by PFA fixation. Fixed cell monolayers were then permeabilized with 0.1 % (v/v) of Triton X-100 in PBS for 20 min and then washed thrice with PBS prior to blocking with 10 % of FBS (v/v) in PBS for 1 h with gentle rocking.

Fixed, permeabilized cell monolayers were then treated with a primary antibody recognizing occludin (Section 2.16, Table 2.6) followed by a species-specific secondary antibody-conjugated to Alexa 546 to highlight TJ structures (Section 2.16 Table 2.7). Subsequently, cell monolayers were washed, as described above, and biotinylated peptides were detected with 1µL/mL of Alex 488-conjugated streptavidin in PBS for 40 min. Nuclei were stained with 1 µL/mL of DAPI in PBS for 20 min. Finally, stained cell monolayer membranes were cut off the Transwell® inserts and placed on glass slides with cells facing up. After a one drop application of Vectashield® mounting medium a glass coverslip was positioned to allow examination by confocal microscopy, as described in Section 2.12.1.

2.12.2.2. Assessment of TJ protein distribution

Caco-2 cell monolayers were treated with the PIP 640 peptide in HBSS, or HBSS only (control), for set times at 37 °C. Subsequently, cell monolayers were washed thrice with 500 µL of HBSS to remove unincorporated peptide, then washed once with the same volume of ice-cold MeOH prior to placing in pre-cooled MeOH at -20 °C for 1 h. Cell monolayers were re-hydrated by incubation in PBS for 15 min before being blocked with 10 % (v/v) FBS in PBS for 1 h. Monolayers were then incubated with primary antibodies against different TJ proteins (Section 2.16, Table 2.6). This was followed by 3 washes with PBS before incubation with the appropriate fluorophore-conjugated secondary antibodies against the primary antibody being used (Section 2.16 Table 2.7). Cell monolayers were then washed thrice with PBS and mounted, as described in Section 2.12.2.1.

2.13. *In vivo* studies

All *in vivo* experiments were performed using male adult (7-8 weeks old) Wistar rats with an average weight ~250 g. All experiments were conducted using non-recovery protocol. Rats were anesthetized using inhaled isoflurane for all experiments and euthanized by inhaled CO_2.

2.13.1. Insulin subcutaneous administration or co-administration with PIP 640 peptide by intraluminal injection (ILI) and tissue collection protocols

Rats were anesthetized with 5% inhaled isoflurane in combination with O_2 (induction rate) using a rodent anaesthesia system equipped with isoflurane vaporizer**.** A 4–5 cm midline abdominal incision was made to access the small intestine (mid-jejunum to proximal ileum regions). After performing the incision, isoflurane concentration was lowered to 2% (maintenance rate). A stock solution of human insulin (30 IU/kg) and (20 mM) PIP 640 peptide was prepared in PBS containing 10 mM citric acid. Using a 1 mL syringe connected to a 27-gauge needle, 50 µL of a prepared stock solution was injected into the rat intestinal lumen. Changes in blood glucose levels over time were measured using a glucometer (AccuChek,UK) in blood samples collected from the tail vein. Negative control treatment was performed by injecting insulin in PBS containing citric acid into the rat intestine. After the desired exposure times, rats were euthanized by CO_2 asphyxiation. At that time, a ~ 1 cm section of rat intestine at the injection site was collected for biochemical studies. A subcutaneous (SC) insulin injection (3 IU/kg) as a positive control was performed in the mid-scapular region followed by assessment of blood glucose levels as described above.

2.13.2. Tissue preparation for immunoblotting

Collected rat tissues, as described in Section 2.13.1, were washed with ice-cold PBS and then maintained in ice-cold PBS for 10 min. Intestinal segments were then sliced into smaller pieces and placed into 5 mL Eppendorf tubes containing 2 mL of RIPA lysis buffer containing a cocktail of protease and phosphatase inhibitors (25 µL/mL, each) followed by a 10 min incubation on ice. Lysates were clarified by centrifugation at 10,000 x g at 4 °C. Supernatants were aliquoted and stored at – 80 °C prior to their analysis in immunoblotting studies, as described in Section 2.11.3.

2.13.3. Rat intestinal tissue processing for immunofluorescence staining

Rat intestine sections were collected and washed with ice-cold PBS as described (Section 2.13.1). Tissues were then fixed overnight at 4 °C in ice-cold PBS containing 4 % (w/v) PFA. On the next day, fixed intestinal sections were opened longitudinally, placed in marked tissue cassettes, and dehydrated using an automated Leica TP 1020 tissue processor (Leica Biosystems, UK) that used sequential immersions into 70 %, 80 %, 90 % and 100 % (v/v) EtOH/water solutions for 2 h each. Dehydrated tissues were embedded in paraffin using a Leica EG 1160 tissue embedding device (Leica Biosystems, UK) and allowed to set at 4 °C overnight. Paraffin-embedded tissues were sectioned using a Leica RM 2155 microtome (Leica Biosynthesis, UK) to obtain 5 µm slices that were placed onto glass slides.

The procedure of immunofluorescent staining of sectioned intestinal tissue on glass slides was initiated by rehydration that involved immersing slides first in Histo-clear™ solution for 10 min followed by 100%, 90 %, 80 %, and 70 % (v/v) EtOH/water solutions for 5 min each. Slides were then washed with PBS

thrice for 5 min before being subjected to an to antigen retrieval step that was performed by placing slides into a beaker containing boiling 10 mM sodium citrate buffer (pH=6) for 10 min. Subsequently, tissue slices were washed thrice with PBS for 5 min, permeabilized with 0.2 % (v/v) Triton X-100 in PBS for 30 min and blocked with 2% (w/v) BSA in PBS for 1 h. Tissues were then incubated with primary antibodies diluted in PBS containing 1% (w/v) BSA overnight at 4 °C (Section 2.16; Table 2.6). On the next day, slides were washed thrice with PBS then incubated with the required dilution of species-specific secondary antibody in PBS (Section 2.16 Table 2.7) for 2 h at room temperature. Slides were then washed thrice with PBS and once with Milli-Q water for 5 min each. Finally, slides were dehydrated by sequential immersion into 70 %, 80 %, 90 % and 100 % (v/v) EtOH/water solutions for 5 min each followed by immersion into Histo-clear™ solution for 10 min prior to cover slip-mounting the tissue with Vectashield® medium, as described in Section 2.12.2.1. Slides were then imaged by confocal microscopy (Section 2.12.1).

2.13.4. Assessment of enhanced calcitonin and exenatide permeability in rats *in vivo*

Rats were anesthetized and their abdominal cavity accessed via surgical incision as described in Section 2.13.1, to allow ILI and blood sample collection from the portal vein. ILI (50 µL) injections were performed for solutions containing either calcitonin or exenatide (0.5 mg), 20 mM PIP 640 and 1.5/mL soybean trypsin inhibitor (SBTI). Control injections were performed with either calcitonin or exenatide and SBTI, but no PIP 640 peptide. Blood samples (100 µL) were collected at set time points from the portal vein and placed into Eppendorf tubes containing 50 mM of EDTA and 0.6 IU/mL aprotinin to prevent blood coagulation and protein degradation, respectively. Blood samples were then centrifuged at 1,600 x g for 15 min at 4 °C and the isolated plasma was stored at -80 °C until use. Calcitonin and exenatide

content in plasma samples were measured by enzyme linked immunosorbent assay (ELISA) using commercially available kits.

2.13.5. Assessment of blood endotoxin levels *in vivo*

Plasma samples that were used to evaluate therapeutic peptide permeability enhancement (Section 2.13.4), were also examined for determining if PIP 640 also enhanced the trans-epithelial uptake of luminal endotoxin. This was performed using a commercial, semi-quantitative assay kit: E-Toxate™ *Limulus* amebocyte lysate (LAL). This kit uses as readout the formation of a gel-like clot with the reagent when reacted with endotoxin [*140*]. Analysis using the LAL kit was performed on 50 µL of a plasma sample and endotoxin standards in separate sterile 10 x 75 mm glass test tubes. This was followed by adding 150 µL of LAL reagent into each tube and incubation for 1 h at 37 °C in a water bath. Afterwards, tubes were inverted 180° to evaluate gel formation; generation of a hard gel, which was not disrupted by tube inversion, was considered a positive test.

2.13.6. Hydrodynamic radius calculation

Hydrodynamic radius was approximated using the relationship established between the molecular weight (MW) and the hydrodynamic radius (R_H) of a protein that assumes the protein have the simple shape of a sphere. [141]:

$$R_H = \left[\frac{3\ MW}{4\ \pi \rho N}\right]^{\frac{1}{3}}$$

Where

R_H in (cm)

MW in (g/mol)

ρ is the average density of a hydrated protein (0.99 g/cm^3)[141]

N is Avogadro's number (6.02x10^{23} mol^{-1})

2.14. Cell viability assay *in vitro*

The extent of viable cells with active mitochondrial metabolism can be correlated with the amount of 3-(4,5-dimethylthiazol-2-yl)-5-(3-carboxymethoxyphenyl)-2-(4-sulfophenyl)-2H tetrazolium (MTS) that can be converted to formazan [142]. This conversion is presumably accomplished by NADPH- or NADH-dependent oxidoreductase and dehydrogenase enzymes in metabolically active cells [142]. The colour intensity of formazan formed by this reaction can be measured at 490 nm.

Caco-2 cells were seeded in 96-well plates at a density of 2 x 10^4 in 100 µL DMEM cell medium supplemented with 10% FBS and 1% P/S and incubated overnight at 37 °C under 5% CO_2. On the next day, cells were treated with different PIP peptides dissolved in 100 µL of cell medium, as described above, for 12 h. Control cells were incubated with 100 µL of cell media that did not contain a PIP peptide. Upon completion of this 12 h incubation period, cells were treated with 20 µL of MTS reagent (at the concentration provided by the supplier) and incubated at 37 °C and 5% CO_2 for 3 h. Finally, absorbance was recorded at 490 nm using the plate reader described in Section 2.5.4.

2.15. Statistical analysis

All data are represented as values ± SEM of three independent experiments, unless otherwise specified. A two-tailed unpaired t test was used for comparison between two groups. Potential differences between treatment groups were examined using one-way ANOVA; Tukey's multiple comparison was used to test for experiments involving three or more treatments. All statistical analysis was performed using GraphPad Prism® software version 7.

2.16. Reagents and materials

Table 2.4: Chemical reagents for peptide synthesis

Reagent	Catalogue number	Supplier
Biotin-ONp	851027	Novabiochem, UK
biotin-PEG Nova Tag™ resin	855055	Novabiochem, UK
DIC	D125407	Sigma-Aldrich, UK
DIEA	D125806	Sigma-Aldrich, UK
DMF	RG2014	Rathburn chemicals, UK
Fmoc-D-Ala-OH	852142	Novabiochem, UK
Fmoc-D-Arg(Pbf)-OH	852165	Novabiochem, UK
Fmoc-D-Asp(OtBu)-OH	852154	Novabiochem, UK
Fmoc-D-Glu(OtBu)-OH	852155	Novabiochem, UK
Fmoc-D-Lys(Boc)-OH	852146	Novabiochem, UK
Fmoc-D-Tyr(tBu)-OH	852151	Novabiochem, UK
Fmoc-D-Val-OH	852152	Novabiochem, UK
HOBt	157260	Sigma-Aldrich, UK
piperidine	411027	Sigma-Aldrich, UK
PyBOP	851009	Novabiochem, UK
Rink amide MBHA resin	855003	Novabiochem, UK
TFA	T62200	Sigma-Aldrich, UK
TIPS	841359	Sigma-Aldrich, UK

Table 2.5: Reagents and materials for cell biology studies

Reagent	Catalogue number	Supplier
Acrylamide/bis-acrylamide (29:1), 40% solution	A7802	Sigma-Aldrich, UK
Aprotinin	10820	Sigma-Aldrich, UK
APS	10744171	Fisher Scientific, UK
Bolt™ empty mini gel cassette combs, 10-well	NW3010	Invitrogen, UK

BSA	A7906	Sigma-Aldrich, UK
Calcitonin (Salmon) - ELISA Kit	EK-014-09	Phoenix Pharmaceuticals, US
Calcitonin, salmon	05-23-2401	Novabiochem, UK
Cell culture flask, 75 cm^2	156499	Fisher Scientific, UK
Citric acid	C1909	Sigma-Aldrich, UK
DAPI	D3571	Invitrogen, UK
DMEM medium	41965039	Fisher Scientific, UK
DMSO	D8418	Sigma-Aldrich, UK
EDTA	BP118	Fisher Scientific, UK
Empty mini 1.0 mm gel cassettes	NC2010	Invitrogen, UK
Ethanol	32221	Sigma-Aldrich, UK
E-Toxate™ kit	E8779	Sigma-Aldrich, UK
Exenatide (Exendin-4)	1933	Tocris Bioscience, UK
Exenatide (Exendin-4) ELISA Kit	MBS031942	2B Scientific Ltd, UK
FBS	10500064	Fisher Scientific, UK
FITC-CM-dextran, 4 kDa	68059	Sigma-Aldrich, UK
FITC-DEAE-dextran, 4 kDa	53557	Sigma-Aldrich, UK
FITC–dextran, 10 kDa	FD10S	Sigma-Aldrich, UK
FITC–dextran, 4 kDa	FD4	Sigma-Aldrich, UK
Gibco™ IFN-γ	10474733	Fisher Scientific, UK
Gibco™ TNFα	10699920	Fisher Scientific, UK
Glass square coverslip	12363138	Fisher Scientific, UK
Glycerol	BP229	Fisher Scientific, UK
Glycine	10061073	Fisher Scientific, UK
HBSS buffer	12352207	Fisher Scientific, UK
Histo-clear™	12358637	Fisher Scientific, UK
Immobilon®-FL PVDF transfer membrane, 0.45 µm,	IPFL00010	Novabiochem, UK
Insulin, recombinant human	91077C	Sigma-Aldrich, UK
Methanol	34860	Sigma-Aldrich, UK
Minisart® syringe filter, 0.2µm	16532	Sartorius, UK
MTS reagent, CellTiter 96® one solution cell proliferation assay	G358A	Promega, UK

Nalgene™ cryogenic tubes	11375644	Fisher Scientific, UK
Native sample gel buffer	1610738	BIO-RAD, UK
NH_4Cl	09718	Sigma-Aldrich, UK
NP-40 detergent	85124	Invitrogen, UK
Nunc™ 96-well microplates	10212811	Fisher Scientific, UK
4X NuPAGE™ LDS sample buffer	NP0007	Invitrogen, UK
10 X NuPAGE™ sample reducing agent material	NP0009	Invitrogen, UK
P/S antibiotics	P0781	Sigma-Aldrich, UK
Paraffin wax	SA4523	Science Services, Germany
PBS tablets	BR0014G	Fisher Scientific, UK
PFA	P6148	Sigma-Aldrich, UK
Phosphatase inhibitor cocktail IV	12851650	Fisher Scientific, UK
Pierce™ detergent compatible Bradford assay kit	23246	Invitrogen, UK
Polysine adhesion slides	10219280	Fisher Scientific, UK
Protease inhibitor cocktail III	12841640	Fisher Scientific, UK
Protein A/G plus agarose beads	sc-2003	Santa Cruz Biotech, UK
RIPA buffer	R0278	Sigma-Aldrich, UK
SBTI	T9128	Sigma-Aldrich, UK
SDS	10090490	Fisher Scientific, UK
Sodium chloride	S9625	Sigma-Aldrich, UK
Sodium citrate dihydrate	W302600	Sigma-Aldrich, UK
Streptavidin Sepharose™ magnetic bead	11791456	Fisher Scientific, UK
Streptavidin, Alexa Fluor™ 488 conjugate	S11223	Invitrogen, UK
TEMED	10549960	Fisher Scientific, UK
Tissue cassette	12026839	Fisher Scientific, UK
Tissue cassette lid	12096829	Fisher Scientific, UK
Transwell® polyester membrane, 0.4 µm, cell culture inserts	3460	Sigma-Aldrich, UK
TRITC-dextran, 4 kDa	T1037	Sigma-Aldrich, UK
TRITC-dextran, 70 kDa	T1162	Sigma-Aldrich, UK

Triton™ X-100	X100	Sigma-Aldrich, UK
Trizma® (Tris) base	T6066	Sigma-Aldrich, UK
Trypsin 10x	SV30037.01	Fisher Scientific, UK
Tween®-20	P1379	Sigma-Aldrich, UK
Vectashield® mounting medium	H-1000	Vector Laboratories, UK

Table 2.6: List of primary antibodies used for western blotting (WB), immunofluorescence (IF), and Immunoprecipitation (IP) studies

Protein target of primary antibody	Host species	Application concentration	Catalogue number	Supplier
Actin	Goat (polyclonal)	WB: 1 µg/mL	Sc-1615	Santa Cruz Biotech, UK
Claudin-1	Rabbit (polyclonal)	WB: 1 µg/mL IF: 1 µg/mL	Ab15098	Abcam, UK
Claudin-15	Rabbit (polyclonal)	WB: 1 µg/mL	Sc-25712	Santa Cruz Biotech, UK
Claudin-2	Rabbit (polyclonal)	WB: 1 µg/mL IF: 5 µg/mL	Ab125293	Abcam, UK
Claudin-2	Rabbit (polyclonal)	IP: 2 µg/mL	Sc-133464	Santa Cruz Biotech, UK
Claudin-3	Rabbit (polyclonal)	WB: 1 µg/mL	Ab15102	Abcam, UK
Claudin-4	Rabbit (polyclonal)	WB: 1 µg/mL IF: 1 µg/mL	Ab15104	Abcam, UK
Claudin-5	Rabbit (polyclonal)	WB: 1 µg/mL	Sc-28670	Santa Cruz Biotech, UK
Claudin-7	Rabbit (polyclonal)	WB: 5 µg/mL IF: 5 µg/mL	Ab27487	Abcam, UK
Claudin-8	Rabbit (polyclonal)	WB: 2 µg/mL	Ab110050	Abcam, UK

MARVELD3	Rabbit (polyclonal)	WB: 1 µg/mL IF: 2 µg/mL	Sc-102018	Santa Cruz Biotech, UK
MYPT1	Rabbit (polyclonal)	WB: 1 µg/mL	Sc-25618	Santa Cruz Biotech, UK
Occludin	Rabbit (polyclonal)	WB: 1 µg/mL IF: 5 µg/mL	Ab31721	Abcam, UK
Occludin	Mouse (monoclonal)	IF: 2 µg/mL	Sc-133255	Santa Cruz Biotech, UK
Phospho-MLC (Ser19)	Rabbit (polyclonal)	WB: 1 µg/mL	3671	Cell Signalling Technologies, UK
PP1β	Mouse (monoclonal)	WB: 1 µg/mL	sc-365678	Santa Cruz Biotech, UK
Total MLC	Rabbit (polyclonal)	WB: 1 µg/mL	Ab79935	Abcam, UK
Tricellulin	Rabbit (polyclonal)	WB: 1 µg/mL IF: 2 µg/mL	48-8400	Invitrogen, UK
ZO-1	Rabbit (polyclonal)	WB: 1 µg/mL IF: 2 µg/mL	40-2200	Invitrogen, UK

Table 2.7: List of primary antibodies used for western blot (WB), immunofluorescence (IF) studies

Secondary antibody	**Host species**	**Application concentration**	**Catalogue number**	**Supplier**
Alexa Fluor® 488-conjugated anti-rabbit IgG	Goat (polyclonal)	IF: 4 µg/mL	A-11008	Invitrogen, UK
Alexa Fluor® 546-conjugated anti-mouse IgG	Donkey (polyclonal)	IF: 4 µg/mL	A-10036	Invitrogen, UK
IRDye® 800CW anti-goat IgG	Donkey (polyclonal)	WB: 1 µg/mL	926-32214	LI-COR, UK

IRDye® 680CW anti-rabbit IgG	Donkey (polyclonal)	WB: 1 µg/mL	926-68073	LI-COR, UK
IRDye® 680CW anti-mouse IgG	Donkey (polyclonal)	WB: 1 µg/mL	926-68072	LI-COR, UK

Chapter 3 : Validation of PIP 640 peptide function *in vitro*

Chapter 3

3.1. Background

Peptide therapeutics have become an increasingly popular type of medication because of their efficient target selectivity and potency [143]. Therefore, the development of peptide-based medications has increased in the global drug market over the last decade [143, 144]. Currently, most of the available peptide therapeutics are only administered parentally by injection [143]. This route of administration usually requires frequent and high dosing with expensive materials and is considered inconvenient for patients [145]. Hence, enabling other routes of administrating therapeutic peptides, such as oral, pulmonary and intranasal, would provide more options to improve the medication's targeting efficiency and patient acceptability. The pharmaceutical industry considers the oral route of administration the desired method for peptide therapeutics [116, 145]. This is probably because of the remarkable acceptance and preference for oral dosage forms. Methods to improve outcomes of such oral dosage forms have benefited from enteric coatings that would provide protection of therapeutic peptides during transit through the harsh environment of the stomach to allow biologically active materials to reach the intestinal lumen where they might be absorbed [13, 116]. However, such oral dosage form-related strategies do not address the ultimate barrier to oral delivery of a peptide therapeutic: restriction of these materials to cross the single layer of epithelial cells that line the intestinal lumen [146].

Most previous efforts to overcome this epithelial barrier were focused on developing or modifying the functional properties of the intestinal epithelium. For example, agents known to enhance drug permeability, such as sodium caprate that function by altering the intestinal epithelial cell-cell contacts, have been co-administered with peptide drugs. The main challenge with this approach is that, in such cases, there is a great deal of uncertainty as to the mechanism of action (MoA) for such permeation enhancing agents [5]. Moreover, the application of some technologies, for example, nanoparticles, have shown benefit for protecting peptide therapeutics from gastric and

intestinal degradation and improving the ability to cross the intestinal epithelial cells [116]. However, the safety of this delivery technology is still controversial and appears to again lack a clear MoA [116]. Therefore, it seems essential to focus on approaches to improve the absorption of peptide therapeutics that might be facilitated by known MoA for alteration of epithelial barrier properties. By taking such an approach where a specific MoA is used, a clear strategy or safety assessment can be planned to optimize a rapid and logical strategy to clinical studies.

Under certain physiological and pathological conditions, TJ structure and thus barrier properties can be modulated to increase paracellular permeability [147]. This is primarily mediated by the reversible phosphorylation of myosin light chain (MLC) protein at the serine 19 of the protein (MLC-pS^{19}); a phosphorylation state controlled by the interplay of a specific kinase (MLCK) and a specific phosphatase (MLCP) [147, 148]. MLCK enzyme contains a pseudosubstrate region that acts as an auto-inhibitory domain, with activation of kinase in epithelial cells being induced by the action of the Ca^{2+} binding protein calmodulin (CaM) [149]. Increased cytosolic Ca^{2+} levels lead to the formation of Ca^{2+}/CaM complexes, which in turn bind to MLCK and interrupt the auto-inhibition caused by its pseudosubstrate domain. As a result, Ca^{2+}/CaM binding causes MLCK activation, allows it to selectively induce MLC-pS^{19} and trigger contraction of TJ-associated actomyosin filaments and enhance TJ permeability [147, 149]. This process is reversed by MLCP, a trimeric protein complex composed of protein phosphatase 1-δ (PP1-δ), a myosin targeting subunit-1 (MYPT-1) and a 20 kDa accessory subunit [91, 150]. Dephosphorylation of MLC-pS^{19} by MLCP is strictly dependent on the binding of PP1-δ to the MYPT1 subunit, because PP1 is a ubiquitous enzyme that has various functions determined by its binding to different regulatory proteins [151-153]. In addition to MLCP components, a protein kinase-C (PKC) dependent protein inhibitor called C-kinase potentiated protein phosphatase-1 inhibitor-17 kDa (CPI-17) has been identified as a specific inhibitor of MLCP [148, 154].

Chapter 3

Previous data have shown that reducing the level of MLC-pS^{19} with a membrane-permeant peptide, called PIK peptide that was designed to mimic the inhibitory domain of MLCK, repaired TJ barrier dysfunction associated with some intestinal inflammatory diseases by closing TJs opened by the action of pro-inflammatory cytokines [53, 103, 129]. By adopting a similar principle to PIK peptide design, membrane permeant peptide inhibitors of MLCP (PIP) were designed to selectively inhibit MLCP to transiently increase MLC-pS^{19} levels to enhance paracellular permeability so that the transient permeability of therapeutic peptide could be briefly increased across intestinal epithelial cells [127]. This was done by synthesizing small peptides targeting interfacial surfaces where PP1 interacts with the MLCP regulatory subunits MYPT-1 or CPI-17 [91, 155, 156].

Two candidates for PIP peptides were identified; PIP 250 (rrfkvktkkrk-NH_2) and PIP 640 (rrdykvevrrkkr-NH_2), which were designed to emulate binding events between PP1 to MYPT1 and interactions between CPI-17 and the MLCP holoenzyme, respectively [127]. Both PIP peptides were able to increase 4 kDa dextran flux across Caco-2 monolayers *in vitro* and also enhance insulin permeability into blood circulation *in vivo* (with bioavailability of 3-4%), as detected in a rat portal vein after direct intestinal loop injection [127]. The PIP 640 peptide induced a more dynamic response (rapid onset and fast recovery of TJ permeability) on Caco-2 cell monolayers *in vitro* compared to the PIP 250 peptide [127]. These results of PIP peptide-mediated enhancement of solute permeability were consistent with the time course observed for increased MLC-pS^{19} levels [127].

Manipulation of MLC-pS^{19} levels is a mechanism used in intestinal epithelial cells to transiently enhance TJ permeability. Work performed in this chapter was focused on increasing our understanding of MoA of the PIP 640

peptide with regard to this endogenous pathway. Moreover, the work in this chapter aimed to characterize the functional properties of the PIP 640 peptide and examine the impact of amino acid changes to the peptide on its action *in vitro*. Finally, toxicity associated with the PIP 640 peptide was examined *in vitro* to estimate the safe application of PIP peptides as a permeability enhancer for poorly absorbed peptide drugs.

3.2. Results

3.2.1. Rationale for PIP 640 peptide design

Abundant data support the role of PKC-mediated phosphorylation of a threonine residue at amino acid position 38 (pT^{38}) of CPI-17 in converting this protein into a potent inhibitor selective for MLCP (*90, 148*). Both *in-silico* simulation and *in-vitro* binding assessments indicate that pT^{38}-CPI-17 binds to both MLCP elements PP1:MYPT1 (*156, 157*). This binding of pT^{38}-CPI-17 to MLCP, which is responsible for the inhibitory function of CPI-17, is mediated by the sequence $R^{36}V(pT)VKYDRR^{44}$ of CPI-17 (*148, 155*). Therefore, a peptide mimicking this CPI-17 sequence was designed to inhibit MLCP and, in turn, increase MLC-pS^{19} levels to enhance TJ permeability, since MLCP inhibition by CPI-17 enhances MLC-pS^{19} (*92*). Because the ultimate application of this peptide will involve delivery to the intestinal lumen, some strategies to limit its rapid digestion are required to provide a reasonable chance of it working in an *in vivo* setting. This was achieved by using the D-retro inverso strategy (*158*). The carboxylic acid at the peptide C-terminus was replaced with a primary amide for two reasons: to stabilize the peptide against carboxypeptidase (*129*), and to mask the negative charge on the C-terminus carboxylic acid for better permeability enhancement. Moreover, an additional basic amino acid, arginine (R), was added at the N-terminus of the PIP 640 peptide to enhance its potential cell-penetrating peptide (CPP)-like properties (*159*). The pT^{38} was substituted with glutamic acid (E) as a stable phosphomimetic analogue of pT^{38} (*148*). Accordingly, a lead candidate, PIP 640 peptide = H_2N-rrdykvevrr-NH_2, was identified (a summary of modifications on the PIP 640 peptide design are in Table 3.1).

Table 3.1: A summary of the cumulative modifications on the emulated pT^{38}-CPI-17 sequence, $R^{36}V(pT)VKYDRR^{44}$, are highlighted in red. Lower case letters indicate the use of D-amino acids. (v = D-valine: k = D-lysine: y = D-tyrosine: d = D-aspartic acid).

Modification	Sequence
Original emulated sequence	NH_2-RVpTVKYDRR-OH
Introducing stable phosphomimetic analogues	NH_2-RVEVKYDRR-OH
Integrating basic amino acids	NH_2-RRVEVKYDRR-OH
D-retro inverso strategy	NH_2-rrdykvevrr-OH
C-terminus amidation	NH_2-rrdykvevrr-NH_2
Parent PIP 640 peptide	NH_2-rrdykvevrr-NH_2

3.2.2. Experimental design to explore the PIP 640 peptide MoA *in vitro*

The PIP 640 peptide was designed to selectively emulate the protein-protein interactions between CPI-17, and the MLCP protein complex, PP1-δ: MYPT-1, with the ultimate aim of inhibiting MLCP to transiently enhance TJ permeability. Because our previous work involved an *in vivo* investigation of PIP 640 peptide-induced permeability enhancement across rat intestinal epithelia, a longer version of PIP 640 peptide with three additional basic resides on the C-terminus, sequence: rrdykvevrrkkr-NH_2, was used to ensure faster cell permeability because the peptide residence time in the intestinal lumen is variable [127]. Therefore, in the current work several lines of effort were made to further refine our understanding of the MoA of the parent PIP 640 peptide, sequence (Table 3.1).

First, an optimal PIP 640 peptide concentration for modulation of epithelial barrier function was determined using the human colorectal adenocarcinoma cell line, Caco-2, grown as confluent monolayers on a semi-permeable support *in vitro*. The PIP 640 peptide was applied to the apical surface, and the change in trans-epithelial electrical resistance (TEER) was monitored over time. As a measure of the change in solute permeability, the apical to basal movement of 4 kDa and 70 kDa fluorescent dextrans was also followed over the same 60 min time course. Caco-2 monolayer recovery from the actions of the PIP 640 peptide was determined by replacement of the apical media with fresh DMEM medium, then measurement of TEER values once again after an overnight incubation.

These studies showed that exposure of Caco-2 monolayers to 10 mM of PIP 640 peptide caused a rapid, significant decrease in TEER values to approximately 20 % of their original value (Figure 3.1 A). This response was dose-dependent, with 5 mM peptide showing a lesser effect on Caco-2 monolayer TEER values compared to 10 mM (Figure 3.1 A). With both 5 mM and 10 mM concentrations, PIP 640 peptide significantly enhanced the flux of both 4 and 70 kDa fluorescent dextrans, the extent of 70 kDa fluorescent dextran transport enhancement by 5 mM peptide being less that that observed for 10 mM treatment (Figure 3.1 B). PIP 640 peptide at a 1 mM apical concentration induced about a 30% reduction in TEER of Caco-2 monolayers upon 60 min exposure (Figure 3.1 A). This reduction in TEER was enough to increase the cumulative flux of only the 4 kDa dextran over 60 min (Figure 3.1 B).

Overnight recovery after 60 min of apical exposure to different concentrations of PIP 640 peptide showed a dose-dependent outcome with monolayers treated with 10 mM and 5 mM showing incomplete TEER recovery, whereas cell monolayers treated with 1 mM achieved almost complete TEER recovery (Figure 3.1 A). Since the basolateral levels of the PIP 640 peptide after 60 min were not measured, it is possible that a reservoir

of PIP 640 peptide could have remained in the Caco-2 monolayers treated with 5 mM and 10 mM after apical media replacement that remained above the concentration to reduce TEER values after an overnight 'washout' that occurred by the same MoA as the initial actions occurring after apical addition. These results supported the use of 1 mM in future *in vitro* studies using Caco-2 cell monolayers to assess the reversible function of PIP 640 peptide and supported the use of changes in the permeability of 4 kDa dextran to characterize its action.

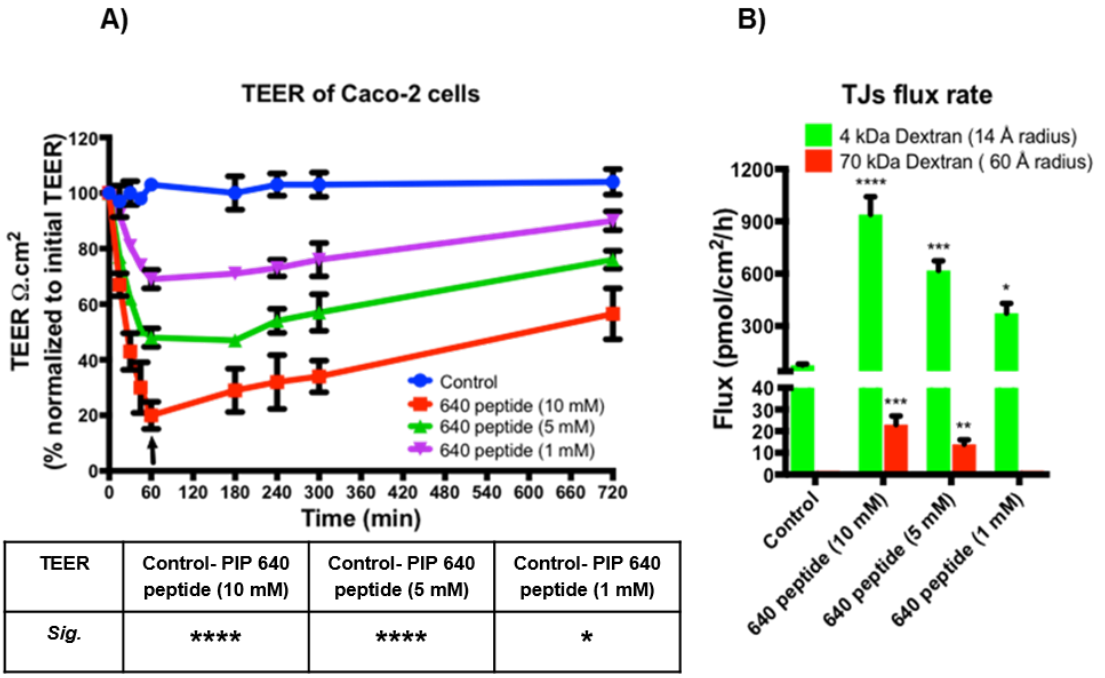

TEER	Control- PIP 640 peptide (10 mM)	Control- PIP 640 peptide (5 mM)	Control- PIP 640 peptide (1 mM)
Sig.	****	****	*

Figure 3.1: Dose-dependent effect of PIP 640 peptide on Caco-2 cell monolayer trans-epithelial electrical resistance (TEER) and permeability properties. **A)** PIP 640 peptide was applied apically at the concentration shown for 60 min, at which time the apical media was replaced with fresh DMEM media lacking PIP 640 peptide (arrow). TEER values were continued to be monitored over the next 12 h to assess functional recovery of the epithelium. **B)** Cumulative apical to basal flux rate of fluorescent dextran (4 and 70 kDa) across Caco-2 cell monolayers measured over 60 min of apical exposure at different concentrations of PIP 640 peptide. For both experiments, values represent means ± SEM of 3 independent experiments; n= 9 for control and 10 mM PIP 640 peptide; n= 6 for PIP 640 peptide at both 5 and 1 mM (**p* value< 0.05, ***p* value< 0.01, ****p* value<0.001 and *****p* value<0.0001).

3.2.3. Validation of PIP 640 peptide functional properties *in vitro*

Studies examining the concentration-dependent effect of PIP 640 peptide suggested that 1 mM of this peptide was sufficient to induce reversible permeation-enhancing actions. The second question that was now asked involved variation of amino acids in the peptide to look for potential modifications to the peptide sequence that might optimize PIP 640 peptide function. To do this, different analogues of PIP 640 peptide were synthesised that replaced specific amino acids with the D-isomer of alanine (a). Sites for this amino acid exchange were selected to ask specific question regarding the cell penetration and CPI-17-mediated actions of the PIP 640 peptide (Table 3.2). These PIP 640 peptide analogues were examined *in vitro* using Caco-2 cell monolayers for their ability to increase MLC-pS[19] levels, decrease TEER, and enhance the permeability of 4 and 70 kDa dextrans. Studies examined the actions of these PIP 640 peptide analogues after a 60 min exposure and functional recovery overnight after washout of the apical compartment.

Table 3.2: Summary of PIP 640 peptide analogue sequences and the aspect being tested. Modifications to the original PIP 640 peptide sequence are shown in red.

Peptide analogues	Sequence	Tested aspect	Analytical characterization
PIP 640 peptide (original)	rrdykvevrr-NH_2	--------	Appendices (Section 7.1 A)
PIP 641 peptide	rrdykv**a**vrr-NH_2	Phosphomimetic	Appendices (Section 7.1 B)
PIP 642 peptide	rrd**a**kvevrr-NH_2	Tyr role	Appendices (Section 7.1 C)
PIP 643 peptide	rr**a**ykvevrr-NH_2	Asp role	Appendices (Section 7.1 D)
PIP 644 peptide	rr**r**ykvevrr-NH_2	Increase in +ve charge	Appendices (Section 7.1 E)

Chapter 3

The parent PIP 640 peptide was designed rationally based upon published structural information regarding binding of CPI-17 to MLCP, an interface that include a threonine at position 38 that must be phosphorylated (pT^{38}) for optimal CPI-17 inhibitory function [154, 156, 157]. To test the phosphomimetic role of D-glutamic acid (e) residue to replace (pT^{38}) in the PIP 640 peptide, the e residue was replaced with a D-alanine (a), resulting in a peptide termed PIP 641 (Table 3.2). An apical exposure to 1 mM of PIP 641 peptide for 60 min showed no significant effect on TEER or dextran flux (Figure 3.2 A and B). These findings validated the role of glutamic acid as a phosphomimetic analogue for pT, and was consistent with the essential role of this structural feature in the PIP 640 peptide.

A previous study showed that certain amino acid residues surrounding the pT^{38}, primarily a tyrosine three residues away, are essential for pT^{38}-CPI-17 targeting to MLCP because replacement of this residue with alanine in the CPI-17 protein eliminated its inhibitory effect [155]. Hence, the PIP 642 peptide where the tyrosine residue (y) was replaced with alanine (a) was synthesized to study the impact of this change on PIP 640 peptide function (Table 3.2). Consistent with the previous study performed on the full-length CPI-17 [155], this substitution eliminated peptide-mediated effects on TEER and dextran flux (Figure 3.2 A and B).

Since the PIP 640 peptide must cross the plasma membrane to reach its intracellular target of MLCP for its desired actions on epithelium to occur, we wished to examine the potential role of specific positive charges in the peptide that had been included to increase its CPP-like character. Exchange of negatively-charged aspartic acid (d) in the PIP 640 peptide with alanine (a) resulted in the PIP 643 peptide (Table 3.2). Apical exposure of Caco-2 monolayers to 1 mM of PIP 643 peptide showed a significant reduction of TEER value, but although this analogue appeared to be slightly less potent

compared to the PIP 640 peptide at the same concentration (Figure 3.2 A). The difference in TEER reduction was not statistically significant (Figure 3.2 A). However, the effect of the PIP 643 peptide on the flux of 4 kDa dextran was only about 50 % of that induced by PIP 640 peptide (Figure 3.2 B). Despite the reduced flux rate observed with the PIP 643 peptide, these results indicated that PIP 640 peptide could function to some extent in the absence of the aspartic acid residue.

After demonstrating that the aspartic acid residue of the PIP 640 peptide was not absolutely required for its actions on Caco-2 cell monolayers, the question of whether this residue in the peptide could be replaced with a positive charge was investigated. The goal here was to determine whether increasing the net positive charge of the PIP 640 peptide could improve its cell penetration properties and hence lower the concentration needed. The PIP 644 peptide was therefore synthesized where the d residue of the PIP 640 peptide was replaced with the D-isomer of arginine (r) (Table 3.2). Apical application of 1 mM PIP 644 peptide to Caco-2 monolayers showed a stronger effect on TEER reduction and a reduced overnight recovery compared to the PIP 640 peptide (Figure 3.2 A). PIP 644 peptide also produced an approximately 3-fold increase in 4 kDa flux rate compared to the PIP 640 peptide, and a significant increase in the cumulative flux of 70 kDa dextran over 60 min, an action that was not observed with the rest of the PIP 640 peptide analogues (Figure 3.2 B).

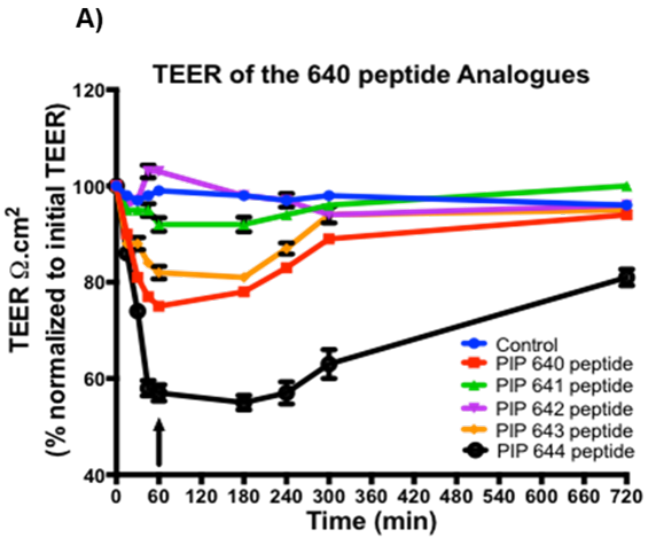

TEER	*Sig.*	TEER contrast	*Sig.*
Control- PIP 640 peptide	*	PIP 640 peptide- PIP 641 peptide	**
Control- PIP 641 peptide	n.s	PIP 640 peptide- PIP 642 peptide	*
Control- PIP 642 peptide	n.s	PIP 640peptide- PIP 643 peptide	n.s
Control- PIP 643 peptide	*	PIP 640 peptide- PIP 644 peptide	*
Control- PIP 644 peptide	**	----------	----

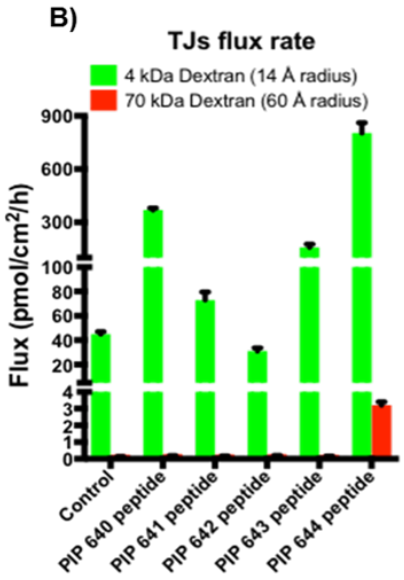

Flux	*Sig.* 4 kDa	*Sig.* 70 kDa	Flux contrast	*Sig.* 4 kDa	*Sig.* 70 kDa
Control- PIP 640 peptide	****	n.s	PIP 640 peptide- PIP 641 peptide	****	n.s
Control- PIP 641 peptide	n.s	n.s	PIP 640 peptide- PIP 642 peptide	****	n.s
Control- PIP 642 peptide	n.s	n.s	PIP 640peptide- PIP 643 peptide	****	n.s
Control- PIP 643 peptide	***	n.s	PIP 640 peptide- PIP 644 peptide	****	****
Control- PIP 644 peptide	****	****	----------	----	----

Figure 3.2: Effect of selected amino acid replacement on PIP 640 peptide actions. **A)** Caco-2 cell monolayers TEER change induced by 1 mM of PIP 640 peptide were compared to that induced by a series of analogues. Apical media was replaced with fresh DMEM medium after 60 min to allow examination of TEER recovery (arrow). **B)** Cumulative apical to basal flux rate of fluorescent 4 and 70 kDa dextran across Caco-2 cell monolayers after 60 min of apical exposure of the PIP 640 peptide and the analogues noted in (A). All peptides were tested in 3 independent experiments, with all analogues being tested in parallel with the PIP 640 peptide and control (untreated cells). Data are means ± SEM; n= 24 for control, n=18 for PIP 640 peptide; n= 8 for PIP 643 peptide; and n= 6 for PIP 641, PIP 642 and PIP 644 peptides. (*p value< 0.05, **p value< 0.01, ***p value<0.001 and ****p value< 0.0001). n.s: not significant.

The data on *in vitro* examination of different PIP 640 peptide analogues presented above probed the role of selected amino acids on the PIP 640 peptide sequence with respect to its presumed function in emulating the actions of the CPI-17 protein. The action of this peptide is based upon its potential to mimic the properties of pT^{38}-CPI-17. If this were true, the decrease in TEER and increase in solute permeability induced by the PIP 640 peptide should correlate with increased MLC-pS^{19} levels that would lead to TJ barrier relaxation by inhibiting MLCP [160, 161]. To address this hypothesis, a time course immunoblotting analysis was conducted to monitor the change in MLC-pS^{19} levels induced by PIP 640 peptide analogues on Caco-2 monolayers. Apical addition of 1 mM PIP 640 peptide showed that the MLC-pS^{19} level relative to total MLC increased within 15 min and remained at an increased level at 45 min (Figure 3.3 A and B). This observation correlated well with the previously described effect of PIP 640 peptide on Caco-2 monolayers TEER (Figure 3.2 A).

Neither the PIP 641 peptide nor the PIP 642 peptide, when tested at 1 mM concentration showed any significant effect on MLC-pS^{19} relative to total MLC (Figure 3.3 A and B), consistent with their lack of effect on TEER (Figure 3.2 A). Although, TEER changes observed for Caco-2 monolayers treated apically with 1 mM of either PIP 640 peptide or PIP 643 peptides were statistically similar (Figure 3.2 A), there was a slower onset of action in changing MLC-pS^{19} relative to total MLC for the PIP 643 peptide compared to the PIP 640 peptide (Figure 3.3 A and B). This delay in the change of the MLC-pS^{19} levels might explain the reduced dextran flux rate obtained with the PIP 643 peptide (Figure 3.2 B). Interestingly, both the PIP 644 and PIP 640 peptides showed a similar onset and intensity of the increase in MLC-pS^{19} compared to total MLC (Figure 3.3 A and B). Assuming that the actions of both peptides are comparable for mimicking CPI-17 function and there is a maximal response in this Caco-2 monolayers system for inducing MLC-pS^{19} relative to total MLC, this finding with the PIP 644 peptide could be explained by improved CPP-like

properties that allows more peptide to enter the cells more rapidly and to be retained in the cell longer compared to the PIP 640 peptide. Thus, its effective activity may look more like 10 mM PIP 640 peptide. Alternately, the activity of the PIP 644 peptide could reflect effects on other cellular pathways that are additional to its presumed inhibitory action on MLCP.

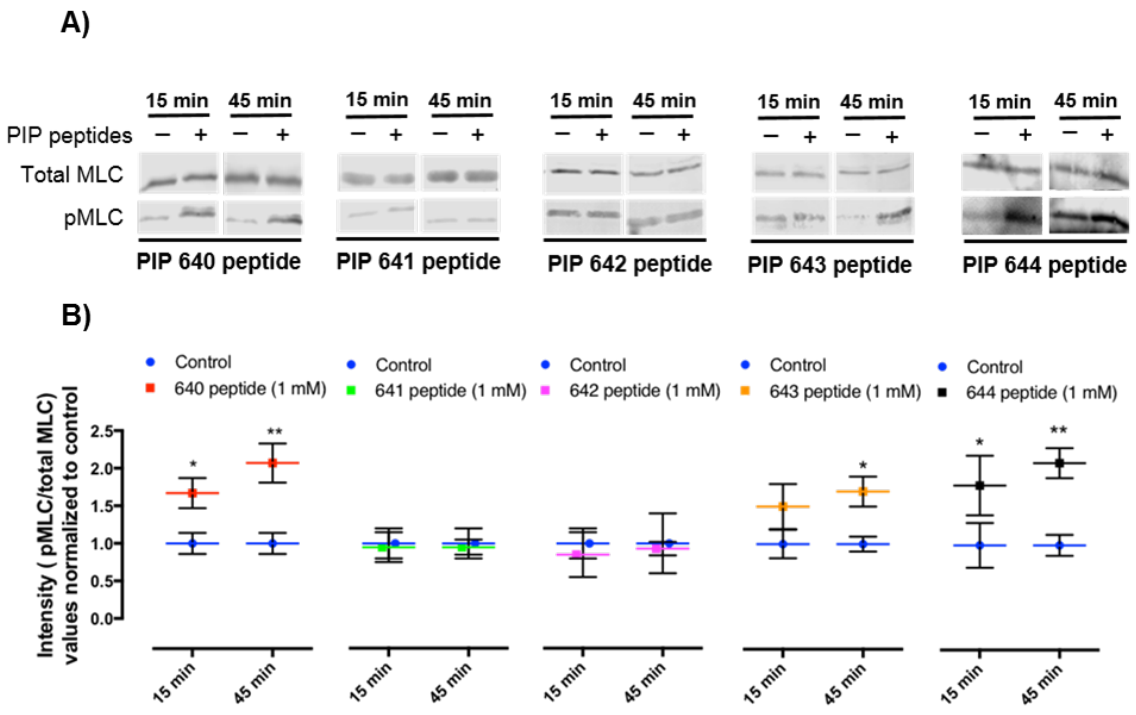

Figure 3.3: Effect of the PIP 640 peptide and selected peptide analogues on MLC-pS[19] levels in Caco-2 monolayers 15 and 45 min after 1 mM apical addition. **A)** Immunoblot assessment of MLC-pS19 compared to total MLC levels. **B)** Quantitative analysis of MLC-pS[19] and MLC levels for immunoblots shown in A). Data represent means ± SEM of independent experiments; PIP 640 peptide (n=4); all PIP 640 peptide analogues (n= 3). (*p value< 0.05, **p value< 0.01).

3.2.4. Intracellular fate of PIP 640 peptide analogues

PIP 640 peptide analogues induced reduction of Caco-2 monolayer TEER values and enhanced paracellular flux of dextran in a manner that correlated with increased MLC-pS^{19} levels. These actions are presumed to occur by inhibiting MLCP that, in turn, alters the function of the actomyosin microfilaments surrounding TJs. A critical aspect in the design of the PIP 640 peptide was to integrate CPP-like elements that would allow it to pass across a cell membrane barrier to reach the cytoplasm and interact with MLCP involved in regulating TJ function. The data described above, showing enhanced levels of MLC-pS^{19} is consistent with this hypothesis. In order to explore this issue further, the PIP 640 peptide and the selected PIP peptide analogues 641, 642, 643, and 644 were synthesized with a N-terminal biotin residue to allow microscopic investigation of these peptides' ability to cross the cell membrane and distribute within the cell at perijunctional actomyosin microfilaments where the phosphorylation of MLC at this location is known to regulate TJ permeability (*103*). Localization of biotin-labelled peptides (analytical characterization in Appendices Section 7.1 F-J) was assessed by immunofluorescence microscopy using fluorophore-labelled streptavidin. Cellular distribution of these N-terminally biotinylated peptides was coordinated with immunofluorescent labelling of TJ protein occludin.

Cell penetration and intracellular distribution of the biotinylated PIP peptides was examined 45 min after the apical addition to Caco-2 monolayers after repeated washing to remove surface-associated peptide, fixation and membrane permeabilization (Figure 3.4 and Figure 3.5). The 45 min time point was a time for which all functional PIP peptides (PIP 640, PIP 643 and PIP 644) showed significant alteration of the amount of MLC-pS^{19} relative to MLC (Figure 3.3 A and B). Biotinylated PIP 640 peptide was located intracellularly and often in close proximity to membrane demonstrated by occludin labelling (Figure 3. 4). This observation is consistent with the hypothesis that the PIP 640 peptide acts on MLCP present at TJ structures to

increase levels of MLC-pS^{19} that then act to modify TJ permeability properties (Figure 3.3 A and B). Similar to biotinylated PIP 640 peptide, both biotinylated PIP 641 and PIP 642 peptides were detected intracellularly, suggesting that the integrated positive residues were sufficient to impart CPP-like activity for these peptides (Figure 3.4). However, both peptides showed random distribution within the cytoplasm rather than localization to the plasma membrane, supporting the premise that the glutamic acid (to emulate a pT residue) and adjacent tyrosine residue are both important for PIP 640 peptide targeting to plasma membrane. It should be noted that in a few cells, the biotinylated PIP 642 peptide aligned along the plasma membrane without co-localization with TJ structures as identified by occludin immunofluorescence.

Biotinylated PIP 643 peptide showed some similarity in cellular distribution to the PIP 640 peptide, but there seemed to be qualitatively less of this peptide associated with the perijunctional areas compared to biotinylated PIP 640 peptide (Figure 3.4). This observation correlated nicely with the slower onset of increased MLC-pS^{19} levels observed with PIP 643 peptide after 15 min of exposure (Figure 3.3 A and B). Moreover, the observed distribution of biotinylated PIP 643 peptide indicated that replacing the aspartic acid residue with an alanine might have reduced the ability of the biotinylated peptide to efficiently engage with MLCP localized to TJ structures. Importantly, removal of the negative charge associated with this amino acid did not dramatically alter its ability to access the cytoplasm but did reduce its ability to target and/or be retained at TJ structures relative to the biotinylated PIP 640 peptide.

Enhancing the net positive charge of the PIP 640 peptide was achieved by substituting the aspartic acid with an arginine in the biotinylated PIP 644 peptide. This peptide showed an intracellular distribution that was distinct from all of the other biotinylated peptide examined: there was an alignment to the plasma membrane, but there was little if any co-localization with occludin that

defined TJ structures (Figure 3.4). Also, the biotinylated PIP 644 peptide was observed to localize at a distinct distance from the plasma membrane as occasionally observed for the biotinylated PIP 642 peptide. Uniquely, the biotinylated PIP 644 peptide was organized in what appeared to be aggregate clusters that were not observed for any of the other biotinylated peptides. This altered intracellular distribution may provide insights into the stronger action of the PIP 644 peptide on TEER reduction and enhanced 70 kDa dextran flux compared to the PIP 640 peptide (Figure 2 A and B). The results could suggest a more intense action on MLCP that results in disorganization of structures typically present at TJs, or that the PIP 644 peptide may engage some cellular structure that organizes at a discrete distance from the plasma membrane.

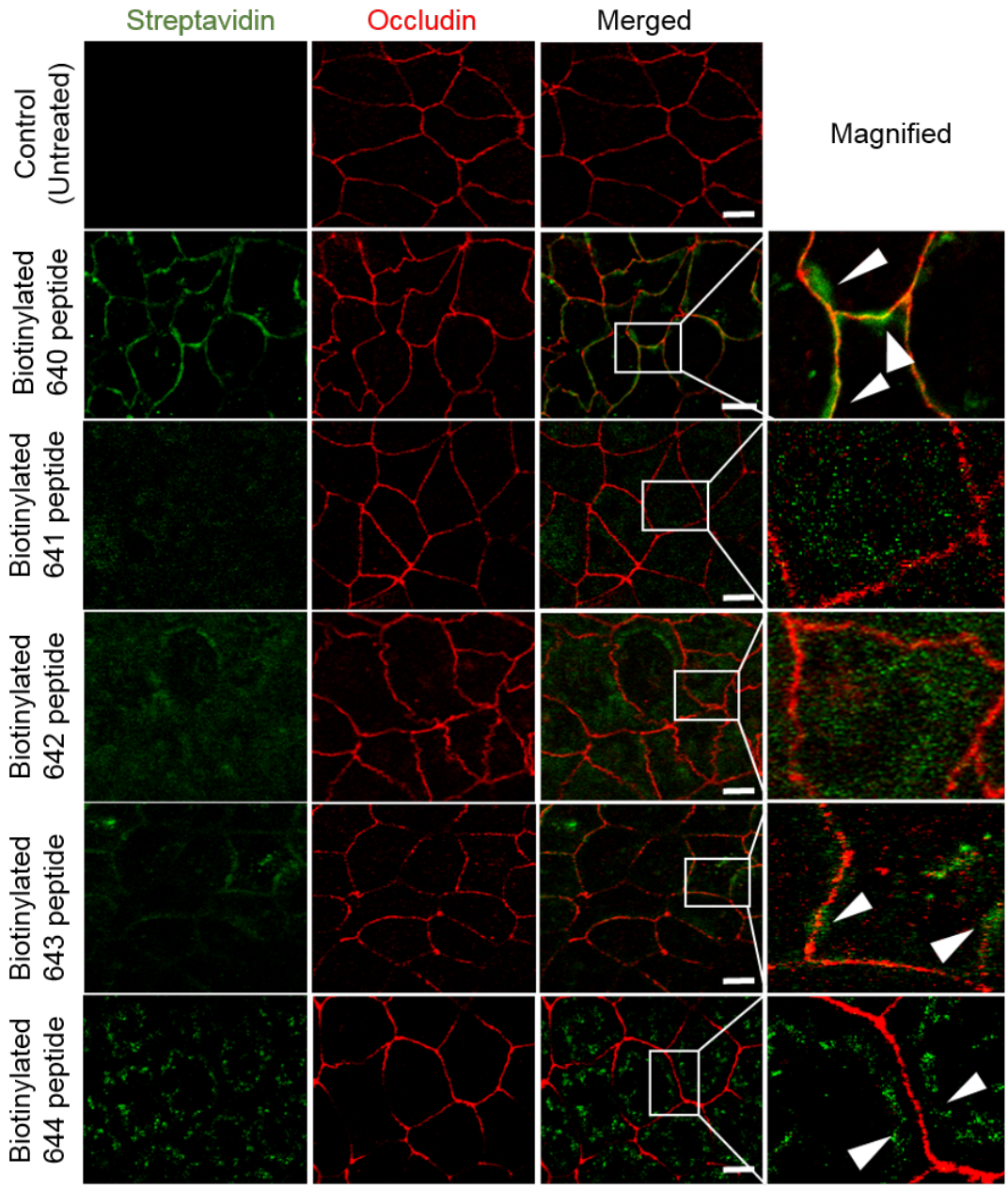

Figure 3.4: Confocal microscopy images of Caco-2 monolayers showing the intracellular distribution of N-terminally biotinylated PIP 640 peptide and analogues 45 min after apical exposure. The first column from the left represents the distribution of of the PIP 640 peptide analogues, as detected by Alexa 488-conjugated streptavidin (green). The second column shows cell distribution of the TJ-associated protein occludin stained with Alexa 546-conjugated secondary antibody against a primary antibody (red). The third column represents merged images showing co-localization of the PIP 640 peptide and analogues with occludin. The last column to the right shows magnified images of the areas highlighted by the white boxes. The arrows show PIP peptide co-localization profile with TJs. Scale bar, 10 μm. Images are representative of 3 independent experments, with n= 3 for all peptides.

A Z-stack analysis (XZ-plane) of Caco-2 cell monolayers treated with biotinylated PIP 640 peptide and its analogues confirmed their intracellular localization suggested in the xy-plane images (Figure 3.5).

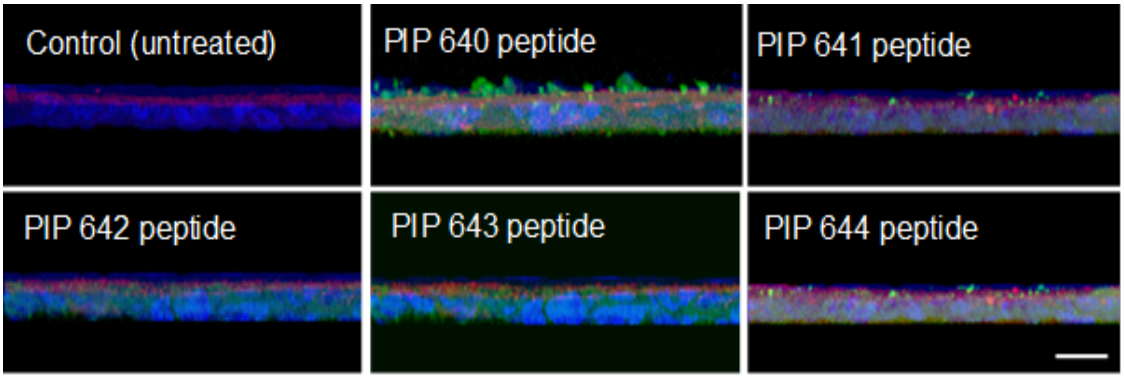

Figure 3.5: Z-stack scan images of Caco-2 monolayers obtained by confocal micorscopy, showing surface and subcellular localization of N-terminally biotinylated PIP 640 peptide analogues after 45 min of apical exposure. PIP 640 peptide or an analogue was detected using by Alexa 488-conjugated streptavidin (green). TJs were stained with Alexa 546-conjugated secondary antibody against occludin primary antibody (red). Nuclei were stained with DAPI (blue). Scale bar, 20 µm. Images are representative of 3 independent experments with n=3 for all peptides.

A C-terminally biotinylated version of PIP 640 peptide was also prepared that contained a polyethylene glycol (PEG) spacer between the peptide and the biotin unit: PIP 640 peptide-PEG-biotin (analytical characterization in Appendices Section 7.1 K). Interestingly, PIP 640 peptide-PEG-biotin behaved differently from the N-terminally biotinylated version, and was associated predominantly with the cell membrane surface (appendices, Figure 7.2 A and B), unlike the N-terminally labelled 640 peptide (Figure 3.5). Moreover, PIP 640-PEG-biotin produced no significant change in Caco-2 monolayers TEER (appendices, Figure 7.2 C). This behaviour supports the suggestion that PIP 640 peptide-PEG-biotin was not able to access the cytoplasm. However, it was not clear whether the lack of cell permeability of PIP 640 peptide-PEG-biotin occurred as a result of changing the location of the biotin label from the N-terminus to the C-terminus or because of changing the physiochemical properties of the peptide by adding a PEG spacer.

3.2.5. PIP 640 peptide functions by blocking MLCP

The studies described above validated the membrane permeability property of the PIP 640 peptide and showed its potential to selectively localize at TJ structures. Such outcomes are consistent with its proposed action on MLCP through a specific, physical association with regulatory subunits (PP1:MYPT1). We further examined this possible interaction using a pull-down protocol with the N-terminally biotinylated version of the PIP 640 peptide as bait under non-denaturing conditions to capture protein binding partners from Caco-2 cell lysates using streptavidin beads. However, despite several attempts using slightly different conditions, neither PP1 nor MYPT1 could be shown to associate with biotinylated PIP 640 peptide (Figure 3.6 A).

Native polyacrylamide gel electrophoresis (PAGE) was employed next to assess the effect of the PIP 640 peptide on the MLCP complex, MYPT1:PP1. This technique has been used extensively to study changes in protein association within protein complexes [162, 163]. In this study, the PIP 640 peptide was incubated with Caco-2 cell lysates under non-denaturing conditions for 60 min prior to analysing with native PAGE. The intensity of detected protein bands on the native PAGE reflects the amount of non-associated MYPT1 and PP1, since under native PAGE conditions individual proteins migrate faster than when they are assembled into a complexes. Under native PAGE conditions, MYPT1 was observed to migrate faster in the gel than PP1 even though MYPT1 has a larger molecular weight than PP1. MYPT1 was detected at ~45 kDa, while PP1 was detected at ~75 kDa relative to protein standard markers (Figure 3.6 B). These findings were consistent with the surface charge properties of these proteins that would have greatly affected their mobility in an electric field [91]. Incubating Caco-2 cell lysates with PIP 640 peptide showed a concentration-dependent reduction of the non-associated PP1 and MYPT1 (Figure 3.6 B). This result supports the contention that PIP 640 peptide function involves binding to both MYPT1 and PP1, similar to the emulated binding site of pT^{38}-CPI-17 that binds to both regulatory subunits of MLCP and blocks its function [90].

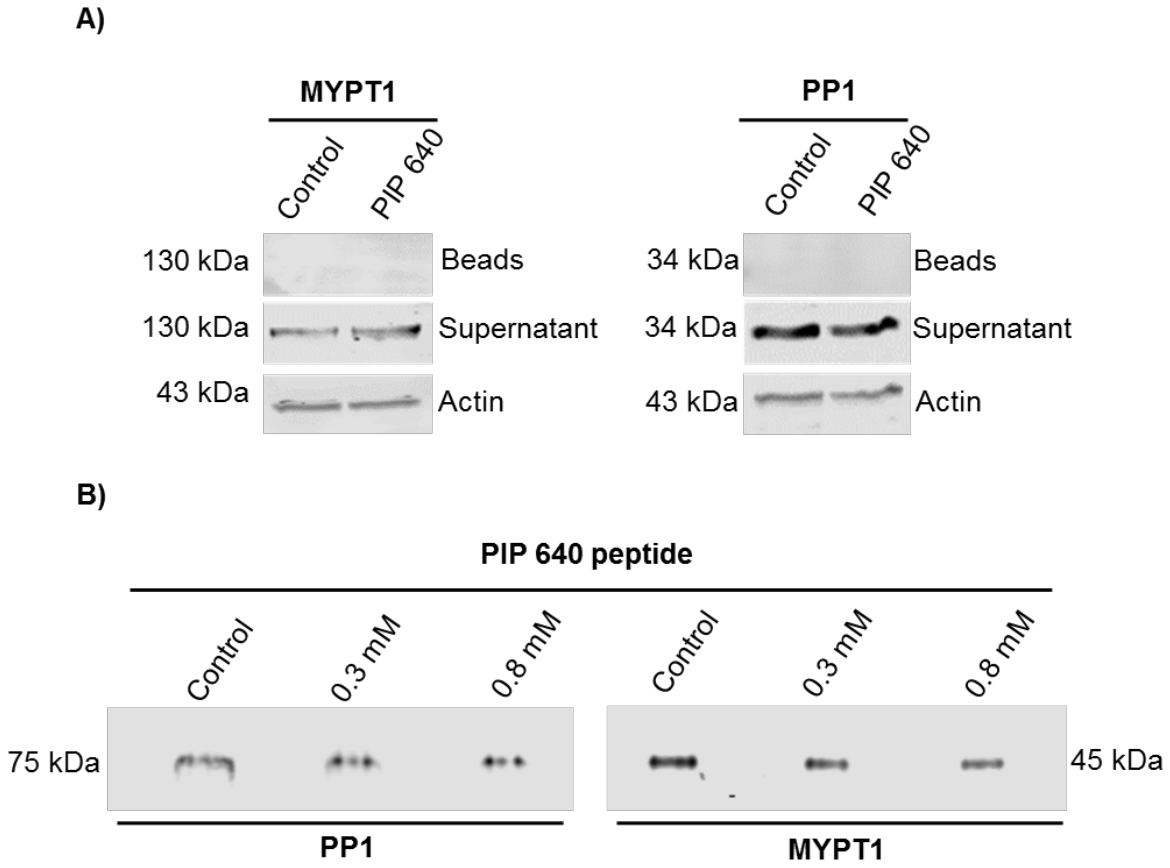

Figure 3.6: A) SDS-immunoblot of MLCP protein components, PP1 and MYPT1, from Caco-2 cell lysates analyzed in a pull-down using biotinylated PIP 640 peptide. No association of these MLCP components with PIP 640 peptide was observed. Actin loading controls were used from supernatants to normalise the amount of lysate probed. Control lanes are streptavidin beads incubated in Caco-2 cell lysates in the absence of biotinylated PIP 640 peptide. Data are representative of 3 independent experiments, n=3. **B)** Immunoblot of MLCP components present in Caco-2 cell lysates treated with different concentrations of PIP 640 peptide for 60 min. Under these native polyacrylamide gel electrophorisis conditions PP1, which has MW of 34 kDa, was detected at ~ 75 kDa and MYPT1, which has a MW of 130 kDa, was detected at ~45 kDa. Data are representative of 2 independent experiments, n=2.

As the anticipated function of the PIP 640 peptide appears to involve binding both regulatory subunits of MLCP, the same method involving native PAGE was applied to explore the impact of sequence modifications in the PIP 640 peptide analoges on binding to MLCP subunits PP1 and MYPT1. Both PIP 641 and 642 peptides failed to interact with either PP1 or MYPT1 under the conditions used (Figure 3.7 A and B), being consistant with their lack of effect on MLC-pS^{19} levels and random distribution in polarized Caco-2 cells. PIP 643 peptide showed a slightly greater interaction with PP1, but a loss of interaction with MYPT1 compared to PIP 640 peptide (Figure 3.7 A and B). This shift in specificity for PP1 over MYPT1 was even greater in the case of PIP 644 peptide (Figure 3.7 A and B). Data obtained with PIP 643 and PIP 644 peptides demonstrated that the loss of negative charge presented by the aspartic acid residue was important for interaction with MYPT1 but supressed its interactions with PP1. Additionally, changing this residue in the peptide from a negative or neutral amino acid to a positively-charged amino acid further enhanced its activity towards PP1 without affecting the loss of MYPT1 interactions. These observations were consistent with the changing in PIP 644 peptide cellular localization from TJ structures to locations adjacent to the plasma membrane. Thus, while possibly improving the CPP-like characateristics for the PIP 643 and PIP 644 peptide, changes made to the PIP 640 peptide sequence to generate these analogues also resulted in loss of selectivity for MYPT1 and shifted it towards PP1, which would likely results in action not related to CPI-17-regulated processes. These studies demonstrated that only the PIP 640 peptide bound to both PP1 and MYPT1 (Figure 3.7 A and B), suggesting an ability to interact with MLCP.

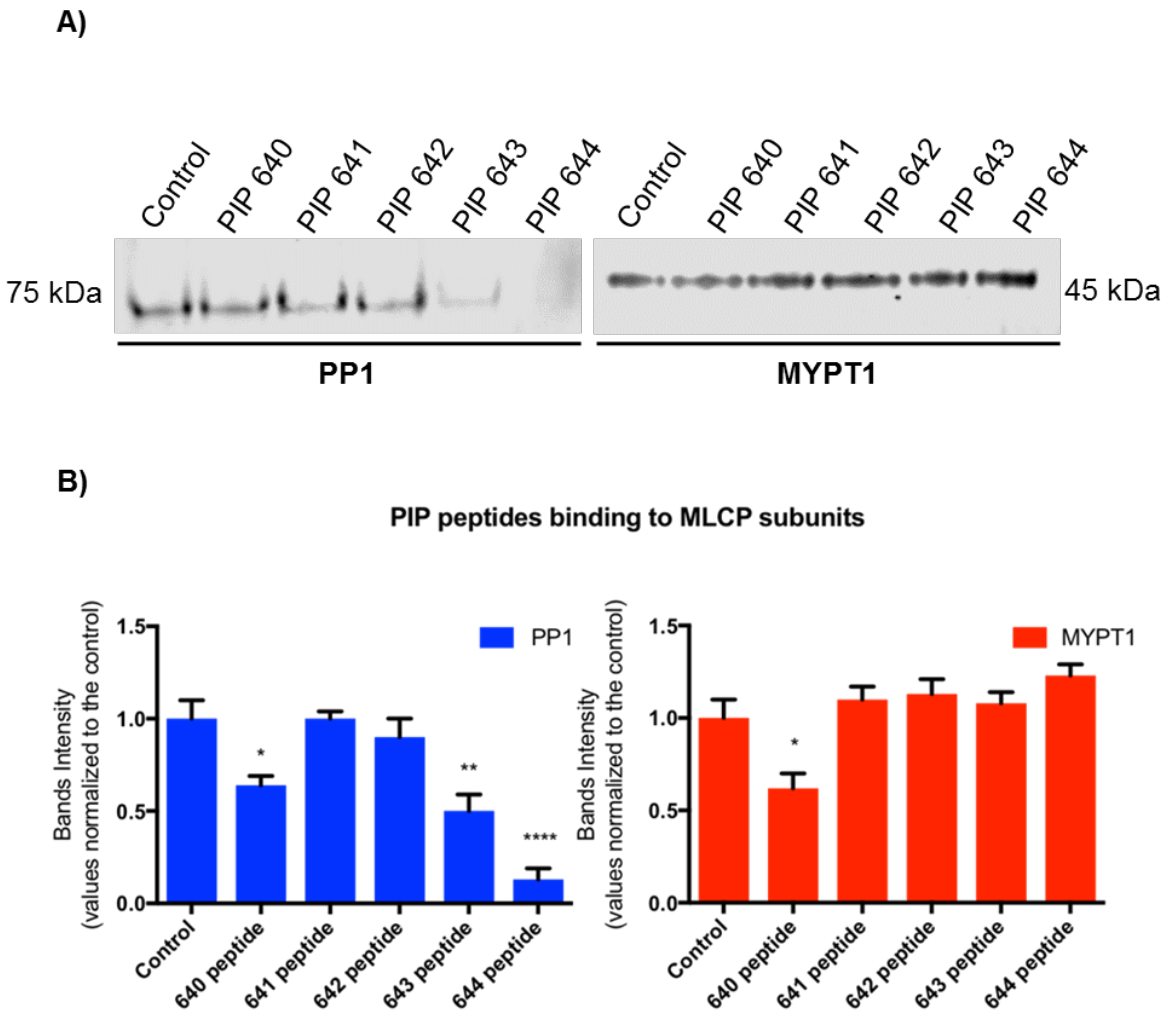

Figure 3.7: Binding of PIP 640 peptide or PIP 640 peptide analogues with MLCP components. Peptides (0.8 mM) were incubated with Caco-2 cell lysates for 60 min prior to analysing using native PAGE. Quantitative determination of capture (depicted as removal from the lysate) for **A)** PP1 and **B)** MYPT1. Data are representative of 4 independent experiments, n=4 for all data. Quantitative analysis of the immunoblots obtained in (A) induced by PIP 640 peptide analogues. Data are means ± SEM of 4 independent experiments, n=4 for all data. (*p value< 0.05, **p value< 0.01, ****p value< 0.0001).

3.2.6. PIP 640 peptide effects on epithelial cell viability

All *in-vitro* data presented above suggested that the PIP 640 peptide could regulate TEER and paracellular permeability properties of Caco-2 monolayers by enhancing MLC-pS^{19} through a blockadge of MLCP function. These effects were either eliminated or altered by mutating specific amino acids in the PIP 640 peptide sequence. Washout of these peptides after 60 min of apical exposure showed that all tested PIP peptides that demonstrate these properties did so through a reversible mechanism (Figure 3.2 A). Such studies however, failed to address the question of whether these peptides and/or the actions they induce interfered with cell viability. To test this possibility, Caco-2 cell viability was investigated by measuring 3-(4,5-dimethylthiazol-2-yl)-5-(3-carboxymethoxyphenyl)-2-(4-sulfophenyl)-2H tetrazolium (MTS) dye conversion to formazan in viable cells. This so-called MTS assay reflects the integrity of the cells' metabolic activity. The formazan that is formed has an intense purple colour, which is proportional to cell viability. All tested PIP peptides were incubated with Caco-2 cells for 12 h prior to adding the MTS reagent. Triton X-100 was used as a positive control to induce cell death, resulting in cell viability levels less than 10 % (Figure 3.8). PIP 640, PIP 641 and PIP 642 peptides showed no significant interference with Caco-2 cell viability compared to untreated cells (Figure 3.8). This indicates that the permeability enhancement function of the PIP 640 peptide occurred without inducing cell toxicity. A lack of effect on cell viability also suggested that these PIP 640 peptide analogues, while retaining their ability to enter cells (Figure 3.4 and Figure 3.5) but having lost their ability to affect Caco-2 cell monolayer TEER and permeability properties (Figure 3.2 A and B), are harmless to epithelial cells. In contrast, PIP 643 and PIP 644 peptides, which showed an ability to enhance permeability (Figure 3.2 A and B), reduced Caco-2 cell viability to approximately 50 % of control values (Figure 3.8). This might occurred in response to shifting the specificity of these two peptides toward PP1 (Figure 3.7 A and B), possibly resulting in the activation of signalling pathways involved in cell viability.

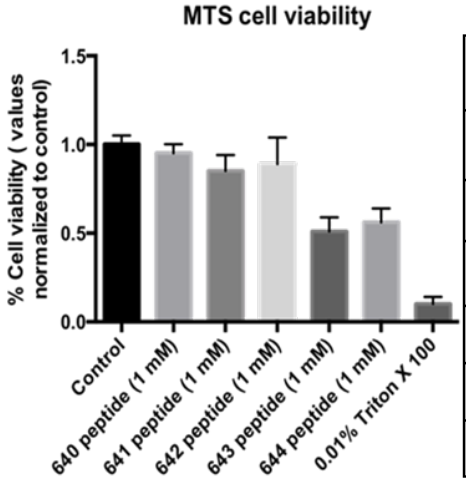

Cell viability contrast	*Sig.*	Cell viability contrast	*Sig.*
Control- 640 peptide	n.s	640 peptide- 641 peptide	n.s
Control- 641 peptide	n.s	640 peptide- 642 peptide	n.s
Control- 642 peptide	n.s	640 peptide- 643 peptide	*
Control- 643 peptide	*	640 peptide- 644 peptide	*
Control- 644 peptide	*	640 peptide- Triton X 100	****
Control- Triton X 100	****	----------	-----

Figure 3.8: Colorimetric cell viability assessments of Caco-2 cells after 12 h exposure to 1 mM of each PIP 640 peptide or PIP 640 peptide analogues as evaluated by MTS dye conversion by cells. Here, Triton x-100 (0.01%) was used as a positive control. Data are means ± SEM of 3 independent experiments, n=9 for all data. (**p* value< 0.05, *****p* value< 0.0001). n.s: not significant.

3.3. Discussion

Oral delivery of peptide therapeutics is typically limited by their sensitivity to intestinal digestive enzymes. Even when strategies are taken to limit this degradation, the physicochemical properties of these molecules restrict their ability to cross the intestinal epithelial barrier [164]. Previous efforts to overcome these issues were mainly focused on the use of agents that alter the barrier function as a means to enhance intestinal permeability [5]. Accordingly, several oral therapeutic peptide formulations have now reached clinical trial stages [117], however, most of these peptide therapeutic formulations failed to make it past the trial stages [117]. In most of these permeability enhancers (PEs), this lack of clinical success is due to unacceptable safety concerns that can be linked to uncertainties regarding a lack of a selective and well-understood MoA [5]. For example, sodium caprate, is a medium chain fatty acid that has been used as a PE in many therapeutic peptide formulations. Studies have proposed that sodium caprate enhances permeability through transcellular routes by general disruption of cell membranes [165]. Other studies suggest that permeability enhancement associated with sodium caprate occurs through paracellular routes by activating MLCK [120], or by redistributing claudin-5 and tricellulin proteins [57]. The lack of clear MoA for sodium caprate could be the reason why its clinical use in a rectal ampicillin suppository was associated with non-specific damage to the rectal mucosa in humans [166].

In the current approach, we have attempted to address the unmet need for the development of an efficient and safe strategy to enhance the permeability of therapeutic peptides across intestinal epithelium. This was done by utilizing rationally designed agents targeting an intracellular mechanism that is naturally involved in transiently regulating the TJ barrier function of the intestinal epithelium associated with enhancing nutrient uptake through paracellular routes [88, 167]. This mechanism of enhancing paracellular permeability of nutrients is mediated by increasing MLC-pS^{19} levels that are induced by activating MLCK by Na^+-nutrient co-transport [88, 168]. It is well

established that manipulating MLC phosphorylation could regulate TJ barrier function. This was first observed with the application of a permeable inhibitor of MLCK (PIK) peptide that was reported to be effective in rectifying the defective TJ barrier function associated with chronic epithelial inflammations that are characterized by leaky epithelia generated by hyper-activation of MLCK (*53, 103, 129*). Recently, we utilized an approach similar to that used to design the PIK peptide to design selective membrane permeant inhibitors for MLCP termed PIP, to transiently open intestinal TJs and enhance the uptake of therapeutic peptides (*127*).

Two PIP peptides, termed 250 and 640, were designed to target different protein-protein interfacial sites that regulate MLCP function. These two peptides were shown to enhance paracellular permeability of insulin *in vivo* (*127*). Their permeability enhancement effect was consistent with transient action induced by increasing MLC-pS^{19}, as this effect was reversed within a few minutes (*127*). Because PIP 640 showed better onset and recovery of paracellular permeability enhancement compared to PIP 250 peptide (*127*), the work in this chapter was aimed at refining the understanding of the PIP 640 peptide MoA *in vitro* and exploring the possibility of optimizing its permeability enhancement function.

PIP 640 peptide was designed to mimic a phosphorylated binding site of CPI-17, R^{36}V(pT)VKYDRR^{44}, which is responsible for selective inhibition of MLCP (*90, 148, 160*). A D-retro inverso strategy was used to produce an enzymatically stable version of the PIP 640 peptide; the peptide was synthesised using D-amino acids in reverse order of sequence (*158*). Thus, orientation of the amino acid side chains of the D-sequences would be similar to the parent L-sequences, though the amide bonds are inverted. This strategy was validated previously for enhancing PIK peptide stability without affecting its targeting ability to MLCK (*129*). PIP 640 peptide was synthesized using

standard 9-fluorenylmethyloxycarbonyl (Fmoc) solid phase peptide synthesis (SPPS) techniques [128]. This technique involves repetitive coupling of amino acids to a growing polypeptide chain bound to a solid support. This solid support is typically composed of small polystyrene beads to which the peptide is attached during the repetitive washing and filtration steps of these processes. The first amino acid is generally bound to the resin through its α-carboxylic acid function, via an ester or amide linkage, depending on the choice of the solid support and desired C-terminal functional group [128]. For synthesis of PIP 640 peptide and its analogues, a Rink amide polystyrene resin was chosen in order to generate a C-terminal peptide amines upon removal of the final peptide from the solid support. In the Fmoc SPPS approach, the α-amino functions of the amino acids that are added successively to the N-terminus of the peptide are blocked by the base-sensitive Fmoc group, which is easily removed by a secondary amine (piperidine) [128]. For synthesis of the PIP 640 peptide and analogues, any side chain amino acid functions were blocked by appropriate acid-labile protecting groups that are stable to the repetitive removal of Fmoc during each coupling cycle. Acid-labile side chain protecting groups were used for lysine (Boc), arginine (Pbf), tyrosine (tBu), glutamic acid and aspartic acid (OtBu), which could all be removed under the same conditions as those required for cleaving the final peptide from the Rink Amide support with a strong acid [128]. Introduction of a glutamic acid residue into the PIP 640 peptide was intended to serve as a stable phosphomimetic analogue of pT because the length of a glutamic acid side chain is similar to pT, allowing for a delocalized negative charge from the ionized carboxylic acid at about the same position as the phosphate group on the side chain of pT. Previous structural studies of pT^{38}-CPI-17 have suggested that the flanking residues of pT^{38} within the $R^{36}V(pT)VKYDRR^{44}$ sequence, except R^{36} and K^{40}, of CPI-17 are involved in binding to MLCP [155-157, 169]. However, Y^{41} seemed to be critical for the inhibitory function of CPI-17, as single alanine substitution to Y^{41} was able to abolish pT^{38}-CPI-17 inhibitory function. Therefore, a single arginine was introduced onto the N-terminus of the PIP 640 peptide sequence to enhance its cell permeability properties

because residues located N-terminally to R^{36} have been reported not to be involved in CPI-17 binding to MLCP (*155*).

Previous *in vivo* studies of PIP 640 peptide functions were focused on proving the concept of the ability of the PIP 640 peptide to enhance paracellular permeability of therapeutic peptides by increasing MLC-pS^{19} levels (*127*). An essential consideration for successful *in vivo* application of the PIP 640 peptide was the onset of peptide cell entry to rapidly increase MLC-pS^{19} and enhance the permeability of a poorly absorbed therapeutic agent in the intestinal lumen. In order to potentially increase the rate of cell uptake of the PIP 640 peptide, a longer version with three additional basic amino acids on the C-terminus was used *in vivo*, sequence: rrdykvevrrkkr-NH_2 (*127*). This longer version of the PIP 640 peptide induced rapid paracellular permeability of insulin across intestinal epithelia by enhancing MLC-pS^{19} that started a few minutes after direct intraluminal injection. Since work in this chapter was to investigate PIP 640 peptide MoA, studies were performed using the parent sequence of PIP 640 peptide, rrdykvevrr-NH_2, which has only one additional arginine at the N-terminus that is not present in the original emulated sequence of CPI-17, R^{36}V(pT)VKYDRR^{44}. This can be used for a more precise assessment of PIP 640 peptide target binding and to potentially reduce the ultimate cost of peptide production if this compound were to be used therapeutically.

An initial step in exploring the MoA of PIP 640 peptide was to define the ideal concentration of the peptide that can induce a regulated TJ permeability to be used in the *in vitro* investigations. This eliminated the possibility that any activity observed with the PIP 640 peptide was due to exposure to high concentrations of the peptide. This was monitored by measuring TEER change and apical to basolateral transport of molecules across epithelial cell monolayers induced by different concentrations of the PIP 640 peptide. Varied sizes of fluorescent dextran, 4 kDa (hydrodynamic radius ~ 14 Å) and 70 kDa

(hydrodynamic radius ~ 60 Å), were used in the permeability assays to estimate the extent of TJ opening. In this regard, insulin has a hydrodynamic radius of ~11 Å, while leaky TJs associated with chronic intestinal inflammatory diseases have been shown to be permeable to macromolecules up to ~ 60 Å [53, 54]. The data in (Figure 3.1 A and B) indicated that 1 mM of PIP 640 peptide seemed to be a realistic concentration for *in vitro* MoA investigations because the permeability of 70 kDa dextran that was observed with higher concentrations of PIP 640 peptide was eliminated at 1 mM. Moreover, a complete TEER recovery of Caco-2 monolayers was only obtained with an application of 1 mM of the PIP 640 peptide.

Manipulating specific phosphatase complexes using small peptides has been a widely-used strategy to study the function of a variety of phosphatases, some of which can deliver therapeutic benefits [153, 170]. It has been reported that pT^{38}-CPI-17 can specifically inhibit MLCP and induce alteration of TJ function by enhancing MLC-pS^{19} [160, 161]. Although the PIP 640 peptide at a low concentration induced a reversible reduction of TJ barrier in Caco-2 monolayer, it was not clear whether the actions of this peptide were indeed achieved by mimicking pT^{38}-CPI-17. The PIP 640 peptide was synthesised using a D-retro inverso strategy, which have shown limited success on some occasions at mimicking the functional properties of parent L-peptides [171]. Therefore, a structure activity relationship (SAR) study was performed on the PIP 640 peptide sequence by substituting specific amino acids. The selection of the residues for these modifications was based on previous structural studies that identified critical residues within the emulated sequence of CPI-17, $R^{36}V(pT)VKYDRR^{44}$, which are essential for inhibiting MLCP. Accordingly, a limited set of PIP 640 peptide analogues were designed and examined *in vitro* to see if they could alter the function of the parent peptide.

Chapter 3

PIP 641 peptide revealed the importance of a negative charge (provided by a glutamic acid) that could function as phosphomimetic analogue of pT. Similarly, the tyrosine residue in the PIP 640 peptide seems critical for permeability enhancement function of PIP 640 peptide, as demonstrated with the PIP 642 peptide. These findings are consistent with structural characterization of pT^{38}-CPI-17 that showed the importance of these two positions for CPI-17 function [148, 155]. Moreover, these outcomes indicated that the D-retro inverso version of the PIP 640 peptide was indeed able to emulate CPI-17 function. A key consideration in optimizing the PIP 640 peptide was to improve the cell penetration function of the peptide by enhancing its net positive charge; this was accomplished by maintaining basic acids and reducing non-essential acidic residues. In this context, *in vitro* permeability enhancement data for PIP 641, sequence: rrdykvavrr-NH_2, and PIP 643, sequence: rraykvevrr-NH_2, demonstrated that the role of the negatively charged glutamic acid residue in PIP 640 peptide is more critical than that of aspartic acid (Figure 3.2 A and B) (Figure 3.3 A and B). Exchange of the negative charge of the aspartic acid for a positive charge to possibly improve the cell permeability properties as in PIP 644 peptide increased the extent of MLC-pS^{19} induction compared to the PIP 640 peptide, but it also dramatically altered the intracellular localization and altered its selectivity between PP1 and MYPT1. This may indicate the possible involvement of other cellular pathways being accessed by the PIP 644 peptide versus the PIP 640 peptide and refines our understanding of how to selectively inhibit MLCP to increase the intestinal paracellular permeability of therapeutic peptide drugs with these compounds.

Since altering specific amino acids in the PIP 640 peptide sequence was associated with changes to permeability enhancement function, as represented by the tested PIP 640 peptide analogues, biotinylated versions of PIP 640 peptide analogues were used to explore the role of these specific mutations on PIP 640 peptide cell penetration properties and to see how the different functions of these peptides could be associated with their intracellular

distribution. Initially, biotin labelling was performed using Fmoc-PEG-biotin resin that produces a C-terminally biotinylated peptide with PEG spacer between the peptide and biotin unit. The use of this labelling technique was expected to be advantageous for a variety of reasons: having a hydrophilic spacer, the PEG chain, should enhance the peptide's water solubility, improve its efficiency in binding assays by separating the biotin functionality from peptide residues that are involved in target binding and, more practically, simplify the synthesis because the biotinylated peptide would be obtained immediately after the cleavage from the solid phase resin [130, 131]. Although this method of biotin labelling has been validated by previously studies involved the intracellular localization of peptides [130], C-terminally biotinylated PIP 640 peptide, PIP 640-PEG-biotin peptide, seemed to be associated with the cell membrane surface instead of entering Caco-2 cells, resulting in an elimination of the permeability enhancement function of the PIP 640 peptide itself (Appendices, Figure 3.2 A-C). It has been reported previously that changing the coupling site of the same cargo may have a significant effect on the cell penetration properties of CPP peptides [172]. Interestingly, when the PIP 640 peptide and its analogues were biotinylated at the N-terminus, using the p-nitrophenyl ester derivative of biotin, all the peptides obtained were able to cross cell membrane (Figures 3.4 and 3.5). The precise reason for the different behaviour of C- and N- terminally labelled PIP 640 peptide is not clear, however, the nature of the spacer between the biotin labels and the peptides in the two cases are quite different, and this may also be significant as well as the point of attachment.

Immunofluorescent images showed that the PIP 640 peptide was localized at the perijunctional areas, an observation consistent with its action of enhancing MLC-pS[19]. Similar to the outcomes obtained in the previous SAR study, removal of either Glu or Tyr in PIP 641 and PIP 642 peptides, respectively, changed their cellular distribution. In an attempt to improve PIP 640 peptide cell penetration properties to optimize its function, PIP 643 was

synthesized with less negatively charged residues, and this showed a substantial loss of the perijunctional distribution obtained with the PIP 640 peptide. Increasing the net positive charge of the PIP 640 peptide by switching Asp to Arg in the PIP 644 peptide shifted the peptide distribution back toward the perijunctional areas in a cluster format that was less associated to TJ compared to the PIP 640 peptide. Overall, data from immunofluorescent images indicate that the probed residues within PIP 640 peptide including Glu, Tyr and Asp are essential for evoking PIP 640 peptide permeability enhancement function.

MYPT1 binding to PP1 generates the MLCP holoenzyme that specifically functions to dephosphorylate MLC-pS^{19} (*91, 153*). Phosphorylation of CPI-17 at pT^{38} enables it to selectively form a complex with MLCP to block its phosphatase function (*90*). Studies characterizing the nature of pT^{38}-CPI-17 binding to MLCP have suggested that a minimal inhibitory domain within CP-17 is essential for recognition of MLCP, which includes R^{36}V(pT)VKYDRR^{44} (*155, 156, 169*). Since PIP 640 was designed to mimic this sequence, we addressed the ability of PIP 640 peptide to bind MLCP. This was performed using native PAGE immunoblotting because it has been shown that native PAGE can be used to anticipate changes in protein complex bindings (*162, 163*). Unlike SDS-PAGE, protein migration in native PAGE depends on both hydrodynamic size and charge of the protein involved. This means that protein complexes would migrate slowly or not enter the native gel. Under the experimental conditions employed, the PIP 640 peptide showed a concentration-dependant association with both the MLCP components, MYPT1 and PP1 (Figure 3.6 B), which is consistent with the binding pattern of pT^{38}-CPI-17 with MLCP. The intensity of the migrating bands of both MYPT1 and PP1 did not change with either the PIP 641 or PIP 642 peptides indicating that these peptides did not bind to MLCP, an observation consistent with their inability to enhance MLC-pS^{19} (Figure 3.3 A and B). A previous study suggested that the emulated sequence of pT^{38}-CPI-17, R^{36}V(pT)VKYDRR^{44},

binds to the MYPT1 subunit of the MLCP complex via Arg^{44} [156]. However, removal of the negatively charged Asp residue in PIP 643 peptide shifted its binding towards PP1, and the effect was further increased by introducing Arg in this position in the PIP 644 peptide (Figure 3.7 A and B). These findings show that Asp might be essential for PIP 640 peptide binding to the MYPT1 subunit of MLCP complex; this probably applies to CPI-17. Although only the PIP 640 peptide seems to associate with both regulatory subunits of MLCP in native PAGE, it was not clear whether the data obtained from native gel experiments represent an absolute effect of the PIP 640 peptide on MLCP, as other cellular proteins present in the cell lysates still might contribute to PIP 640 peptide binding to MLCP regulatory subunits under native PAGE conditions.

Native PAGE immunoblotting data indicated that the different permeability enhancement profiles between the PIP 640 peptide and several analogues of this peptide (Figure 3.2 A and B) could be correlated to differences in binding nature to MLCP components (Figure 3.7 A and B). Indeed, loss of the ability to enhance TJ permeability by PIP 641 and PIP 642 peptides correlated with their inability to induce MLC-pS^{19} (Figure 3.3 A and B). PIP 643 and PIP 644 peptides, however, both retained the ability to decrease TEER and enhance paracellular permeability and this was correlated with a retained ability to induce MLC-pS^{19} (Figure 3.3 A and B). There was no strong correlation between the ability of these peptides to alter TJ permeability and their binding pattern with MLCP compared to the PIP 640 peptide (Figure 3.2 A and B) (Figure 3.7 A and B), as the PIP 643 and PIP 644 peptides showed similar or stronger TEER reduction, respectively, compared to the PIP 640 peptide but showed more association to PP1 instead of MYPT1. This shift in PIP 643 and PIP 644 binding towards PP1 suggested that they acquired greater non-specific PP1 inhibitory function that might have involved MLC-pS^{19} increases in locations of the cell not directly involving TJs.

In essence, PIP 643 and PIP 644 peptides may have acquired greater non-specific protein phosphatase inhibitory function. Such actions may be similar to okadaic acid (OA), a toxin produced by dinoflagellates that can inhibit multiple protein phosphatases including protein phosphatase 2 A (PP2A) and PP1, which is known to cause cell toxicity at high concentrations [173]. It has been reported that OA is responsible for causing diarrhetic shellfish poisoning characterized by a leaky TJ barrier, which has been suggested to be induced by sustaining phosphorylation of various proteins, including MLC-pS^{19} [173, 174]. Cell viability data of the PIP peptides tested in these studies support the idea that non-specific functions of both PIP 643 and PIP 644 peptides could be the cause of their associated cytotoxicity (Figure 3.8). This might suggest that PIP 643 and PIP 644 peptides caused general protein phosphatase inhibition that is responsible for increasing MLC-pS^{19} associated with reducing cell viability and changing permeability enhancement profiles; in particularly, the enhanced permeability of 70 kDa dextran induced by the PIP 644 peptide.

In conclusion, the present studies have provided a greater understanding of the MoA for a novel agent, PIP 640 peptide, which was designed to increase the intestinal absorption of protein therapeutics. PIP 640 peptide was designed to be stable in the intestinal lumen and access the cytoplasm of enterocytes to alter the phosphorylation state of MLC in order to transiently alter epithelial TJ barrier function. These studies characterized the permeability properties, recovery of TEER properties, intracellular localization, protein target selectivity and potential cytotoxicity for the PIP 640 peptide, but importantly examined these same properties for a selected series of PIP 640 peptide analogues. In doing so, a greater understanding has been acquired for how the PIP 640 peptide functions as a relatively safe and effective agent by enhancing MLC-pS^{19} to manipulate an endogenous mechanism regulating TJ permeability. Although the next logical step in the development of the PIP 640 peptide technology will likely be a large animal safety and efficacy study to improve the uptake of poorly absorbed peptide therapeutic, the data presented here have

characterized a series of peptides that could be used as tools by researchers interested in studying the role and function of MLCP in epithelial cells.

Chapter 4 : Characterization of tight junction opening induced by PIP 640 peptide

Chapter 4

4.1. Background

Functional integrity of the body's epithelia is essential for their ability to allow the body to maintain its homeostasis and protect it from the casual entry of unwanted and potentially dangerous materials [14]. This barrier function requires polarized epithelia to generate, maintain and regulate a set of structures organized between adjacent epithelial cells that are collectively known as the apical junctional complex (AJC) [14, 15]. The tight junction (TJ) is the most apical structural element of the AJC and it consists of protein complexes that establish a size- and charge-selective barrier that can selectively restrict the transport of ions and small molecules ~< 4 Å through the paracellular space located between adjacent epithelial cells [14, 175]. TJ structures contain many transcellular proteins that include the claudin protein family [35], junctional adhesion molecule (JAM) proteins [64] and TJ-associated Marvel proteins (TAMPs) members: occludin, tricellulin and MarvelD3 [36]. These transmembrane TJ proteins are connected to a network of peripheral scaffolding proteins, which function as adaptors connecting transmembrane TJ proteins to adjacent elements of the cell's cytoskeleton; *zonula occluden* (ZO) proteins represent a prominent family of these adaptor proteins [74].

Claudin proteins exist in at least 27 different isoforms that are naturally expressed in various patterns and combinations in different organs' epithelia, which determine the distinct properties of TJ barrier demonstrated by each epithelium of the body [176]. Distinct isoforms are primarily known to either seal (sealing claudins) or to function in the charge selective ion properties (pore-forming claudin) of the different TJs [38]. While most of the functions of claudin proteins are associated with altered permeability of ions and low molecular weight solutes. Some studies have also suggested that claudin proteins may be involved in regulating the paracellular permeability of macromolecules. It has been shown that knockout or disruption of some claudin proteins result in the enhanced passage of large solutes [26, 39, 40]. In contrast, TAMPs and ZO proteins have been closely linked to enhancement of macromolecule

permeability through TJs [36, 53, 84, 118], while JAM proteins play a role in TJ stability and immune cell migration [65, 66].

TJ proteins bind to each other through complicated interactions that have been studied using techniques such as fluorescence recovery after photobleaching (FRAP) and fluorescence loss in photobleaching (FLIP). FRAP and FLIP studies have revealed that TJ proteins are highly dynamic in the resting state, meaning that the TJ protein complex is subject to continuous remodelling. Moreover, different TJ proteins have distinct dynamic behaviours to provide a fence function that is essential for the separation of apical and basolateral domains of the plasma membrane. For example, claudin-1 was found to be less dynamic than occludin and *zonula occluden*-1 (ZO-1) [46, 95, 177]. The discovery that TJ proteins exist at AJC structures in a dynamic manner has led to the hypothesis that modulation of TJ protein components could be a mechanism by which TJ barrier function could be rapidly regulated in response to different stimuli.

In intestinal epithelia, for example, it was found that TJ pore permeability is regulated by induction of the Na^+-glucose co-transporter, which induces TJ permeability by activating myosin light chain kinase (MLCK) [88]. These events were associated with increased ZO-1 mobility without altered expression at TJ structures through a mechanism that could be reversed by inhibiting MLCK [95]. Casein kinase-2 (CK2)-mediated phosphorylation of occludin at the serine 408 (occludin-pS^{408}) increased TJ pore permeability of cations by changing TJ protein organization and dynamic behaviour of TJ elements [46]. CK2-mediated increases in occludin-pS^{408} enhanced occludin mobility at TJs and occludin dimerization, resulting in dissociation from ZO-1, claudin-1, and claudin-2 proteins [46]. These events coincide with the formation of claudin-2 pore channels between adjacent epithelial cells, which enhances TJ cation paracellular permeability [46].

Consistent with the role of altering TJ protein composition induced by different stimuli in determining barrier properties, proinflammatory cytokines such as tumour necrosis factor-α (TNF-α) and interferon-γ (INF-γ) are known to induce the loss of TJ barrier function and increase macromolecular solute permeability associated with intestinal inflammatory diseases, such as Crohn's disease [53, 103, 137]. Proinflammatory cytokine-induced TJ barrier loss is associated with occludin endocytosis induced by prolonged activation of MLCK [53, 103, 137]. Sodium caprate has been shown to function as a TJ permeability-enhancing (PE) agent, increasing paracellular permeability across the human intestinal cell line HT-29/B6 *in vitro* for dextran molecules up to 10 kDa [118]. The action(s) of sodium caprate on epithelial TJ structure, similar to proinflammatory cytokines, also affected TAMP and claudin protein family members; in this case the redistribution of tricellulin and claudin-5 were observed without a striking alteration of their cellular expression [118].

We have hypothesized that pharmacological activation of MLCK could increase TJ solute permeability to produce a transient state where paracellular permeability is sufficiently increased to provide an enhancement of therapeutic peptide absorption from the intestinal lumen. To achieve this, a membrane-permeant peptide capable of regulating myosin light chain phosphatase (MLCP) activity to induce myosin light chain phosphorylation in the serine 19 (MLC-pS^{19}) was identified through a rational design process. The results presented in Chapter 1 showed that a membrane-permeant inhibitor of MLCP (PIP), termed the PIP 640 peptide, was able to enter Caco-2 cell monolayers, co-localize with TJ structures, increase cellular MLC-pS^{19} levels, and enhance the permeability of 4 kDa dextran through the TJ. The observed co-localization of PIP 640 peptide with the TJ structures, induction of MLC phosphorylation, and changes in paracellular solute permeability properties were all consistent with the anticipated MoA for this PIP peptide.

Chapter 4

The studies performed in this chapter were aimed at providing a preliminary characterization of biochemical changes associated with TJ proteins induced by the actions of the PIP 640 peptide. With this information, we hope to increase our understanding of how TJ components involved in controlling TJ barrier function are affected by the PIP 640 peptide. Also, this work investigates the potential impact of alteration of TJ proteins induced by PIP 640 peptide on the permeability enhancement properties of TJs.

4.2. Results

4.2.1. Effect of PIP 640 peptide on TJ proteins

TJ protein structures function as gates regulating the paracellular permeability of an epithelium [38]. Studies have shown that the paracellular permeability of solutes through intestinal TJs in both physiological and pathological conditions are associated with reorganization of TJ protein complexes [53, 94, 95]. The data discussed in Chapter 1 showed that PIP 640 peptide-enhanced TJ permeability of 4 kDa dextran (hydrodynamic radius ~ 14 Å), which is unable to cross epithelial cell TJs under baseline physiological conditions [88], moved across Caco-2 cell monolayers *in vitro* in a manner consistent with increased levels of MLC-pS^{19}. However, it is not yet known whether the permeability enhancement induced by PIP 640 peptide involves alteration of TJ proteins. To address this, immunoblotting analysis of total cell lysates as well as immunofluorescent imaging of Caco-2 cell monolayers were performed to assess possible changes in the protein levels and cellular distribution of TJ protein elements in response to exposure to the PIP 640 peptide.

Initially, this work focused on studying the effect of PIP 640 peptide on the TAMP protein family and the scaffolding protein ZO-1, as these proteins are the most commonly studied TJ proteins for regulating large solute permeability through intestinal epithelial TJs [36, 53, 84, 118]. Therefore, the effect of apical exposure to 1 mM of PIP 640 peptide for 60 min on TAMPs and ZO-1 was investigated. The results of immunoblotting showed no significant changes in the cellular levels of occludin, tricellulin, MarvelD3 and ZO-1 in association with increase in MLC-pS^{19} induced by PIP 640 peptide (Figure 4.1 A and B). Further, apical PIP 640 peptide treatment of these confluent monolayers of Caco-2 cell line *in vitro* failed to demonstrate any striking changes to the cellular distribution of TAMPs and ZO-1 proteins as assessed by immunofluorescent microscopy (Figure 4.1 C). These results indicate that the

Chapter 4

PIP 640 peptide enhances the permeability of epithelial cells impermeable molecules, such as 4 kDa dextran, without interfering with TAMPs or ZO-1.

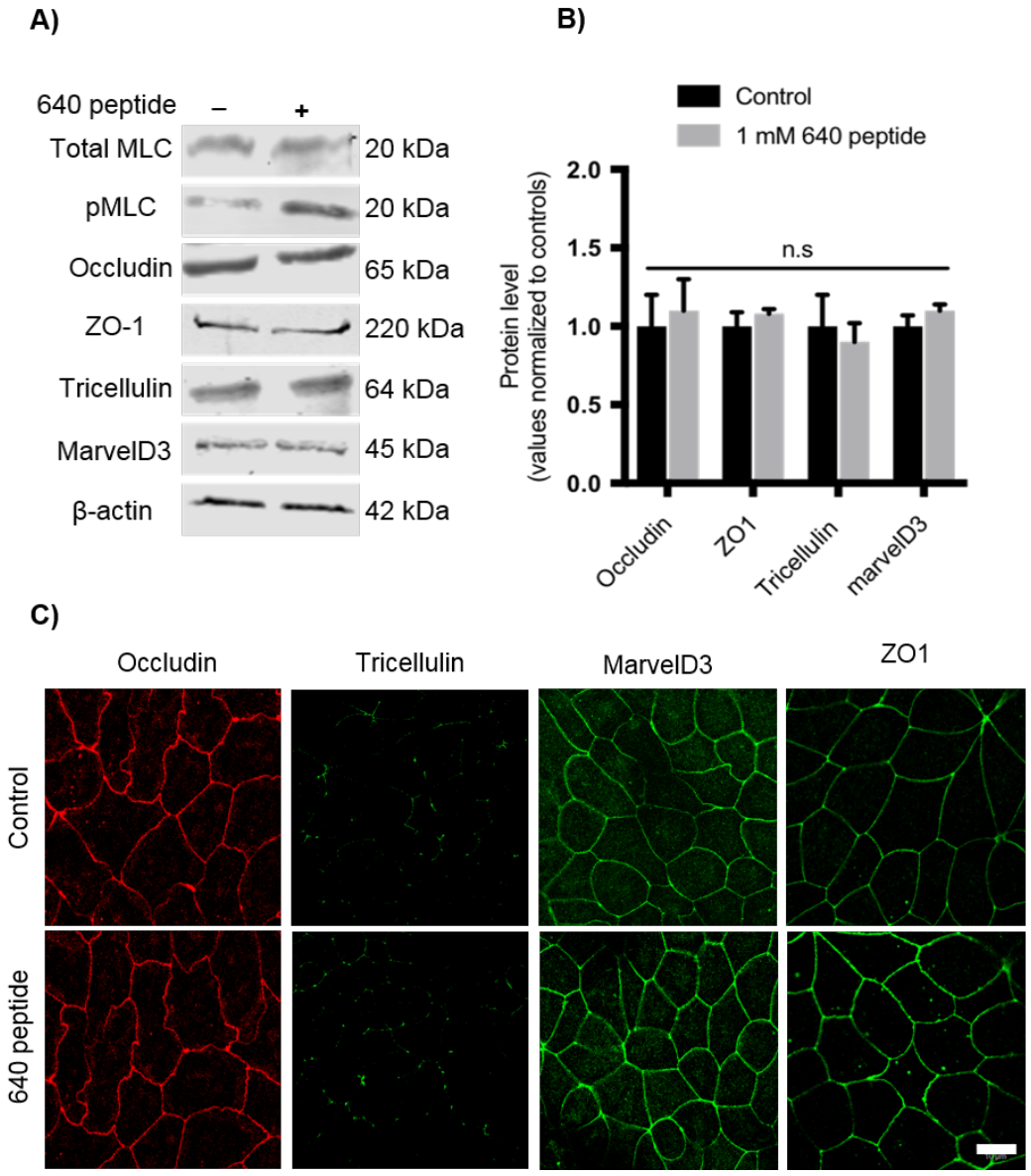

Figure 4.1: Evaluation of the changes in the cellular level and distribution of TAMPs (occludin, tricellulin, and MarvelD3) and the scaffolding protein ZO-1 induced by 1 mM of PIP 640 peptide. **A)** Immunoblotting analysis showing the effect of MLC-pS[19] induction by an apical exposure to 1 mM of PIP 640 peptide for 60 min on the cellular level of TAMPs and ZO-1 in Caco-2 cell monolayers. **B)** Quantitative analysis of the immunoblots obtained in A). Data are means ± SEM of 3 independent experiments, n=6 for control and treated monolayers. **C)** Immunofluorescent images of Caco-2 monolayers showing normal TJ localization of TAMPs and ZO-1 between monolayers treated with PIP 640 peptide and untreated monolayers. Images are representative of 3 independent experiments, n=3. Scale bar, 10 µm. n.s: not significant.

Although claudins have been recognised as paracellular ion channels [38], it is been observed in many cases that macromolecule permeability across TJ was associated with changes in the expression or distribution of distinct claudin family members [26, 39, 40]. Therefore, it is possible that the permeability enhancment function induced by PIP 640 peptide might be corelated with changes in a specific set of claudins either through changes in cellular levels and/or distribution at the TJ. To test this hypothesis, we examined polarized Caco-2 monolayers *in vitro* following a 60 min apical treatment of 1 mM PIP 640 peptide for biochemical changes and cellular distribution of claudin proteins present in human intestinal epithelial cells [176]. It is important to note that some of the tested claudins have been reported to regulate the permeability of TJ solute permeability [25, 26, 39, 118]. Examination of the total cellular protein levels of claudin-1, -2, -3, -4, -5, -7, -8 and -15 via immunoblotting analysis showed that only claudin-2 cellular levels were altered in response to the PIP 640 peptide and consistent with the increased MLC-pS^{19} levels (Figure 4.2 A and B). The observed increase in total claudin-2 cell levels observed by western blot analysis were consistent with increased levels of this protein at the plasma membrane, presumably where it had integrated into the functional TJ structure (Figure 4.3).

The immunofluorescence microscopy studies of TJ protein elements in reponse to PIP 640 peptide were performed using a similar fixation process reported in a previous study [87]. Application of the -20 °C methanol cell fixation method, which has been reported to effectively preserve intracellular localization of TJ proteins [87], provided a more refined prespective and revealed that, in untreated Caco-2 monolayers, intracellular claudin-2 was concentrated in specific regions of the cell cytoplasm, while claudin-2 was widely distributed in the cytoplasm of monolayers treated with PIP 640 peptide (Figure 4.3), an effect was not observed with TAMPs or ZO-1 (Figure 4.1 C). No significant differences were observed in the intracellular or TJ distributions of claudin-1, -4 and -7 between the treated and untreated Caco-2 cell

monolayers with the same concentration of the PIP 640 peptide within the indicated time (Figure 4.3). This observation suggests that claudin-2 was redistributed from its intracellular locations to the plasma membrane and possibly into TJ structures in response to PIP 640 peptide exposure.

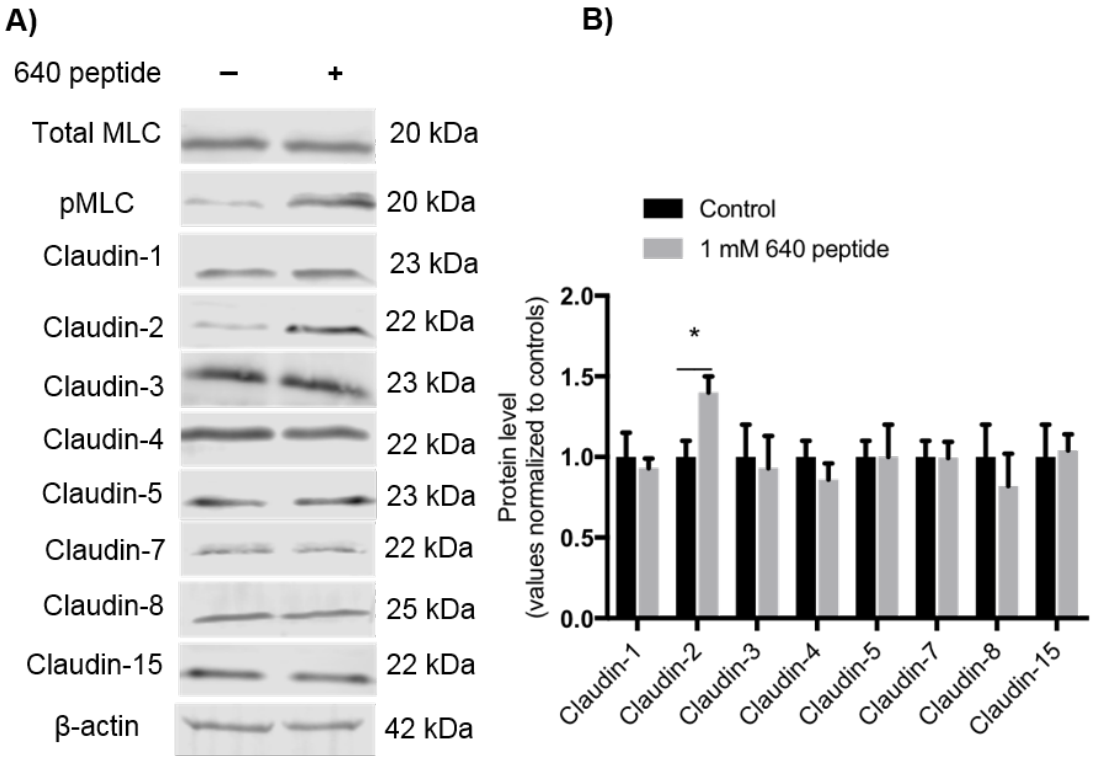

Figure 4.2: Effect of apical treatment of Caco-2 monolayers with 1 mM of PIP 640 peptide for 60 min on different claudin proteins. **A)** Immunoblotting analysis showing the effect of MLC-pS[19] induction by PIP 640 peptide on the cellular levels of claudin-1, -2, -3, -4, -5, -7, -8 and -15. **B)** Quantitative analysis of the immunoblots obtained in A). Data are means ± SEM of 3 independent experiments, n=6 for the control and treated monolayers, (**p* value< 0.05).

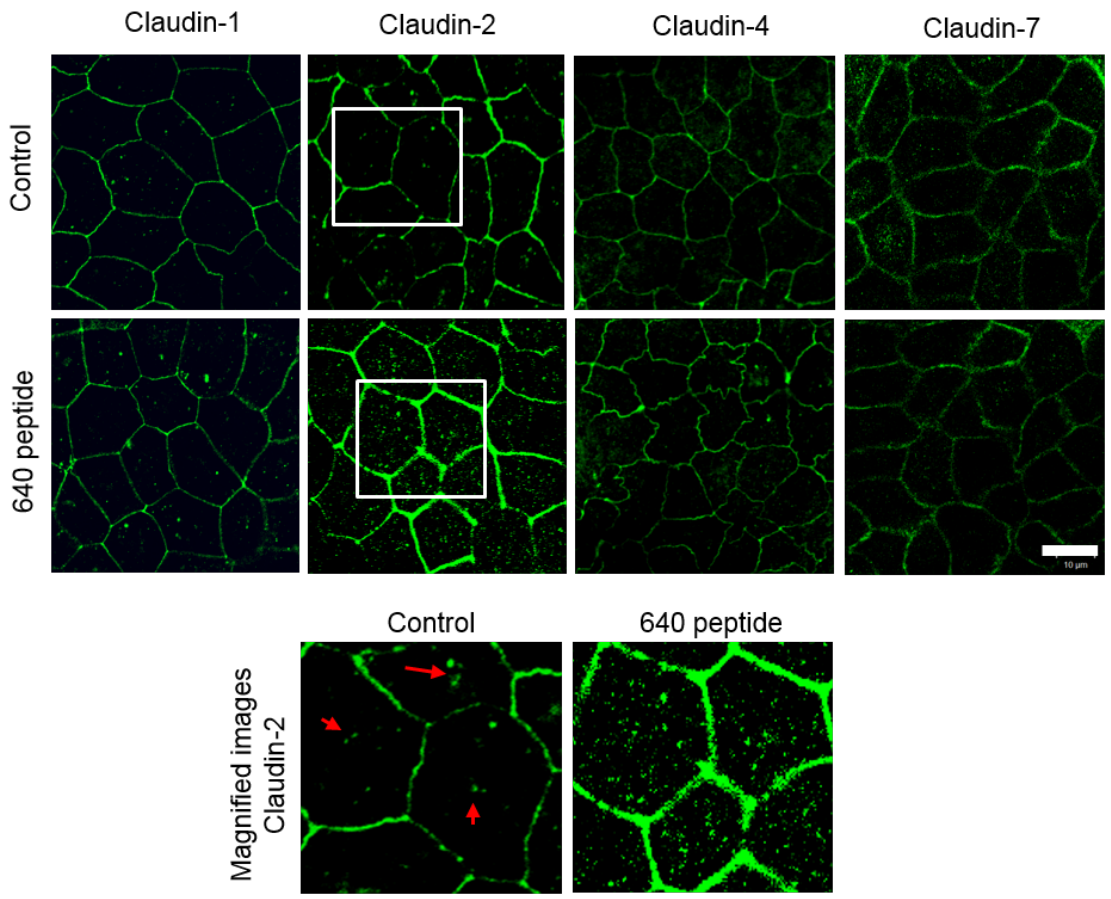

Figure 4.3: Immunofluorescent images of Caco-2 monolayers showing the cellular localization of claudin-1, -2, -4 and -7 before (top row) and after exposure to the PIP 640 peptide (second row). PIP 640 peptide increased TJ localization of claudin-2. Areas highlighted as white boxes in the top and second rows are magnified areas shown in the third row. Intracellular locations of claudin-2 in untreated Caco-2 cell monolayers that changed after exposure to PIP 640 peptide is highlighted by red arrows (third row). Images are representative of 3 independent experiments, n=3. Scale bar, 10 µm.

4.2.2. PIP 640 peptide-induced enhancement of claudin-2 at the TJ correlates with the induction of MLC-pS^{19}.

Reduction of TJ barrier function that correlates with enhanced paracellular permeability is usually associated with the remodelling of TJ protein complexes [45]. The mechanism of this remodelling can range from redistribution to changes in expression of TJ proteins [102, 118]. Hence, changes in the cellular levels and distribution of different TJ proteins were examined after exposure to 1 mM of PIP 640 peptide. The data presented above showed that only claudin-2 of the TJ proteins examined was affected over a time-course that associated with changes in paracellular permeability and TEER of Caco-2 monolayers. Claudin-2 levels as determined by western blotting were significantly increased and the localization of claudin-2 at the TJ as determined by immunofluorescence microscopy was increased in response to exposure to PIP 640 peptide for 60 min (Figure 4.1 and Figure 4.2). Studies have shown that modulation of claudin-2 alone or in combination with other TJ proteins could result in changes to TJ permeability properties [39, 102, 178]. Importantly, we observed that the PIP 640 peptide-enhanced TJ permeability also correlated with increased MLC-pS^{19} levels. Based on the current outcomes, it is unclear how increased claudin-2 levels are related to the increased MLC-pS^{19} in response to the PIP 640 peptide treatment.

To examine a potential relationship between increased claudin-2 levels and the elevation of MLC-pS^{19} in response to the PIP 640 peptide, a time-course study that monitored these two parameters over time was performed. At different time points, the TEER of Caco-2 cell monolayers was measured after exposure to 1 mM of PIP 640 peptide to monitor changes in the TJ barrier function. Subsequently, immunoblotting and immunofluorescent analyses were used to evaluate changes in the total cellular level and distribution of claudin-2 within cells. TEER reduction in response to apical exposure of the PIP 640 peptide was found to be associated with a time-dependent increase in claudin-

2 that was detectable by 10 min after exposure to the PIP 640 peptide, but it was only observed significantly after 20 min of treatment when compared to control cell monolayers (Figure 4.4 A, B and C). This time course for the increase in claudin-2 was correlated with an increase in MLC-pS^{19} levels over time, but MLC-pS^{19} seems to increase faster than claudin-2, as the increase of MLC-pS^{19} levels induced by the PIP 640 peptide was observed significantly after 10 min (Figure 4.4 B and C). Thus, time course studies are consistent with the hypothesis that increased levels of claudin-2 occur secondarily to increased levels in cellular MLC-pS^{19}.

A time-course immunofluorescent assessment of cellular claudin-2 distribution in Caco-2 monolayers after exposure to PIP 640 peptide was also performed to determine whether the increase in claudin-2 levels observed by immunoblotting data correlated with increased claudin-2 at the TJ. The data showed that the claudin-2 localization at the TJ increased over time (Figure 4.5). In addition, these changes in the intracellular distribution of claudin-2 were observed a few minutes after PIP 640 peptide exposure (Figure 4.5). This rapid onset of changes in the intracellular organization of claudin-2 and an increase in its level at the TJ suggested that redistribution of intracellular claudin-2 to the TJs occurred in response to the PIP 640 peptide treatment rather than the synthesis of new proteins because stimuli-inducing protein synthesis, particularly that of claudin-2, should take longer than 10 minutes [*102*]. Removal of PIP 640 peptide from Caco-2 monolayers after 60 min of apical treatment followed by overnight incubation with fresh medium led to complete recovery of both TEER and claudin-2 distribution (Figure 4.4 A and Figure 4.5).

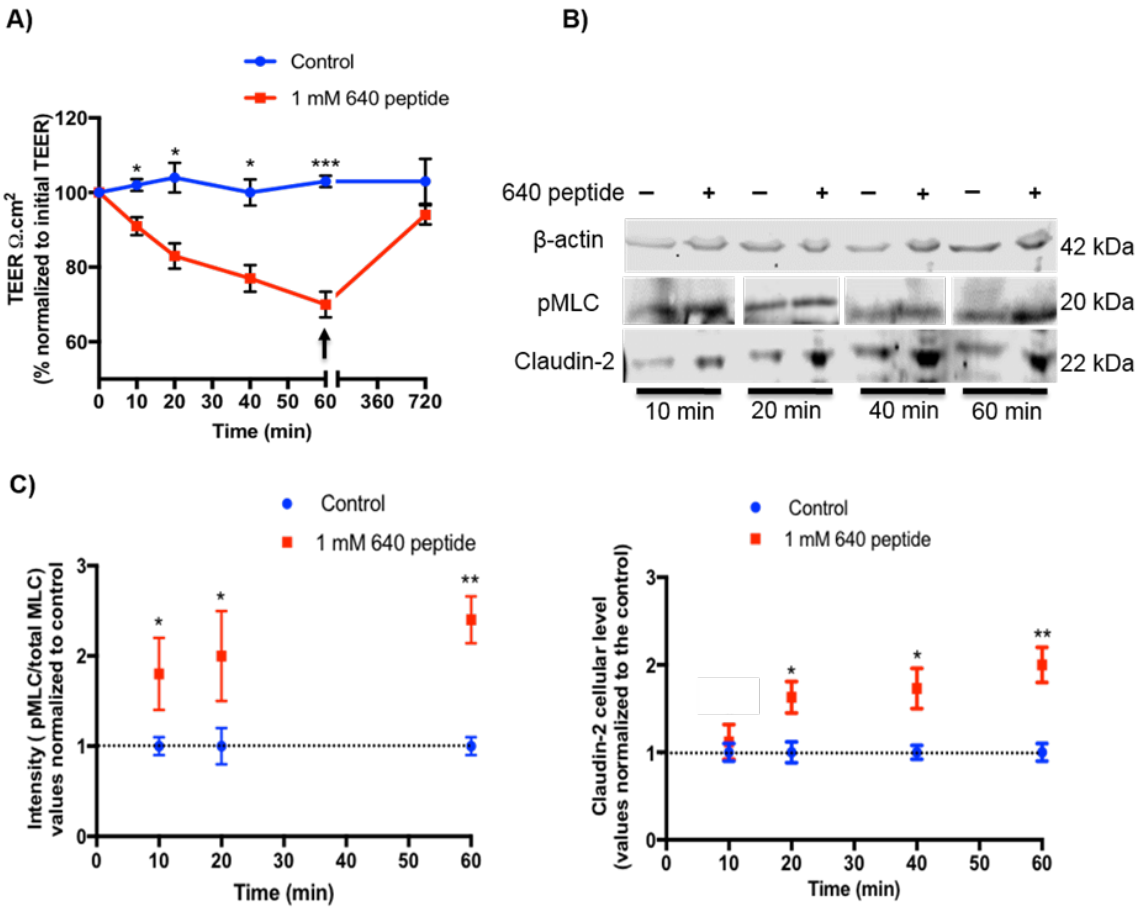

Figure 4.4: Time-course assessment of changes in claudin-2 levels relative to changes of MLC-pS^{19} levels associated with changes in permeability properties induced by PIP 640 peptide. **A)** TEER changes in Caco-2 cell monolayers induced by 1 mM of PIP 640 for 60 min. Removal of apical PIP 640 peptide to initiate recovery of actions is highlighted with an arrow. **B)** Representative immunoblots showing correlation of MLC-pS^{19} levels and claudin-2 levels over time following apical application of 1 mM of PIP 640 peptide. **C)** Quantitative analysis of immunoblots obtained for MLC-pS^{19} and claudin-2 induced by PIP 640 peptide in B). Data points represent means ± SEM of 3 independent experiments with n=6 for TEER data, n= 3 for both MLC-pS^{19} and claudin-2 immunoblotting data at all time points, immunoblot data obtained for MLC-pS^{19} for 40 min exposure n=1 (*p value< 0.05, **p value< 0.01 and ***p value<0.001).

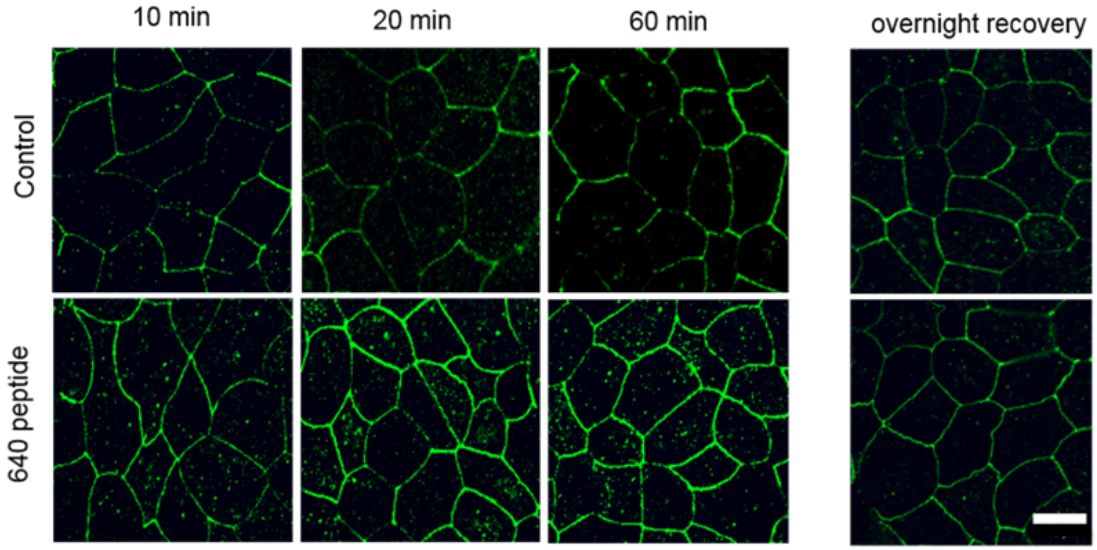

Figure 4.5: Time-course assessments of cellular claudin-2 distribution as assessed by immunofluorescence microscopy following exposure to 1 mM of PIP 640 peptide. Images of Caco-2 monolayers suggest redistribution of claudin-2 to TJ structures in response to the PIP 640 peptide exposure for the indicated period of time. Images are representative of 3 independent experiments, n=3. Scale bar, 10 μm.

To verify that the increase in claudin-2 at the plasma membrane (possible at TJ structures) is a function of modulating MLCP activity by the PIP 640 peptide, the action of a PIP peptide mutant was examined. PIP 644 peptide (sequence: rrrdykvevrr-NH_2), as shown in Chapter 3, non-specifically induces an increase in MLC-pS^{19} via an association with PP1 instead of the MLCP complex (MYPT1:PP1) to produce a more pronounced reduction of TJ barrier function compared to the PIP 640 peptide. Caco-2 monolayers were treated with 1 mM of both the PIP 640 and the PIP 644 peptides for 10 and 60 minutes. Consistent with the data discussed in Chapter 3, both peptides induced MLC-pS^{19} over time, but, only the PIP 640 peptide increased claudin-2 levels (Figure 4.6 A and B). Additionally, the distribution of claudin-2 in Caco-2 cell monolayers treated with the PIP 644 peptide was similar to that in the untreated cell monolayers, while the level of claudin-2 increased at TJs after exposure to the PIP 640 peptide (Figure 4. 5 C). Together, these data are consistent with the hypothesis that changes in claudin-2 associated with the inhibitory action of the PIP 640 peptide possibly involve the redistribution of claudin-2 to the TJs.

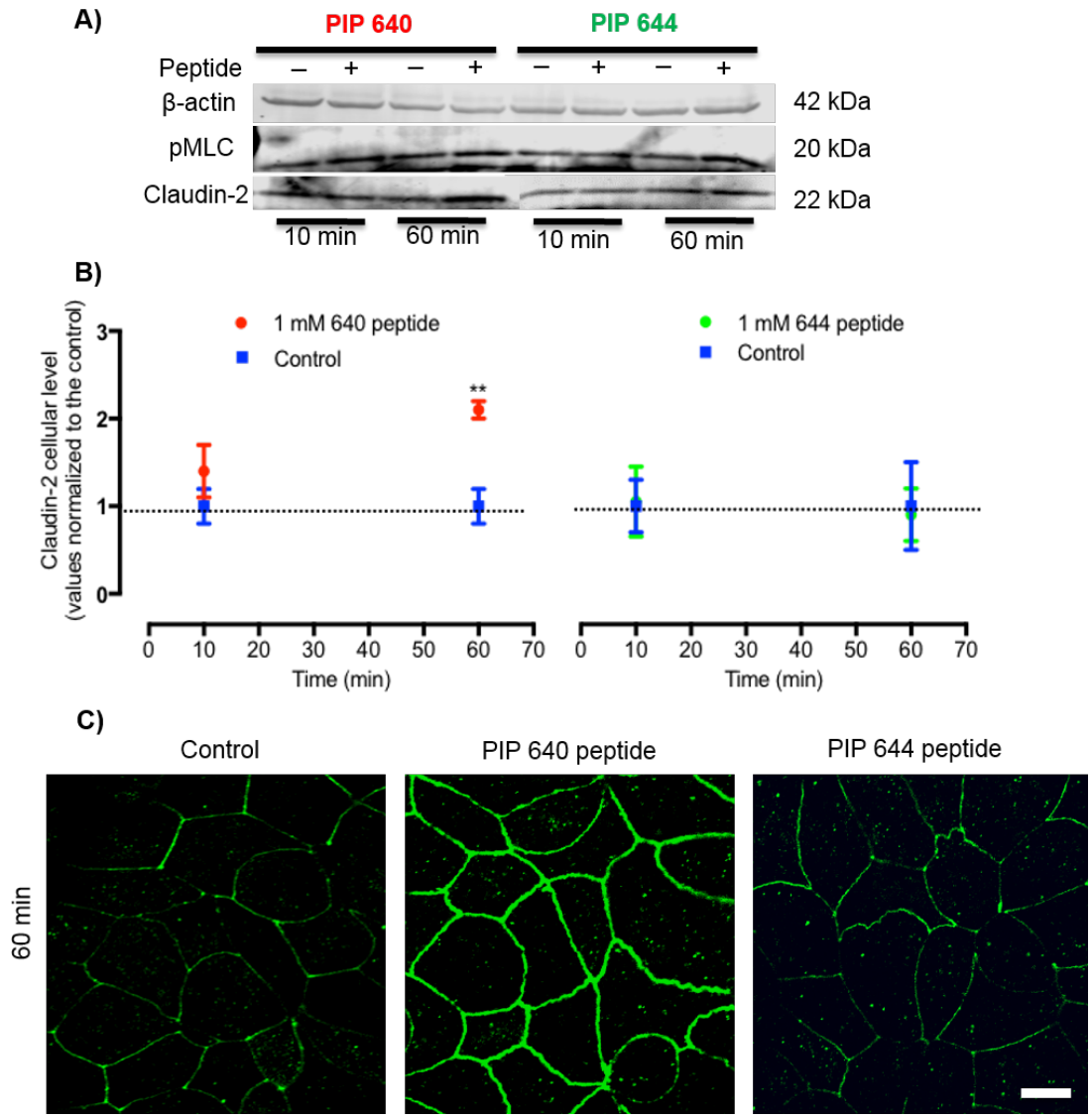

Figure 4.6: PIP 640 but not PIP 644 peptides alters claudin-2 following induction of increased MLC-pS^{19} levels in Caco-2 cell monolayers. **A)** Immunoblots showing cellular levels of MLC-pS^{19} and claudin-2 levels over time following apical application of 1 mM of PIP 640 or PIP 644 peptides. **B)** Quantitative analysis of the immunoblots obtained for MLC-pS^{19} and claudin-2 induced by PIP 640 peptide in A). Data are means ± SEM of 3 independent experiments with n=3 for both MLC-pS^{19} and claudin-2 immunoblotting data at all time points (**p value< 0.01). **C)** Immunofluorescent staining of claudin-2 in Caco-2 cell monolayers treated with PIP 640 or PIP 644 peptide for 60 min. Images are representative of 3 independent experiments, n=3. Scale bar, 10 µm.

4.2.3. Effect of PIP 640 peptide on the phosphorylation of serine residues of claudin-2

Growing evidence suggests that the molecular organization of epithelial TJ proteins is subject to continuous remodelling that regulates TJ barrier and permeability functions in the resting state and in response to changes in the environment experienced by the epithelial cells [95, 175, 177]. It has been reported that this dynamic function of TJ proteins could be modified by either altering expression or post-translational modifications, such as phosphorylation, of TJ proteins. For example, induction of interleukin-13 (IL-13) release by the intestinal mucosa is associated with intestinal inflammatory diseases and this event has been correlated with increased claudin-2 expression and enhanced TJ permeability [39, 102, 179]. Additionally, TJ barrier function can be regulated by phosphorylation of serine residue at position 208 of claudin-2 (claudin-2-pS^{208}), and this post-translational process has been suggested to reduce claudin-2 trafficking to lysosomal degradation and increase its TJ localization [180, 181].

Since PIP 640 peptide induced rapid redistribution of claudin-2 to TJs and phosphorylation of TJ proteins is often responsible for alteration of TJ barrier function [46, 180], we investigated the potential effect of PIP 640 peptide on the phosphorylation of serine residues of claudin-2. Immunoprecipitation of claudin-2 isolated from confluent Caco-2 cells grown in 75 cm^2 flasks were assessed for the phosphorylation state of serine residues using an anti-phosphoserine antibody following treatment with 1 mM of PIP 640 peptide for 10 or 60 min. Under control conditions, claudin-2 was phosphorylated at the serine residues, but this level of phosphorylation was increased following the application of the PIP 640 peptide (Figure 4. 6). This observation was consistent with recent reports showing that increasing claudin-2-pS^{208} is associated with increased TJ localization of claudin-2 [180, 181]. These results indicate that the PIP 640 peptide enhances claudin-2 recruitment to TJs by increasing its phosphorylation at serine residues, potentially the serine residue at position 208.

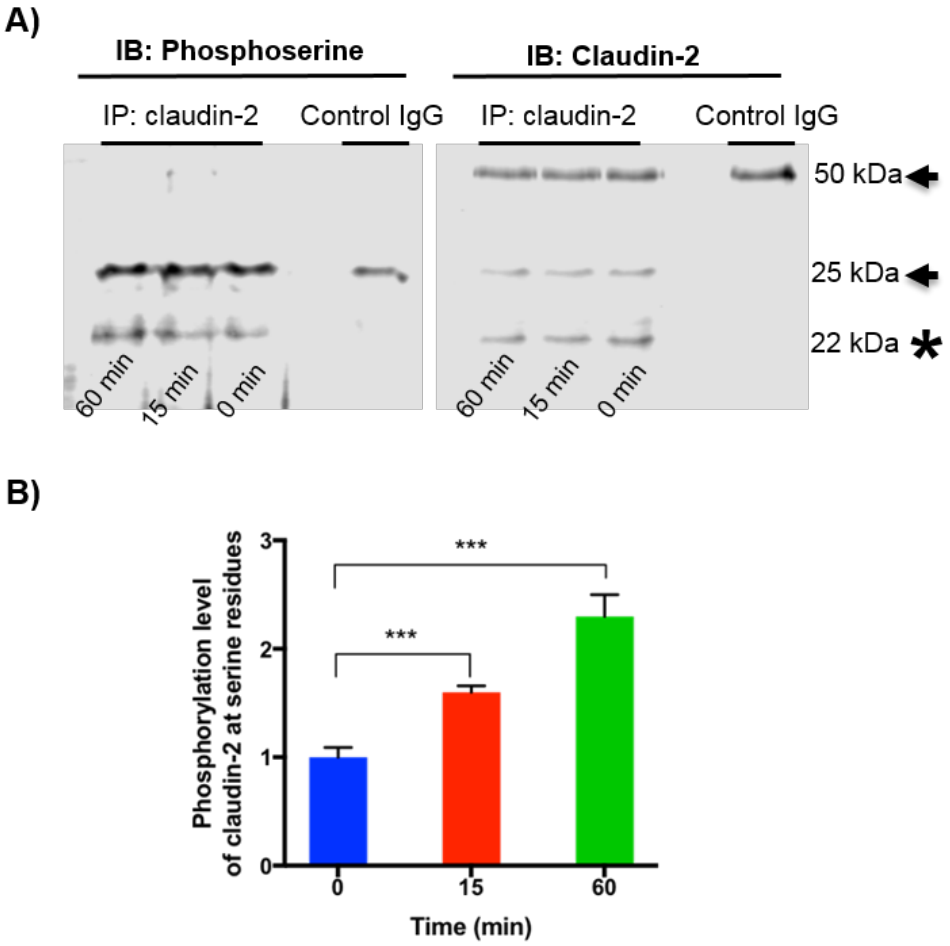

Figure 4.7: Effect of the PIP 640 peptide on phosphorylation of claudin-2 serine residues. **A)** Confluent Caco-2 cells seeded in 75 cm^2 were treated with 1 mM of the PIP 640 peptide for the indicated period of time. Cell lysates were immunoprecipitated (IP) with anti-claudin-2 IgG or a control IgG and immunoblotted (IB) with anti-claudin-2 IgG or anti-phosphoserine IgG. Arrows indicate the heavy chain (50 kDa) and the light chain (25 kDa) of the IgGs used. Claudin-2 and phosphoserine-claudin-2 bands are indicated by the star symbol (22 kDa). **B)** Levels of claudin-2 phosphorylation at serine residues in response to PIP 640 peptide over time were quantitated. Change in phosphorylation is expressed as a ratio of band intensity for phosphoserine-claudin-2/claudin-2. Data represent means ± SEM of 5 independent experiments with n=5 (***p value<0.001).

4.2.4. PIP 640 peptide induced a perm-selective TJ permeability

Studies have shown that enhancement of intestinal TJ permeability is induced by different intestinal inflammatory disorders, such as inflammatory bowel diseases (IBD), and these changes have been demonstrated to involve MLC-pS^{19} induction by prolonged activation of MLCK. This process, in turn, results in rearrangement of TJ proteins, such as induction of occludin endocytosis and/or claudin-2 upregulation, which results in increased paracellular solute permeability [53, 102, 179, 182]. The data presented above indicate that cellular changes induced by PIP 640 peptide were associated with increased levels of claudin-2 at the TJs that was correlated with increased levels of MLC-pS^{19} levels, similar to mechanisms demonstrated for TJ barrier dysfunction associated with IBD. Thus, it was important to compare the extent to which permeability was enhanced by the PIP 640 peptide in comparison to effects induced by pro-inflammatory cytokines that have been demonstrated to drive this increased permeability associated with IBD-like conditions. To do so, apical to basal permeability of different size fluorescent molecules, 4 kDa, 10 kDa and 70 kDa dextran, across Caco-2 monolayers was assessed after exposure to either PIP 640 peptide or a mixture of pro-inflammatory cytokines, tumour necrosis factor-α and interferon-γ (TNF-α/INFγ), which have been identified as essential mediators of IBD [138, 183].

Monolayers TEER changes and the cumulative flux of fluorescent dextrans were monitored for 60 min after apical PIP 640 peptide application to Caco-2 monolayers and these parameters were compared to the action of basal treatment with TNF-α/INFγ after 4h to ensure induction of an inflammatory process [54]. Exposure to PIP 640 peptide for 60 min reduced the TEER values of Caco-2 monolayers to ~ 70 % of the initial TEER values, whereas treating the monolayers with TNF-α/INFγ for the indicated time induced a decrease in TEER to ~ 55 % of the initial TEER values (Figure 4.8 A). Both PIP 640 peptide and TNF-α/INFγ treatments induced MLC-pS^{19}, but occludin down-regulation was only observed following TNF-α/INFγ treatment (Figure 4.8 B).

This is consistent with studies showing occludin down-regulation is required for pro-inflammatory cytokine-induced TJ barrier dysfunction [54, 137]. In response to TEER reduction induced by both PIP 640 peptide and TNF-α/INFγ, apical to basal flux of 4 kDa dextran was significantly increased compared to controls (Figure 4.9). However, TNF-α/INFγ allowed more 4 kDa dextran to cross the monolayers compared to PIP 640 peptide (Figure 4.9). Apical to basal flux of 10 kDa and 70 kDa dextran across Caco-2 monolayers was enhanced in monolayers treated with TNF-α/INFγ but, not following PIP 640 peptide treatment (Figure 4.9).

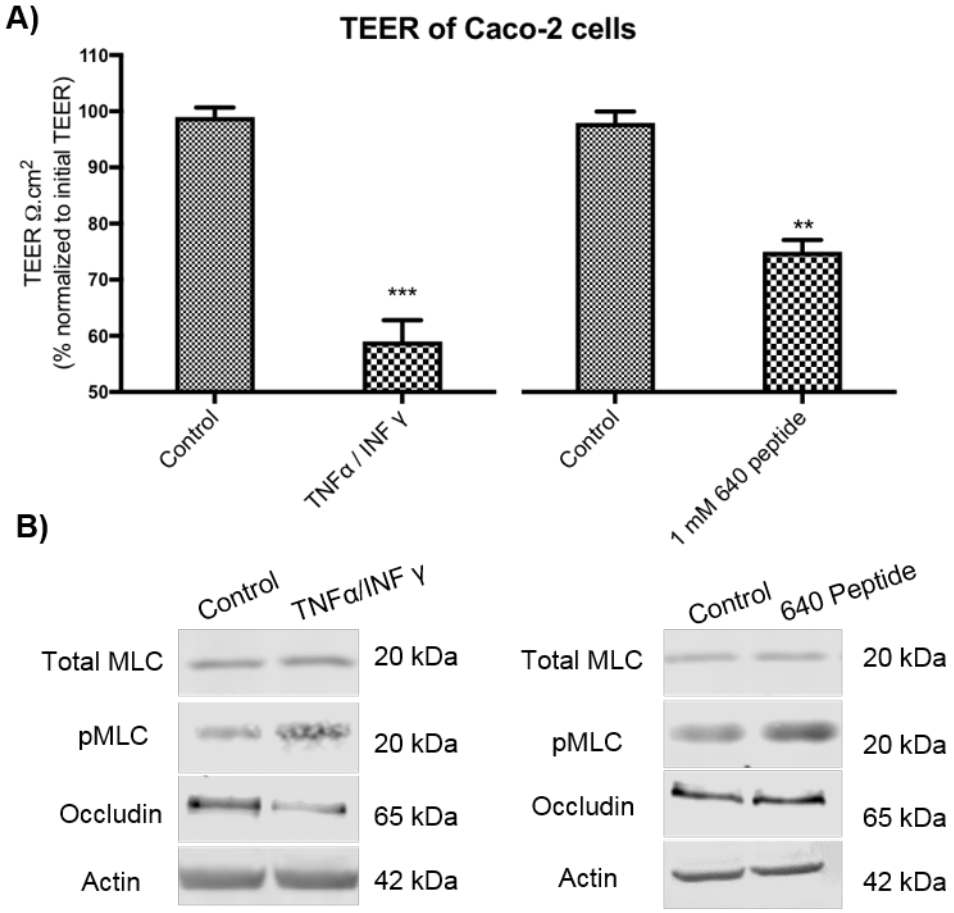

Figure 4.8: Effect of TNF-α/INFγ or PIP 640 peptide on the barrier properties of Caco-2 cell monolayers. **A)** Change in the TEER of Caco-2 monolayers after 60 min of apical exposure to 1 mM of PIP 640 peptide and after 4 h of basal exposure to TNF-α (5 ng/mL)/ INF-γ (10 ng/mL). Data are means ± SEM of 3 independent experiments, with n=9 (**p value< 0.01 and ***p value< 0.001). **B)** Immunoblotting assessment of changes in MLC-pS[19] and occludin levels induced by both PIP 640 peptide and TNF-α/INF-γ treatment after time indicated in A). Data are representative of 4 independent experiments, n=4. Data are means ± SEM of 3 independent experiments, with n=9 (**p value< 0.01 and ****p value<0.0001).

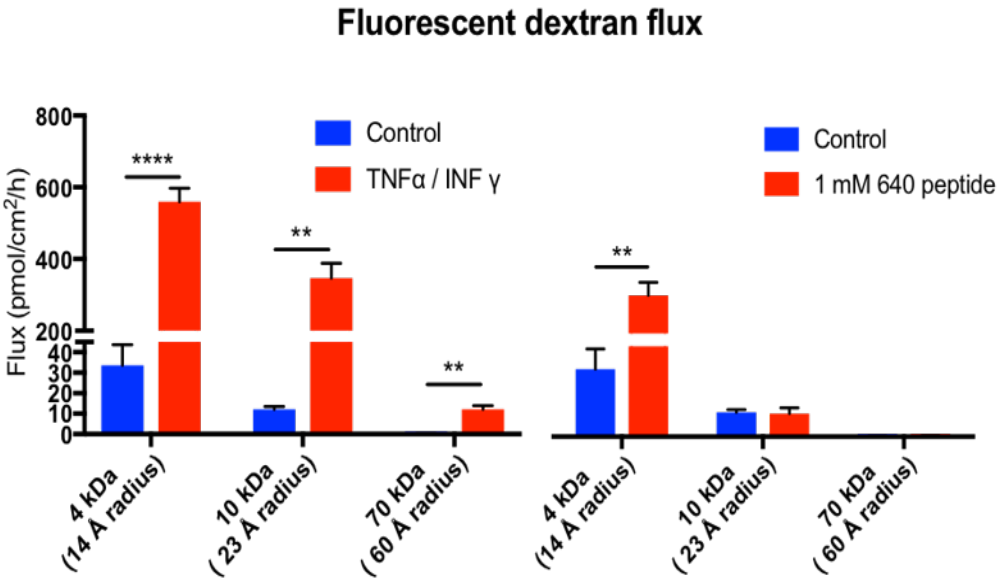

Figure 4.9: Cumulative apical to basolateral flux of fluorescent dextran (4 kDa, 10 kDa and 70 kDa) across Caco-2 cell monolayers induced by basal TNF-α/INF-γ or apical PIP 640 peptide treatment. The extent of fluorescent dextran across monolayers was monitored for 60 min after induction of barrier dysfunction by pre-treatment TNF-α/INF-γ while these values were similarly determined for PIP 640 peptide added apically at the time of dextran application. Data are means ± SEM of 3 independent experiments, with n=9 (**p value< 0.01 and ****p value<0.0001).

4.2.5. Perm-selectivity of PIP 640 peptide solute transport

Claudin proteins are known to regulate ion flux through TJs between the apical and basolateral sides of epithelial cells [38, 45]. At TJs, claudin-2 establish an ion channel that is selectively permeable to small cations and water [27, 184]. Claudin-2 ion channels are involved in generating essential gradients that also mediate the paracellular permeability of molecules [38, 45]. Studies have shown that claudin-2 regulation is involved in the induction of physiological gradient-dependent paracellular flux of nutrient molecules [178]. Increased levels of claudin-2 at TJ structure, however, have also been linked with many intestinal disorders characterized by a leaky epithelium [102, 179, 182]. The data presented above showed that treatment of both the PIP 640 peptide and TNF-α/INF-γ increased MLC-pS^{19} levels and led to changes in the TJ permeability properties of Caco-2 cell monolayers. However, the PIP 640 peptide increased Caco-2 monolayers permeability to 4 kDa dextran but not 10 kDa dextran, while TNF-α/INF-γ enhanced the permeability of dextrans as large as 70 kDa (Figure 4.9). In addition, TNF-α/INF-γ-induced permeability changes to Caco-2 monolayers were associated with occludin down-regulation [53], whereas TJ permeability induced by the PIP 640 peptide did not appear to alter occludin protein levels (Figure 4.8 B).

PIP 640 peptide increased claudin-2 levels at TJ structures and also caused an increase in the permeability of a macromolecular solute, in this case 4 kDa dextran. We next asked whether these PIP 640 peptide-mediated changes to TJ function also affected the charge selectivity of macromolecular solutes through the paracellular route in a manner consistent with the nature of claudin-2 perm-selectivity. To study this, TEER changes of Caco-2 cell monolayers and apical to basal transport of fluorescent dextrans with either an overall positive or negative charge were compared to that of neutral dextran *in vitro*. In separate monolayers, 4 kDa size forms of positively-charged diethylaminoethyl-dextran (DEAE-dextran; structure shown in Figure 4.10 A) or negatively-charged carboxymethyl-dextran (CM-dextran; structure shown in

Figure 4.10 B) were mixed with neutral 4 kDa dextran and applied apically to Caco-2 monolayers treated with 1 mM of the PIP 640 peptide. After 60 min the extent of apical to basal compartment transfer for the dextrans being tested were determined and the apical media was replaced with fresh media and TEER values for the Caco-2 cell monolayers were monitored over the next 5 h to ensure recovery of TJ function (Figure 4.10 C and D). These studies showed that Caco-2 monolayers treated with PIP 640 peptide were more permeable to 4 kDa positively-charged DEAE-dextran than neutral 4 kDa dextran, but that the permeability changes induced by PIP 640 peptide were similar for 4 kDa negatively-charged CM-dextran and 4 kDa neutral dextran (Figure 4.10 D). These findings might indicate that the positively charged molecule selectivity of claudin-2 might contribute to PIP 640 peptide permeability enhancement function to some extent, as Caco-2 monolayer were preferentially permeable to DEAE-dextran over neutral and negatively-charged dextran derivatives.

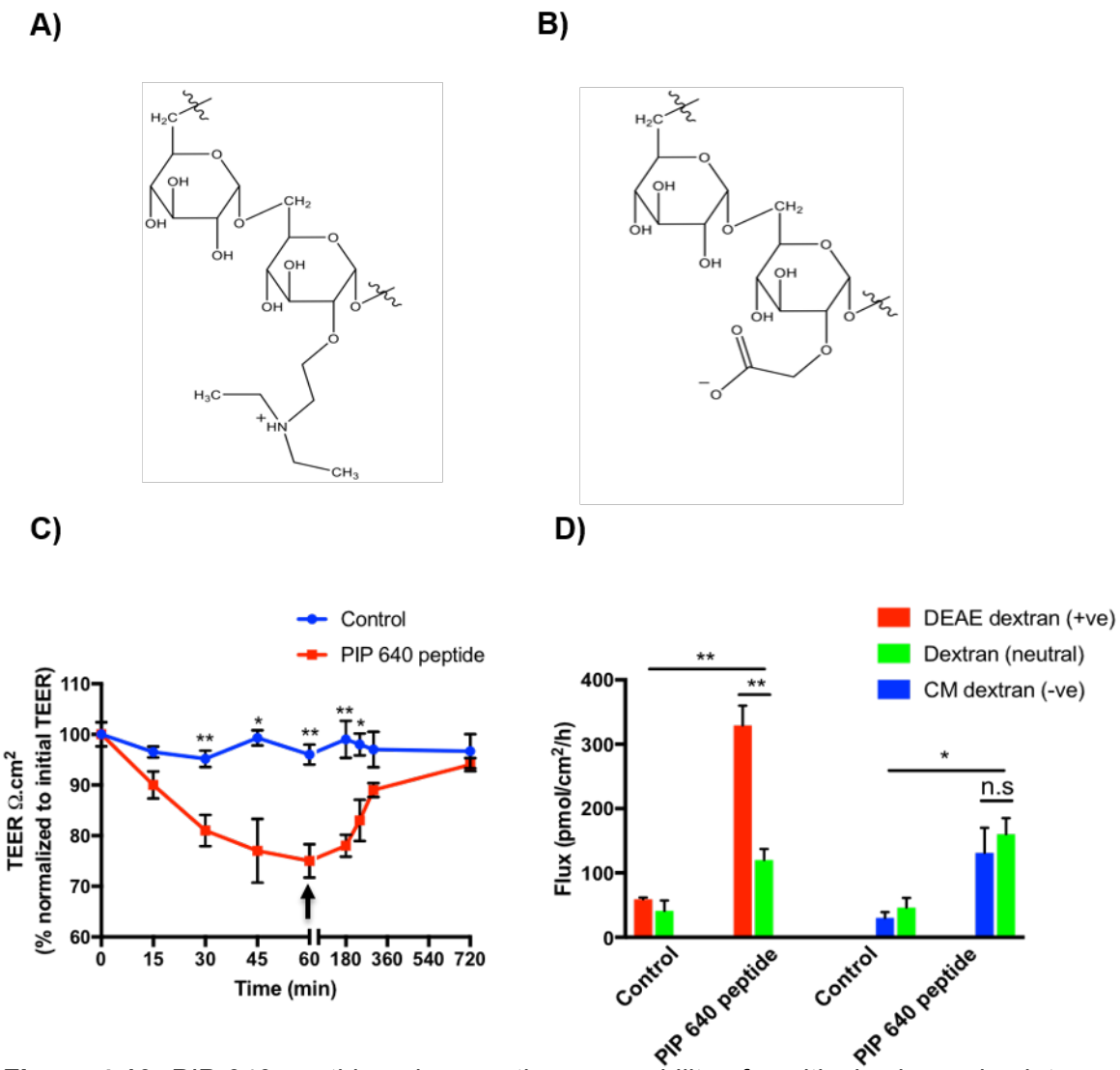

Figure 4.10: PIP 640 peptide enhances the permeability of positively-charged solutes relative to neutral or negatively-charged solutes. Chemical structures of the charged dextran derivatives used, **A)** Diethylaminoethyl-dextran (DEAE-dextran) and **B)** Carboxymethyl-dextran (CM-dextran). **C)** Change in TEER of Caco-2 cells monolayers induced by 640 peptide. Apical media containing PIP 640 peptide and dextrans was replaced with fresh DMEM medium after 60 min to allow examination of TEER recovery over a subsequent 5 h period. **D)** Cumulative apical to basal transport across Caco-2 monolayers treated with fluorescent DEAE-dextran or CM-dextran with neutral dextran (all 4 kDa in size) over 60 min. Data are means ± SEM (*P < 0.05 and **P < 0.01).

4.3. Discussion

The intestinal epithelial barrier performs a critical task of protecting the human body from the invasion of harmful agents or pathogens that might induce systemic disorders and/or local inflammation to the intestine [45, 101]. However, the barrier characteristics that grant this protection also hinder the absorption of therapeutic peptides [5]. Accordingly, most of the available therapeutic peptides are limited to parenteral applications, which are considered inconvenient for patients that require long-term treatment. Therefore, various approaches have been investigated to enhance the oral delivery of such drugs across the intestinal epithelial barrier [5, 117]. For example, many permeability enhancers (PEs) have shown to effectively enhance drug permeability across epithelial cells [5, 117], with most of them acting non-selectively on the epithelial barrier by disorganizing TJ proteins or generally disrupting the epithelial cell membrane [13, 119].

The TJ barrier is comprised of complex protein structures that consist of many cell membrane integral proteins, organized as a network of membrane peripheral proteins linking to the TJ-associated actomyosin cytoskeleton [14]. TJ proteins possess a distinct dynamic behaviour by which association of TJ integral membrane proteins and their organization within the TJ can be modulated [175, 177]. The restricted transport of solutes across the TJ barrier is regulated by a wide array of intracellular signalling molecules that modulate TJ protein components [45]. Application of agents to enhance the paracellular permeability of therapeutic peptides across the TJs of intestinal epithelial cells has gained wide acceptance as a drug delivery strategy [5, 117], as TJ routes are more suitable for hydrophilic medication that are unable to cross the lipid bilayers of epithelial cell membranes, being the mechanism used in the oral absorption of small molecule drugs [5]. However, opening the TJs non-specifically for drug delivery may lead to epithelial damage and/or inflammation that might occur as result of co-absorption of pathogens [13].

Chapter 4

It is well established that induction of MLC-pS^{19} in the intestinal epithelium can trigger dynamic modulation of TJ protein structures that reversibly regulate the TJ barrier properties [88, 95, 103], an endogenous mechanism involved in the regulation of physiological uptake of molecules, such as nutrients, through paracellular routes [88, 167]. The main goal of the current project was to examine a strategy to improve oral delivery of therapeutic peptides by enhancing their ability to cross the intestinal epithelial barrier. Accordingly, we designed a small cell permeant peptide, PIP 640 peptide, to regulate MLCP activity, inducing MLC-pS^{19} levels that would result in the induction of a transient TJ opening to allow for enhanced therapeutic peptide absorption. The data presented in Chapter 1 showed that the PIP 640 peptide was able to reversibly reduce the TEER of Caco-2 cell monolayers and enhance the permeability of 4 kDa dextran through the TJ *in vitro* by the proposed MoA. However, it was not clear whether the permeability enhancement function of PIP 640 peptide was associated with changes in TJ protein elements. In addition, the studies presented in Chapter 1 that investigated intracellular distribution of PIP 640 peptide in Caco-2 cell monolayers showed that the peptide was closely associated with the TJ protein structure, as it was co-localized with the integral membrane protein occludin. These observations led us to the hypothesis that PIP 640 peptide might induce TJ permeability by altering the structure of TJ proteins. Therefore, the studies performed in the current chapter were aimed to investigate biochemical changes in TJ proteins associated with the permeability enhancement function of the PIP 640 peptide.

Major determinants of TJ barrier properties in different epithelial barriers are regulated by the composition of specific TJ proteins and their expression levels [21, 45]. Hence, based upon such differences, TJ barrier of epithelial cells lining organs such as the intestine and kidney tubules are relatively more permeable than those covering the urinary bladder lumen [21, 45]. Studies have determined that TJs are naturally permeable to ions and small solutes < 4 Å [175]. The data presented in Chapter 1 showed that the PIP 640 peptide

enhanced the permeability of 4 kDa dextran (~ 14 Å radius) across Caco-2 monolayers *in vitro*. It has been suggested that the permeability of macromolecules of this size through TJ routes is associated with the displacement of TJ proteins, especially TAMPs and ZO-1. For example, occludin endocytosis that is associated with TNF-induced MLCK hyperactivity in IBD that induces macromolecules permeability across epithelial TJs [53, 185]. Similarly, disruption of tricellulin has been recognized as a pathway to enhance TJ permeability in cultured monolayers to molecules such as 10 kDa dextran [118]. Knockdown of the third member of TAMP, MarvelD3, in Caco-2 cells was also associated with changing TJ barrier properties [59]. The scaffolding protein ZO-1 has a major role in the assembly of TJ proteins, and it has been shown that ZO-1 down-regulation was associated with enhancement of the flux of large solutes across epithelial cells *in vitro* [186, 187]. In addition, TAMPs and ZO-1 were shown to be highly dynamic at the TJs compared to other TJ proteins such as claudin-1 that seems to be more stable at TJ [36, 177]. Therefore, our initial thought was that the permeability enhancement induced by the PIP 640 peptide might be regulated by modulating these TJ proteins. Accordingly, we investigated the potential effect of the PIP 640 peptide on TAMP family and ZO-1 proteins. Immunoblot analysis of total cell lysates of Caco-2 monolayers before and after treatment with PIP 640 peptide showed no significant difference on TAMPs and ZO-1 levels (Figure 4.1 A and B). Similarly, immunostaining of these proteins in Caco-2 monolayers treated with PIP 640 peptide showed normal TJ localization and no marked difference compared to the control (Figure 4.1 C).

Since data investigating the effect of the PIP 640 peptide on TJ proteins revealed that the peptide does not seem to interfere with TAMPs and ZO-1 functions, we explored the status of other membrane integrated TJ proteins such as members of the claudin family, as disruption or reorganization of some claudin proteins have been shown to enhance the paracellular permeability of large solutes [26, 39, 40]. In our investigation of PIP 640 peptide effect on

claudins, we focused on different claudin isoforms that are expressed in intestinal epithelium and contribute differently to TJ barrier function with the assumption that changes in these proteins might explain TJ permeability property changes induced by the PIP 640 peptide. These include claudins-1, -3 and -5, which have been shown to act as sealing proteins to the paracellular routes to reduce paracellular permeability [25, 40]. In addition, we explored the alterations to claudin-4, -7 and -8 that have been shown to contribute to the regulation of TJ permeability to negatively charged ions [29, 188]. Also, we investigated changes to claudin-2 and -15 that promote the passage of positively charged ions [28, 115]. Immunoblotting data showed that PIP 640 peptide-induced MLC-pS^{19} was associated with an apparent increase in claudin-2 in Caco-2 monolayers and no effect was observed on the other tested claudins (Figure 4.2 A and B). This increase in claudin-2 was consistent with TJ localization (Figure 4.3). Moreover, claudin-2 was widely distributed intracellularly, which might suggest that the PIP 640 peptide induced claudin-2 recruitment to TJ structures (Figure 4.3).

It is been shown that the pore size of claudin-2 permits the permeability to small cations but not larger molecules such as 4 kDa dextran [115]. This might suggest that the permeability enhancement of 4 kDa dextran associated with PIP 640 peptide might be primarily mediated by other untested TJ proteins and claudin-2 likely contributes to charge selectivity of the permeability enhancement function of the PIP 640 peptide. In addition, imaging of fixed tissues and cell monolayers might not reveal some of the changes in the organization of TJ proteins that are associated with paracellular permeability. For example, paracellular permeability induced by activation of MLCK associated with Na^+-glucose co-transport showed normal distribution of ZO-1 protein at the TJs [94]. However, application of FRAP techniques in living cells revealed that the dynamic behaviour of ZO-1 changes during Na^+-glucose-induced MLCK. This appeared as less ZO-1 protein was associated with the TJ [95]. Therefore, live imaging using techniques such as FRAP might be

necessary in future for precise assessment of the action of the PIP 640 peptide on the organization of TJ proteins that mediate macromolecule permeability, such as occludin.

PIP 640 peptide was designed to mimic the inhibitory function of CPI-17 towards MLCP by emulating the binding properties of CPI-17 to MLCP components (MYPT1:PP1). This was done to increase MLC-pS^{19} levels, an intracellular mechanism that is known to regulate TJ barrier properties (*88, 160, 161*), in order to enhance the paracellular permeability of peptide therapeutics. The data presented in chapter 1 suggest that PIP 640 peptide regulates MLCP activity by increasing MLC-pS^{19} levels. This induced reversible TJ permeability of molecules with a radius of ~ 14 Å. We then attempted to characterize changes to the TJ proteins associated with PIP 640 peptide-induced TJ permeability. The data showed that of the many TJ integral membrane proteins examined, only claudin-2 was significantly increased at the TJ. Analysis of the cellular levels and distribution of claudin-2 over time in response to exposure to the PIP 640 peptide revealed a time-dependent increase of claudin-2, reduction of TEER and increase in MLC-pS^{19} levels (Figure 4.3, and Figure 4.4). However, the PIP 644 peptide, an analogue of PIP 640 peptide described in chapter 1 that increases MLC-pS^{19} levels by acting as a general phosphatase inhibitor instead of acting specifically on MLCP, had no significant effect on claudin-2 (Figure 4.6). These findings might indicate that the increase in claudin-2 induced by the PIP 640 peptide was due to regulation of MLCP activity and not by enhancing MLC-pS^{19} levels, as PIP 644 peptide did not change claudin-2 levels. Moreover, the delayed onset of claudin-2 increases compared to MLC-pS^{19} increases observed in (Figure 4.3) might suggest that PIP 640 peptide-induced claudin-2 increase at the TJ is regulated by a secondary mechanism triggered by regulating MLCP activity.

Various studies have defined mechanisms mediating TJ protein trafficking that are essential for modulating TJ barrier function. For example, TNF-induced barrier loss was shown to occur due to occludin endocytosis that is

mediated by caveolin-1, a lipid raft protein that plays a role in protein endocytosis [189]. Moreover, it was found that phosphorylation of occludin at threonine residues at positons 403 and 404 increases occludin recruitment to the TJs and accordingly enhances TJ barrier function [190]. Our data showed that the PIP 640 peptide increased claudin-2 levels at the TJ significantly after 20 min, an effect that seems to occur secondarily to the increase observed in MLC-pS^{19} levels (Figure 4.3, and Figure 4.4). Studies have shown that claudin-2 expression increases in response to cytokines [39, 102, 179]. This cytokine-induced claudin-2 up-regulation appears to be a slower onset and more durable process compared to the more dynamic actions of the PIP 640 peptide on Caco-2 cell monolayers *in vitro*. Therefore, we excluded the possibility that the effect of PIP 640 peptide on claudin-2 levels was related to expression level. Instead PIP 640 peptide seems to redistribute claudin-2 to TJs.

It is been established that the TJ proteins, including claudin-2, are found in a cholesterol-enriched glycolipids raft (lipid raft) of plasma membranes, which forms a tightly packed detergent-insoluble region [196]. Studies have suggested that claudin-2 disassembled from TJ is rapidly targeted to lysosomal degradation [181, 191]. Cellular trafficking of claudin-2 has been shown to be regulated by different signalling pathways. For example, Rab-14, a small guanosine triphosphatase (GTPase), has been shown to play a regulatory role in the delivery of claudin-2 to TJs and the internalization of claudin-2 [191]. In addition, claudin-2-pS^{208} was found to be essential for the recruitment of claudin-2 to TJ structures [181]. Also, phosphorylation of claudin-2 at this position was shown to enhance claudin-2 detergent solubility [181]. These mechanisms were also found involved in regulating claudin-2 targeting to lysosomes [181, 191]. Expression of mutated claudin-2 in the serine residue at position 208 in MDCK I cells caused claudin-2 down-regulation by lysosomal degradation [181]. Similarly, knockdown of Rab-14 in MDCK II cells was associated with a reduction in claudin-2 and increase in the TJ barrier function, an effect that was reversed by re-expression of Rab-14 [191]. The role of Rab-

14 in regulating claudin-2 levels was linked to directing claudin-2 to lysosomes, as inhibiting lysosomal degradation in Rab-14 knock-down MDCK II cells resulted in maintenance of claudin-2 levels [191]. In our investigation of the effect of PIP 640 peptide treatment of Caco-2 monolayers on TJ proteins, we observed a rapid time-dependent increase of claudin-2 localization at the TJ, an effect that was also detected in the immunoblot data using total cell lysates. This increase in claudin-2 was associated with a rapid enhancement of claudin-2-pS^{208} (Figure 4.7). Since the half-life of claudin proteins has been suggested to be ~ 6 h [181], such a rapid alteration in claudin-2 levels that was observed in the immunoblot data is unlikely to occur by reducing claudin-2 degradation, a process that is regulated by claudin-2-pS^{208} as discussed earlier [180, 181]. However, this increase in claudin-2 levels that was induced by the PIP 640 peptide might resulted from enhancing claudin-2 detergent solubility from lipid raft, a function of enhanced claudin-2-pS^{208} [181]. This can be confirmed by performing differential detergent extraction and sucrose density centrifugation.

Increased intestinal TJ permeability is commonly associated with cytokine-induced inflammatory disorders, such as IBD [53, 102, 179, 182]. Elevation of TNF-α in intestinal mucosa enhances MLCK activation and has been shown to be the major cause of leaky TJs, which are permeable to macromolecules in patients with Crohn's disease [53, 103]. Other cytokines, such as INF-γ, were found to have a boosting effect to the barrier dysfunction induced by TNF-α [138, 183]. Short exposure to TNF-α/INF-γ was shown in the current studies to induce barrier dysfunction characterized by activation of MLCK-induced MLC-pS^{19} levels and occludin endocytosis [53, 54, 103, 138, 183]. Chronic exposure to these pro-inflammatory cytokines was shown to cause more changes to the TJ structure, such as increasing claudin-2 expression, and consequent epithelial cell damage [138, 192]. The data presented above showed that PIP 640 peptide induced TJ permeability of 4 kDa dextran by enhancing MLC-pS^{19} levels, an effect that was associated with claudin-2 increase, although it is currently unclear if and how claudin-2 alone might affect such an outcomes in solute

transport. Thus, additional TJ modifications may be induced by PIP 640 peptide. Since TNF-α/INF-γ-induced TJ permeability is activated by increasing MLC-pS[19], the same endogenous mechanism that regulates TJ permeability induced by the PIP 640 peptide, it is particularly interesting to note that changes of TJ barrier properties induced by PIP 640 peptide were distinct from those induced by TNF-α/INF-γ.

Our data showed that Caco-2 cell monolayers treated with either PIP 640 peptide or TNF-α/INF-γ decreased TEER associated with elevated MLC-pS[19] levels (Figure 4.8 A and B). However, the pattern of TEER reduction is different for each treatment. TNF-α/INF-γ induced further TEER reduction than did the PIP 640 peptide. This might have occurred in response to occludin down-regulation that was only observed in Caco-2 monolayers treated with TNF-α/INF-γ (Figure 4.8 B). Data concerning the permeability of solutes of different sizes across Caco-2 monolayers revealed that the PIP 640 peptide induced perm-selective permeability of TJs that allowed the passage of molecules with ~ $\leq$ 14 Å radius size (Figure 4.9). However, Caco-2 monolayers treated with TNF-α/INF-γ were also permeable to 70 kDa dextran (~60 Å radius) (Figure 4.9). This outcome was consistent with previous reports concerning TJ permeability associated with TNF-α/INF-γ [(54)]. Another well-defined characteristic of TJ barrier dysfunction associated with TNF-induced MLCK activation is the irregular, undulating distribution of the scaffolding protein ZO-1 at the TJ [(53, 183)]. This was not observed for PIP 640 peptide treated Caco-2 monolayers (Figure 4.1 C). These data imply that PIP 640 peptide and TNF-α/INF-γ enhance TJ permeability by distinct mechanisms, although they are both able to increase MLC-pS[19].

Claudin-2 is a tetraspan pore-forming TJ protein that is size- and charge-selective [(27, 32, 115)]. Similar to most claudin proteins, the charge-selectivity of claudin-2 is mediated by charged amino acids located on its extracellular loop-

1 (ECL-1), which is stabilized by two cysteine residues [32]. The charge-selective property of paracellular routes in tissue epithelial barriers, which is dependent upon the type of claudin proteins expressed in that epithelium, is typically determined by studying the flow of ions across the epithelial cells [29, 115, 188]. In our *in vitro* investigations, we have determined that PIP 640 peptide induced a modification of TJs that resulted in an enhanced transport of small macromolecules in a perm-selective manner. Such changes are distinct from that observed for TJ changes induced by pro-inflammatory cytokines (Figure 4.9). This means that the PIP 640 peptide changed the pore size-selectivity of TJ from being permeable to molecules with $\leq$ 4 Å radius, such as mannitol [175, 193], to molecules with $\leq$ 14 Å radius, 4 kDa dextran.

The TJs of Caco-2 cell monolayers are generally more permeable to positively charged and neutral molecules than negatively charged ones, all with $\leq$ 5 Å radius [194]. This preference was maintained for the same solutes after changing TJ pore size to ~ 15 Å by treating the monolayers with palmitoylcarnitine [194], a PE that was shown to non-specifically enhance TJ permeability [5]. In agreement with this report of the charge preference of Caco-2 cells, TJ permeability induced by sodium caprate across Caco-2 monolayers was higher for neutral 4 kDa dextran than negatively charged Lucifer yellow (LY) dye [122], although that the latter has a smaller radius ~ 5 Å [195] compared to 4 kDa dextran ~14 Å. However, sodium caprate has been shown to induce changes to different TJ proteins [118, 196]. A study has shown that one such change is displacement of claudin-4 [196], which has been shown to contribute to the regulation of passage of negatively charged molecules [29, 197], from TJs. Thus, claudin-4 displacement induced by sodium caprate might be the reason for the reduced permeability of LY across Caco-2 monolayers. Our results show that charge-preferential paracellular permeability changes induced by PIP 640 peptide were only significant for DEAE-dextran (Figure 4.9 D). These findings suggest that claudin-2 might contribute to PIP 640 peptide-induced TJ permeability of positively charged molecules. However, it is not clear whether

claudin-2 is the only protein responsible for enhancing the TJ permeability function of PIP 640 peptide.

In conclusion, in this Chapter we have studied biochemical changes to TJ protein associated with the permeability enhancement function of the PIP 640 peptide, which is mediated by enhancing MLC-pS^{19} levels through the modulation of MLCP activity. Our results showed that PIP 640 peptide induced a time-dependent increase of claudin-2 cellular level that was correlated with increase of MLC-pS^{19}, whereas no changes were observed for a wide range of other integral membrane TJ proteins that were examined. The PIP 640 peptide-induced increase in claudin-2 correlated with an enhancement of claudin-2 phosphorylation at serine residues, potentially claudin-2-pS^{208}, which could result in increased detergent extractability and enhancement of its cellular distribution at TJs. In addition, the PIP 640 peptide was shown to induce a perm-selective permeability increase in TJ pore size in a manner that differed from that induced by proinflammatory cytokines. Finally, this increase in claudin-2 at TJ structures induced by the PIP 640 peptide seems to contribute to regulating paracellular permeability of charged molecules, preferentially to positively charged molecules with a radius of at least 14 Å but less than 23 Å.

Chapter 5 : Application of PIP 640 peptide to enhance intestinal epithelial TJ permeability of therapeutic peptide *in vivo*

5.2. Background

Most of the currently-known therapeutic peptides have poor oral bioavailability. This is due to their undesired physiochemical characteristics of being too large and hydrophilic to cross the intestinal epithelial barrier in a manner similar to small molecule drugs [117]. Many strategies have been explored to improve the oral delivery of such therapeutics; some of these strategies have shown promising outcomes in terms of overcoming the intestinal epithelial barrier [5]. For example, application of permeability enhancer (PE) agents that have been used to transiently enhance the transport of a co-administered peptide therapeutic across the intestinal epithelium. Previously described strategies to enhance the oral delivery of peptide therapeutics usually define their effectiveness in enhancing the permeability by using *in vitro* cell culture models of the intestinal epithelium or an excised intestinal tissue [5, 13, 135]. This is typically is done by examining the transport of various stable solutes that have physicochemical properties similar to peptide therapeutics as a way to predict whether the strategy can enhance the permeability of a desired peptide drug *in vivo* [5, 135]. In addition, *in vitro* models have been widely used in efforts to define the mechanism of action (MoA) by which a delivery strategy enhances the permeability of molecules. This information is critical to explore potential toxicity events associated with a given delivery strategy [5, 13].

A human colorectal adenocarcinoma cell line, Caco-2 cells, is one of the intestinal epithelial cell models most frequently used to study drug permeability across the intestine because it is simple to use and can provide reproducible results [135, 198]. These advantages have lowered the reliance on animal models for the initial examination of delivery strategies across the intestinal epithelium [198]. Fully differentiated Caco-2 cells are able to show many features of the small intestine epithelial barrier, a status that can be achieved when these cells are grown on semi-permeable filters to form a single layer of polarized epithelial cells that develop functional tight junctions (TJs) [135]. In addition,

these Caco-2 cell monolayers has been found to contain various membrane transporters and metabolic enzymes known to exist in human intestinal epithelium [135, 198]. However, the Caco-2 cell model is not an optimum model to study drug permeability across the intestinal epithelial cells, as it does not exactly reflect how a drug permeability enhancement approach will behave *in vivo* [5]. Importantly, Caco-2 cells lack some of the naturally existing elements in the intestine that have been suggested to affect the drug absorption process, such as the mucus layer, and these elements need to be considered when developing a strategy to enhance oral delivery of therapeutic peptides *in vivo* [199].

The mucus layer consists of mucin glycoproteins that form a viscous gel-like structure that covers intestinal epithelial cells, thereby providing a protective barrier against a spectrum of potential pathogens [199]. While the mucus layer allows the transport of small molecules, such as nutrients, it has the potential to entrap poly-ionic macromolecules [199]. Studies have shown that the intestinal mucus layer is a factor that could slow the diffusion of poly-ionic macromolecules to the epithelial surface, thus reducing their absorption rate [10, 200]. For example, chitosan, a PE agent that can improve the intestinal permeability of a poorly absorbed drug such as atenolol, was more effective when tested *in vitro* using Caco-2 cell monolayers that do not secrete a mucus layer versus HT-29 cell monolayers that do produce a mucus layer [200]. This effect of the mucus layer has also been shown to influence the permeability of peptide therapeutics [5, 10, 199].

The need to evaluate safety is one of the major concerns of using PE agents to enhance the intestinal permeability of a peptide therapeutic and this cannot be accomplished by only using *in vitro* models [13].These *in vitro* models can overestimate toxicity associated with PE agents as they lack elements and mechanisms that protect the intestine from damage such as the mucus layer, blood supply and intestinal transit time [13, 201]. Moreover, *in vitro* models of

intestinal epithelium are usually unable to predict the effect of long-term (repeated) exposure to PE agents on the intestinal epithelium or the potential induction of co-permeability of harmful elements present in the intestinal lumen [13]. Hence, it is important to address the limitations of *in vitro* models in a more complex animal model *in vivo*.

In our work, we sought to develop a novel PE agent: a small membrane-permeant peptide to regulate the activity of myosin light chain phosphatase (MCLP). This PE agent, known as the PIP 640 peptide, was designed to increase myosin light chain phosphorylation at the serine 19 (MLC-pS^{19}) to alter TJ properties and enhance the intestinal epithelial TJs permeability of peptide therapeutics. PIP 640 peptide at a concentration of 1 mM, showed an ability to reversibly enhance TJ permeability properties of Caco-2 monolayers *in vitro* without affecting cell viability, as discussed in Chapters 1 and 2. The next logical step was to assess PIP 640 peptide efficacy and validate its MoA in an *in vivo* model in order to predict its possible actions in an ultimate clinical application. This is particularly important because, typically, both the performance and the effective concentration of a PE agent tend to vary between *in vitro* and *in vivo* models [118, 202]. For example, the PE agent sodium caprate at a concentration of 10 mM was able to improve the permeability of dextran molecules with molecular weight of 4 kDa and 10 kDa in HT-29 cell monolayers *in vitro* [118], while a concentration of 100 mM was required to enhance *in vivo* bioavailability of 4 kDa dextran to ~2 % in a rat animal model after intra-jejunal loop injection [202].

The current chapter examines different aspects of PIP 640 peptide-induced permeability enhancement *in vivo* by measuring the systemic bioavailability of different peptide therapeutics in a rat model following co-administration with the PIP 640 peptide by direct intraluminal intestine injection (ILI). Moreover, the experiments in this study examined whether the permeability enhancement induced by the PIP 640 peptide increases the permeability of other harmful substances in the intestinal lumen across the epithelial barrier, such as

lipopolysaccharide (LPS). This chapter also sought to validate the defined MoA of the PIP 640 peptide from *in vitro* studies *in vivo*. Such results could provide valuable information regarding the *in vivo* permeability enhancement performance and safety strategy for the translation of the PIP 640 peptide to clinical study.

5.3. Results

5.3.1. Co-administration of the PIP 640 peptide with insulin lowered blood glucose level *in vivo*

Our initial investigation of the PIP 640 peptide action *in vivo* involved using a longer version of the peptide that has three additional basic amino acids at the C-terminus of the peptide sequence, rrdykvevrrkkr-NH_2, as it was thought that these additional amino acids would be important to increase the rate of intracellular uptake of the PIP 640 peptide in order to compensate for intestinal transit that could not be modelled *in vitro* [127]. This longer version of the PIP 640 peptide was tested to determine its ability to enhance insulin absorption in rat intestine following intraluminal intestinal injection (ILI). This peptide at a concentration of 20 mM showed an ability to enhance insulin transport to blood circulation and accordingly lowered blood glucose levels [127]. In an effort to decrease the number of synthetic steps and lower the cost of peptide, as a part of the PIP 640 peptide optimization process, we tested the ability of the original PIP 640 peptide sequence: rrdykvevrr-NH_2, to enhance the absorption of therapeutic peptides *in vivo* after validating its effectiveness and MoA *in vitro,* which was shown in Chapter 1 and 2.

To explore the actions of the PIP 640 peptide *in vivo*, we applied the same conditions that were used to examine the *in vivo* actions of the longer version of the PIP 640 peptide [127]. Rats were used because the intracellular protein targets of the PIP 640 peptide, MLCP components (MYPT1:PP1), are highly conserved between humans and rats [156, 203]. Human insulin alone (control), or in combination with the PIP 640 peptide, was administered to non-diabetic rats by ILI with blood glucose level being monitored for the next 80 min. Citric acid at a concentration of 10 mM was used in the tested formulations to reduce intestinal proteolysis [204]. A subcutaneous (SC) injection of insulin served as a positive control for changes in blood glucose levels. In our previous *in vivo* study, we found that human insulin alone showed comparable

pharmacodynamics (PD) outcomes in rats at a concentration of 3 IU/kg after SC injection and 30 IU/kg when co-administered with 20 mM of the longer version of the PIP 640 peptide via ILI [127]. Thus, we used the same concentrations to explore the *in vivo* performance of the original PIP 640 peptide.

SC injection of 3 IU/kg of human insulin reduced the blood glucose level in these non-diabetic rats to ~50% of their initial value after 30 min (Figure 5.1 A). This hypoglycaemic effect started to recover after ~50 min and it reached 70 % of the initial values after ~80 min, the time of study termination. ILI co-administration of 30 IU/kg of human insulin with 20 mM of the PIP 640 peptide showed slower action in reducing blood glucose levels in comparison to the SC injection of 3 IU/kg of insulin. The blood glucose levels started to decrease significantly after 20 min, and reached ~55 % of the initial value after 40 min (Figure 5.1 B). However, the recovery profile that was observed with the ILI co-administration of insulin and the PIP 640 peptide was faster in comparison to the SC injection of insulin (Figure 5.1 B). As expected, insulin alone administered by ILI at a concentration of 30 IU/kg, had no effect on blood glucose levels (Figure 5.1 B).

In vitro data presented in Chapter 1 and 2 demonstrated that the PIP 640 peptide can enhance the TJ permeability of intestinal epithelial cells over a time course consistent with increased MLC-pS^{19} levels. Therefore, we performed a similar biochemical analysis with rat intestinal tissues exposed to PIP 640 *in vivo*. Toward that end, we measured MLC-pS^{19} levels in rat intestinal tissue at the site of ILI 40 min after insulin alone or insulin co-administrated with the PIP 640 peptide. Immunoblotting data showed that the MLC-pS^{19} level was only increased in rat intestine exposed to the PIP 640 peptide (Figure 5.1 C and D). Together, these *in vivo* data are consistent with outcomes observed *in vitro* and suggest that the PIP 640 peptide can enhance

insulin absorption across intestinal epithelial TJs with a simultaneous increase in MLC-pS^{19} levels.

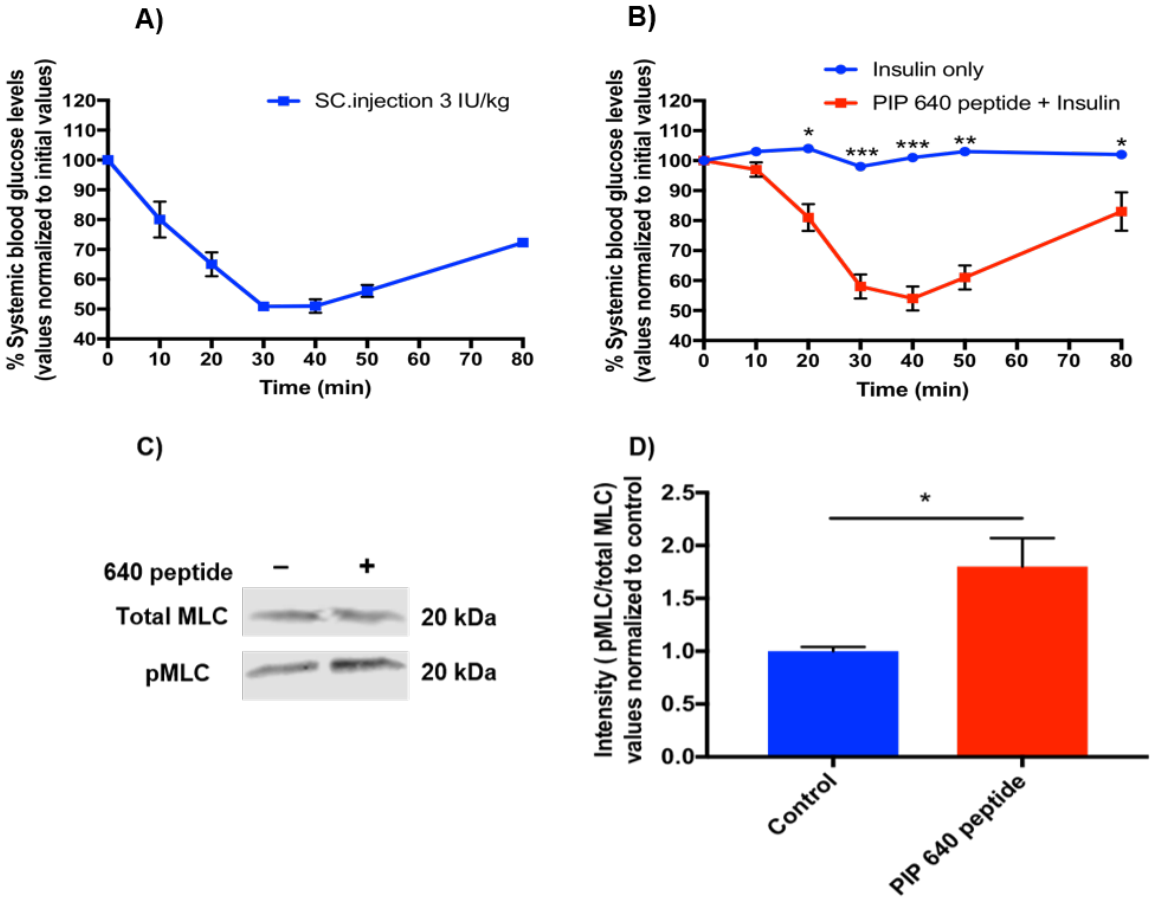

Figure 5.1: Effect of co-administration the PIP 640 peptide and insulin on blood glucose levels and MLC-pS^{19} levels in rats *in vivo*. Blood samples from the tail vein were used to monitor glucose levels. **A)** Effect of subcutaneous (SC) injection of 3 IU/kg insulin alone on blood glucose levels. **B)** Effect of co-administration of 30 IU/kg of insulin and 20 mM of the PIP 640 peptide by intraluminal intestinal injection (ILI) on blood glucose levels. **C)** Immunoblot of MLC-pS^{19} compared to total MLC levels 40 min after ILI of insulin with or without PIP 640 peptide. **D)** Quantitative assessment of MLC-pS^{19} levels immunoblots shown in A). Data represent means ± SEM of 3 independent experiments; n=3 (*p value< 0.05, **p value< 0.01, ***p value< 0.001).

5.3.2. PIP 640 peptide enhanced claudin-2 localization at TJs *in vivo*

Claudin-2 expression at TJ structures is associated with reduced barrier properties and enhanced epithelial permeability of small molecules with a radius < ~4 Å [27, 115]. In the intestine, claudin-2 is highly expressed and was found to play an essential role in regulating intestinal physiological functions that include the regulation of Na^+ transport from the submucosa to the lumen that seemed to be essential for nutrient absorption [178]. In addition, increased claudin-2 levels are associated with many intestinal inflammatory disorders, such as Crohn's disease [39, 102, 182]. Data presented in Chapter 2 demonstrated that the PIP 640 peptide-mediated enhancement of the permeability across Caco-2 cell monolayers *in vitro* correlated with increased MLC-pS^{19} levels as well as an increase in total claudin-2 levels and increased levels of claudin-2 at TJ structures. Consistent with this possible MoA identified *in vitro*, the data presented above (Figure 5.1) suggests that the PIP 640 peptide also enhanced insulin permeability *in vivo* by enhancing MLC-pS^{19} levels. In order to fully compare the proposed MoA identified in vitro with *in vivo* outcomes, we sought to validate the PIP 640 peptide action on claudin-2 in rat intestine.

Rat intestinal epithelial tissues were exposed to 20 mM of the PIP 640 peptide by ILI for 40 min when the tissues were collected and analysed by immunoblotting and immunofluorescence microscopy to monitor the amount and cellular distribution of claudin-2. In agreement with our *in vitro* data, immunoblotting analysis detected an increase in claudin-2 that was correlated with an enhancement to MLC-pS^{19} level *in vivo* (Figure 5.2). We then examined the expression levels and distribution of claudin-2 using immunofluorescence staining. In un-treated (control) rat intestinal tissue, claudin-2 expression was observed to decrease in a crypt to villus tip direction (Figure 5.3 A); consistent with previous studies describing claudin-2 expression *in vivo* [205-207]. Claudin-2 expression was distributed at the TJs and the basolateral membranes of epithelial cells located in the middle of the villus (Figure 5.3 A), but it was restricted to the basolateral membrane of cells

located at the villus tips (Figure 5.3 A, arrowheads, control image). Claudin-2 expression in rat intestinal tissues following exposure to the PIP 640 peptide for 40 min seemed similar to the control, with no striking change observed in the signal intensity. However, claudin-2 distribution at the TJ structures seemed to increase in cells located at the villus tips (Figure 5.3 A, arrowheads, PIP 640 peptide image). Epithelial cells located in the middle of the villus of control tissue showed that caludin-2 was distributed in both TJs and basolateral membranes, forming connected lines along some paracellular spaces. After exposure to the PIP 640 peptide, claudin-2 within these enterocytes was concentrated more at TJs than at the basolateral membrane (Figure 5.3 B). These results suggest that more claudin-2 was recruited to TJ structures in response to PIP 640 peptide exposure. No striking effect was observed on claudin-1 or occludin following exposure to the PIP 640 peptide (Figure 5. 3 B).

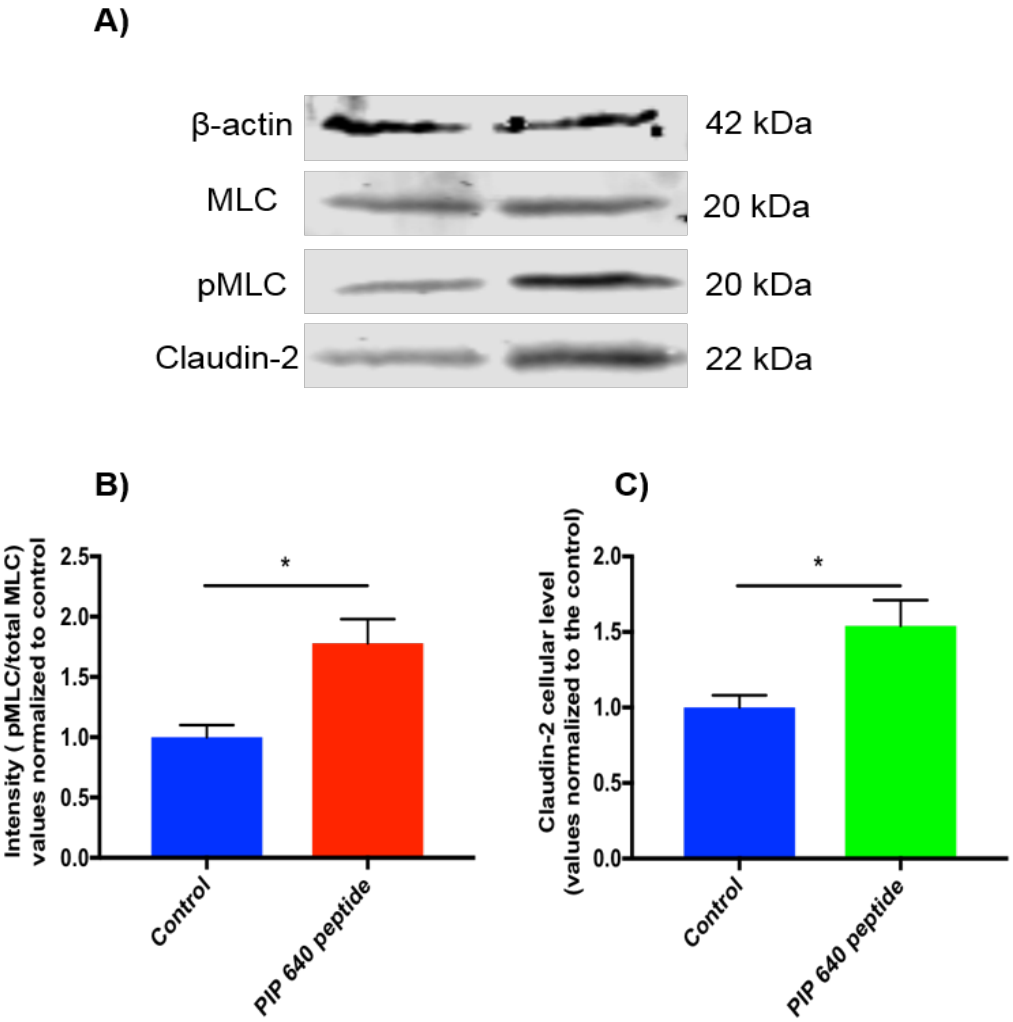

Figure 5.2: Changes in MLC-pS[19] and claudin-2 levels following ILI exposure to 20 mM of the PIP 640 peptide in non-diabetic rats *in vivo.* **A)** Immunoblots of rat intestine exposed to 20 mM of the PIP 640 peptide for 40 min showed an increase in both MLC-pS[19] and claudin-2 levels. **B)** Quantitative representation of the immunoblots obtained in A). Data are means ± SEM of 3 independent experiments; n= 3. (**p* value< 0.05).

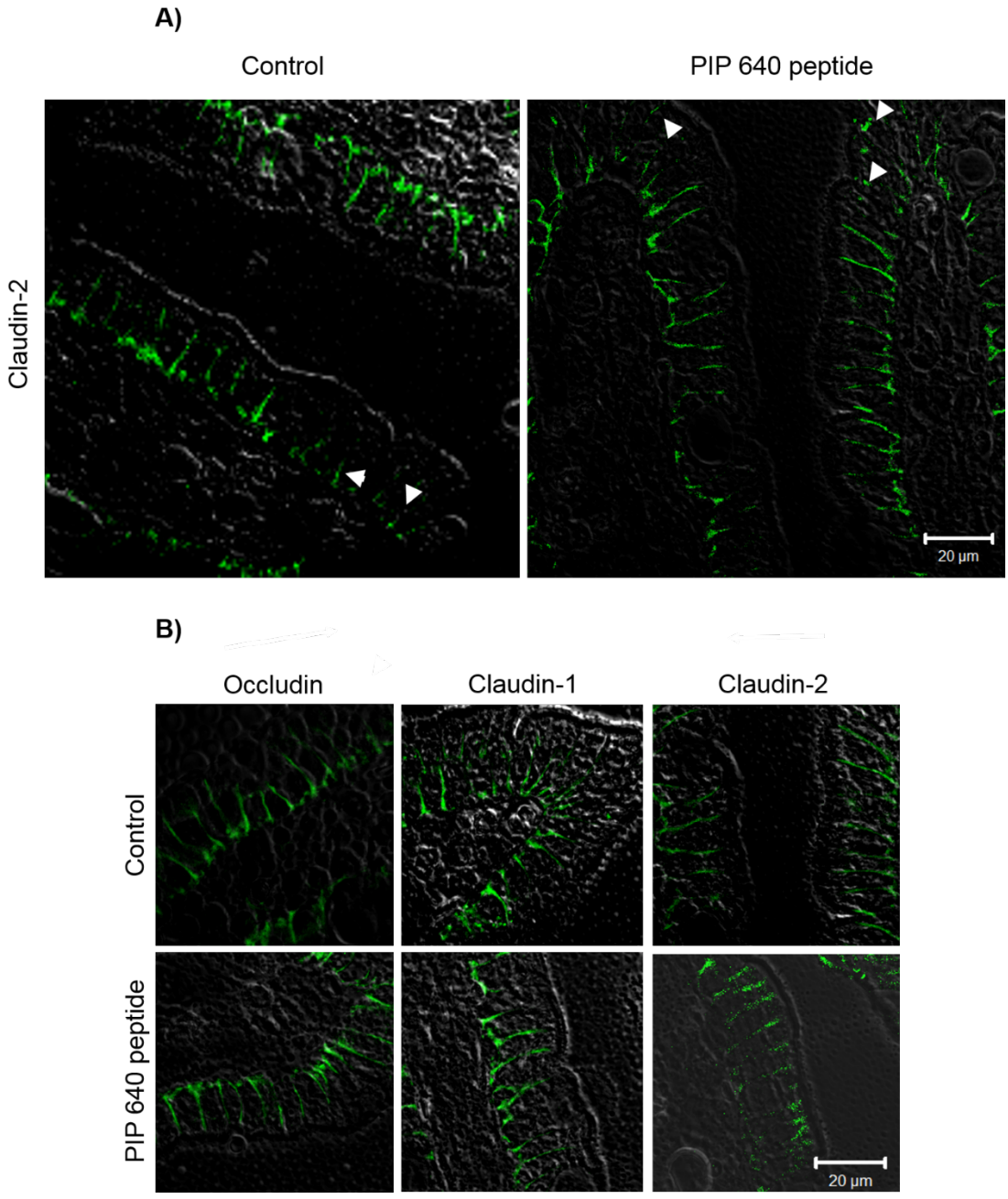

Figure 5.3: Immunofluorescence microscopy of rat jejunum epithelium showing the effect of the PIP 640 peptide on TJ proteins *in vivo.* **A)** Claudin-2 distribution in villi before and after exposure to 20 mM of the PIP 640 peptide for 40 min. Changes in claudin-2 distribution in the villi tips are highlighted with arrowheads. **B)** Claudin-2 is predominantly located at the TJs of rat intestinal epithelium after exposure to the PIP 640 peptide, while it is located in both TJs and lateral membranes in the control tissues. Images show no significant effect on claudin-1 and occludin. Images are representative of 3 independent experiments, n=3. Scale bar, 20 µm.

5.3.3. Validation of the charge-preferential paracellular permeability induced by the PIP 640 peptide *in vivo*

TJs are organized to restrict macromolecular flux but selectively permit the permeability of small and hydrophilic molecules between adjacent epithelial cells, known as the paracellular route [5]. Transient alteration of TJ function by PE agents can increase the permeability of the paracellular route to peptide therapeutics [93]. The permeability of peptide therapeutics through TJs is limited by molecular size and surface charge [208, 209]. In our *in vitro* data presented in Chapter 2, we showed that the PIP 640 peptide induced a perm-selective TJ permeability that was preferentially permeable to positively charged dextran with a molecular weight of 4 kDa (~14 Å radius). This was associated with an increase in claudin-2 at TJ structures of Caco-2 cell monolayers used for these *in vitro* studies. Since claudin-2 at TJ structures is known to correlate with increased flux of positively charged ions, we hypothesized that PIP 640 might affect a charge-preferential TJ permeability change that favoured positively charged molecules.

To examine the possibility that PIP 640 produced a charge-preferential TJ permeability change *in vivo*, we measured the potential for enhanced uptake of either calcitonin (salmon) or exenatide. Both of these therapeutic peptides have a similar hydrodynamic size of ~11 Å radius, but they differ in their isoelectric point (pI) values. Since calcitonin has a pI value of 8.8 and exenatide has a pI values of 4.9, the net charge of these peptides at the physiological pH of the small intestine (*i.e*. jejunum; 5.7- 7.4) where they will be administered by ILI will be net positive and net negative, respectively [3, 210, 211]. Unlike the previous study investigating insulin permeability enhancement that was discussed above (Figure 5.1), soybean trypsin inhibitor (SBTI) (1.5 mg/mL) was used with both calcitonin and exenatide (0.5 mg) instead of citric acid to reduce local luminal proteolysis because it was shown that this concentration of SBTI increased the stability of therapeutic peptides without

inducing significant permeability enhancement [126]. Additionally, the presence of 10 mM citric acid could significantly alter the local pH at the site of ILI, potentially negating the goal of this study. Additionally, uptake of exenatide or calcitonin following ILI was assessed in serum obtained from portal vein blood collections, and not tail vein as with the insulin studies, in order to eliminate the potential for unequal hepatic extraction.

Injecting similar amounts exenatide or calcitonin with 20 mM of the PIP 640 peptide into rat jejunum by ILI resulted in an enhancement of portal vein plasma concentrations in comparison to control animals that received an ILI of exenatide or calcitonin without PIP 640 (Figure 5.4 A and B). Examination of the portal vein concentration-time profiles suggested that calcitonin concentration after 30 min of exposure were slightly higher than exenatide, but the difference was not statistically significant (Figure 5.4 A and B). Both therapeutic peptides showed a similar maximum plasma concentration (C_{max}) at 40 min of co-administration with PIP 640 (Figure 5.4 A and B) (Table 5.1). However, the data indicated that the area under the curve (AUC) value of calcitonin when co-administered with PIP 640 was elevated ~10-fold relative to control, while PIP 640 peptide enhancement of exenatide uptake had an increase in AUC value of ~5-fold in comparison to exenatide alone (Table 5.1). Although the complete pharmacokinetic (PK) parameters required to properly calculate bioavailability were not available, the AUC values presented here suggest that the PIP 640 peptide enhanced the bioavailability of positively-charged calcitonin slightly more than negatively-charged exenatide. This finding is consistent with the observed charge-preferential TJ permeability function induced by the PIP 640 peptide in Caco-2 cell monolayer model *in vitro*.

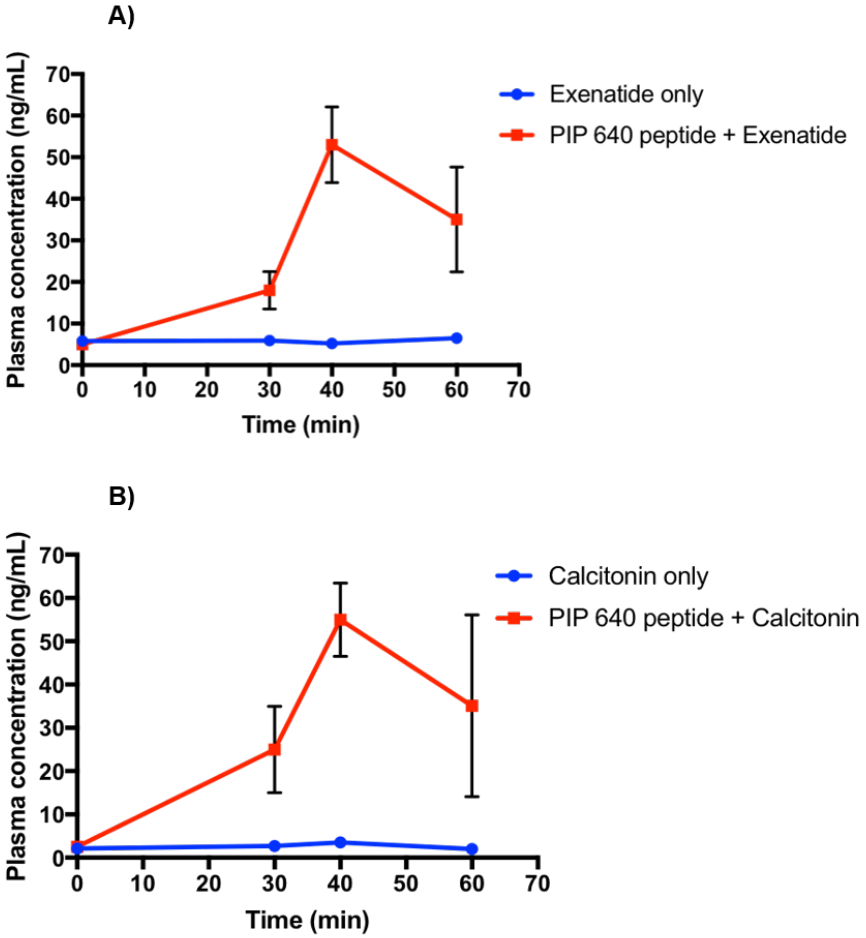

Figure 5.4: Permeability enhancement of calcitonin or exenatide as measured in blood collected from the portal vein of rats after co-administeration with 20 mM of PIP 640 peptide by ILI. All injected formulations (including calcitonin or exenatide only; control) contained 1.5 mg/mL soybean trypsin inhibitor (SBTI). **A)** Portal vein concentration-time profiles of exenatide alone or in combination with PIP 640. **B)** Time-course measurements of the plasma concentration of calcitonin alone or in combination with the PIP 640 peptide. Data are means ± SEM of 3 independent experiments; n= 3. One-way ANOVA indicated a significant difference between the data sets (***p* value< 0.01).

Table 5.1: Physicochemical properties and portal vein pharmacokinetics (PK) parameters following intraluminal injection of calcitonin and exenatide with and without PIP 640.

Peptide drug	MW (kDa)	Hydrodynamic size (Å)(calculated)	$AUC_{(t\ 0-60)}$ (ng/ml*min)		C_{max} (ng/ml)	
			Control	PIP 640	Control	PIP 640
Calcitonin	3.4	11	155	1734	3.3	55.6
Exenatide	4.2	11	340	1577	6.5	53

MW = molecular weight, calculated hydrodynamic radius and pharmacokinetic (PK) parameters obtained from data in Figure 5.4. The hydrodynamic radius was estimated as described in Section 2.13.6. The area under the curve between 0-60 min ($AUC_{t\ 0-60}$) was calculated with the trapezoid rule using the PK-Solver tool in Microsoft Excel (*212*).

5.3.4. TJ permeability enhancement of therapeutic peptides induced by the PIP 640 peptide did not permit co-absorption of endotoxins

Intestinal epithelium is normally exposed to different enteric bacteria that produce endotoxins, in particular lipopolysaccharide (LPS) [213, 214]. LPS are small fragments of the gram-negative bacteria cell wall released by dead bacteria [214]. Transport of LPS into systemic circulation is normally hindered by the epithelial cell barrier [13]. Studies have shown that high LPS levels in blood is usually associated with both local and/or systemic inflammation [13]. Thus, researchers have increased their focus on evaluating potential co-absorption of LPS when altering intestinal epithelial permeability for enhancing therapeutic peptides absorption when using PE agents [13, 215]. The PIP 640 peptide was shown to enhance the uptake of therapeutic peptides following ILI into rat jejunum. We asked whether the PIP 640 peptide could also enhance intestinal permeability of endotoxins along with increasing the uptake of therapeutic peptides. To address this, we used a *Limulus* amebocyte lysate (LAL) assay to semi-quantitatively detect endotoxin levels in blood plasma samples collected from the portal vein of rats following administration of the PIP 640 peptide with a therapeutic peptide by ILI, as described above in Section 2.13.

LAL reagent, which was obtained commercially, is prepared from a lysate of amebocytes of the horseshoe crab, *Limulus polyphemus* [140]. When LAL is exposed to a sample containing Lipopolysaccharide (LPS) endotoxins for 1 h at 37 °C, the LAL reaction with endotoxin results in the formation of a gel-like clot [140]. Depending on the endotoxin concentration in the sample, LAL reagent results could range from increasing the viscosity to formation of a hard gel; samples are only considered positive for endotoxin when the formed gel does not collapse after the sample tube is inverted 180° [140]. Inverted test tubes are thus used to determine the endotoxin level are shown in Figure 5. Gel formation was not observed in any of the blood plasma samples collected before and after exposure to the PIP 640 peptide by ILI (Figure 5.5). The last

endotoxin standard tube with a concentration of 0.01 EU/mL formed a softer gel-like clot that collapsed as soon as the tube was inverted, which is considered to be a negative result. This indicates that endotoxin levels in the exposure was < 0.01 EU/mL

.

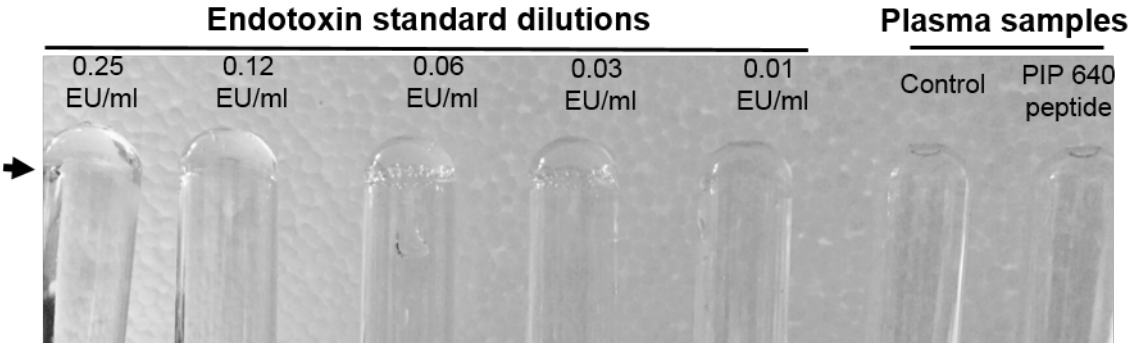

Figure 5.5: Semi-quantitative *Limulus* amebocyte lysate (LAL) assay measuring the endotoxin levels in the blood plasma samples collected from the portal veins of rats following administration of the PIP 640 peptide by ILI. Images show inverted test tubes of different endotoxin standard dilutions and tested blood plasma samples. The surface of the generated gels in the standard tubes (except 0.01 EU/mL) is highlighted with a black arrow. Images are representative of 2 independent experiments, n=2.

5.4. Discussion

The complexity of *in vivo* models used to study oral absorption has increased the reliance on *in vitro* models mainly because the latter provides an easier and faster way to predict the ability of a PE agent to effectively enhance oral bioavailability of poorly absorbed drugs [5, 135, 198]. However, even if a PE agent enhanced the intestinal permeability of a poorly absorbed drug in an *in vitro* model, this does not ensure similar outcomes *in vivo*. Various epithelial cell lines have been developed to mimic the intestinal epithelium with each cell line emulating certain features of the intestinal epithelial barrier *in vivo* but failing to emulate other aspects [216]. For example, Caco-2 cell monolayers can develop functional TJ structures as well as express a variety of metabolic enzymes and membrane transporters present in the intestinal epithelium *in vivo* [198, 216]. However, polarized Caco-2 monolayers develop a TEER range of ~ 250-400 $\Omega.cm^2$ [135, 217]; this is higher than the physiological TEER value of intestinal epithelium *in vivo*, which is less than 100 $\Omega.cm^2$ [45, 135]. In addition, use of these cell line-based *in vitro* models to evaluate the performance of a PE agent usually involves an apical application that remains at the cell's surface for a period of time (often > 60 min) that is much greater than what might be expected in the intestine *in vivo* due to the movement of luminal contents resulting from complex muscular contractions [5, 13]. These contractions mean that the intestinal transit *in vivo* can decrease the exposure time to a PE agent, altering its potential efficacy to enhance permeability of a poorly absorbed drug. Therefore, in our previous *in vivo* work we designed a longer version of the PIP 640 peptide with three additional positively charged amino acids: rrdykvevrrkkr-NH_2, in an attempt to improve its rate of cell penetration to reach its intended intracellular target [127]. *In vitro* studies presented in Chapter 1 and 2 assessed the performance and defined a potential MoA of the original PIP 640 peptide: rrdykvevrr-NH_2. Those studies demonstrated that the original PIP 640 peptide can enhance TJ permeability in Caco-2 cell monolayer *in vitro*. Therefore, the main aim of the current chapter was to validate our *in vitro* outcomes in a rat model *in vivo*.

First, we studied the ability of the original PIP 640 peptide, which does not have three additional basic amino acid residues, to overcome intestinal transit time and enhance the paracellular permeability of intestinal epithelial cells to therapeutic peptides following a direct ILI. This step was performed before tackling the formulation-related challenges associated with the oral delivery of therapeutic peptides, such as bypassing the stomach acidic environment and limiting the actions of pancreatic proteolytic enzymes, an issue that can be solved with existing pharmaceutical technologies such as use of an enteric coating [5]. To do this, we studied the efficacy of the PIP 640 peptide to enhance human insulin permeability in rat intestine *in vivo*. Human insulin was used because it has rapid and easily measured pharmacodynamics (PD) once it is absorbed by simply monitoring the blood glucose levels [127]. Moreover, insulin was chosen to compare the efficacy of the original PIP 640 peptide to the long version of the PIP 640 peptide because we already have defined the PK/PD profiles of insulin *in vivo* when co-administered with the longer version of the PIP 640 peptide [127]. In addition, insulin has a hydrodynamic radius of ~11 Å [218], which is consistent with the extent of TJ opening induced by the PIP 640 peptide; in Chapter 2 TJs were shown to be more permeable to 4 kDa dextran (~ 14 Å radius) but not larger dextrans. Citric acid was used as an acidifying agent in the injected formulation of insulin and PIP 640 peptide by ILI, as it has been shown to benefit therapeutic peptides by enhancing the stability of a peptide therapeutic against luminal proteolytic enzymes by lowering the luminal pH to < 6.5, which is below the optimal pH for the activity of these enzymes [204]. In addition, application of an acidifying agent is beneficial particularly when studying the intestinal permeability of insulin, because insulin tends to have low solubility in a pH environment equal to or higher that its pI value of ~5.3, such as in the intestinal environment of pH 5.7-7.4 [3, 5].

Chapter 5

Success in enhancing the intestinal epithelial TJ permeability of a therapeutic peptide using a PE agent *in vivo* requires their simultaneous arrival at the site of absorption with effective concentrations [5, 13]. The ability to meet this requirement can be limited by the intestinal transit time and large surface of the intestinal epithelium: there could be different spreading and/or dilution of a PE agent and therapeutic peptide after oral gavage [5]. Therefore, we attempted to translate *in vitro* information to *in vivo* outcomes by co-administration in an ILI format, such an approach might be most readily achieved by an oral dosage form. This approach, however, does not completely correlate *in vitro* to *in vivo* outcomes since the issues of movement and dilution within the intestinal lumen cannot be emulated *in vitro*. For example, sodium caprate can effectively function as a PE *in vitro* with a concentration ~10 mM [118], while it was used at a high concentration, up to 100 mM, to enhance permeability *in vivo* [202]. Hence, in the current study we used a higher concentration of the original PIP 640 peptide (20 mM) relative to the concentration tested in our *in vitro* studies (1 mM) in Chapters 1 and 2. The data presented above suggests that co-administration of the PIP 640 peptide with insulin enhanced the TJ permeability of the latter by increasing MLC-pS^{19} levels. This action induced a hypoglycaemic effect similar to the one induced by SC administration of insulin (Figure 5.1 A and B). Since the PD profile of insulin achieved by the original PIP 640 peptide (Figure 5. 1 B) is similar to the one obtained in our previous results using the longer version of the PIP 640 peptide [127], we assumed that the original PIP 640 peptide achieved enhancement of insulin bioavailability that was similar to the longer version of the peptide, which enhanced the bioavailability to ~1.5 % [127]. Consequently, we concluded that the original PIP 640 peptide was as effective as the longer version of the PIP 640 peptide.

One of the aims of the current work was to validate the role of the PIP 640 peptide in enhancing clauidn-2 at TJ structures, which was observed in the *in vitro* data (Chapter 2). Claudin-2 is known to be a pore-forming TJ protein,

which is highly expressed in tissues with leaky epithelia such as the intestine (*115, 206, 207*). Consistent with our *in vitro* studies, immunoblotting data presented above showed that treating rat intestinal epithelium *in vivo* with the PIP 640 peptide can increase claudin-2 levels over a time frame that correlated with increased MLC-pS^{19} levels (Figure 5. 2). This presumably occurred, as suggested in Chapter 2, by decreasing claudin-2 trafficking to lysosomes. Studies have shown that claudin-2 distribution pattern varies between the small intestine and colon in different species (*178, 205-207*). In both foetal and adult human small intestines, claudin-2 is expressed in epithelial cells located in both the villus and crypt of the intestinal mucosa, while claudin-2 in the colon is limited to crypt base (*206*). In contrast, claudin-2 expression in the small intestine in rats and mice was found to decrease from the crypt to the villus (*178, 207*), while claudin-2 expression and distribution have been found to be similar in the colons of rodents and humans, where it occurs in the crypt (*178, 207*). Consistent with the findings reported in these studies, our immunofluorescence microscopy data suggest a crypt to villus decrease of claudin-2 expression in rat intestine as previously described (Figure 5.3 A). Treating rat intestine with the PIP 640 peptide seemed to induce recruitment of more claudin-2 to the TJs (Figure 5. 3 A and B). These data support our *in vitro* findings that suggested a potential contribution of claudin-2 in PIP 640 function.

Previous studies have suggested that diffusion of therapeutic peptides through aqueous pores, such as TJs, can be affected by their surface charge, which is determined by their pI values and the pH of the surrounding environment (*5, 208, 209*). One study has shown that the paracellular permeability of a positively charged hexapeptide across Caco-2 monolayers was higher than a negatively charged peptide with the same size (*208*). In Chapter 2, we showed that PIP 640 peptide-induced claudin-2 at TJs in Caco-2 cell monolayers was associated with greater TJ permeability to positively-charged 4 kDa dextran relative to neutral or negatively-charge dextran of the same size. Therefore, we explored the potential effect of this charge-preferential

permeability induced by the PIP 640 peptide for therapeutic peptides. To test this hypothesis we measured the extent of permeability enhancement of both exenatide (pI=4.9) and calcitonin (pI=8.8) across rat intestinal epithelium following co-administration with the PIP 640 peptide by ILI. Based on pI values of these therapeutic peptides, exenatide and calcitonin should exhibit a net negative and positive charge, respectively, in the small intestine pH range (5.7-7.4) [3]. To maintain the same pH of the intestine, we used SBTI to protect the therapeutic peptides used from luminal proteolysis instead of citric acid, which was used earlier to examine the permeability of insulin (Figure 5.1).

Our data showed that the TJ opening induced by the PIP 640 peptide *in vivo* was more permeable to calcitonin than exenatide (Figure 5.4), based upon calculated PK parameters (Table.1) that suggested a 10-fold increase in the calculated calcitonin AUC compared to a 5-fold increase for the calculated AUC value of exenatide relative to controls (Figure 5.4). It is important to note that both control treatments, calcitonin and exenatide injected into rat intestine without the PIP 640 peptide, showed a slight increase in AUC values, which appeared to be higher with exenatide (Table.1). This is probably caused by SBTI because it was shown that application of SBTI at a concentration of 1.5 mg/mL can enhance insulin absorption to small extent [126]. These observations correlate well with our *in vitro* findings of the preferential TJ permeability of positively charged molecules induced by the PIP 640 peptide. Since the PIP 640 peptide enhanced claudin-2 localization at TJs, the data suggest that claudin-2 might play a role in the charge-preferential permeability obtained *in vivo*. This information could help define the appropriate physiochemical properties of a peptide drug that can benefit from our delivery strategy, such as being positively charged.

An essential function of the intestinal epithelium is to prevent uncontrolled uptake of luminal contents into the blood circulation [13]. Therefore,

pharmaceutically-acceptable PE agents to enhance drug permeability across the intestinal epithelium should not cause toxicity. In studies reporting the permeability enhancement effect of PE agents, it is common to evaluate their actions on cell viability, which only assesses epithelial cell integrity [5]. However, less attention is paid to whether PE agents might enhance the permeability of toxic substances, such as endotoxins, which are present in the intestinal lumen; this has become one of the major safety concerns associated with PE agents [5, 13]. Studies have shown that systemic endotoxin levels commonly range from 0 to $\leq$ 2 EU/mL in healthy individuals [219, 220], while in patients with intestinal epithelial inflammatory disorders characterized by leaky epithelial barrier, such as Crohn's disease, systemic endotoxin levels can be as high as 20-100 EU/mL [220]. Therefore, we aimed to evaluate the potential enhancement of the intestinal luminal endotoxin permeability associated with PIP 640 peptide-induced TJ permeability. The LAL assay results showed that endotoxin uptake into the blood circulation was not enhanced in rats following induction of TJ permeability by the PIP 640 peptide.

In conclusion, studies described in the current chapter validated the *in vitro* efficacy and MoA of the PIP 640 peptide in enhancing the intestinal epithelial TJ permeability of therapeutic peptides *in vivo*. In agreement with the *in vitro* studies demonstrated in Chapter 1 and 2, the results presented above showed that the PIP 640 peptide can effectively enhance intestinal TJ permeability of therapeutic peptides *in vivo*. This enhancement was associated with increased MLC-pS^{19} levels and increased localization of claudin-2 at TJs. Moreover, the data suggest that the TJ opening induced by the PIP 640 peptide was preferentially permeable to peptide drugs that are positively charged at the intestinal pH range, as the PIP 640 peptide enhanced the permeability of calcitonin more than exenatide. Finally, the PIP 640 peptide does not seem to induce co-absorption of intestinal endotoxin.

Chapter 5

Chapter 6 : General conclusion and future work

Chapter 6

TJ proteins of epithelial cells are subject to continuous remodelling events that provide a mechanism for dynamically altering their permeability properties through the paracellular pathway (*89, 177, 221*). The structural remodelling of TJ proteins are regulated by a wide array of intracellular signalling processes (*89, 221*). One of the key players within these intracellular events in altering TJ permeability involves the phosphorylation status of myosin light chain at serine 19 (MLC-pS^{19}). The phosphorylation status of S^{19} in MLC is regulated by the reciprocal actions of MLC kinase (MLCK) and MLC phosphatase (MLCP), with MLC affecting the function of perijunctional actomyosin filaments (*53, 88, 89, 92*). MLCK activation by various stimuli increases MLC-pS^{19} levels and opens TJs, an event that is reversed by MLCP activation (*53, 88, 89, 92*). Identification of this intracellular pathway has led to the discovery of MLCK hyperactivation having a role in reducing TJ barrier function associated with intestinal epithelial inflammatory disorders, such as Crohn's disease (*53, 103*). One of the tools used to study this role of MLCK was the application of a membrane permeant peptide inhibitor for MLCK, called PIK peptide. This peptide was shown to correct TJ barrier dysfunction induced by MLCK hyperactivation and suggested that modulation of MLCK function could represent a potential therapeutic strategy for diseases characterised by TJ barrier dysfunction (*53, 103*).

While studies have defined a role for MLCP in regulating MLC-pS^{19} levels and altering TJ permeability (*92, 160, 161*), nevertheless, there are still many questions about the precise role that MLCP plays in regulating TJ permeability. In this regard, the current studies focused on extending our previous work of developing specific membrane permeant peptide inhibitors for MLCP, PIP peptides, that were designed to enhance TJ permeability transiently by increasing MLC-pS^{19} levels via modulating MLCP activity (*127*). The current work was focused on the best PIP peptide candidates, PIP 640 peptide (rrdykvevrr-NH_2), to explore potential modifications of its sequence to optimize its activity and to validate its intracellular target and mechanism of action (MoA) *in vitro*. Moreover, this work explored changes to TJ protein structure associated with increasing MLC-pS^{19} levels achieved by regulation of MLCP activity. Finally, we assessed the potential ability of the PIP 640 peptide to

regulate TJ permeability *in vivo*. The overall motivations behind this work were to develop a strategy to improve oral delivery of therapeutic peptides through intestinal epithelial TJs through a hypothesis-driven strategy of modulating TJ permeability properties, as opposed to previous approaches to identify permeation enhancer (PE) agents that have used an essentially stochastic process. In addition, this work would improve our knowledge of TJ biology and the role of MLCP in regulating TJ permeability.

We designed the PIP 640 peptide to mimic the binding domain of CPI-17 to MLCP, which contains a phosphorylated threonine residue (pT^{38}), in the sequence $R^{36}V(pT)VKYDRR^{44}$. Several strategies were employed to identify a version of this peptide that allowed it to be more stable in the intestinal lumen and access the cytoplasm of intestinal epithelial cells; both of these properties were assumed essential for use of the peptide to alter MLCP activity and increase MLC-pS^{19} levels in order to transiently alter epithelial TJ permeability *in vivo*. Data presented in Chapter 3 showed that the peptide induced a reversible TJ permeability by increasing MLC-pS^{19} levels in Caco-2 cell monolayers without interfering with cell viability. In addition, both the intracellular distribution of the PIP 640 peptide and its binding profile to the regulatory subunits of MLCP, when compared to series mutants of the PIP 640 peptide, suggested an intracellular action of the PIP 640 peptide that was specified by a few essential amino acids. Since the results in Chapter 3 suggested the importance of the glutamic acid residue in the peptide sequence in mimicking the pT^{38} residue, we plan in the future to explore the potential optimization of PIP 640 peptide function by introducing a phosphatase stable-phosphothreonine mimetic, such as the 2-amino-3-methyl-4-phosphonobutyric acid [222] (Figure 6.1).

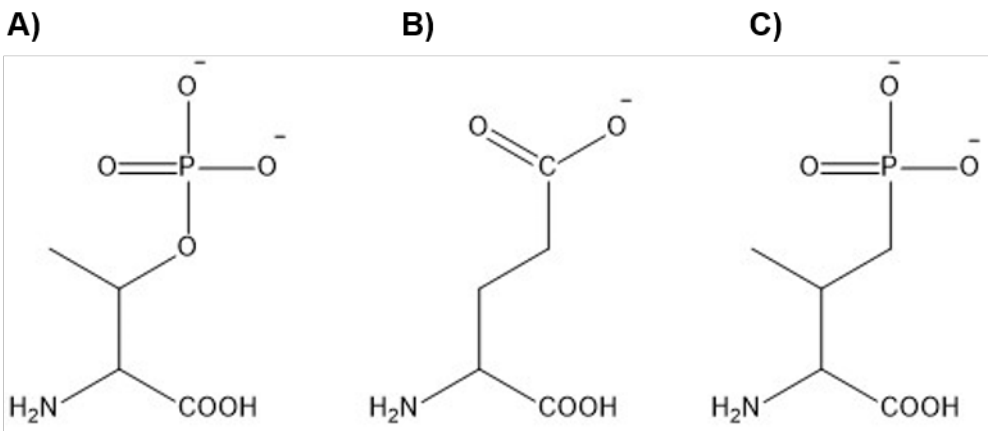

Figure 6.1: Comparison of the structure of phosphothreonine with potential stable mimetics. **A)** Phosphothreonine, **B)** Glutamic acid, and **C)** Stable phosphothreonine.

Studies discussed in Chapter 4, explored biochemical changes of TJ proteins associated with PIP 640 peptide-induced TJ permeability changes associated with increased MLC-pS[19]. Our results showed that, of the many TJ proteins evaluated, only claudin-2 protein levels were altered (increased) in response to the PIP 640 peptide and that there was an increase in the amount of claudin-2 at TJ structures. These modifications to claudin-2 correlated with an increased phosphorylation status, presumably at the serine residue in position 208, which has been shown to enhance claudin-2 detergent extractability and enhance its localization at TJs [(181)]. These changes in TJ structure induced by the PIP 640 peptide were associated with opening of the TJ in a way that was preferentially permeable to positively charged molecules, suggesting a potential contribution of claudin-2 to the TJ permeability function of the PIP 640 peptide (Figure 6.2). In the future, live imaging studies using fluorescence microscopy could be performed to examine the actions of the PIP 640 peptide on a Caco-2 cell line that constitutively expresses fluorescent TJ proteins, such as claudin-2 and occludin. Such a study would provide critical information regarding TJ structural changes associated with altered paracellular permeability induced by the PIP 640 peptide. In addition, more efforts could be focused on defining the intracellular signalling pathways involved in inducing claudin-2 localization at TJs induced by the PIP 640 peptide.

Chapter 6

In Chapters 3 and 4, we showed that the PIP 640 peptide is able to induce TJ permeability by increasing MLC-pS^{19} levels that were associated with increased claudin-2 localization at TJs in Caco-2 cell monolayers *in vitro*. Thus, in Chapter 5, we aimed to test this presumed mechanism of action (MoA) in an *in vivo* model. In addition, we sought to ensure that the extent of TJ opening induced by the PIP 640 peptide observed *in vitro*, could effectively enhance permeability of a therapeutic peptide *in vivo*. The results obtained showed that the PIP 640 peptide can effectively enhance the intestinal TJ permeability of three therapeutic peptides *in vivo*: insulin, calcitonin, and exenatide. Increased uptake of these therapeutic peptides from the rat jejunum following intra-luminal injection was associated with enhancement of MLC-pS^{19} levels and increased claudin-2 at TJ structures. Moreover, the PIP 640 peptide induced similar charge-preferential permeability changes to those observed *in vitro*. One next logical step would be to develop an appropriate oral dosage form of the PIP 640 peptide with a therapeutic peptide to evaluate its safety and efficacy *in vivo* after repeat exposure.

Overall, we have evaluated a small cell-permeant peptide, PIP 640 peptide, for its ability to open TJs for the enhanced uptake of a therapeutic peptide. The hypothesis-driven strategy for this approach focused on altering permeability across the intestinal epithelial barrier by manipulating an endogenous mechanism controlled by the phosphorylation status of MLC. This approach represents an advantage over most of other permeation enhancement strategies, which can act non-selectively and without a defined MoA to enhance intestinal epithelial TJ permeability. Data presented in this thesis show that the PIP 640 peptide is capable of acting selectively on this endogenous mechanism and induces a perm-selective TJ permeability *in vivo* and *in vitro*. Accordingly, we believe that application of the PIP 640 peptide in combination with other pharmaceutical technologies could lead to the development of a new oral delivery strategy for therapeutic peptides.

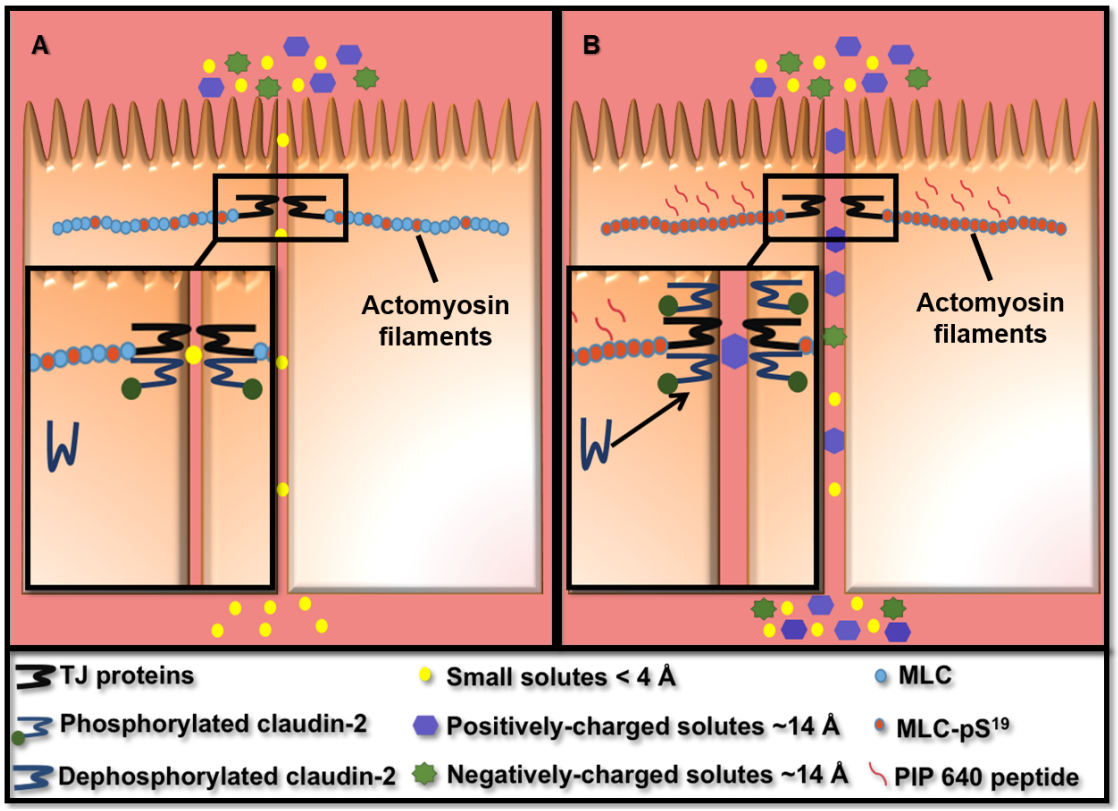

Figure 6.2: Cartoon image summarizing changes in cellular signalling events associated with the TJ permeability enhancement induced by the PIP 640 peptide. **A)** Limited permeability of TJs occurring at steady state. **B)** Perm-selective increase in TJ permeability induced by the PIP 640 peptide.

Chapter 7 : Appendices

7.1. PIP Peptides analytical characterization

The following peptides were synthesized on a 0.15 mmol scale (0.25 g resin).

A) PIP 640 peptide (157 mg, 44 % yield); HPLC: t_R= 4.3 min; ESI-MS$^+$ calculated for $C_{58}H_{102}N_{24}O_{15}$: m/z = 1375.80; found m/z = 1375.82 $[M+H]^+$. HPLC analysis (Figure 7.3) and MS analysis (Figure 7.14).

B) PIP 641 peptide (125 mg, 39 % yield); HPLC: t_R = 4.1 min; ESI-MS$^+$ calculated for $C_{56}H_{99}N_{23}O_{14}$: m/z = 1317.77; found m/z = 1317.77 $[M+H]^+$. HPLC analysis (Figure 7.4) and MS analysis (Figure 7.15).

C) PIP 642 peptide (118 mg, 38 % yield); HPLC: t_R = 3.8 min; ESI-MS$^+$ calculated for $C_{52}H_{98}N_{24}O_{14}$: m/z = 1283.77; found m/z = 1283.78 $[M+H]^+$. HPLC analysis (Figure 7.5) and MS analysis (Figure 7.16).

D) PIP 643 peptide (162 mg, 51 % yield); HPLC: t_R = 4.1 min; ESI-MS$^+$ calculated for $C_{57}H_{100}N_{23}O_{14}$: m/z = 1331.78; found m/z = 1331.80 $[M+H]^+$. HPLC analysis (Figure 7.6) and MS analysis (Figure 7.17).

E) PIP 644 peptide (174 mg, 49 % yield); HPLC: t_R = 4 min; ESI-MS$^+$ calculated for $C_{60}H_{109}N_{27}O_{13}$: m/z = 1416.87; found m/z = 1416.89 $[M+H]^+$. HPLC analysis (Figure 7.7) and MS analysis (Figure 7.18).

F) N-terminally biotinylated PIP 640 peptide (133 mg, 52 % yield); HPLC: t_R = 4.4 min; ESI-MS$^+$ calculated for $C_{68}H_{116}N_{26}O_{17}S$: m/z = 1601.88; found m/z = 1601.88 $[M+H]^+$.. HPLC analysis (Figure 7.8) and MS analysis (Figure 7.19).

G) N-terminally biotinylated PIP 641 peptide (124 mg, 37 % yield); HPLC: t_R = 4.4 min; ESI-MS$^+$ calculated for $C_{65}H_{112}N_{27}O_{15}S$: m/z = 1543.86; found m/z = 1543.87 $[M+H]^+$. HPLC analysis (Figure 7.9) and MS analysis (Figure 7.20).

H) N-terminally biotinylated PIP 642 peptide (129 mg, 39 % yield); HPLC: t_R = 4.2 min; ESI-MS$^+$ calculated for $C_{62}H_{110}N_{25}O_{17}S$: m/z = 755.41; found m/z = 755.44 $[M+2H]^{2+}$. HPLC analysis (Figure 7.10) and MS analysis (Figure 7.21).

I) N-terminally biotinylated PIP 643 peptide (118 mg, 47 % yield); HPLC: t_R = 4.5 min; ESI-MS$^+$ calculated for $C_{67}H_{116}N_{26}O_{15}S$: m/z = 1557.89; found m/z = 1557.86 $[M+H]^+$. HPLC analysis (Figure 7.11) and MS analysis (Figure 7.22).

J) N-terminally biotinylated PIP 644 peptide (135 mg, 37 % yield); HPLC: t_R = 4.3 min; ESI-MS$^+$ calculated for $C_{70}H_{121}N_{28}O_{15}S$: m/z = 821.96; found m/z = 821.99 $[M+2H]^{2+}$. HPLC analysis (Figure 7.12) and MS analysis (Figure 7.23).

The following peptide was synthesized on a 0.085 mmol scale (0.25 g resin)

K) C-terminally biotinylated PIP 640 peptide (PIP 640-PEG-biotin) (93 mg, 43 % yield); HPLC: t_R = 4.9 min; ESI-MS$^+$ calculated for $C_{78}H_{137}N_{27}O_{20}S$: m/z = 903.02; found m/z = 903.02 $[M+2H]^{2+}$. HPLC analysis (Figure 7.13) and MS analysis (Figure 7.24).

7.2. Additional figures

A) **C-terminally biotinylated PIP 640 peptide (PIP 640-PEG-biotin)**

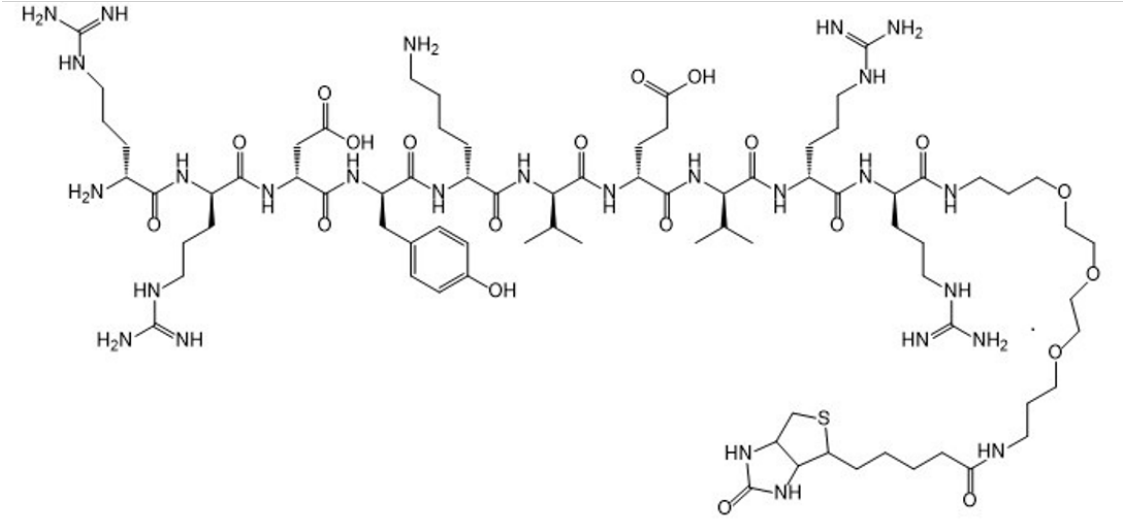

B) **N-terminally biotinylated PIP 640 peptide**

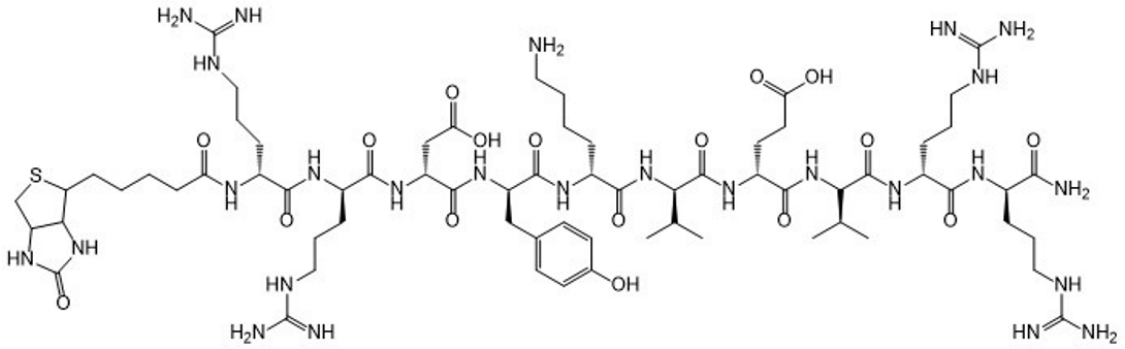

Figure 7.1: Chemical structures of **A)** C-terminally biotinylated PIP 640 PIP peptide (PIP 640-PEG-Biotin) with an additional PEG spacer between the peptide and biotin. **B)** N-terminally biotinylated PIP 640 peptide that coupled directly to the biotin unit.

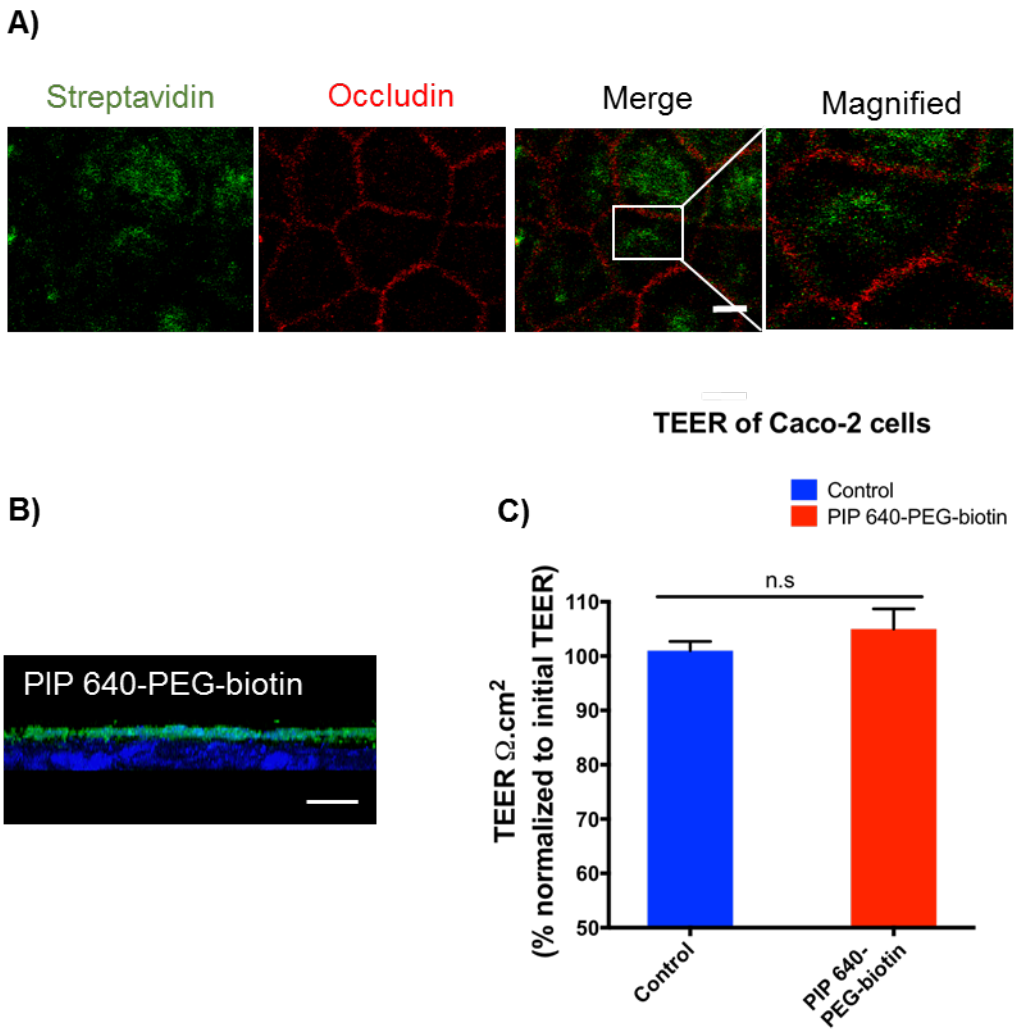

Figure 7.2: **A)** Confocal microscopy images of Caco-2 monolayers showing distribution of C-terminally biotinylated PIP 640 peptide (PIP 640-PEG-biotin) after 45 min of apical exposure. PIP 640-PEG-biotin was detected by Alexa 488-conjugated streptavidin (green). TJs are stained with Alexa 546-conjugated secondary antibody against occludin primary antibody (red). Scale bar, 10 µm. **B)** Z-stack scan image of Caco-2 monolayers obtained by confocal micrscopy showing surface and subcellular localization of PIP 640-PEG-biotin peptide after 45 min of apical exposure. Nuclei were stained with DAPI (blue). Scale bar, 20 µm. Images are repesentative of 3 independent experiments with n=3 for all peptide. **C)** TEER change of Caco-2 cell monolayers induced by 1 mM of PIP 640-PEG-biotin. This data shows that PIP 640-PEG-biotin peptide has no effect on the cell TEER. Data are means ± SEM of 3 independent experiments, n= 6 for Control and PIP 640-PEG-biotin peptide.

7.3. HPLC and mass spectrometry characterization

7.3.1. HPLC analysis

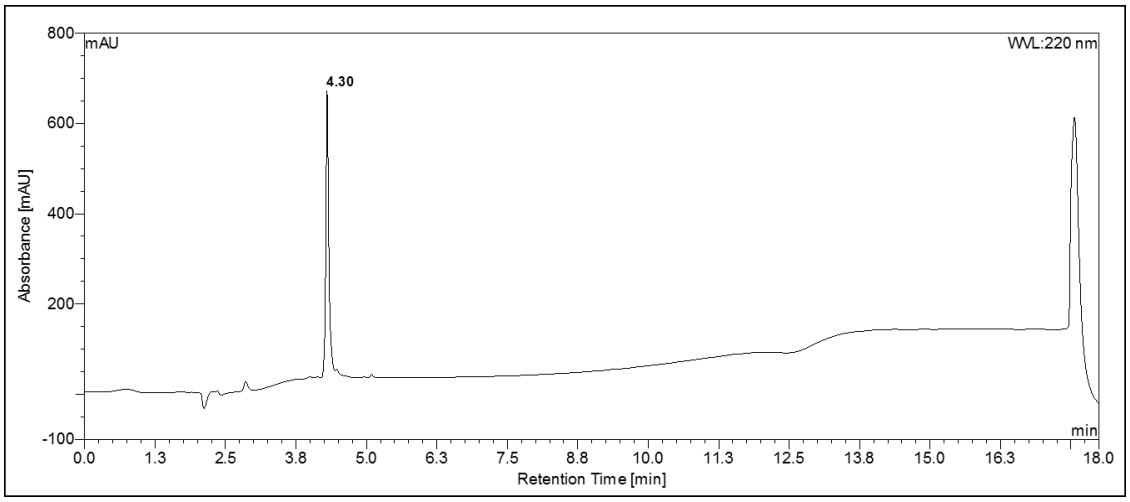

Figure 7.3: HPLC chromatogram of purified PIP 640 peptide, rrdykvevrr-NH_2, detected at 220 nm

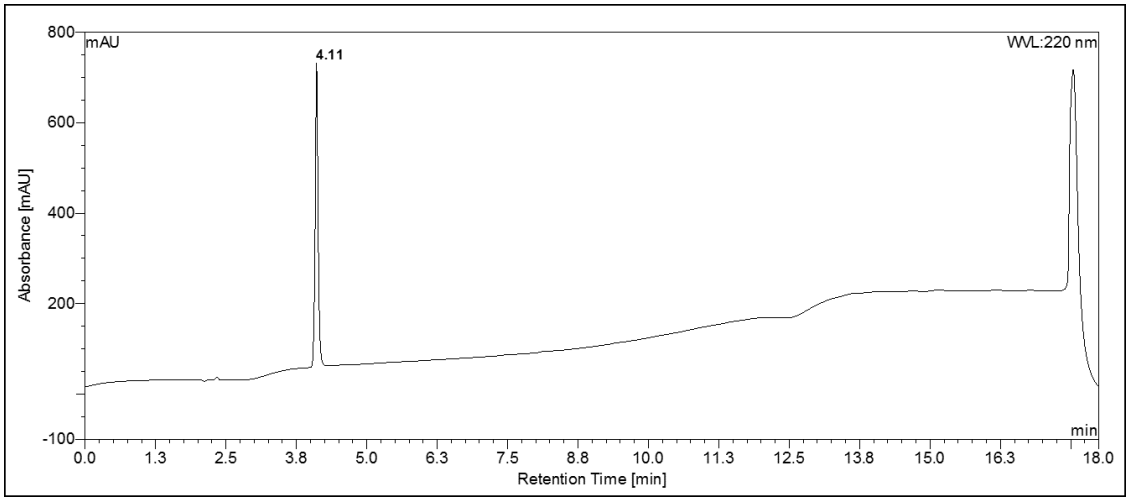

Figure 7.4: HPLC chromatogram of purified PIP 641 peptide, rrdykvavrr-NH_2, detected at 220 nm

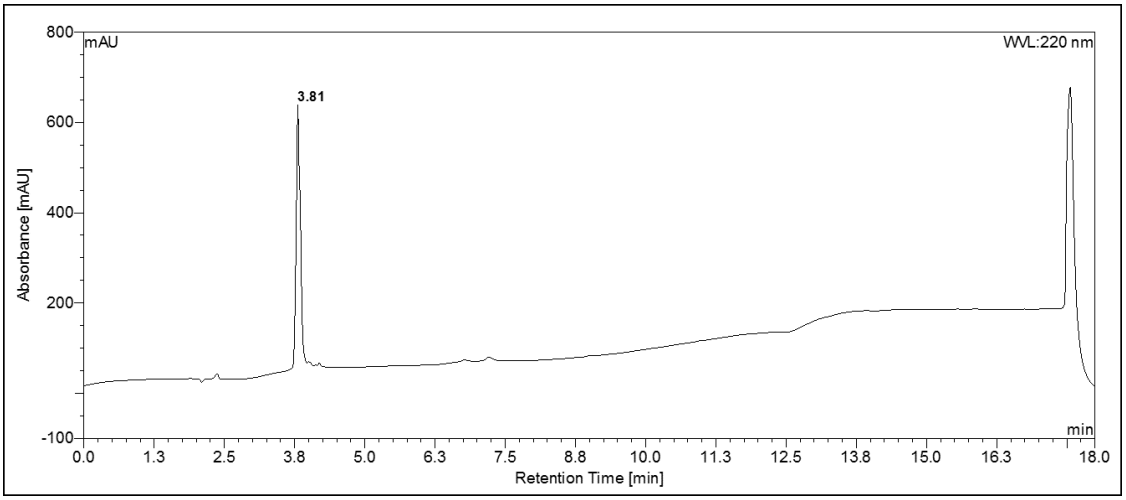

Figure 7.5: HPLC chromatogram of purified PIP 642 peptide, rrdakvevrr-NH_2, detected at 220 nm

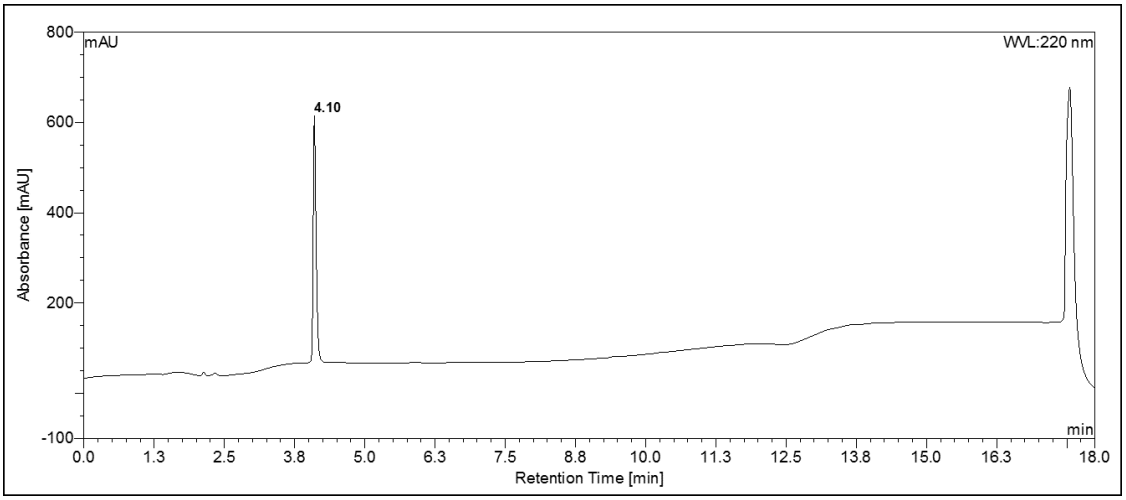

Figure 7.6: HPLC chromatogram of purified PIP 643 peptide, rraykvevrr-NH_2, detected at 220 nm

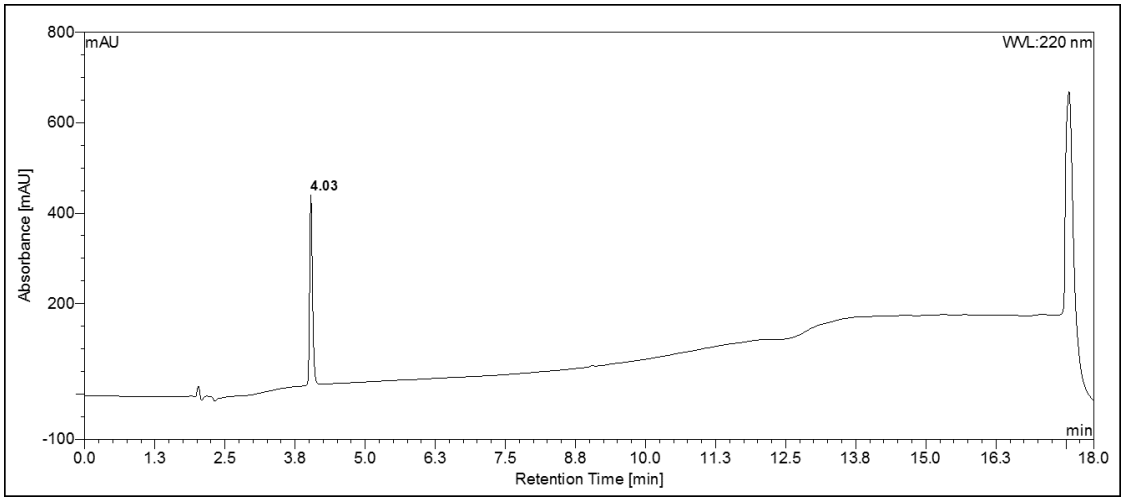

Figure 7.7: HPLC chromatogram of purified PIP 644 peptide, rrrykvevrr-NH_2, detected at 220 nm

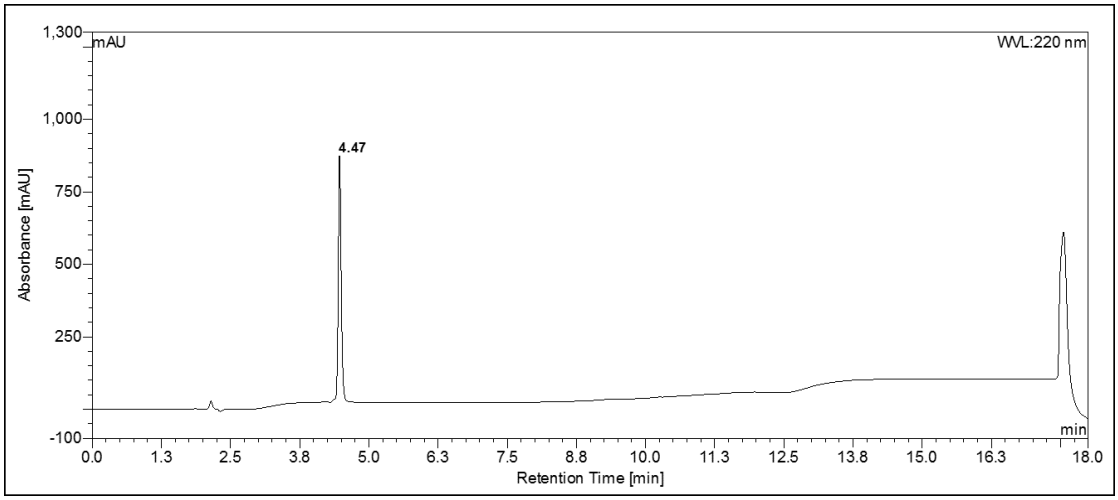

Figure 7.8: HPLC chromatogram of purified N-terminally biotinylated PIP 640 peptide, biotin-rrdykvevrr-NH_2, detected at 220 nm

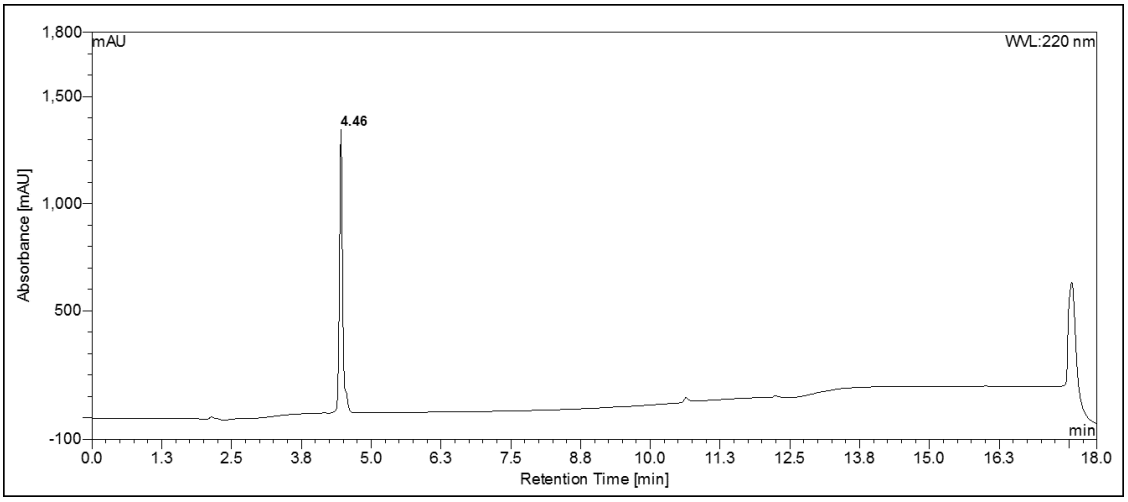

Figure 7.9: HPLC chromatogram of purified N-terminally biotinylated PIP 641 peptide, biotin-rrdykvavrr-NH_2, detected at 220 nm

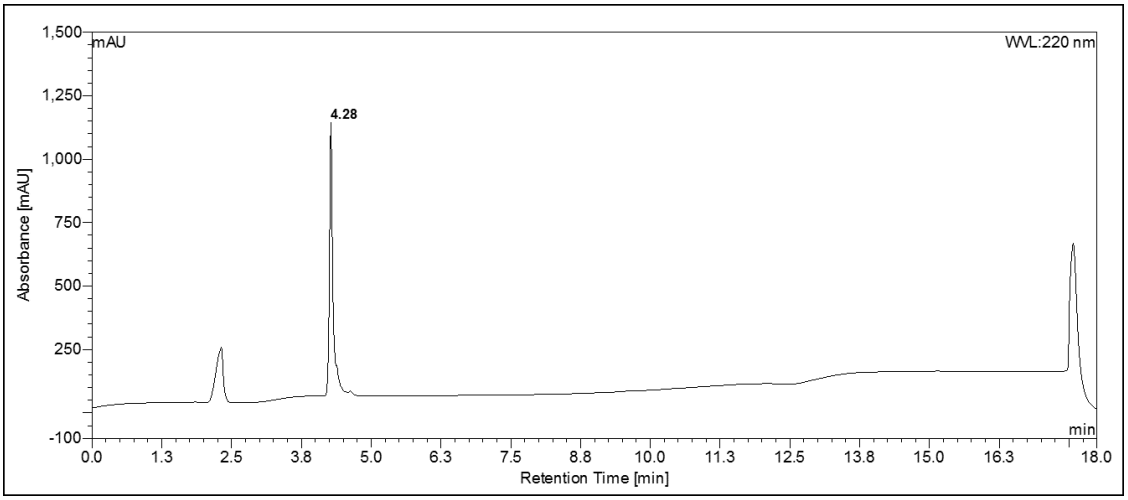

Figure 7.10: HPLC chromatogram of purified N-terminally biotinylated PIP 642 peptide, biotin-rrdakvevrr-NH_2, detected at 220 nm

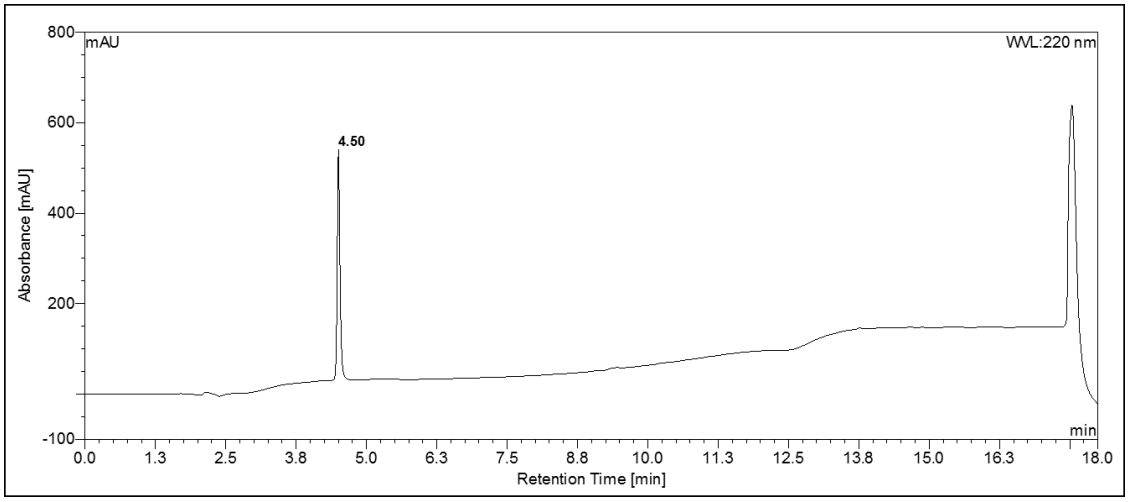

Figure 7.11: HPLC chromatogram of purified N-terminally biotinylated PIP 643 peptide, biotin-rraykvevrr-NH_2, detected at 220 nm

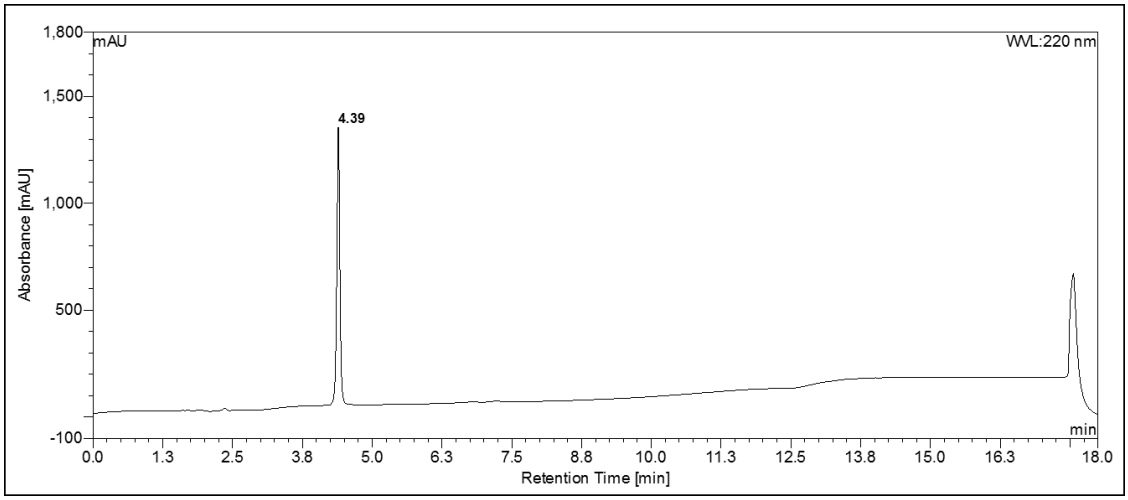

Figure 7.12: HPLC chromatogram of purified N-terminally biotinylated PIP 644 peptide, biotin-rrrykvevrr-NH_2, detected at 220 nm

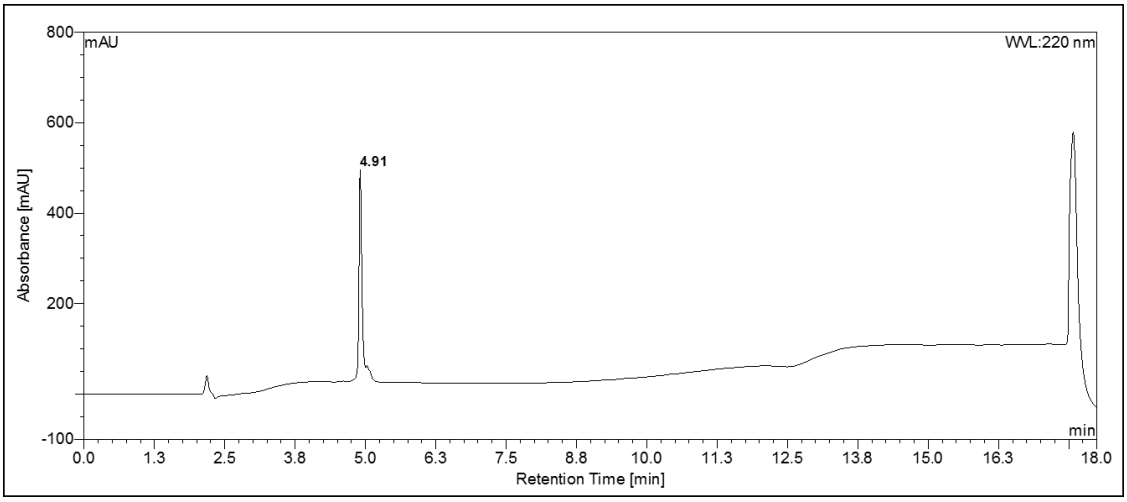

Figure 7.13: HPLC chromatogram of purified C-terminally biotinylated PIP 640 peptide, rraykvevrr-PEG-biotin, detected at 220 nm

7.3.2. Mass spectrometry data

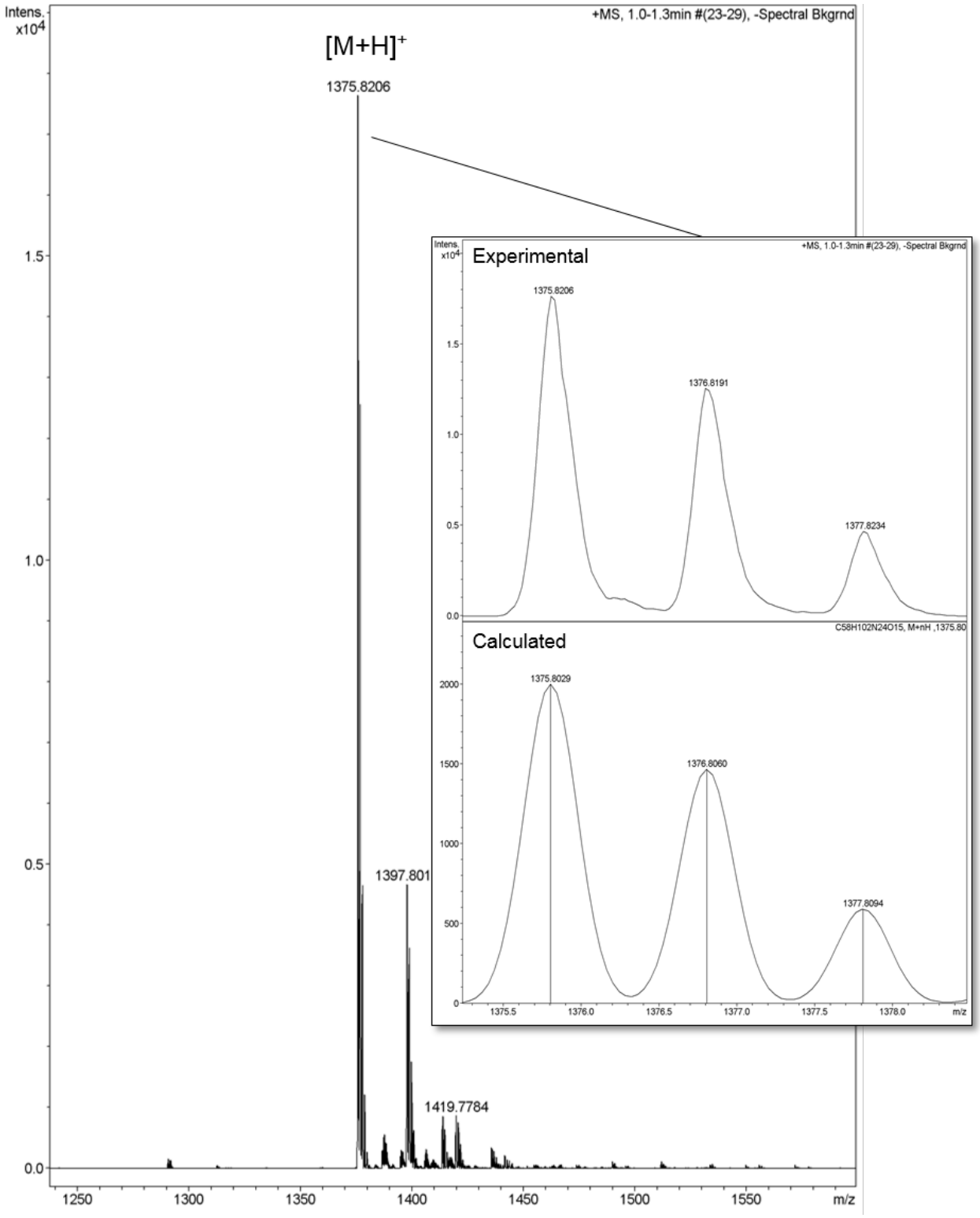

Figure 7.14: ESI-MS$^+$ spectrum of the PIP 640 peptide. Inset, the experimental isotopic pattern (top) in comparison with the calculated isotopic pattern (bottom) for the $[M+H]^+$ species.

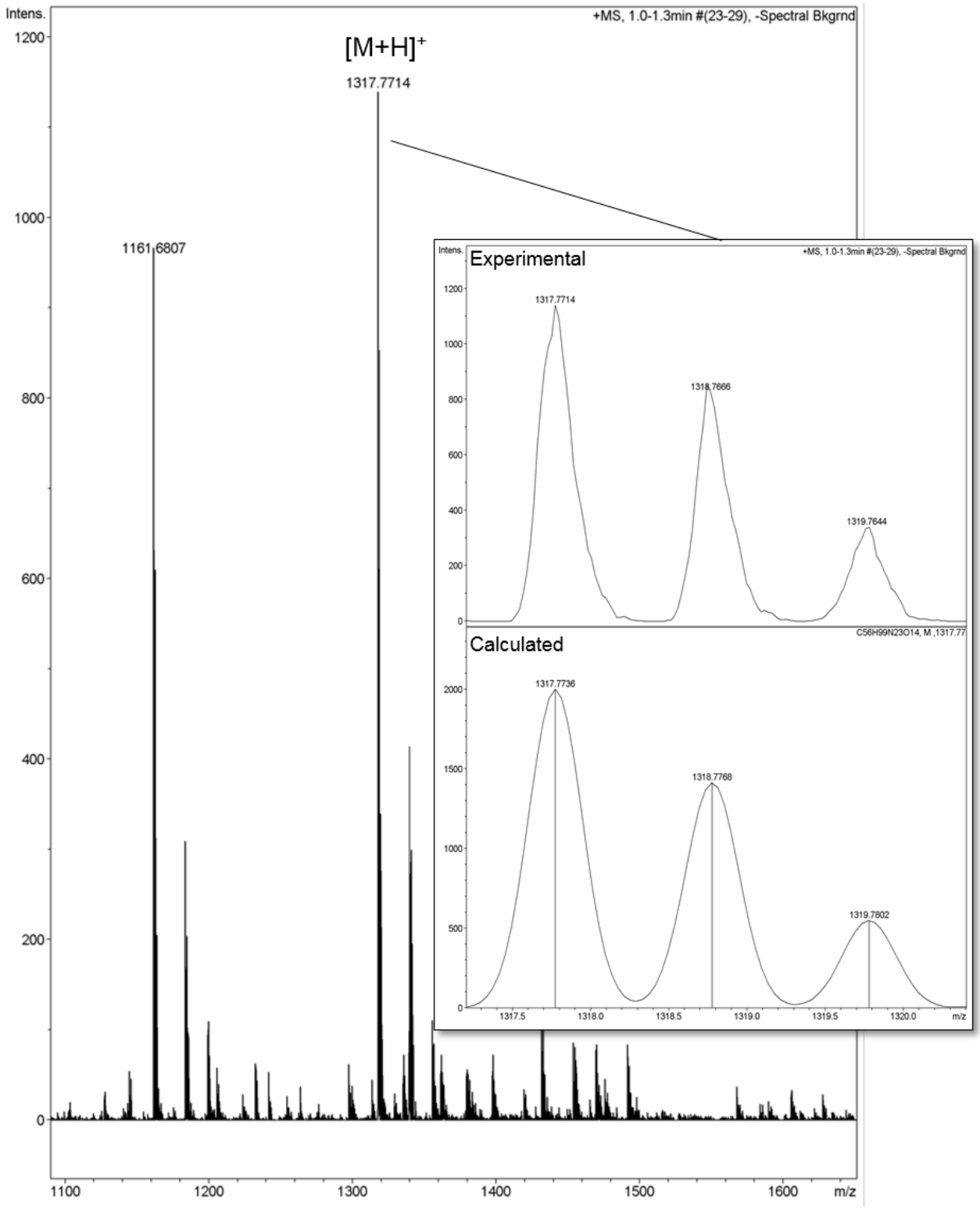

Figure 7.15: ESI-MS$^+$ spectrum of the PIP 641 peptide. Inset, the experimental isotopic pattern (top) in comparison with the calculated isotopic pattern (bottom) for the $[M+H]^+$ species.

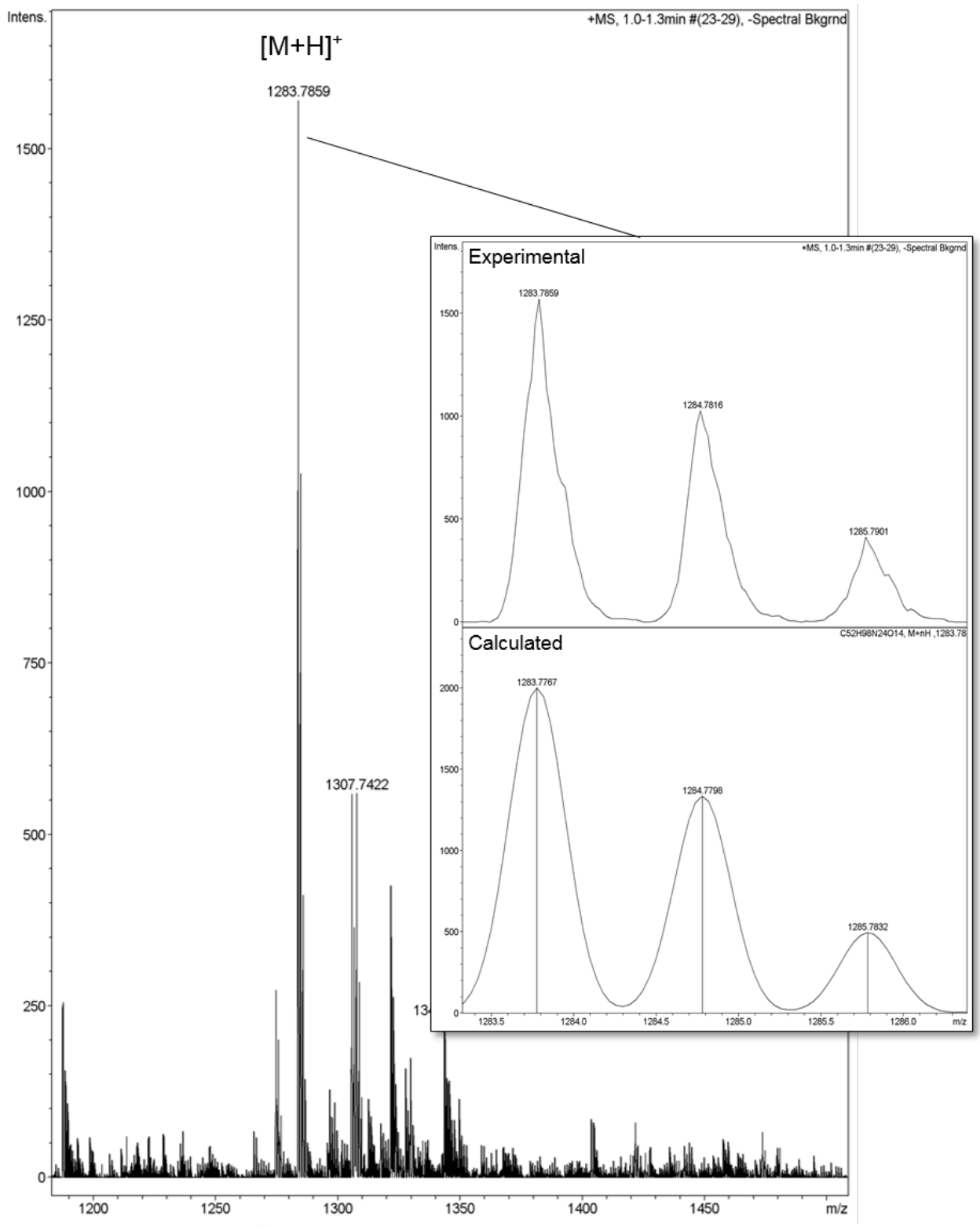

Figure 7.16: ESI-MS$^+$ spectrum of the PIP 642 peptide. Inset, the experimental isotopic pattern (top) in comparison with the calculated isotopic pattern (bottom) for the $[M+H]^+$ species.

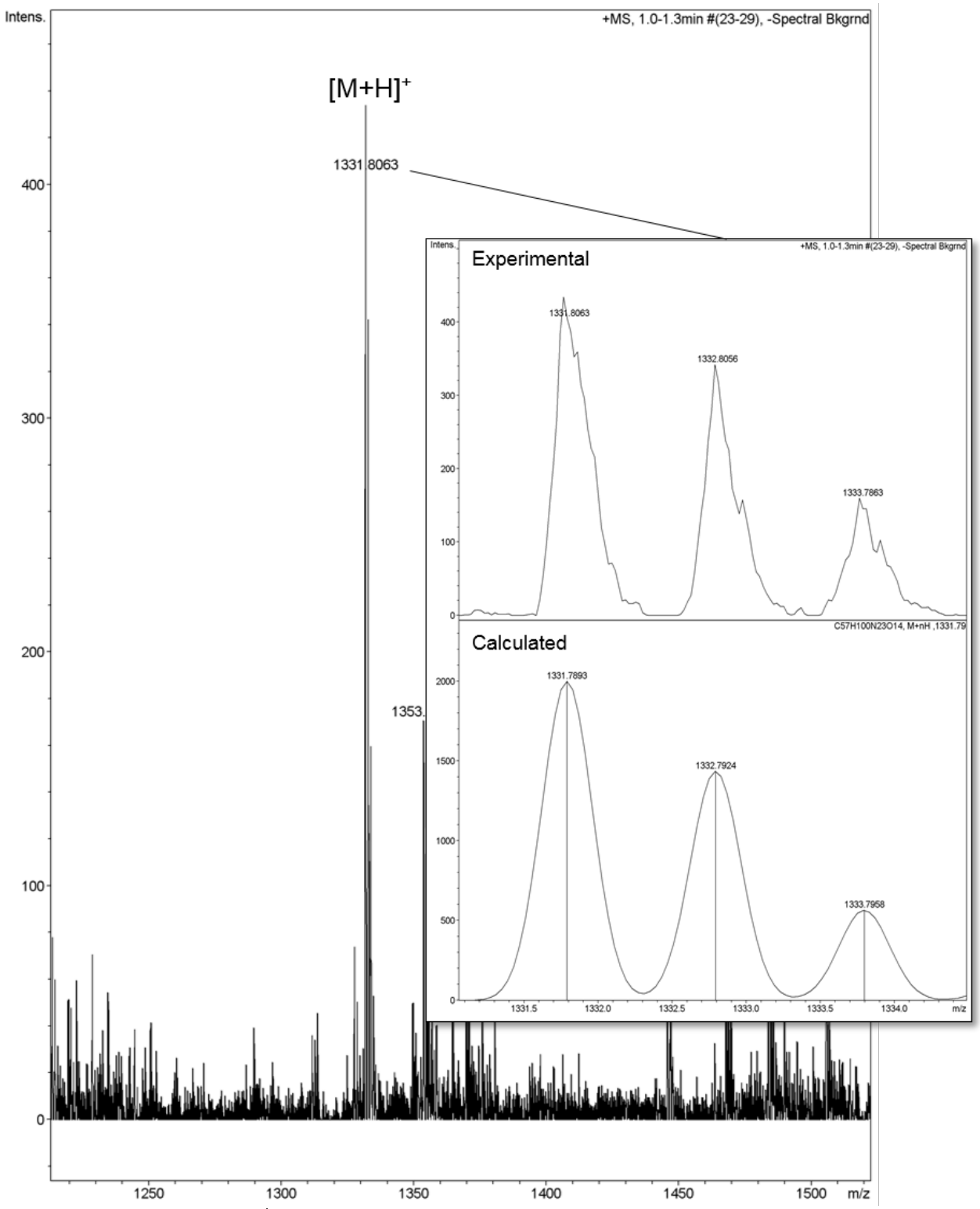

Figure 7.17: ESI-MS$^+$ spectrum of the PIP 643 peptide. Inset, the experimental isotopic pattern (top) in comparison with the calculated isotopic pattern (bottom) for the $[M+H]^+$ species.

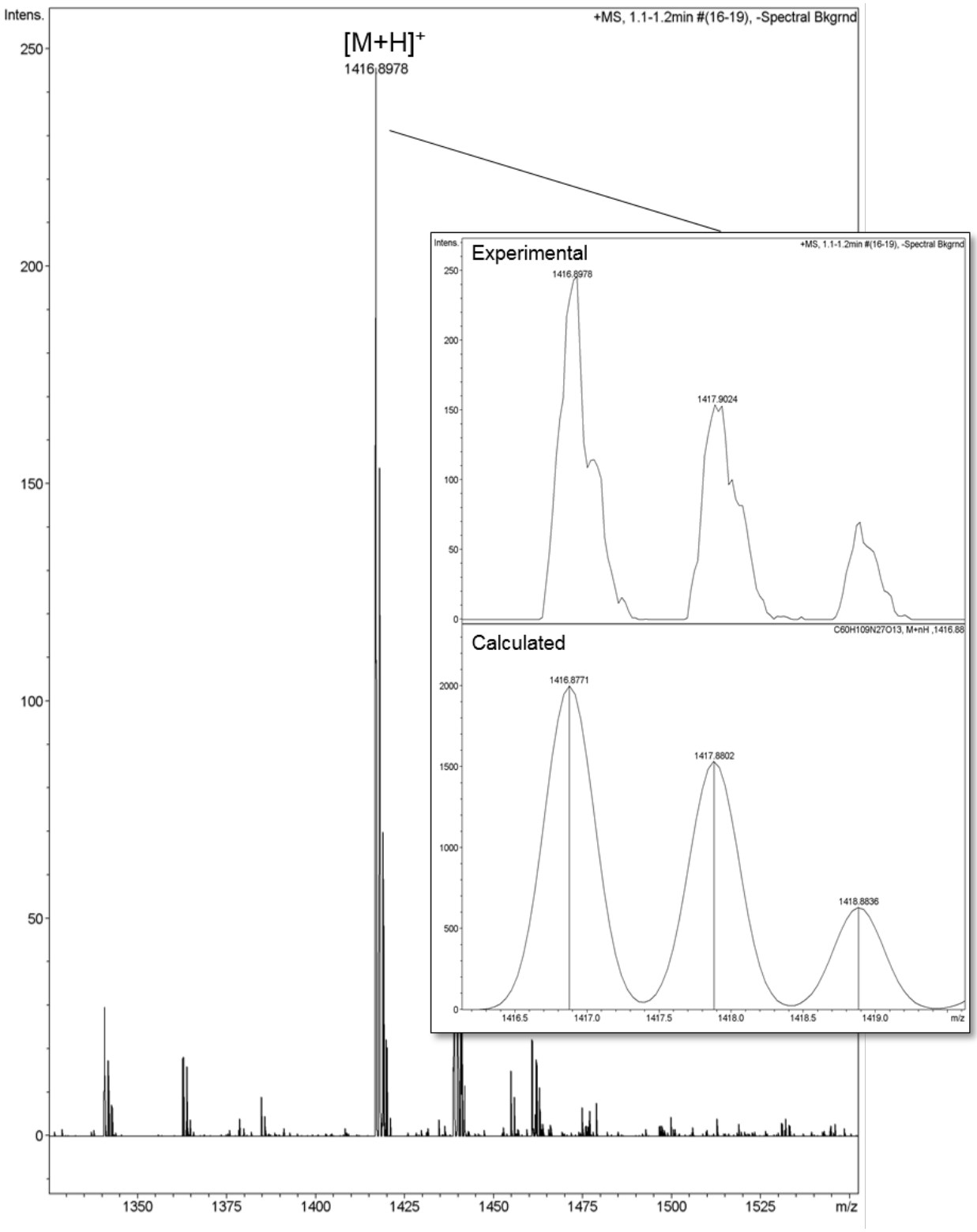

Figure 7.18: ESI-MS$^+$ spectrum of the PIP 644 peptide. Inset, the experimental isotopic pattern (top) in comparison with the calculated isotopic pattern (bottom) for the $[M+H]^+$ species.

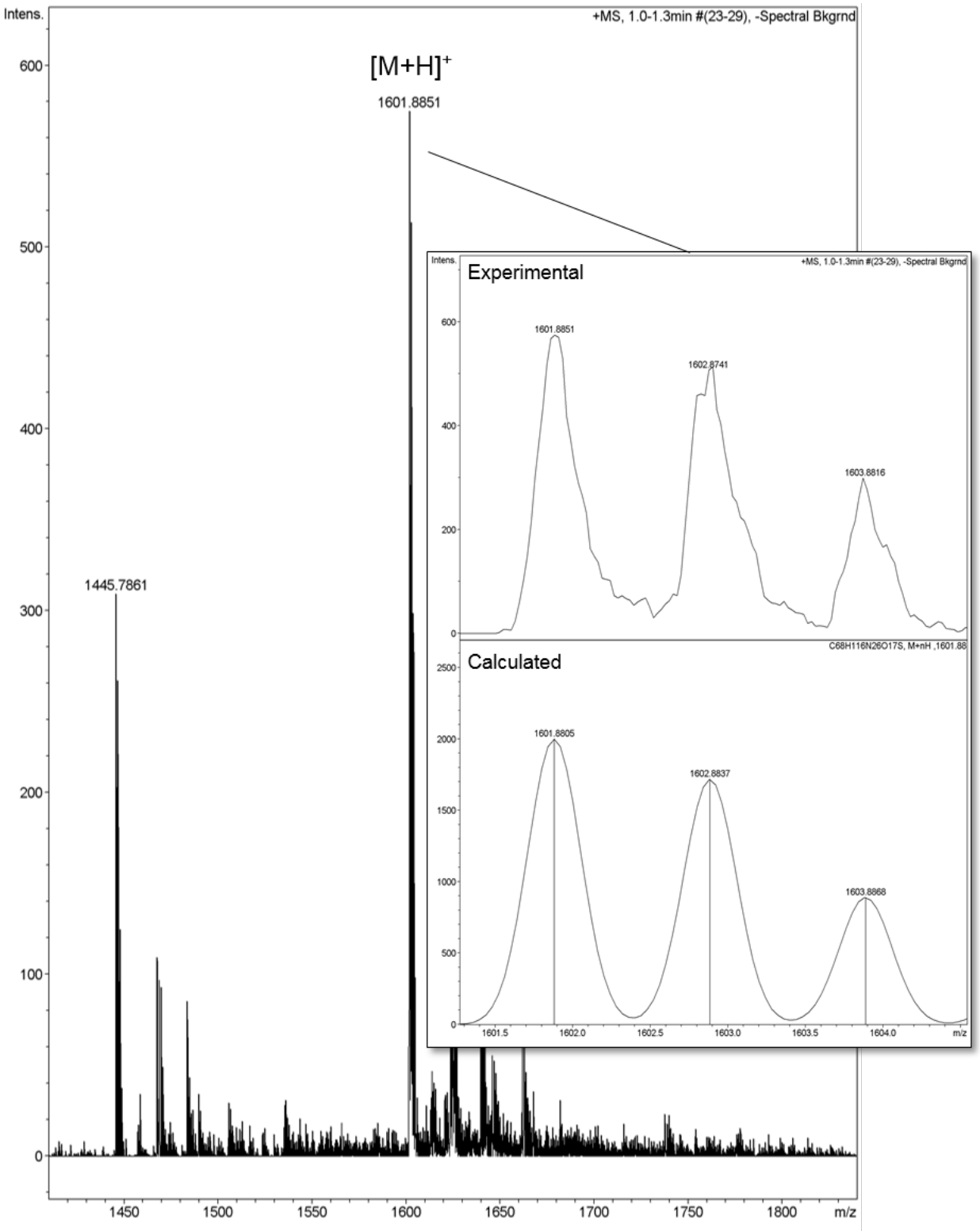

Figure 7.19: ESI-MS$^+$ spectrum of the N-terminally biotinylated PIP 640 peptide. Inset, the experimental isotopic pattern (top) in comparison with the calculated isotopic pattern (bottom) for the $[M+H]^+$ species.

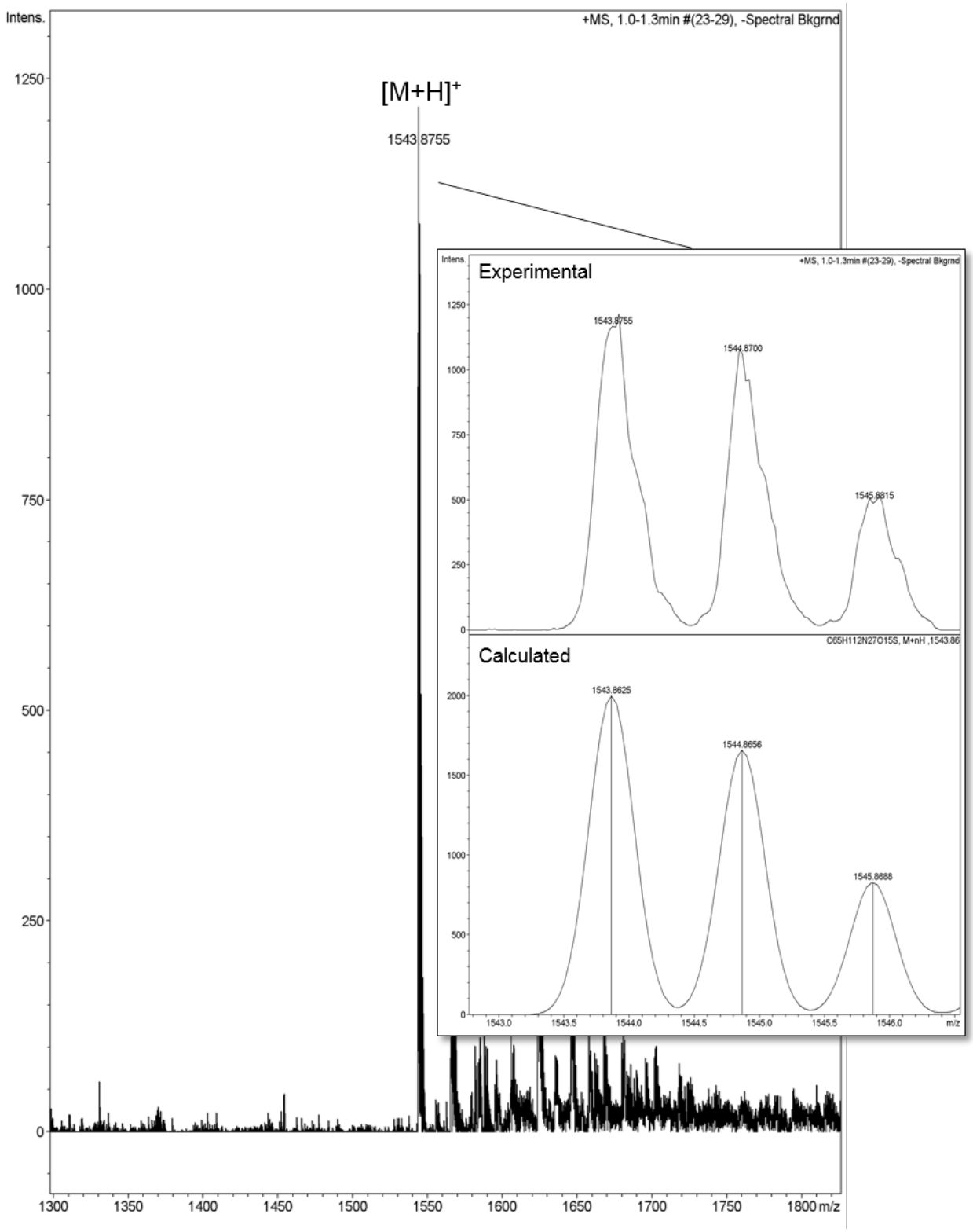

Figure 7.20: ESI-MS$^+$ spectrum of the N-terminally biotinylated PIP 641 peptide. Inset, the experimental isotopic pattern (top) in comparison with the calculated isotopic pattern (bottom) for the $[M+H]^+$ species.

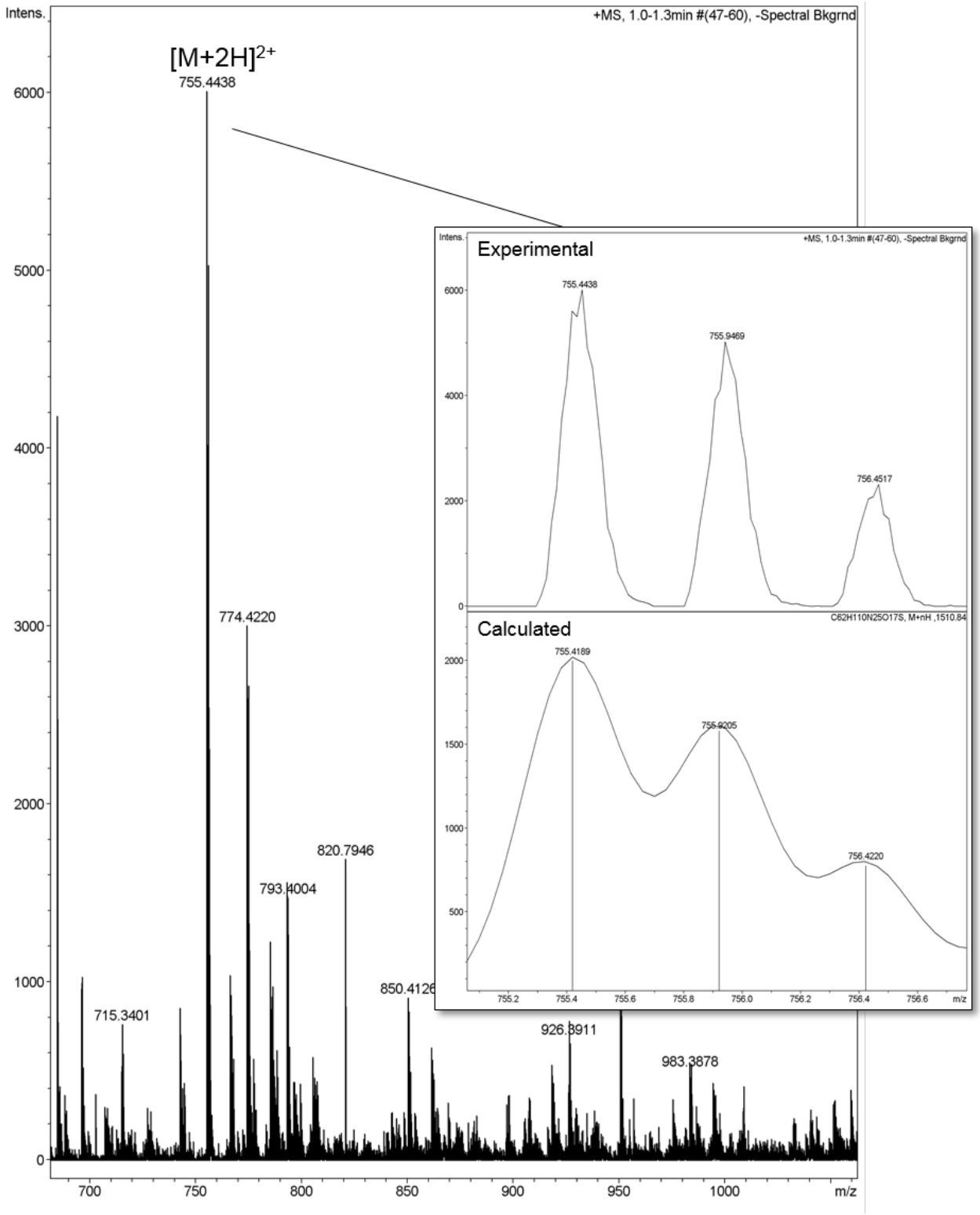

Figure 7.21: ESI-MS$^+$ spectrum of the N-terminally biotinylated PIP 642 peptide. Inset, the experimental isotopic pattern (top) in comparison with the calculated isotopic pattern (bottom) for the $[M+2H]^{2+}$ species.

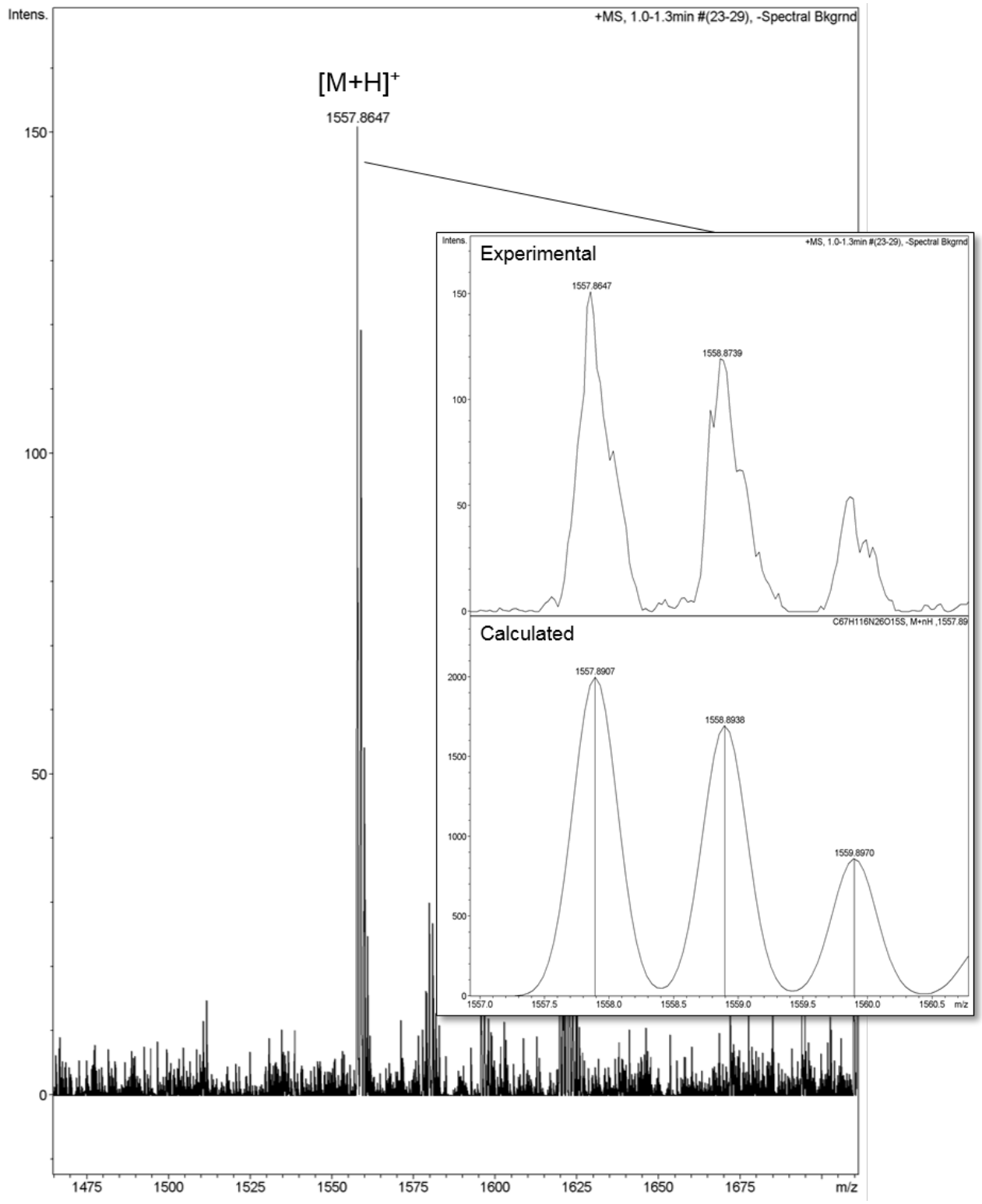

Figure 7.22: ESI-MS$^+$ spectrum of the N-terminally biotinylated PIP 643 peptide. Inset, the experimental isotopic pattern (top) in comparison with the calculated isotopic pattern (bottom) for the $[M+H]^+$ species.

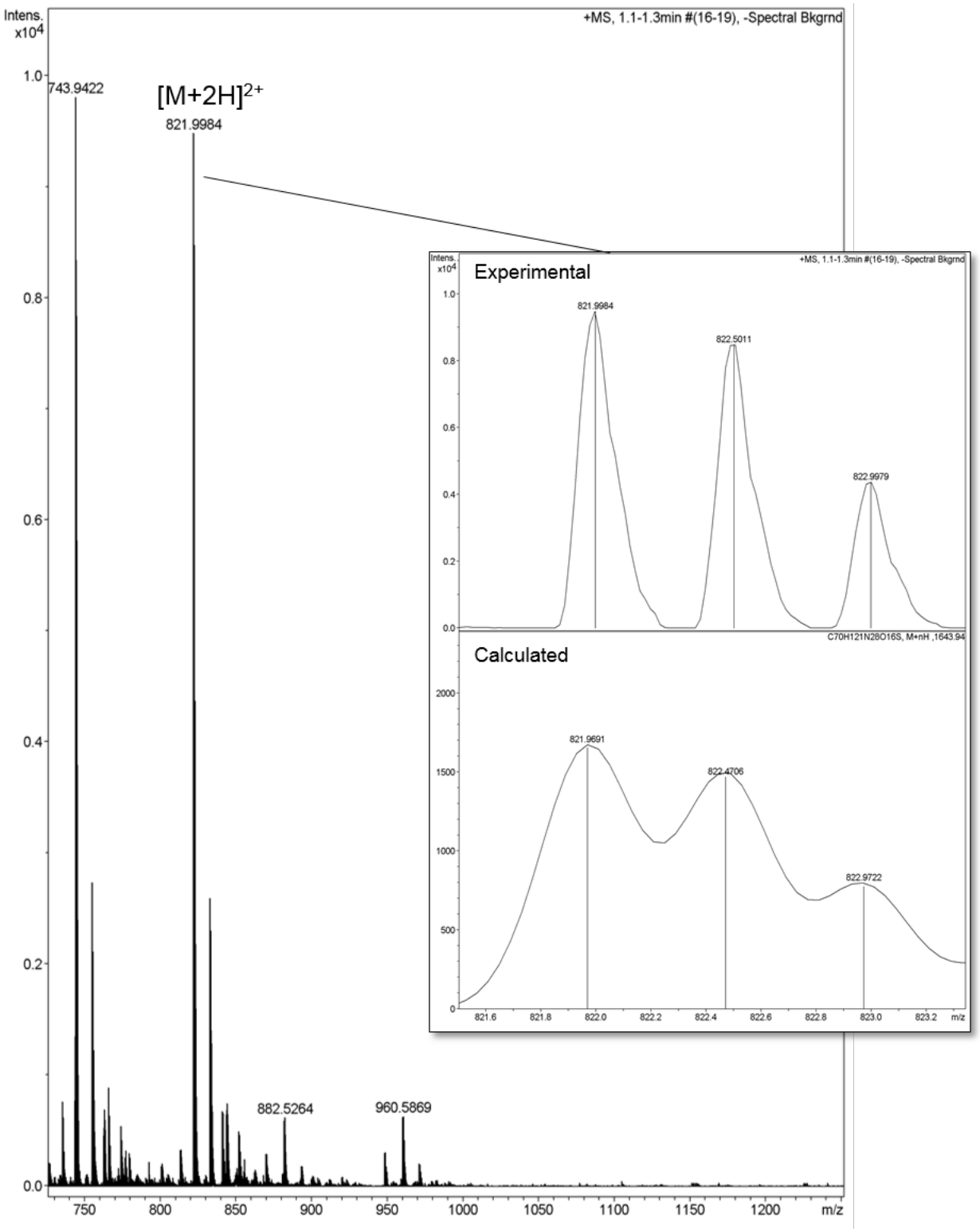

Figure 7.23: ESI-MS$^+$ spectrum of the N-terminally biotinylated PIP 644 peptide. Inset, the experimental isotopic pattern (top) in comparison with the calculated isotopic pattern (bottom) for the $[M+2H]^{2+}$ species.

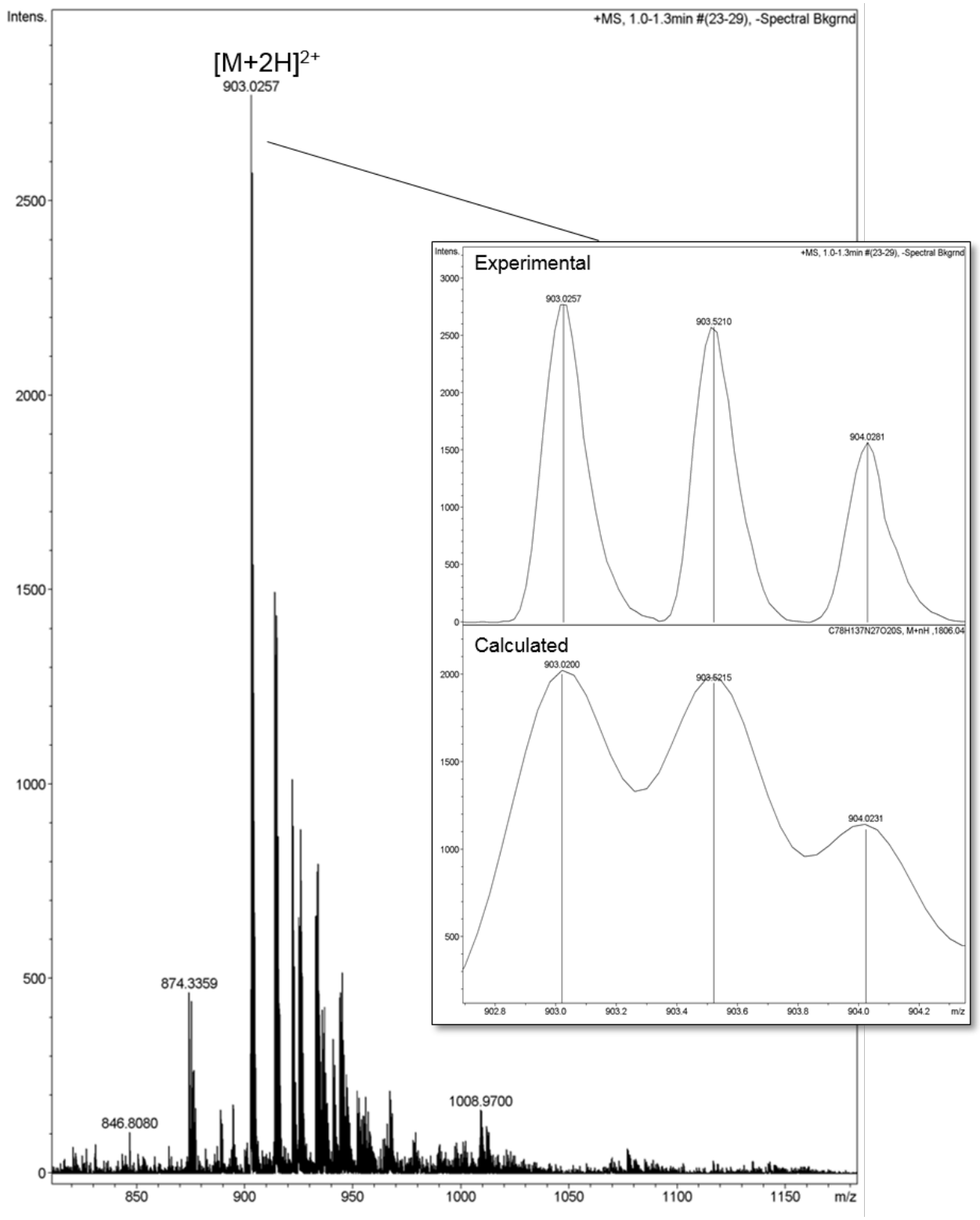

Figure 7.24: ESI-MS$^+$ spectrum of the C-terminally biotinylated PIP 640 peptide. Inset, the experimental isotopic pattern (top) in comparison with the calculated isotopic pattern (bottom) for the $[M+2H]^{2+}$ species.

Chapter 8 : References

1. Scanlon, V., and Sanders, T. (2014) *Essentials of anatomy and physiology*, F. A. Davis company, Philadelphia, United States.
2. Peterson, L. W., and Artis, D. (2014) Intestinal epithelial cells: regulators of barrier function and immune homeostasis, *Nat Rev Immunol 14*, 141-153.
3. Renukuntla, J., Vadlapudi, A. D., Patel, A., Boddu, S. H., and Mitra, A. K. (2013) Approaches for enhancing oral bioavailability of peptides and proteins, *Int J Pharm 447*, 75-93.
4. Peters, T. J. (1970) Intestinal peptidases, *Gut 11*, 720-725.
5. Maher, S., Mrsny, R. J., and Brayden, D. J. (2016) Intestinal permeation enhancers for oral peptide delivery, *Adv Drug Deliv Rev 106*, 277-319.
6. Wilson, C. G. (2011) The organization of the gut and the oral absorption of drugs: Anatomical, biological and physiological considerations in oral formulation development, in *Controlled release in oral drug delivery* (Wilson, C. G., and Crowley, P. J., Eds.), pp 27-48, Springer US, Boston, MA.
7. Hooton, D., Lentle, R., Monro, J., Wickham, M., and Simpson, R. (2015) The secretion and action of brush border enzymes in the mammalian small intestine, in *Reviews of physiology, biochemistry and pharmacology* (Nilius, B., Gudermann, T., Jahn, R., Lill, R., Petersen, O. H., and de Tombe, P. P., Eds.), pp 59-118, Springer international publishing, Cambridge.
8. Masaoka, Y., Tanaka, Y., Kataoka, M., Sakuma, S., and Yamashita, S. (2006) Site of drug absorption after oral administration: assessment of membrane permeability and luminal concentration of drugs in each segment of gastrointestinal tract, *Eur J Pharm Sci 29*, 240-250.
9. Elphick, D. A., and Mahida, Y. R. (2005) Paneth cells: their role in innate immunity and inflammatory disease, *Gut 54*, 1802-1809.
10. Aoki, Y., Morishita, M., and Takayama, K. (2005) Role of the mucous/glycocalyx layers in insulin permeation across the rat ileal membrane, *Int J Pharm 297*, 98-109.
11. Moran-Ramos, S., Tovar, A. R., and Torres, N. (2012) Diet: friend or foe of enteroendocrine cells-how it interacts with enteroendocrine cells, *Adv Nutr (Bethesda, Md.) 3*, 8-20.
12. Turner, J. R. (2006) Molecular basis of epithelial barrier regulation: from basic mechanisms to clinical application, *Am J Pathol 169*, 1901-1909.
13. McCartney, F., Gleeson, J. P., and Brayden, D. J. (2016) Safety concerns over the use of intestinal permeation enhancers: A mini-review, *Tissue Barriers 4*, e1176822.
14. Zihni, C., Mills, C., Matter, K., and Balda, M. S. (2016) Tight junctions: from simple barriers to multifunctional molecular gates, *Nat Rev Mol Cell Biol 17*, 564-580.
15. Giepmans, B. N. G., and van Ijzendoorn, S. C. D. (2009) Epithelial cell–cell junctions and plasma membrane domains, *Biochim Biophys Acta 1788*, 820-831.

16. Daugherty, A. L., and Mrsny, R. J. (1999) Transcellular uptake mechanisms of the intestinal epithelial barrier part one, *Pharm Sci Technolo Today 2*, 144-151.
17. Bellmann, S., Carlander, D., Fasano, A., Momcilovic, D., Scimeca, J. A., Waldman, W. J., Gombau, L., Tsytsikova, L., Canady, R., Pereira, D. I. A., and Lefebvre, D. E. (2015) Mammalian gastrointestinal tract parameters modulating the integrity, surface properties, and absorption of food-relevant nanomaterials, *Wiley Interdiscip Rev Nanomed Nanobiotechnol 7*, 609-622.
18. Doherty, G. J., and McMahon, H. T. (2009) Mechanisms of endocytosis, *Annu Rev Biochem 78*, 857-902.
19. Farquhar, M. G., and Palade, G. E. (1963) Junctional complexes in various epithelia, *J Cell Biol 17*, 375-412.
20. Claude, P., and Goodenough, D. A. (1973) Fracture faces of zonulae occludentes from "tight" and "leaky" epithelia, *J Cell Biol 58*, 390-400.
21. Tamura, A., and Tsukita, S. (2014) Paracellular barrier and channel functions of TJ claudins in organizing biological systems: advances in the field of barriology revealed in knockout mice, *Semin Cell Dev Biol 36*, 177-185.
22. Krause, G., Winkler, L., Mueller, S. L., Haseloff, R. F., Piontek, J., and Blasig, I. E. (2008) Structure and function of claudins, *Biochim Biophys Acta 1778*, 631-645.
23. Guillemot, L., Paschoud, S., Pulimeno, P., Foglia, A., and Citi, S. (2008) The cytoplasmic plaque of tight junctions: A scaffolding and signalling center, *Biochim Biophys Acta 1778*, 601-613.
24. Furuse, M., Sasaki, H., and Tsukita, S. (1999) Manner of interaction of heterogeneous claudin species within and between tight junction strands, *J Cell Biol 147*, 891-903.
25. Milatz, S., Krug, S. M., Rosenthal, R., Günzel, D., Müller, D., Schulzke, J.-D., Amasheh, S., and Fromm, M. (2010) Claudin-3 acts as a sealing component of the tight junction for ions of either charge and uncharged solutes, *Biochim Biophys Acta 1798*, 2048-2057.
26. Furuse, M., Hata, M., Furuse, K., Yoshida, Y., Haratake, A., Sugitani, Y., Noda, T., Kubo, A., and Tsukita, S. (2002) Claudin-based tight junctions are crucial for the mammalian epidermal barrier: a lesson from claudin-1-deficient mice, *J Cell Biol 156*, 1099-1111.
27. Amasheh, S., Meiri, N., Gitter, A. H., Schoneberg, T., Mankertz, J., Schulzke, J. D., and Fromm, M. (2002) Claudin-2 expression induces cation-selective channels in tight junctions of epithelial cells, *J Cell Sci 115*, 4969-4976.
28. Wada, M., Tamura, A., Takahashi, N., and Tsukita, S. (2013) Loss of claudins 2 and 15 from mice causes defects in paracellular Na^+ flow and nutrient transport in gut and leads to death from malnutrition, *Gastroenterology 144*, 369-380.
29. Hou, J., Renigunta, A., Yang, J., and Waldegger, S. (2010) Claudin-4 forms paracellular chloride channel in the kidney and requires claudin-8 for tight junction localization, *Proc Natl Acad Sci U S A 107*, 18010-18015.
30. Yu, A. S., Cheng, M. H., Angelow, S., Gunzel, D., Kanzawa, S. A., Schneeberger, E. E., Fromm, M., and Coalson, R. D. (2009) Molecular

basis for cation selectivity in claudin-2-based paracellular pores: identification of an electrostatic interaction site, *J Gen Physiol 133*, 111-127.
31. Wen, H., Watry, D. D., Marcondes, M. C., and Fox, H. S. (2004) Selective decrease in paracellular conductance of tight junctions: role of the first extracellular domain of claudin-5, *Mol Cell Biol 24*, 8408-8417.
32. Li, J., Angelow, S., Linge, A., Zhuo, M., and Yu, A. S. (2013) Claudin-2 pore function requires an intramolecular disulfide bond between two conserved extracellular cysteines, *Am J Physiol Cell Physiol 305*, C190-196.
33. Piontek, J., Winkler, L., Wolburg, H., Muller, S. L., Zuleger, N., Piehl, C., Wiesner, B., Krause, G., and Blasig, I. E. (2008) Formation of tight junction: determinants of homophilic interaction between classic claudins, *FASEB J 22*, 146-158.
34. Piehl, C., Piontek, J., Cording, J., Wolburg, H., and Blasig, I. E. (2010) Participation of the second extracellular loop of claudin-5 in paracellular tightening against ions, small and large molecules, *Cell Mol Life Sci 67*, 2131-2140.
35. Furuse, M., Sasaki, H., Fujimoto, K., and Tsukita, S. (1998) A single gene product, claudin-1 or -2, reconstitutes tight junction strands and recruits occludin in fibroblasts, *J Cell Biol 143*, 391-401.
36. Raleigh, D. R., Marchiando, A. M., Zhang, Y., Shen, L., Sasaki, H., Wang, Y., Long, M., and Turner, J. R. (2010) Tight junction-associated MARVEL proteins marveld3, tricellulin, and occludin have distinct but overlapping functions, *Mol Biol Cell 21*, 1200-1213.
37. Cording, J., Berg, J., Käding, N., Bellmann, C., Tscheik, C., Westphal, J. K., Milatz, S., Günzel, D., Wolburg, H., Piontek, J., Huber, O., and Blasig, I. E. (2013) In tight junctions, claudins regulate the interactions between occludin, tricellulin and marvelD3, which, inversely, modulate claudin oligomerization, *J Cell Sci 126*, 554-564.
38. Lingaraju, A., Long, T. M., Wang, Y., Austin Ii, J. R., and Turner, J. R. (2015) Conceptual barriers to understanding physical barriers, *Semin Cell Dev Biol 42*, 13-21.
39. Zeissig, S., Burgel, N., Gunzel, D., Richter, J., Mankertz, J., Wahnschaffe, U., Kroesen, A. J., Zeitz, M., Fromm, M., and Schulzke, J. D. (2007) Changes in expression and distribution of claudin 2, 5 and 8 lead to discontinuous tight junctions and barrier dysfunction in active Crohn's disease, *Gut 56*, 61-72.
40. Staat, C., Coisne, C., Dabrowski, S., Stamatovic, S. M., Andjelkovic, A. V., Wolburg, H., Engelhardt, B., and Blasig, I. E. (2015) Mode of action of claudin peptidomimetics in the transient opening of cellular tight junction barriers, *Biomaterials 54*, 9-20.
41. Sanchez-Pulido, L., Martin-Belmonte, F., Valencia, A., and Alonso, M. A. (2002) MARVEL: a conserved domain involved in membrane apposition events, *Trends Biochem Sci 27*, 599-601.
42. Furuse, M., Hirase, T., Itoh, M., Nagafuchi, A., Yonemura, S., Tsukita, S., and Tsukita, S. (1993) Occludin: a novel integral membrane protein localizing at tight junctions, *J Cell Biol 123*, 1777-1788.

43. Li, Y., Fanning, A. S., Anderson, J. M., and Lavie, A. (2005) Structure of the conserved cytoplasmic C-terminal domain of occludin: identification of the ZO-1 binding surface, *J Mol Biol 352*, 151-164.
44. Nusrat, A., Chen, J. A., Foley, C. S., Liang, T. W., Tom, J., Cromwell, M., Quan, C., and Mrsny, R. J. (2000) The coiled-coil domain of occludin can act to organize structural and functional elements of the epithelial tight junction, *J Biol Chem 275*, 29816-29822.
45. Turner, J. R., Buschmann, M. M., Romero-Calvo, I., Sailer, A., and Shen, L. (2014) The role of molecular remodeling in differential regulation of tight junction permeability, *Semin Cell Dev Biol 36*, 204-212.
46. Raleigh, D. R., Boe, D. M., Yu, D., Weber, C. R., Marchiando, A. M., Bradford, E. M., Wang, Y., Wu, L., Schneeberger, E. E., Shen, L., and Turner, J. R. (2011) Occludin S408 phosphorylation regulates tight junction protein interactions and barrier function, *J Cell Biol 193*, 565-582.
47. Wong, V., and Gumbiner, B. M. (1997) A synthetic peptide corresponding to the extracellular domain of occludin perturbs the tight junction permeability barrier, *J Cell Biol 136*, 399-409.
48. Van Itallie, C. M., and Anderson, J. M. (1997) Occludin confers adhesiveness when expressed in fibroblasts, *J Cell Sci 110 (Pt 9)*, 1113-1121.
49. Medina, R., Rahner, C., Mitic, L. L., Anderson, J. M., and Van Itallie, C. M. (2000) Occludin localization at the tight junction requires the second extracellular loop, *J Biol Chem J Membr Biol 178*, 235-247.
50. Saitou, M., Furuse, M., Sasaki, H., Schulzke, J. D., Fromm, M., Takano, H., Noda, T., and Tsukita, S. (2000) Complex phenotype of mice lacking occludin, a component of tight junction strands, *Mol Biol Cell 11*, 4131-4142.
51. Schulzke, J. D., Gitter, A. H., Mankertz, J., Spiegel, S., Seidler, U., Amasheh, S., Saitou, M., Tsukita, S., and Fromm, M. (2005) Epithelial transport and barrier function in occludin-deficient mice, *Biochim Biophys Acta 1669*, 34-42.
52. Ikenouchi, J., Sasaki, H., Tsukita, S., Furuse, M., and Tsukita, S. (2008) Loss of occludin affects tricellular localization of tricellulin, *Mol Biol Cell 19*, 4687-4693.
53. Clayburgh, D. R., Barrett, T. A., Tang, Y., Meddings, J. B., Van Eldik, L. J., Watterson, D. M., Clarke, L. L., Mrsny, R. J., and Turner, J. R. (2005) Epithelial myosin light chain kinase-dependent barrier dysfunction mediates T cell activation-induced diarrhea *in vivo*, *J Clin Invest 115*, 2702-2715.
54. Buschmann, M. M., Shen, L., Rajapakse, H., Raleigh, D. R., Wang, Y., Wang, Y., Lingaraju, A., Zha, J., Abbott, E., McAuley, E. M., Breskin, L. A., Wu, L., Anderson, K., Turner, J. R., and Weber, C. R. (2013) Occludin OCEL-domain interactions are required for maintenance and regulation of the tight junction barrier to macromolecular flux, *Mol Biol Cell 24*, 3056-3068.
55. Ikenouchi, J., Furuse, M., Furuse, K., Sasaki, H., Tsukita, S., and Tsukita, S. (2005) Tricellulin constitutes a novel barrier at tricellular contacts of epithelial cells, *J Cell Biol 171*, 939-945.

56. Riazuddin, S., Ahmed, Z. M., Fanning, A. S., Lagziel, A., Kitajiri, S., Ramzan, K., Khan, S. N., Chattaraj, P., Friedman, P. L., Anderson, J. M., Belyantseva, I. A., Forge, A., Riazuddin, S., and Friedman, T. B. (2006) Tricellulin is a tight-junction protein necessary for hearing, *Am J Hum Genet 79*, 1040-1051.
57. Krug, S. M., Amasheh, S., Richter, J. F., Milatz, S., Gunzel, D., Westphal, J. K., Huber, O., Schulzke, J. D., and Fromm, M. (2009) Tricellulin forms a barrier to macromolecules in tricellular tight junctions without affecting ion permeability, *Mol Biol Cell 20*, 3713-3724.
58. Takasawa, A., Kojima, T., Ninomiya, T., Tsujiwaki, M., Murata, M., Tanaka, S., and Sawada, N. (2013) Behavior of tricellulin during destruction and formation of tight junctions under various extracellular calcium conditions, *Cell Tissue Res 351*, 73-84.
59. Steed, E., Rodrigues, N. T., Balda, M. S., and Matter, K. (2009) Identification of MarvelD3 as a tight junction-associated transmembrane protein of the occludin family, *BMC Cell Biol 10*, 95.
60. Osler, M. E., Chang, M. S., and Bader, D. M. (2005) Bves modulates epithelial integrity through an interaction at the tight junction, *J Cell Sci 118*, 4667-4678.
61. Wada, A. M., Reese, D. E., and Bader, D. M. (2001) Bves: prototype of a new class of cell adhesion molecules expressed during coronary artery development, *Development 128*, 2085-2093.
62. Martìn-Padura, I., Lostaglio, S., Schneemann, M., Williams, L., Romano, M., Fruscella, P., Panzeri, C., Stoppacciaro, A., Ruco, L., Villa, A., Simmons, D., and Dejana, E. (1998) Junctional adhesion molecule, a novel member of the immunoglobulin superfamily that distributes at intercellular junctions and modulates monocyte transmigration, *J Cell Biol 142*, 117-127.
63. Luissint, A. C., Nusrat, A., and Parkos, C. A. (2014) JAM-related proteins in mucosal homeostasis and inflammation, *Semin Immunopathol 36*, 211-226.
64. Ebnet, K., Suzuki, A., Ohno, S., and Vestweber, D. (2004) Junctional adhesion molecules (JAMs): more molecules with dual functions?, *J Cell Sci 117*, 19-29.
65. Laukoetter, M. G., Nava, P., Lee, W. Y., Severson, E. A., Capaldo, C. T., Babbin, B. A., Williams, I. R., Koval, M., Peatman, E., Campbell, J. A., Dermody, T. S., Nusrat, A., and Parkos, C. A. (2007) JAM-A regulates permeability and inflammation in the intestine *in vivo*, *J Exp Med 204*, 3067-3076.
66. Williams, L. A., Martin-Padura, I., Dejana, E., Hogg, N., and Simmons, D. L. (1999) Identification and characterisation of human junctional adhesion molecule (JAM), *Mol Immunol 36*, 1175-1188.
67. Arrate, M. P., Rodriguez, J. M., Tran, T. M., Brock, T. A., and Cunningham, S. A. (2001) Cloning of human junctional adhesion molecule 3 (JAM3) and its identification as the JAM2 counter-receptor, *J Biol Chem 276*, 45826-45832.
68. Itoh, M., Sasaki, H., Furuse, M., Ozaki, H., Kita, T., and Tsukita, S. (2001) Junctional adhesion molecule (JAM) binds to PAR-3: a possible mechanism for the recruitment of PAR-3 to tight junctions, *J Cell Biol 154*, 491-497.

69. Knust, E. (2000) Control of epithelial cell shape and polarity, *Curr Opin Genet Dev 10*, 471-475.
70. Lemmers, C., Medina, E., Delgrossi, M. H., Michel, D., Arsanto, J. P., and Le Bivic, A. (2002) hINADl/PATJ, a homolog of discs lost, interacts with crumbs and localizes to tight junctions in human epithelial cells, *J Biol Chem 277*, 25408-25415.
71. Makarova, O., Roh, M. H., Liu, C.-J., Laurinec, S., and Margolis, B. (2003) Mammalian Crumbs3 is a small transmembrane protein linked to protein associated with Lin-7 (Pals1), *Gene 302*, 21-29.
72. Masuda, S., Oda, Y., Sasaki, H., Ikenouchi, J., Higashi, T., Akashi, M., Nishi, E., and Furuse, M. (2011) LSR defines cell corners for tricellular tight junction formation in epithelial cells, *J Cell Sci 124*, 548-555.
73. Higashi, T., Tokuda, S., Kitajiri, S., Masuda, S., Nakamura, H., Oda, Y., and Furuse, M. (2013) Analysis of the 'angulin' proteins LSR, ILDR1 and ILDR2--tricellulin recruitment, epithelial barrier function and implication in deafness pathogenesis, *J Cell Sci 126*, 966-977.
74. Van Itallie, C. M., and Anderson, J. M. (2014) Architecture of tight junctions and principles of molecular composition, *Semin Cell Dev Biol 36*, 157-165.
75. Stevenson, B. R., Siliciano, J. D., Mooseker, M. S., and Goodenough, D. A. (1986) Identification of ZO-1: a high molecular weight polypeptide associated with the tight junction (zonula occludens) in a variety of epithelia, *J Cell Biol 103*, 755-766.
76. Gumbiner, B., Lowenkopf, T., and Apatira, D. (1991) Identification of a 160-kDa polypeptide that binds to the tight junction protein ZO-1, *Proc Natl Acad Sci U S A 88*, 3460-3464.
77. Haskins, J., Gu, L., Wittchen, E. S., Hibbard, J., and Stevenson, B. R. (1998) ZO-3, a novel member of the MAGUK protein family found at the tight junction, interacts with ZO-1 and occludin, *J Cell Biol 141*, 199-208.
78. González-Mariscal, L., Betanzos, A., and Ávila-Flores, A. (2000) MAGUK proteins: structure and role in the tight junction, *Semin Cell Dev Biol 11*, 315-324.
79. Fanning, A. S., and Anderson, J. M. (2009) Zonula occludens-1 and-2 are cytosolic scaffolds that regulate the assembly of cellular junctions, in *Molecular structure and function of the tight junction: From basic mechanisms to clinical manifestations* (Fromm, M., and Schulzke, J. D., Eds.), pp 113-120, Blackwell Publishing, Oxford.
80. Adachi, M., Inoko, A., Hata, M., Furuse, K., Umeda, K., Itoh, M., and Tsukita, S. (2006) Normal establishment of epithelial tight junctions in mice and cultured cells lacking expression of ZO-3, a tight-junction MAGUK protein, *Mol Cell Biol 26*, 9003-9015.
81. Guillemot, L., Schneider, Y., Brun, P., Castagliuolo, I., Pizzuti, D., Martines, D., Jond, L., Bongiovanni, M., and Citi, S. (2012) Cingulin is dispensable for epithelial barrier function and tight junction structure, and plays a role in the control of claudin-2 expression and response to duodenal mucosa injury, *J Cell Sci 125*, 5005-5014.
82. Katsuno, T., Umeda, K., Matsui, T., Hata, M., Tamura, A., Itoh, M., Takeuchi, K., Fujimori, T., Nabeshima, Y., Noda, T., Tsukita, S., and Tsukita, S. (2008) Deficiency of zonula occludens-1 causes embryonic

lethal phenotype associated with defected yolk sac angiogenesis and apoptosis of embryonic cells, *Mol Biol Cell 19*, 2465-2475.
83. Xu, J., Kausalya, P. J., Phua, D. C., Ali, S. M., Hossain, Z., and Hunziker, W. (2008) Early embryonic lethality of mice lacking ZO-2, but Not ZO-3, reveals critical and nonredundant roles for individual zonula occludens proteins in mammalian development, *Mol Cell Biol 28*, 1669-1678.
84. Umeda, K., Matsui, T., Nakayama, M., Furuse, K., Sasaki, H., Furuse, M., and Tsukita, S. (2004) Establishment and characterization of cultured epithelial cells lacking expression of ZO-1, *J Biol Chem 279*, 44785-44794.
85. Van Itallie, C. M., Fanning, A. S., Bridges, A., and Anderson, J. M. (2009) ZO-1 stabilizes the tight junction solute barrier through coupling to the perijunctional cytoskeleton, *Mol Biol Cell 20*, 3930-3940.
86. Madara, J. L. (1987) Intestinal absorptive cell tight junctions are linked to cytoskeleton, *Am J Physiol 253*, C171-175.
87. Shen, L., and Turner, J. R. (2005) Actin depolymerization disrupts tight junctions via caveolae-mediated endocytosis, *Mol Biol Cell 16*, 3919-3936.
88. Turner, J. R., Rill, B. K., Carlson, S. L., Carnes, D., Kerner, R., Mrsny, R. J., and Madara, J. L. (1997) Physiological regulation of epithelial tight junctions is associated with myosin light-chain phosphorylation, *Am J Physiol 273*, C1378-1385.
89. Shen, L., Black, E. D., Witkowski, E. D., Lencer, W. I., Guerriero, V., Schneeberger, E. E., and Turner, J. R. (2006) Myosin light chain phosphorylation regulates barrier function by remodeling tight junction structure, *J Cell Sci 119*, 2095-2106.
90. Eto, M., and Kitazawa, T. (2017) Diversity and plasticity in signaling pathways that regulate smooth muscle responsiveness: Paradigms and paradoxes for the myosin phosphatase, the master regulator of smooth muscle contraction, *J Smooth Muscle Res 53*, 1-19.
91. Terrak, M., Kerff, F., Langsetmo, K., Tao, T., and Dominguez, R. (2004) Structural basis of protein phosphatase 1 regulation, *Nature 429*, 780-784.
92. Dimopoulos, G. J., Semba, S., Kitazawa, K., Eto, M., and Kitazawa, T. (2007) Ca^{2+}-dependent rapid Ca^{2+} sensitization of contraction in arterial smooth muscle, *Circ Res 100*, 121-129.
93. Pappenheimer, J. R., and Reiss, K. Z. (1987) Contribution of solvent drag through intercellular junctions to absorption of nutrients by the small intestine of the rat, *J Biol Chem J Membr Biol 100*, 123-136.
94. Madara, J. L., Carlson, S., and Anderson, J. M. (1993) ZO-1 maintains its spatial distribution but dissociates from junctional fibrils during tight junction regulation, *Am J Physiol 264*, C1096-1101.
95. Yu, D., Marchiando, A. M., Weber, C. R., Raleigh, D. R., Wang, Y., Shen, L., and Turner, J. R. (2010) MLCK-dependent exchange and actin binding region-dependent anchoring of ZO-1 regulate tight junction barrier function, *Proc Natl Acad Sci U S A 107*, 8237-8241.
96. Maher, S., Leonard, T. W., Jacobsen, J., and Brayden, D. J. (2009) Safety and efficacy of sodium caprate in promoting oral drug absorption: from *in vitro* to the clinic, *Adv Drug Deliv Rev 61*, 1427-1449.

97. Tran, C. D., Ball, J. M., Sundar, S., Coyle, P., and Howarth, G. S. (2007) The role of zinc and metallothionein in the dextran sulfate sodium-induced colitis mouse model, *Dig Dis Sci 52*, 2113-2121.
98. Finamore, A., Massimi, M., Conti Devirgiliis, L., and Mengheri, E. (2008) Zinc deficiency induces membrane barrier damage and increases neutrophil transmigration in Caco-2 cells, *J Nutr 138*, 1664-1670.
99. Miyoshi, Y., Tanabe, S., and Suzuki, T. (2016) Cellular zinc is required for intestinal epithelial barrier maintenance via the regulation of claudin-3 and occludin expression, *Am J Physiol Gastrointest Liver Physiol 311*, G105-116.
100. Hooper, L. V., Midtvedt, T., and Gordon, J. I. (2002) How host-microbial interactions shape the nutrient environment of the mammalian intestine, *Annu Rev Nutr 22*, 283-307.
101. Funderburg, N. T., Stubblefield Park, S. R., Sung, H. C., Hardy, G., Clagett, B., Ignatz-Hoover, J., Harding, C. V., Fu, P., Katz, J. A., Lederman, M. M., and Levine, A. D. (2013) Circulating CD4(+) and CD8(+) T cells are activated in inflammatory bowel disease and are associated with plasma markers of inflammation, *Immunology 140*, 87-97.
102. Weber, C. R., Raleigh, D. R., Su, L., Shen, L., Sullivan, E. A., Wang, Y., and Turner, J. R. (2010) Epithelial myosin light chain kinase activation induces mucosal interleukin-13 expression to alter tight junction ion selectivity, *J Biol Chem 285*, 12037-12046.
103. Zolotarevsky, Y., Hecht, G., Koutsouris, A., Gonzalez, D. E., Quan, C., Tom, J., Mrsny, R. J., and Turner, J. R. (2002) A membrane-permeant peptide that inhibits MLC kinase restores barrier function in *in vitro* models of intestinal disease, *Gastroenterology 123*, 163-172.
104. Capaldo, C. T., Farkas, A. E., Hilgarth, R. S., Krug, S. M., Wolf, M. F., Benedik, J. K., Fromm, M., Koval, M., Parkos, C., and Nusrat, A. (2014) Proinflammatory cytokine-induced tight junction remodeling through dynamic self-assembly of claudins, *Mol Biol Cell 25*, 2710-2719.
105. Heller, F., Florian, P., Bojarski, C., Richter, J., Christ, M., Hillenbrand, B., Mankertz, J., Gitter, A. H., Burgel, N., Fromm, M., Zeitz, M., Fuss, I., Strober, W., and Schulzke, J. D. (2005) Interleukin-13 is the key effector Th2 cytokine in ulcerative colitis that affects epithelial tight junctions, apoptosis, and cell restitution, *Gastroenterology 129*, 550-564.
106. Purohit, V., Bode, J. C., Bode, C., Brenner, D. A., Choudhry, M. A., Hamilton, F., Kang, Y. J., Keshavarzian, A., Rao, R., Sartor, R. B., Swanson, C., and Turner, J. R. (2008) Alcohol, intestinal bacterial growth, intestinal permeability to endotoxin, and medical consequences: summary of a symposium, *Alcohol 42*, 349-361.
107. Sheth, P., Seth, A., Thangavel, M., Basuroy, S., and Rao, R. K. (2004) Epidermal growth factor prevents acetaldehyde-induced paracellular permeability in Caco-2 cell monolayer, *Alcohol Clin Exp Res 28*, 797-804.
108. Sheth, P., Seth, A., Atkinson, Katherine J., Gheyi, T., Kale, G., Giorgianni, F., Desiderio, Dominic M., Li, C., Naren, A., and Rao, R. (2007) Acetaldehyde dissociates the PTP1B–E-cadherin–β-catenin complex in Caco-2 cell monolayers by a phosphorylation-dependent mechanism, *Biochem J 402*, 291-300.

109. Chen, P., Starkel, P., Turner, J. R., Ho, S. B., and Schnabl, B. (2015) Dysbiosis-induced intestinal inflammation activates tumor necrosis factor receptor I and mediates alcoholic liver disease in mice, *Hepatology (Baltimore, Md.) 61*, 883-894.
110. de Punder, K., and Pruimboom, L. (2015) Stress induces endotoxemia and low-grade inflammation by increasing barrier permeability, *Front Immunol 6*, 223.
111. Yu, Y., Liu, Z. Q., Liu, X. Y., Yang, L., Geng, X. R., Yang, G., Liu, Z. G., Zheng, P. Y., and Yang, P. C. (2013) Stress-derived corticotropin releasing factor breaches epithelial endotoxin tolerance, *PloS one 8*, e65760.
112. Nusrat, A., Brown, G. T., Tom, J., Drake, A., Bui, T. T., Quan, C., and Mrsny, R. J. (2005) Multiple protein interactions involving proposed extracellular loop domains of the tight junction protein occludin, *Mol Biol Cell 16*, 1725-1734.
113. Mrsny, R. J., Brown, G. T., Gerner-Smidt, K., Buret, A. G., Meddings, J. B., Quan, C., Koval, M., and Nusrat, A. (2008) A key claudin extracellular loop domain is critical for epithelial barrier integrity, *Am J Pathol 172*, 905-915.
114. Zwanziger, D., Hackel, D., Staat, C., Böcker, A., Brack, A., Beyermann, M., Rittner, H., and Blasig, I. E. (2012) A peptidomimetic tight junction modulator to improve regional analgesia, *Mol Pharm 9*, 1785-1794.
115. Weber, C. R., Liang, G. H., Wang, Y., Das, S., Shen, L., Yu, A. S., Nelson, D. J., and Turner, J. R. (2015) Claudin-2-dependent paracellular channels are dynamically gated, *eLife 4*, e09906.
116. Mrsny, R. J. (2012) Oral drug delivery research in Europe, *J Control Release 161*, 247-253.
117. Aguirre, T. A., Teijeiro-Osorio, D., Rosa, M., Coulter, I. S., Alonso, M. J., and Brayden, D. J. (2016) Current status of selected oral peptide technologies in advanced preclinical development and in clinical trials, *Adv Drug Deliv Rev 106*, 223-241.
118. Krug, S. M., Amasheh, M., Dittmann, I., Christoffel, I., Fromm, M., and Amasheh, S. (2013) Sodium caprate as an enhancer of macromolecule permeation across tricellular tight junctions of intestinal cells, *Biomaterials 34*, 275-282.
119. Tscheik, C., Blasig, I. E., and Winkler, L. (2013) Trends in drug delivery through tissue barriers containing tight junctions, *Tissue Barriers 1*, e24565.
120. Feighery, L. M., Cochrane, S. W., Quinn, T., Baird, A. W., O'Toole, D., Owens, S. E., O'Donoghue, D., Mrsny, R. J., and Brayden, D. J. (2008) Myosin light chain kinase inhibition: correction of increased intestinal epithelial permeability *in vitro*, *Pharm Res 25*, 1377-1386.
121. Lindmark, T., Kimura, Y., and Artursson, P. (1998) Absorption enhancement through intracellular regulation of tight junction permeability by medium chain fatty acids in Caco-2 cells, *J Pharmacol Exp Ther 284*, 362-369.
122. Suzuki, T., and Hara, H. (2006) Difructose anhydride III and sodium caprate activate paracellular transport via different intracellular events in Caco-2 cells, *Life Sci 79*, 401-410.

123. Van Itallie, C. M., Gambling, T. M., Carson, J. L., and Anderson, J. M. (2005) Palmitoylation of claudins is required for efficient tight-junction localization, *J Cell Sci 118*, 1427-1436.
124. Usmani, S. S., Bedi, G., Samuel, J. S., Singh, S., Kalra, S., Kumar, P., Ahuja, A. A., Sharma, M., Gautam, A., and Raghava, G. P. S. (2017) THPdb: Database of FDA-approved peptide and protein therapeutics, *PloS one 12*, e0181748.
125. Leader, B., Baca, Q. J., and Golan, D. E. (2008) Protein therapeutics: a summary and pharmacological classification, *Nat Rev Drug Discov 7*, 21-39.
126. Yamamoto, A., Taniguchi, T., Rikyuu, K., Tsuji, T., Fujita, T., Murakami, M., and Muranishi, S. (1994) Effects of various protease inhibitors on the intestinal absorption and degradation of insulin in rats, *Pharm Res 11*, 1496-1500.
127. Taverner, A., Dondi, R., Almansour, K., Laurent, F., Owens, S.-E., Eggleston, I. M., Fotaki, N., and Mrsny, R. J. (2015) Enhanced paracellular transport of insulin can be achieved via transient induction of myosin light chain phosphorylation, *J Control Release 210*, 189-197.
128. Palomo, J. M. (2014) Solid-phase peptide synthesis: an overview focused on the preparation of biologically relevant peptides, *RSC Adv 4*, 32658-32672.
129. Owens, S. E., Graham, W. V., Siccardi, D., Turner, J. R., and Mrsny, R. J. (2005) A strategy to identify stable membrane-permeant peptide inhibitors of myosin light chain kinase, *Pharm Res 22*, 703-709.
130. Carraz, M., Zwart, W., Phan, T., Michalides, R., and Brunsveld, L. (2009) Perturbation of estrogen receptor α localization with synthetic nona-arginine LXXLL-peptide coactivator binding inhibitors, *Chem Biol 16*, 702-711.
131. Kumar, V., and Aldrich, J. V. (2003) A solid-phase synthetic strategy for labeled peptides: synthesis of a biotinylated derivative of the δ opioid receptor antagonist TIPP (Tyr-Tic-Phe-Phe-OH), *Org Lett 5*, 613-616.
132. Amblard, M., Fehrentz, J. A., Martinez, J., and Subra, G. (2006) Methods and protocols of modern solid phase peptide synthesis, *Mol Biotechnol 33*, 239-254.
133. Kaiser, E., Colescott, R. L., Bossinger, C. D., and Cook, P. I. (1970) Color test for detection of free terminal amino groups in the solid-phase synthesis of peptides, *Anal Biochem 34*, 595-598.
134. Winkler, D. F., and McGeer, P. L. (2008) Protein labeling and biotinylation of peptides during spot synthesis using biotin p-nitrophenyl ester (biotin-ONp), *Proteomics 8*, 961-967.
135. Rubas, W., Cromwell, M. E., Shahrokh, Z., Villagran, J., Nguyen, T. N., Wellton, M., Nguyen, T. H., and Mrsny, R. J. (1996) Flux measurements across Caco-2 monolayers may predict transport in human large intestinal tissue, *J Pharm Sci 85*, 165-169.
136. Balda, M. S., Whitney, J. A., Flores, C., Gonzalez, S., Cereijido, M., and Matter, K. (1996) Functional dissociation of paracellular permeability and transepithelial electrical resistance and disruption of the apical-basolateral intramembrane diffusion barrier by expression of a mutant tight junction membrane protein, *J Cell Biol 134*, 1031-1049.

137. Van Itallie, C. M., Fanning, A. S., Holmes, J., and Anderson, J. M. (2010) Occludin is required for cytokine-induced regulation of tight junction barriers, *J Cell Sci 123*, 2844-2852.
138. Wang, F., Schwarz, B. T., Graham, W. V., Wang, Y., Su, L., Clayburgh, D. R., Abraham, C., and Turner, J. R. (2006) IFN-γ-induced TNFR2 expression is required for TNF-dependent intestinal epithelial barrier dysfunction, *Gastroenterology 131*, 1153-1163.
139. Bradford, M. M. (1976) A rapid and sensitive method for the quantitation of microgram quantities of protein utilizing the principle of protein-dye binding, *Anal Biochem 72*, 248-254.
140. Wachtel, R. E., and Tsuji, K. (1977) Comparison of *Limulus amebocyte* lysates and correlation with the United States Pharmacopeial pyrogen test, *Appl Environ Microbiol 33*, 1265-1269.
141. Venturoli, D., and Rippe, B. (2005) Ficoll and dextran *vs*. globular proteins as probes for testing glomerular permselectivity: effects of molecular size, shape, charge, and deformability, *Am J Physiol Renal Physiol 288*, F605-613.
142. Berridge, M. V., Herst, P. M., and Tan, A. S. (2005) Tetrazolium dyes as tools in cell biology: new insights into their cellular reduction, *Biotechnol Annu Rev 11*, 127-152.
143. Fosgerau, K., and Hoffmann, T. (2015) Peptide therapeutics: current status and future directions, *Drug Discov Today 20*, 122-128.
144. Kaspar, A. A., and Reichert, J. M. (2013) Future directions for peptide therapeutics development, *Drug Discov Today 18*, 807-817.
145. Antosova, Z., Mackova, M., Kral, V., and Macek, T. (2009) Therapeutic application of peptides and proteins: parenteral forever?, *Trends Biotechnol 27*, 628-635.
146. Koch, S., and Nusrat, A. (2009) Dynamic regulation of epithelial cell fate and barrier function by intercellular junctions, *Ann N Y Acad Sci 1165*, 220-227.
147. Cunningham, K. E., and Turner, J. R. (2012) Myosin light chain kinase: pulling the strings of epithelial tight junction function, *Ann N Y Acad Sci 1258*, 34-42.
148. Eto, M. (2009) Regulation of cellular protein phosphatase-1 (PP1) by phosphorylation of the CPI-17 family, C-kinase-activated PP1 inhibitors, *J Biol Chem 284*, 35273-35277.
149. Hong, F., Haldeman, B. D., Jackson, D., Carter, M., Baker, J. E., and Cremo, C. R. (2011) Biochemistry of smooth muscle myosin light chain kinase, *Arch Biochem Biophys 510*, 135-146.
150. Hartshorne, D. J., Ito, M., and Erdodi, F. (1998) Myosin light chain phosphatase: subunit composition, interactions and regulation, *J Muscle Res Cell Motil 19*, 325-341.
151. Hendrickx, A., Beullens, M., Ceulemans, H., Den Abt, T., Van Eynde, A., Nicolaescu, E., Lesage, B., and Bollen, M. (2009) Docking Motif-Guided Mapping of the Interactome of Protein Phosphatase-1, *Chem Biol 16*, 365-371.
152. Bollen, M., Peti, W., Ragusa, M. J., and Beullens, M. (2010) The extended PP1 toolkit: designed to create specificity, *Trends Biochem Sci 35*, 450-458.

153. Cohen, P. T. (2002) Protein phosphatase 1-targeted in many directions, *J Cell Sci 115*, 241-256.
154. Eto, M., Ohmori, T., Suzuki, M., Furuya, K., and Morita, F. (1995) A novel protein phosphatase-1 inhibitory protein potentiated by protein kinase c. isolation from porcine aorta media and characterization, *J Biochem 118*, 1104-1107.
155. Hayashi, Y., Senba, S., Yazawa, M., Brautigan, D. L., and Eto, M. (2001) Defining the structural determinants and a potential mechanism for inhibition of myosin phosphatase by the protein kinase C-potentiated inhibitor protein of 17 kDa, *J Biol Chem 276*, 39858-39863.
156. Eto, M., Kitazawa, T., Matsuzawa, F., Aikawa, S., Kirkbride, J. A., Isozumi, N., Nishimura, Y., Brautigan, D. L., and Ohki, S. Y. (2007) Phosphorylation-induced conformational switching of CPI-17 produces a potent myosin phosphatase inhibitor, *Structure 15*, 1591-1602.
157. Eto, M., Kitazawa, T., and Brautigan, D. L. (2004) Phosphoprotein inhibitor CPI-17 specificity depends on allosteric regulation of protein phosphatase-1 by regulatory subunits, *Proc Natl Acad Sci U S A 101*, 8888-8893.
158. Goodman, M., and Chorev, M. (1979) On the concept of linear modified retro-peptide structures, *Acc Chem Res 12*, 1-7.
159. Madani, F., Lindberg, S., Langel, U., Futaki, S., and Graslund, A. (2011) Mechanisms of cellular uptake of cell-penetrating peptides, *J Biophys 2011*, 414729.
160. Kolosova, I. A., Ma, S. F., Adyshev, D. M., Wang, P., Ohba, M., Natarajan, V., Garcia, J. G., and Verin, A. D. (2004) Role of CPI-17 in the regulation of endothelial cytoskeleton, *Am J Physiol Lung Cell Mol Physiol 287*, L970-980.
161. Srinivas, S. P., Satpathy, M., Guo, Y., and Anandan, V. (2006) Histamine-induced phosphorylation of the regulatory light chain of myosin II disrupts the barrier integrity of corneal endothelial cells, *Invest Ophthalmol Vis Sci 47*, 4011-4018.
162. Lamberti, A., Sgammato, R., Desiderio, D., Punzo, C., Raimo, G., Novellino, E., Carotenuto, A., and Masullo, M. (2015) Native PAGE to study the interaction between the oncosuppressor p53 and its protein ligands, *Electrophoresis 36*, 552-555.
163. Sgammato, R., Desiderio, D., Lamberti, A., Raimo, G., Novellino, E., Carotenuto, A., and Masullo, M. (2015) Nondenaturing polyacrylamide gel electrophoresis to study the dissociation of the p53.MDM2/X complex by potentially anticancer compounds, *Electrophoresis 36*, 3101-3104.
164. Bruno, B. J., Miller, G. D., and Lim, C. S. (2013) Basics and recent advances in peptide and protein drug delivery, *Ther Deliv 4*, 1443-1467.
165. Tomita, M., Hayashi, M., Horie, T., Ishizawa, T., and Awazu, S. (1988) Enhancement of colonic drug absorption by the transcellular permeation route, *Pharm Res 5*, 786-789.
166. Lindmark, T., Soderholm, J. D., Olaison, G., Alvan, G., Ocklind, G., and Artursson, P. (1997) Mechanism of absorption enhancement in humans after rectal administration of ampicillin in suppositories containing sodium caprate, *Pharm Res 14*, 930-935.

167. Pappenheimer, J. R. (1993) On the coupling of membrane digestion with intestinal absorption of sugars and amino acids, *Am J Physiol 265*, G409-417.
168. Madara, J. L., and Carlson, S. (1991) Supraphysiologic L-tryptophan elicits cytoskeletal and macromolecular permeability alterations in hamster small intestinal epithelium *in vitro*, *J Clin Invest 87*, 454-462.
169. Ohki, S.-y., Eto, M., Shimizu, M., Takada, R., Brautigan, D. L., and Kainosho, M. (2003) Distinctive solution conformation of phosphatase inhibitor CPI-17 substituted with aspartate at the phosphorylation-site threonine residue, *J Mol Biol 326*, 1539-1547.
170. Chatterjee, J., Beullens, M., Sukackaite, R., Qian, J., Lesage, B., Hart, D. J., Bollen, M., and Kohn, M. (2012) Development of a peptide that selectively activates protein phosphatase-1 in living cells, *Angew Chem Int Ed Engl 51*, 10054-10059.
171. Li, C., Pazgier, M., Li, J., Li, C., Liu, M., Zou, G., Li, Z., Chen, J., Tarasov, S. G., Lu, W. Y., and Lu, W. (2010) Limitations of peptide retro-inverso isomerization in molecular mimicry, *J Biol Chem 285*, 19572-19581.
172. El-Andaloussi, S., Jarver, P., Johansson, H. J., and Langel, U. (2007) Cargo-dependent cytotoxicity and delivery efficacy of cell-penetrating peptides: a comparative study, *Biochem J 407*, 285-292.
173. Munday, R. (2013) Is protein phosphatase inhibition responsible for the toxic effects of okadaic acid in animals?, *Toxins 5*, 267-285.
174. Shasby, D. M., Kamath, J. M., Moy, A. B., and Shasby, S. S. (1995) Ionomycin and PDBU increase MDCK monolayer permeability independently of myosin light chain phosphorylation, *Am J Physiol 269*, L144-150.
175. Weber, C. R. (2012) Dynamic properties of the tight junction barrier, *Ann N Y Acad Sci 1257*, 77-84.
176. Günzel, D., and Yu, A. S. L. (2013) Claudins and the modulation of tight junction permeability, *Physiol Rev 93*, 525-569.
177. Shen, L., Weber, C. R., and Turner, J. R. (2008) The tight junction protein complex undergoes rapid and continuous molecular remodeling at steady state, *J Cell Biol 181*, 683-695.
178. Wada, M., Tamura, A., Takahashi, N., and Tsukita, S. (2013) Loss of claudins 2 and 15 from mice causes defects in paracellular Na^+ flow and nutrient transport in gut and leads to death from malnutrition, *Gastroenterology 144*, 369-380.
179. Heller, F., Florian, P., Bojarski, C., Richter, J., Christ, M., Hillenbrand, B., Mankertz, J., Gitter, A. H., Bürgel, N., Fromm, M., Zeitz, M., Fuss, I., Strober, W., and Schulzke, J. D. (2005) Interleukin-13 is the key effector Th2 cytokine in ulcerative colitis that affects epithelial tight junctions, apoptosis, and cell restitution, *Gastroenterology 129*, 550-564.
180. Fujii, N., Matsuo, Y., Matsunaga, T., Endo, S., Sakai, H., Yamaguchi, M., Yamazaki, Y., Sugatani, J., and Ikari, A. (2016) Hypotonic stress-induced down-regulation of claudin-1 and -2 mediated by dephosphorylation and clathrin-dependent endocytosis in renal tubular epithelial cells, *J Biol Chem 291*, 24787-24799.
181. Van Itallie, C. M., Tietgens, A. J., LoGrande, K., Aponte, A., Gucek, M., and Anderson, J. M. (2012) Phosphorylation of claudin-2 on serine 208

promotes membrane retention and reduces trafficking to lysosomes, *J Cell Sci 125*, 4902-4912.
182. Su, L., Nalle, S. C., Shen, L., Turner, E. S., Singh, G., Breskin, L. A., Khramtsova, E. A., Khramtsova, G., Tsai, P. Y., Fu, Y. X., Abraham, C., and Turner, J. R. (2013) TNFR2 activates MLCK-dependent tight junction dysregulation to cause apoptosis-mediated barrier loss and experimental colitis, *Gastroenterology 145*, 407-415.
183. Wang, F., Graham, W. V., Wang, Y., Witkowski, E. D., Schwarz, B. T., and Turner, J. R. (2005) Interferon-γ and tumor necrosis factor-α synergize to induce intestinal epithelial barrier dysfunction by up-regulating myosin light chain kinase expression, *Am J Pathol 166*, 409-419.
184. Rosenthal, R., Milatz, S., Krug, S. M., Oelrich, B., Schulzke, J. D., Amasheh, S., Gunzel, D., and Fromm, M. (2010) Claudin-2, a component of the tight junction, forms a paracellular water channel, *J Cell Sci 123*, 1913-1921.
185. Clayburgh, D. R., Musch, M. W., Leitges, M., Fu, Y. X., and Turner, J. R. (2006) Coordinated epithelial NHE3 inhibition and barrier dysfunction are required for TNF-mediated diarrhea *in vivo*, *J Clin Invest 116*, 2682-2694.
186. Fanning, A. S., Van Itallie, C. M., and Anderson, J. M. (2012) Zonula occludens-1 and -2 regulate apical cell structure and the zonula adherens cytoskeleton in polarized epithelia, *Mol Biol Cell 23*, 577-590.
187. Rodgers, L. S., Beam, M. T., Anderson, J. M., and Fanning, A. S. (2013) Epithelial barrier assembly requires coordinated activity of multiple domains of the tight junction protein ZO-1, *J Cell Sci 126*, 1565-1575.
188. Alexandre, M. D., Jeansonne, B. G., Renegar, R. H., Tatum, R., and Chen, Y. H. (2007) The first extracellular domain of claudin-7 affects paracellular Cl- permeability, *Biochem Biophys Res Commun 357*, 87-91.
189. Marchiando, A. M., Shen, L., Graham, W. V., Weber, C. R., Schwarz, B. T., Austin, J. R., 2nd, Raleigh, D. R., Guan, Y., Watson, A. J., Montrose, M. H., and Turner, J. R. (2010) Caveolin-1-dependent occludin endocytosis is required for TNF-induced tight junction regulation *in vivo*, *J Cell Biol 189*, 111-126.
190. Suzuki, T., Elias, B. C., Seth, A., Shen, L., Turner, J. R., Giorgianni, F., Desiderio, D., Guntaka, R., and Rao, R. (2009) PKCη regulates occludin phosphorylation and epithelial tight junction integrity, *Proc Natl Acad Sci U S A 106*, 61-66.
191. Lu, R., Johnson, D. L., Stewart, L., Waite, K., Elliott, D., and Wilson, J. M. (2014) Rab14 regulation of claudin-2 trafficking modulates epithelial permeability and lumen morphogenesis, *Mol Biol Cell 25*, 1744-1754.
192. Mankertz, J., Amasheh, M., Krug, S. M., Fromm, A., Amasheh, S., Hillenbrand, B., Tavalali, S., Fromm, M., and Schulzke, J. D. (2009) TNF- α up-regulates claudin-2 expression in epithelial HT-29/B6 cells via phosphatidylinositol-3-kinase signaling, *Cell Tissue Res 336*, 67-77.
193. Jenkins, R. T., and Bell, R. A. (1987) Molecular radii of probes used in studies of intestinal permeability, *Gut 28*, 110-111.
194. Knipp, G. T., Ho, N. F., Barsuhn, C. L., and Borchardt, R. T. (1997) Paracellular diffusion in Caco-2 cell monolayers: effect of perturbation

on the transport of hydrophilic compounds that vary in charge and size, *J Pharm Sci 86*, 1105-1110.
195. Heyman, N. S., and Burt, J. M. (2008) Hindered diffusion through an aqueous pore describes invariant dye selectivity of Cx43 junctions, *Biophys J 94*, 840-854.
196. Sugibayashi, K., Onuki, Y., and Takayama, K. (2009) Displacement of tight junction proteins from detergent-resistant membrane domains by treatment with sodium caprate, *Eur J Pharm Sci 36*, 246-253.
197. Colegio, O. R., Van Itallie, C. M., McCrea, H. J., Rahner, C., and Anderson, J. M. (2002) Claudins create charge-selective channels in the paracellular pathway between epithelial cells, *Am J Physiol Cell Physiol 283*, C142-147.
198. Sun, H., Chow, E. C., Liu, S., Du, Y., and Pang, K. S. (2008) The Caco-2 cell monolayer: usefulness and limitations, *Expert Opin Drug Metab Toxicol 4*, 395-411.
199. Hamman, J. H., Enslin, G. M., and Kotze, A. F. (2005) Oral delivery of peptide drugs: barriers and developments, *BioDrugs 19*, 165-177.
200. Schipper, N. G., Varum, K. M., Stenberg, P., Ocklind, G., Lennernas, H., and Artursson, P. (1999) Chitosans as absorption enhancers of poorly absorbable drugs. 3: Influence of mucus on absorption enhancement, *Eur J Pharm Sci 8*, 335-343.
201. Narkar, Y., Burnette, R., Bleher, R., Albrecht, R., Kandela, A., and Robinson, J. R. (2008) Evaluation of mucosal damage and recovery in the gastrointestinal tract of rats by a penetration enhancer, *Pharm Res 25*, 25-38.
202. Maher, S., Wang, X., Bzik, V., McClean, S., and Brayden, D. J. (2009) Evaluation of intestinal absorption and mucosal toxicity using two promoters. II. Rat instillation and perfusion studies, *Eur J Pharm Sci 38*, 301-311.
203. Grassie, M. E., Moffat, L. D., Walsh, M. P., and MacDonald, J. A. (2011) The myosin phosphatase targeting protein (MYPT) family: a regulated mechanism for achieving substrate specificity of the catalytic subunit of protein phosphatase type 1delta, *Arch Biochem Biophys 510*, 147-159.
204. Welling, S. H., Hubálek, F., Jacobsen, J., Brayden, D. J., Rahbek, U. L., and Buckley, S. T. (2014) The role of citric acid in oral peptide and protein formulations: Relationship between calcium chelation and proteolysis inhibition, *Eur J Pharm Biopharm 86*, 544-551.
205. Holmes, J. L., Van Itallie, C. M., Rasmussen, J. E., and Anderson, J. M. (2006) Claudin profiling in the mouse during postnatal intestinal development and along the gastrointestinal tract reveals complex expression patterns, *Gene expression patterns 6*, 581-588.
206. Escaffit, F., Boudreau, F., and Beaulieu, J. F. (2005) Differential expression of claudin-2 along the human intestine: Implication of GATA-4 in the maintenance of claudin-2 in differentiating cells, *J Cell Physiol 203*, 15-26.
207. Rahner, C., Mitic, L. L., and Anderson, J. M. (2001) Heterogeneity in expression and subcellular localization of claudins 2, 3, 4, and 5 in the rat liver, pancreas, and gut, *Gastroenterology 120*, 411-422.

208. Pauletti, G. M., Okumu, F. W., and Borchardt, R. T. (1997) Effect of size and charge on the passive diffusion of peptides across Caco-2 cell monolayers via the paracellular pathway, *Pharm Res 14*, 164-168.
209. Chittchang, M., Mitra, A. K., and Johnston, T. P. (2007) Interplay of secondary structure and charge on the diffusion of a polypeptide through negatively charged aqueous pores, *Pharm Res 24*, 502-511.
210. Kim, J. Y., Lee, H., Oh, K. S., Kweon, S., Jeon, O. C., Byun, Y., Kim, K., Kwon, I. C., Kim, S. Y., and Yuk, S. H. (2013) Multilayer nanoparticles for sustained delivery of exenatide to treat type 2 diabetes mellitus, *Biomaterials 34*, 8444-8449.
211. Torres-Lugo, M., and Peppas, N. A. (1999) Molecular design and *in vitro* studies of novel pH-sensitive hydrogels for the oral delivery of calcitonin, *Macromolecules 32*, 6646-6651.
212. Zhang, Y., Huo, M., Zhou, J., and Xie, S. (2010) PKSolver: An add-in program for pharmacokinetic and pharmacodynamic data analysis in Microsoft Excel, *Comput Methods Programs Biomed 99*, 306-314.
213. Walker, R. I., and Owen, R. L. (1990) Intestinal barriers to bacteria and their toxins, *Annu Rev Med 41*, 393-400.
214. Gutsmann, T., Schromm, A. B., and Brandenburg, K. (2007) The physicochemistry of endotoxins in relation to bioactivity, *Int J Med Microbiol 297*, 341-352.
215. Sonaje, K., Lin, K. J., Tseng, M. T., Wey, S. P., Su, F. Y., Chuang, E. Y., Hsu, C. W., Chen, C. T., and Sung, H. W. (2011) Effects of chitosan-nanoparticle-mediated tight junction opening on the oral absorption of endotoxins, *Biomaterials 32*, 8712-8721.
216. Balimane, P. V., and Chong, S. (2005) Cell culture-based models for intestinal permeability: a critique, *Drug Discov Today 10*, 335-343.
217. Natoli, M., Leoni, B. D., D'Agnano, I., Zucco, F., and Felsani, A. (2012) Good Caco-2 cell culture practices, *Toxicol In vitro 26*, 1243-1246.
218. Hovgaard, L., Jacobs, H., Wilson, D. E., and Kim, S. W. (1996) Stabilization of insulin by alkylmaltosides. B. Oral absorption in vivo in rats, *Int J Pharm132*, 115-121.
219. Schaumberger, S., Ladinig, A., Reisinger, N., Ritzmann, M., and Schatzmayr, G. (2014) Evaluation of the endotoxin binding efficiency of clay minerals using the *Limulus amebocyte* lysate test: an *in vitro* study, *AMB Express 4*, 1.
220. Guo, S., Al-Sadi, R., Said, H. M., and Ma, T. Y. (2013) Lipopolysaccharide causes an increase in intestinal tight junction permeability *in vitro* and *in vivo* by inducing enterocyte membrane expression and localization of TLR-4 and CD14, *Am J Pathol 182*, 375-387.
221. Turner, J. R., Buschmann, M. M., Romero-Calvo, I., Sailer, A., and Shen, L. (2014) The role of molecular remodeling in differential regulation of tight junction permeability, *Semin Cell Dev Biol 36*, 204-212.
222. Liu, F., Park, J. E., Lee, K. S., and Burke, T. R., Jr. (2009) Preparation of orthogonally protected-2-amino-3-methyl-4-phosphonobutyric acid (Pmab) as a phosphatase-stable phosphothreonine mimetic and its use in the synthesis of Polo-box domain-binding peptides, *Tetrahedron 65*, 9673-9679.

Chapter 9 : Dissemination

Publications:

1- **Almansour, K**., Taverner, A., Turner, J. R., Eggleston, I. M., and Mrsny. R. J. (2018) An Intestinal Paracellular Pathway Biased for Positively-Charged Macromolecules**,** *J Control Release*. (Manuscript in preparation).

2- **Almansour, K**., Taverner, A., Eggleston, I. M., and Mrsny, R. J. (2018) Mechanistic studies of a cell-permeant peptide designed to enhance myosin light chain phosphorylation in polarized intestinal epithelia, *J Control Release* 279, 208- 219.

3- Taverner, A., Dondi, R., **Almansour, K**., Laurent, F., Owens, S.-E., Eggleston, I. M., Fotaki, N., and Mrsny, R. J. (2015) Enhanced paracellular transport of insulin can be achieved via transient induction of myosin light chain phosphorylation, *J Control Release 210*, 189-197.

Conference Abstracts:

1- **Almansour, K**., Eggleston, I. M., and Mrsny, R. J. (July 2017) Regulation of intestinal epithelial tight junction (TJ) by a permeability-enhancing peptide, CRS annual meeting, Boston, USA.

2- **Almansour, K**., Eggleston, I. M., and Mrsny, R. J. (September 2016) Characterizing the opening of the tight junctions (TJs) induced by a permeability-enhancing peptide for the application of improving the oral absorption of protein drugs, 7th APS international PharmSci conference, Glasgow, UK.

3- **Almansour, K**., Eggleston, I. M., and Mrsny, R. J. (July 2015) Novel approach to enhance the oral absorption of peptide and protein drugs through an endogenous pathway, CRS annual meeting, Edinburgh, UK.

4- **Almansour, K**., Eggleston, I. M., and Mrsny, R. J. (July 2014) Application of retro-inverso cell penetrating peptides to selectively inhibit myosin light chain phosphatase (MLCP), chemistry and biology of peptides meetings by the RSC, London, UK.

Oral Presentations:

1- **Almansour, K**., Eggleston, I. M., and Mrsny, R. J. (March 2017) Therapeutic peptides delivery over the intestinal epithelial tight junctions, CNS barrier congress meeting by KISACO research, London, UK.